

Lab-on-a-chip technologies for manipulation and imaging of *C. elegans* worms and embryos

THÈSE N° 8438 (2018)

PRÉSENTÉE LE 22 MARS 2018

À LA FACULTÉ DES SCIENCES ET TECHNIQUES DE L'INGÉNIEUR
LABORATOIRE DE MICROSYSTÈMES 2
PROGRAMME DOCTORAL EN MICROSYSTÈMES ET MICROÉLECTRONIQUE

ÉCOLE POLYTECHNIQUE FÉDÉRALE DE LAUSANNE

POUR L'OBTENTION DU GRADE DE DOCTEUR ÈS SCIENCES

PAR

Li DONG

acceptée sur proposition du jury:

Dr G. Boero, président du jury
Prof. M. Gijs, Dr T. Lehnert, directeurs de thèse
Prof. P. Dittrich, rapporteuse
Prof. H. Bringmann, rapporteur
Prof. P. Gónczy, rapporteur



ÉCOLE POLYTECHNIQUE
FÉDÉRALE DE LAUSANNE

Suisse
2018

Acknowledgements

How time flies! Though it's such a simple sentence, I cannot find out a more magnificent sentence to express my feelings now. The four and half years in Lausanne has been the most rich and meaningful of my life. I feel to have experienced, learned and received a lot. And this is owing to a number of people I want to acknowledge here.

I cannot achieve this goal if **Martin** have not supported me. As my supervisor and mentor, he has an incredible ability to find the perfect balance between: allowing me to develop and explore my own ideas, research plans and projects; providing me with expert guidance, direction when needed; and most importantly providing the inspiration to achieve my best. I need freedom to 'smell the food' as *C. elegans* worms. If my experiment appears to be going wrong I need to try and understand why. A good supervisor appreciates these differences and does not try and fit square pegs in round holes. Martin knows when to back off and allow students to make their own decisions and when to come in and offer support and sympathy. Outside science, he is my one of my most trusted friends. I still remember the first time when he took me to go hiking, which was also my first real hike in my life. I was collapse and he even tried to call helicopter! After four and half years' training from him, I would say I have survived in this mountainous nation.

I can hardly advance my scientific output without the help of my co-director **Thomas**. Rather than directly providing me with interesting ideas or test method, he is always able to ask the right questions to lead me step back to think about the deficiencies of my experiments, research plans and manuscript works. It is him who cultivate me a scientific critical thinking, and lead me to create more positive and optimistic attitude towards life and pioneering sense of innovation.

Life could not be so wonderful without a good environment. Thanks to all my LMIS2 friends and colleagues, my PhD Life is sweetened by friendships we encounter along the highways that journey into our dreams. **Xiaopeng**, who is like my little brother, I enjoyed spending time together with him both in- and outside science. He is a great scientist and I hope he can achieve his ideal – to be a professor. **Tuan** and **Cristina**, we joined this lab together. It is wonderful to grow up together with you. After four and half years, I am 30. I have seen many people lost their hair... I am happy to see Einstuan's hair is still so dense and Cristina is as beautiful as the first day we met on her interview. We made such swell friends. **Matteo**, a great scientist and collaborator. His passion has no limits and I hope his attitude will pay him back for his startup. Thanks for the time he discussed science with me. **Greg** and I are like sport teammates. We went biking, skiing, bodybuilding, badminton... Unbelievable, I am slim like before while you become 'bigger'. **Roger** and **Baris**, these boys are like twins. They always bring joy to the lab. I will never forget I went for being a dad for them during our trip in Washington. And we had to stop to look for toilets since Baris had trouble with diarrhea. Here, I am especially thankful to Roger for translating my abstract into German version. **Hui**, not only for her collaboration but also for her great help when I arrived at Lausanne and started my PhD study. Finally, I would like to thank my present and former colleagues in LMIS2, **Raphael**, **Gopal**, **Daniel**,

Vittorio, Federico, Chiara, Jalil, Chaobo, Tuna, Diego, Rima, Jingwei, Deborah, Pierre, Antoine, Giuseppe, Paolo. Special thanks to **Melis, Lucie, Marie** and **Sylvie** for our nice chats and for their so prompt and efficient help, whatever I needed.

Worm-on-chip is a cross disciplinary science that centralizes biology and Lab-on-a-chip technology. I am extremely grateful for the support I received from the biologist: **Radek, Vincenzo, Laurent, Qiujian, Evan, Olli, Virginija, Elena, Marie, Kerstin.**

I would like to acknowledge the financial support of the EU Ideas program (ERC-2012-AdG-320404). Many thanks to **Professor Pierre Gönczy** and **Professor Johan Auwerx** for their collaboration and help during the work on drug studies during early embryogenesis and reversible *C. elegans* immobilization. My sincere thanks to all the CMI staff members for their support and for sharing their microfabrication expertise whenever required.

I express my gratitude to all my Chinese friends in Switzerland who offer me numerous assistances in the aspect of my daily life. Particular thanks to **KUNG Yen-Cheng, LOU Ye, SU Zongming, LIU Ke, WANG Ya, REN Yufei, XIE Shenqi, DU Huachuan, CHANG Rui-Chia, ZHANG Junrui, WANG Jian, LI Hao, QIU Jian, TANG Wei, MENG Zhenzhu, CAO Linlin, FAN Haifeng, YANG Fei, REN Wuwei, LI Tao, YU Xiaoyun, CAO Jin, CHEN Evelyn, NI Ruiqing, PAN Rensheng, XU Yuanping,**

Last but not least, I am truly grateful to my parents and my girlfriend for their unconditional and constant love, support and belief in me. My parents, **FENG Xiaoyan** and **DONG Jianqiu**, not only take care of me all these years, but always teach me and show me how can be an honest and hard-working person. My girlfriend, **LUAN Peiling**, always encourages me, gives me constructive suggestions and extraordinary feedbacks. This thesis is dedicated to them, with all my love.

Li Dong

9 March, 2018 Lausanne

Abstract

The nematode *Caenorhabditis elegans* is an attractive model organism, owing notably to its short life cycle, genetic tractability, optical transparency facilitating microscopic observation, and absence of ethical issues related to experimentation. In the last decade, lab-on-chip or microfluidic techniques have enabled many *C. elegans* experiments that could not be performed with conventional methods. Microfluidics facilitates animal manipulation and permits achieving precise environmental conditions and controlled delivery of chemicals. This thesis deals with the realization of technological tools for the manipulation of worms and for studying thereby biologically relevant questions. The novel microfluidic devices that were developed are:

#1 A microfluidic approach for size-dependent sorting of *C. elegans* nematodes on-chip.

We take advantage of the external pressure-deformable profile of polydimethylsiloxane (PDMS) transfer channels that connect two on-chip worm chambers. The pressure-controlled effective cross-section of these channels creates adjustable filter structures that can be easily tuned for a specific worm sorting experiment, without changing the design parameters of the device itself. By optimizing the control pressure settings, we can extract larvae of a specific development stage from a mixed worm culture with an efficiency close to 100% and with a throughput of up to 3.5 worms per second. Our approach also allows to generate mixed populations of larvae of adjacent stages, or to adjust the ratio of these directly in the microfluidic chamber. Moreover, using the same device, we demonstrated extraction of embryos from adult worm populations for subsequent culture of accurately age-synchronized nematode populations or embryo-based assays. Considering that our sorting device is merely based on geometrical parameters and operated by simple fluidic and pressure control, we believe that it has strong potential for further use in advanced, automated, microfluidic *C. elegans*-based assay platforms.

#2 A microfluidic device for studying signaling via diffusive secreted compounds between two specific *C. elegans* populations over prolonged durations.

In particular, we designed a microfluidic assay to investigate the biological process of male-induced demise, *i.e.* lifespan shortening and accelerated age-related phenotype alterations, in *C. elegans* hermaphrodites in the presence of a physically separated male population. For this purpose, male and hermaphrodite worm populations were confined in adjacent microchambers on the chip, whereas molecules secreted by males could be exchanged between both populations by periodically activating controlled fluidic transfer of μl -volume aliquots of male-conditioned medium. For male-conditioned hermaphrodites, we observe a reduction in mean lifespan of 4 days compared to non-conditioned on-chip culture. An enhanced muscle decline was also noticed, as expressed by a faster decrease of the thrashing frequency and the appearance of vacuolar-like structures indicative of accelerated aging. The chip was placed in an incubator at 20°C for accurate control of the lifespan assay conditions. An on-demand

bacteria feeding protocol was applied and worms were observed during long-term on-chip culture over the whole worm lifespan.

#3 Development of two reversible *C. elegans* immobilization methods for imaging applications.

The first immobilization method takes advantage of a biocompatible and temperature-responsive hydrogel-microbead matrix. Our gel-based immobilization technique does not require a specific chip design and enables fast and reversible immobilization, thereby allowing successive imaging of the same single worm or of small worm populations at all development stages for several days. We successfully demonstrated the applicability of this method in challenging worm imaging contexts, in particular by applying it for high-resolution confocal imaging of the mitochondrial morphology in worm body wall muscle cells and for the long-term quantification of number and size of specific protein aggregates in different *C. elegans* neurodegenerative disease models. Our approach can also be extended into the immobilization of other small organisms, such as the larvae of the fruit fly *Drosophila melanogaster* and the unicellular parasite *Trypanosoma brucei*. We anticipate that this versatile technique will significantly simplify biological assay-based longitudinal studies and long-term observation of small model organisms.

The second immobilization method takes advantage of the elastic properties of PDMS. We present two distinct microdevices, namely a micropillar array and a serpentine microchannel, for on-chip feeding and high-resolution imaging studies, respectively. Both devices consist of size-tunable PDMS structures that allow the same chips to be used for immobilization of worms at all development stages. Our microfluidic approach provides appropriate physiological conditions for long-term studies and enables worm recovery after the experiment. The performance of our devices is demonstrated by two different imaging experiments. The pillar array chip is used for *in vivo* live imaging of *C. elegans* embryo fertilization and early embryogenesis, whereas 3D cross-sectional image and bacterial colonization of a worm's intestine was observed by means of the stretchable microchannel device.

#4 A fully integrated microfluidic approach for the exploration of *C. elegans* early embryogenesis including the possibility of testing small-molecule inhibitors with increased throughput and versatility.

Our set up enables robust on-chip extraction of embryos from adult worms in a dedicated pillar array chamber by mechanical compression, followed by rapid fluidic transfer of embryos into an adjacent microtrap array. Here, up to 100 embryos can be immobilized in parallel for simultaneous high-resolution time-lapse imaging of embryonic development from the 1-cell stage to hatching. We demonstrate time-controlled and reversible drug delivery to on-chip immobilized embryos, which is of relevance for biochemical and pharmacological assays.

#5 A “Single Embryo Pipette” (SEP) for rapid and highly efficient dispensing of single *C. elegans* embryos, from an embryo suspension directly into standard microtiter plates.

Our microfluidic device takes advantage of pressure-tuned flexible embryo microtraps to easily capture and release single embryos on-demand. SEP fluidic manipulations do not have an adverse impact on embryo or worm physiology as indicated by the monitoring results of normal development of the embryos after dispensing.

Keywords :

Microfluidics, *Caenorhabditis elegans*, *C. elegans* early embryo, on-chip worm culture, worm sorting, reversible worm immobilization, biocommunication, male-induced demise, neurodegenerative disease, protein aggregation, drug studies, 3D imaging, long-term high-resolution imaging.

Zusammenfassung

Der Nematode *Caenorhabditis elegans* ist ein attraktiver Modellorganismus dank seines kurzen Lebenszyklus, der Zugänglichkeit für genetische Manipulationen, seiner optische Transparenz für einfache Beobachtung mit Mikroskopen und dem Nichtvorhandensein von ethischen Problemen. Mikrofluidische Technologien («Lab-on-a-chip») ermöglichten im letzten Jahrzehnt Experimente mit *C. elegans*, welche mit konventionellen Methoden nicht realisiert werden konnten. Diese Technologien vereinfachen die Handhabung der Nematoden und ermöglichen eine präzise Regelung der experimentellen Bedingungen sowie die kontrollierte Verabreichung von Reagenzien. In dieser Dissertation wird die Realisation von auf mikrofluidischen Technologien basierenden Mikrosystemen für die Manipulation von Nematoden sowie deren Anwendung für die Studie von biologisch relevanten Fragestellungen beschrieben. Wir haben folgende Systeme entwickelt:

#1 Ein mikrofluidisches System für die größenabhängige on-chip Sortierung von *C. elegans* Nematoden.

Die Elastizität des Materials Polydimethylsiloxane (PDMS) ermöglicht es, Kanäle zwischen zwei on-chip Kammern für Nematoden zu verformen. Der durch Druck gesteuerte, effektive Querschnitt dieser Kanäle resultiert in anpassbaren Filtrierstrukturen, um Nematoden verschiedener Größen voneinander zu trennen. Durch sorgfältige Optimierung des angelegten Drucks können Larven von spezifischen Stadien mit einer Effizienz von fast 100% und mit einem Durchsatz von 3.5 Nematoden pro Sekunde extrahiert werden. Unser Ansatz erlaubt auch die Erstellung von gemischten Populationen in angrenzenden Larvenstadien in einem definierbaren Verhältnis. Ebenfalls möglich ist die Trennung von Embryos und ausgewachsenen *C. elegans* für die darauffolgende Züchtung von alterssynchronisierten Nematodenpopulationen oder für Experimente an Embryos. Aufgrund der einfachen Geometrie unseres Sortierchips und der einfachen on-chip Steuerung der Flüsse und des Drucks glauben wir, dass diese Technologie ein großes Potenzial in komplexen, automatisierten on-chip *C. elegans* Experimenten hat.

#2 Ein mikrofluidisches System zum Studium von biochemischer Kommunikation zwischen zwei spezifischen *C. elegans* Populationen über längere Zeiträume.

Wir entwickelten einen mikrofluidischen Chip, um eine durch Nematodenmännchen herbeigeführte Lebensverkürzung und verfrühtes Altern in *C. elegans* Hermaphroditen zu zeigen. Bei diesen Experimenten werden Männchen und Hermaphroditen getrennt voneinander in nahe beieinanderliegenden Mikrokammern gehalten, zwischen welchen der Austausch von Medium gewährleistet ist. Medium aus der Kammer mit Männchen wurde periodisch in die Kammer mit Hermaphroditen injiziert und die Auswirkungen auf die Hermaphroditen untersucht. Wir beobachteten eine im Durchschnitt 4 Tage kürzere Lebensdauer bei den konditionierten Hermaphroditen im Vergleich zu nicht konditionierten Kulturen. Ebenfalls beobachtet wird ein verstärkter Muskelabbau, ausgedrückt durch eine Verlangsamung der Schlängelbewegung, und vakuolartige Strukturen, die beschleunigtes

Altern andeuten. Der Chip wurde in einem Inkubator bei 20°C gelagert, um gleichbleibende Bedingungen zu garantieren. Die Nematoden wurden während ihrer ganzen Lebensdauer beobachtet. Bei Bedarf wurden Bakterien als Futter gegeben.

#3 Zwei verschiedene temporäre *C. elegans* Immobilisierungsmethoden für bildgebende Anwendungen.

Die erste Methode zur Immobilisierung basiert auf einer biokompatiblen und temperatursensitiven Hydrogel-microbead Matrix. Die auf diesem Gel basierende Methode ermöglicht eine schnelle und reversible Immobilisierung, welche aufeinanderfolgende Abbildungen desselben Nematoden oder von kleinen Nematodenpopulationen in allen Lebensstadien über mehrere Tage ermöglicht. Diese Methode konnte in für Mikroskopie schwierigen Bedingungen, wie zum Beispiel hochauflösende Konfokalmikroskopie, angewendet werden. Wir bildeten damit die Morphologie der Mitochondrien in Muskelzellen der äußeren Nematodenwand sowie von Proteinaggregaten in verschiedenen *C. elegans* Mutanten ab. Dieser Ansatz kann auch für die Immobilisierung von anderen kleinen Organismen, wie zum Beispiel der Fruchtfliege *Drosophila melanogaster* und des einzelligen Parasiten *Trypanosoma brucei* angewendet werden. Wir erwarten, dass diese Methode biologische Langzeitbeobachtungen von kleinen Modellorganismen bedeutsam vereinfachen wird.

Die zweite Methode nutzt die elastischen Eigenschaften von PDMS. Wir entwickelten zwei verschiedene Chipstrukturen: Ein Array bestehend aus Mikrosäulen, das auch on-chip Wurmütterung erlaubt, und ein Chip mit einem schlangenförmigen Mikrokanal für hochauflösende Mikroskopieaufnahmen. Diese beiden Chips bestehen aus verformbaren PDMS Strukturen, welche für die Immobilisierung von Nematoden aller Lebensstadien genutzt werden können. Unsere on-chip Immobilisierungsmethoden fügen den Nematoden keine sichtbaren mechanische Schäden zu, stellen die für normales Wachstum benötigte Bedingungen her und erlauben eine Wiederverwendung der Nematoden nach dem Experiment.

Die Funktionsfähigkeit der Chips wird durch zwei verschiedene Experimente gezeigt. Der Chip mit den Mikrosäulen wird für *in vivo* Mikroskopie der Befruchtung von *C. elegans* Embryos und früher Embryogenese verwendet, während 3D Querschnittsaufnahmen und Beobachtungen der bakteriellen Kolonisierung des Darms der Nematoden im Chip mit dem dehnbaren Mikrokanal gemacht wurden.

#4 Ein integriertes Mikrosystem zur Erforschung der frühen *C. elegans* Embryogenese verbunden mit der Möglichkeit, niedermolekulare Inhibitoren mit erhöhtem Durchsatz zu testen.

Unser Mikrosystem ermöglicht die Extraktion von *C. elegans* Embryos durch Kompression von erwachsenen Nematoden, welche in einer Mikrokammer gefangen sind. Im Anschluss werden die Embryos in ein anliegendes Array transferiert. Bis zu 100 Embryos können in diesem Array gleichzeitig immobilisiert werden, um hochauflösende Zeitrafferaufnahmen der Embryogenese vom 1-Zell Stadium bis zum Ausschlüpfen durchzuführen. Wir zeigen auch die Möglichkeit für zeitgesteuerte on-chip Dosierung von aktiven Substanzen zu den immobilisierten Embryos, was relevant für biochemische und pharmakologische Experimente ist.

#5 Eine "Single Embryo Pipette" (SEP) für schnelle und hocheffektive Verteilung von einzelnen *C. elegans* Embryos aus einer Suspension direkt in standardisierte Mikrotiterplatten.

Unser mikrofluidisches Device nutzt druckgeregelter, flexibler Embryofänger, mit denen einzelne Embryos nach Bedarf eingefangen und freigesetzt werden können. Handhabung mit der SEP hat keinen negativen Einfluss auf die Embryos oder die Physiologie der Nematode, wie wir durch Beobachtung der Entwicklung der Embryos nach ihrer Verteilung feststellen konnten.

Stichwörter :

Mikrofluidik, *Caenorhabditis elegans*, *C. elegans* früher Embryo, On-Chip-Wurmkultur, Wurmsortierung, reversible Wurmimmobilisierung, Biokommunikation, männlich-induzierter Niedergang, neurodegenerative Erkrankung, Proteinaggregation, Arzneimittelstudien, 3D-Bildgebung, langfristige hochauflösende Bildgebung.

Contents

Acknowledgements	i
Abstract	iii
Zusammenfassung	vii
Contents	xi
List of Figures	xv
List of Tables	xvii
List of Equations	xix
Chapter 1 Introduction	1
1.1 <i>C. elegans</i> as an emerging model organism	1
1.2 The rise of microfluidic technologies.....	3
1.3 Microfluidic systems for <i>C. elegans</i> studies	4
1.4 Thesis objectives and outline	4
Chapter 2 Sorting of <i>C. elegans</i> nematodes and embryos on a microfluidic chip	7
2.1 Challenges and opportunities for <i>C. elegans</i> sorting	8
2.2 Microfluidic device design and operation	10
2.2.1 Overview of the microfluidic device.....	10
2.2.2 Principle of size-selective sorting.....	11
2.2.3 Evaluation of D_{pass} for different PDMS membrane thicknesses and mixing ratios	13
2.2.4 Device operation and sorting procedure	15
2.3 Worm sorting experiments	16
2.3.1 Larvae and adult worm sorting	16
2.3.2 Male and hermaphrodites worm sorting	20
2.3.3 Worm sorting purity and efficiency	21
2.3.4 Analysis of throughput of the sorting experiments.....	23
2.3.5 Embryo sorting	24
2.4 Materials and methods.....	25
2.4.1 Materials	25
2.4.2 Worm strains culture.....	26
2.4.3 Device fabrication	26
2.5 Conclusions.....	27
Chapter 3 Microfluidic biocommunication assay for studying male-induced demise in <i>C. elegans</i> hermaphrodites	29

3.1	Introduction.....	30
3.1.1	Molecular signaling in <i>C. elegans</i> populations.....	30
3.1.2	Challenges and opportunities for <i>C. elegans</i> controlled chemical stimuli sensing	31
3.2	Microfluidic device design and operation	33
3.2.1	Overview of the microfluidic device.....	33
3.2.2	Device operation	34
3.3	Male-conditioned <i>vs</i> non-conditioned on-chip assays	36
3.3.1	On-chip assays for studying male-induced phenotype alterations.....	36
3.3.2	Non-conditioned on-chip assays.....	37
3.3.3	Male-conditioned on-chip assays.....	41
3.4	Materials and methods.....	46
3.4.1	Materials	46
3.4.2	Worm strains culture and preparation	46
3.4.3	Device fabrication	47
3.5	Conclusions.....	47
Chapter 4	Reversible immobilization of <i>C. elegans</i> worms for high-resolution imaging	49
4.1	Challenges and opportunities for <i>C. elegans</i> immobilization.....	50
4.2	<i>C. elegans</i> immobilization using a hydrogel-microbead matrix.....	53
4.2.1	Gel-based immobilization protocol.....	53
4.2.2	Thermogelling of aqueous Pluronic solutions	54
4.2.3	Immobilization of <i>C. elegans</i> larvae	55
4.2.4	Adult worm immobilization using a gel-microbead matrix.....	55
4.2.5	Quantification of worm motility in different media.....	57
4.2.6	Worm recovery after immobilization.....	59
4.2.7	Study of <i>C. elegans</i> models of neurodegenerative disease with a hydrogel-microbeads technique.....	60
4.2.8	Immobilization of other small model organisms	63
4.2.9	Materials and methods	65
4.3	<i>C. elegans</i> immobilization using deformable microfluidics	66
4.3.1	Micropillar array device for embryo fertilization and embryogenesis studies.....	66
4.3.2	Stretchable channel device for linear alignment of <i>C. elegans</i> worms.....	69
4.3.3	Materials and methods	72
4.4	Conclusions.....	73
Chapter 5	On-chip drug studies during <i>C. elegans</i> early embryogenesis	75
5.1	Early <i>C. elegans</i> embryos as model system	76
5.2	<i>C. elegans</i> embryogenesis	76
5.2.1	The reproductive system of <i>C. elegans</i> hermaphrodites.....	76
5.2.2	The timeline of embryogenesis	77
5.2.3	The early stage <i>C. elegans</i> embryo.....	78

5.2.4	The role of actin and myosin II in cytokinesis.....	80
5.3	The challenges and opportunities for drug studies during <i>C. elegans</i> early embryogenesis	82
5.4	Microfluidic platform for early embryo trapping and drug delivery.....	85
5.4.1	Chip design for embryo extraction and trapping	85
5.4.2	Chip operation	86
5.5	<i>C. elegans</i> early embryos on-chip drug assays.....	88
5.5.1	Study of complete <i>C. elegans</i> embryogenesis on-chip	88
5.5.2	Study of drug treatment in <i>C. elegans</i> embryogenesis.....	89
5.5.3	Materials and methods	92
5.6	Conclusions.....	92
Chapter 6	Single embryo pipette for accurate <i>C. elegans</i> bioassays	95
6.1	Challenges and opportunities for <i>C. elegans</i> single embryo pipette	96
6.2	Microfluidic device design and operation	97
6.2.1	Overview of the microfluidic device.....	97
6.2.2	Device operation and sorting procedure	97
6.3	Materials and methods.....	100
6.3.1	Materials	100
6.3.2	Worm strains culture and embryo preparation.....	101
6.3.3	Device fabrication	101
6.4	Conclusions.....	101
Chapter 7	Conclusions.....	103
7.1	Main results achieved in this thesis	103
7.2	Future opportunities for microfluidics-based <i>C. elegans</i> studies	105
References	107
Curriculum Vitae		117

List of Figures

Figure 1.1 Development of the <i>C. elegans</i> nematode.	2
Figure 1.2 Historical timeline of <i>C. elegans</i> for drug discovery	3
Figure 1.3 Microfluidic <i>C. elegans</i> platforms.	6
Figure 2.1 COPAS Biosort platform overview.	8
Figure 2.2 Microfluidic technologies for <i>C. elegans</i> sorting studies.....	9
Figure 2.3 <i>C. elegans</i> sorting device.....	11
Figure 2.4 Operation of the sorting device.	12
Figure 2.5 Finite Element Method (FEM) simulations of the deflected PDMS filter valve membrane.	14
Figure 2.6 Worm sorting protocol.....	15
Figure 2.7 Images of size-selective on-chip sorting of L2 larvae from a mixed population of worms.18	
Figure 2.8 Images of sorting of worms having adjacent development stages.....	19
Figure 2.9 Sorting of adult males from same-aged hermaphrodites.	20
Figure 2.10 Worm counting before and after sorting.....	22
Figure 2.11 Time-dependent throughput during the lapse of a sorting experiment, in particular for L2 & L3 and L4 & adult sorting (2 experiments for each case).	23
Figure 2.12 Embryo and adult count before and after sorting.....	25
Figure 3.1 Microfluidic technologies for <i>C. elegans</i> controlled chemical stimuli sensing.	32
Figure 3.2 Microfluidic worm biocommunication device.....	34
Figure 3.3 On-chip worm handling.....	36
Figure 3.4 On-chip assays for studying male-induced phenotype alterations in <i>C. elegans</i> hermaphrodites.....	37
Figure 3.5 Early development of WT <i>C. elegans</i> hermaphrodites.....	38
Figure 3.6 Validation of <i>C. elegans</i> hermaphrodite on-chip culture over the whole lifespan.....	39
Figure 3.7 Survival rate and behavioral study for WT <i>C. elegans</i> hermaphrodites cultured on-chip.43	
Figure 3.8 WT hermaphrodites with male-induced demise.	45
Figure 3.9 Hallmarks for male-induced demise.	46
Figure 4.1 Microfluidic devices as tools for <i>C. elegans</i> immobilization and imaging.	51
Figure 4.2 Pluronic (PF127) as a tool for <i>C. elegans</i> immobilization and imaging.	52
Figure 4.3 <i>C. elegans</i> immobilization protocol using a hydrogel-microbead matrix.	54
Figure 4.4 Characterization of different Pluronic (PF127) solutions.	55

Figure 4.5 The mechanism of <i>C. elegans</i> worm immobilization in the hydrogel-microbead matrix.	56
Figure 4.6 Evaluation of <i>C. elegans</i> immobilization and recovery for different conditions.	58
Figure 4.7 High-resolution confocal imaging of mitochondrial morphology in <i>C. elegans</i>	61
Figure 4.8 Longitudinal analysis of mitochondrial morphology in the body wall muscle cells of <i>C. elegans</i> worms under different RNAi conditions.	62
Figure 4.9 Protein aggregate morphology and progression in different <i>C. elegans</i> neurodegenerative disease models.	64
Figure 4.10 Gel-based immobilization of other small organisms.	65
Figure 4.11 Micropillar array device for <i>C. elegans</i> immobilization.....	67
Figure 4.12 Live imaging (bright field) of a <i>C. elegans</i> wild-type worm immobilized on the pillar array chip over long periods.	68
Figure 4.13 <i>In vivo</i> observation of early embryo development on the pillar array chip.	68
Figure 4.14 PDMS device with stretchable channel sections for immobilization and linear alignment of <i>C. elegans</i> worms.....	69
Figure 4.15 visOCM 3D imaging of an adult <i>C. elegans</i> worm.....	71
Figure 4.16 High-resolution <i>in vivo</i> imaging of bacterial colonization of the intestine of an aligned adult <i>C. elegans</i> worm.....	72
Figure 5.1 The <i>C. elegans</i> hermaphrodite reproductive system.	77
Figure 5.2 Timeline of <i>C. elegans</i> embryogenesis.....	78
Figure 5.3 Embryogenesis of the early <i>C. elegans</i> embryo.....	79
Figure 5.4 <i>C. elegans</i> 1-cell embryo stage.....	80
Figure 5.5 Generation of the contractile ring during cytokinesis.	81
Figure 5.6. Actin-binding small-molecule drugs.	82
Figure 5.7 Conventional <i>C. elegans</i> embryo slide preparation.	84
Figure 5.8 A microdevice for immobilization of permeable embryos, imaging and small-molecule drug application.....	84
Figure 5.9 Microfluidic embryo harvesting and drug delivery chip.....	86
Figure 5.10 Fluidic operations and embryo handling.	87
Figure 5.11 Study of complete <i>C. elegans</i> embryogenesis on-chip.....	89
Figure 5.12 Early embryogenesis and on-chip drug treatment.	91
Figure 6.1 Microdevices for capturing and monitoring single worms.....	96
Figure 6.2 Microfluidic “Single Embryo Pipette” (SEP).....	97
Figure 6.3 Single Embryo Pipette operation.	98
Figure 6.4 Microfluidic “Single Embryo Pipette” (SEP) characterization.	99
Figure 6.5 Live imaging of single embryo dispensing.	100
Figure 6.6 Embryogenesis of an embryo after dispensing with the SEP.	100

List of Tables

Table 2.1 Relevant parameters of the sorting device.	13
Table 2.2 Material constants of the Mooney-Rivlin model.	14
Table 2.3 Possible worm sorting experiments.	17
Table 2.4 Separation purity and efficiency.	21
Table 3.1 Male-conditioned and non-conditioned on-chip assays.	43
Table 5.1 Embryo transfer and trapping rate.	88
Table 5.2 Hatching rate for on-chip embryogenesis assays.	88

List of Equations

Equation 2.1 Diameter of the biggest worm that can pass the filter.	11
Equation 2.2 The strain energy density in the Mooney-Rivlin model.	13
Equation 3.1 Semi-empirical Wilke–Chang equation.....	41

Chapter 1 Introduction

1.1 *C. elegans* as an emerging model organism

Approximately 40% of the about 20,000 *Caenorhabditis elegans* (*C. elegans*) protein coding genes are functional orthologues of their human counterparts. This is only one of the reasons why, over the last decades, *C. elegans* has become one of the most popular model organisms to understand, among others, human disease and aging [1-4]. The nematode shares many conserved systemic, molecular and genetic mechanisms with humans [5-7]. Furthermore, each hermaphrodite has only 302 neurons of which the physical connections have been fully mapped out [1, 2, 8, 9]. *C. elegans* is therefore widely used for genetic studies, developmental biology, molecular biology, neurobiology, biochemistry and human disease research [10-12].

In addition to merely biological reasons, more practical features make *C. elegans* a powerful tool for these studies. First, *C. elegans* is usually simply cultured at or close to room temperature on agar plates or in liquid medium with *Escherichia coli* strains OP50 or HT115 as food source [13]. As culture conditions are quite robust, it is easy to maintain *C. elegans* populations in any, also non-biological, laboratories. Second, even adult *C. elegans* worms are of small size (length ~1 mm, diameter ~60 μm) and have a transparent body. Various imaging techniques may be readily applied to study the animal's anatomy, inner organs, nervous systems etc., including high-resolution transmission bright-field microscopy and fluorescent imaging. Most biological assays can be directly carried out on the agar plate or in liquid medium on-chip. Third, it has a relatively short development time from embryo stage to adulthood. The life cycle of *C. elegans* is temperature-dependent and it lives happily between 16°C and 24°C. At 16°C, the animal develops from egg throughout four larval stages to a fertile animal in ~6 days, while at 24°C this takes merely ~3 days (Fig. 1.1). The brood size of a wild-type (WT) *C. elegans* hermaphrodite is ~300 embryos. Each development stage, in particular the four larval stages (L1-L4), can be clearly distinguished by the worms' body size and specific morphological features. *C. elegans* presents several advantages in elucidating genetic pathways controlling important cellular processes such as development [4], cell death [14], aging [15] and RNA-mediated interference of gene expression (RNAi) [16] among others. In the past decades, it has been extensively used to model complex human diseases including Alzheimer's disease [17], Parkinson's disease [18] diabetes [19], and cancer [20]. Low culture costs and very large populations make *C. elegans* potentially useful in high-throughput screens for drug development and discovery. The review of O'Reilly *et al.* showed a historical timeline of the major milestones of *C. elegans*-based drug screening format (Fig. 1.2) [21]. Different classes of active compounds have been already investigated in *C. elegans*, as reviewed in [22]. The fundamental problem in the drug studies related to aging is to identify what molecular intake in the worm leads to an extended lifespan. Due to its short lifespan, *C. elegans* is particularly suitable for studying aging and identifying longevity compounds. Furthermore, *C. elegans* has already played an important role in elucidating molecular aspects

of anthelmintic resistance and identifying anthelmintic compounds due to its closely evolutionary tie with parasites [23]. Moreover, in their natural habitat, *C. elegans* is continuously exposed to bacteria and fungi, which can be either just a food source or even human disease-causing pathogens. Therefore, *C. elegans* is a convenient organism model in which to identify or assay anti-infective compounds in a high-throughput fashion [24]. Besides, since the neuronal connectivity in *C. elegans* has already been established, *C. elegans* is also advantageous in modeling neurodegenerative diseases such as Alzheimer's disease (AD), Parkinson's and Huntington's disease, and in discovery of compounds that treat these neurodegenerative diseases [25, 26].

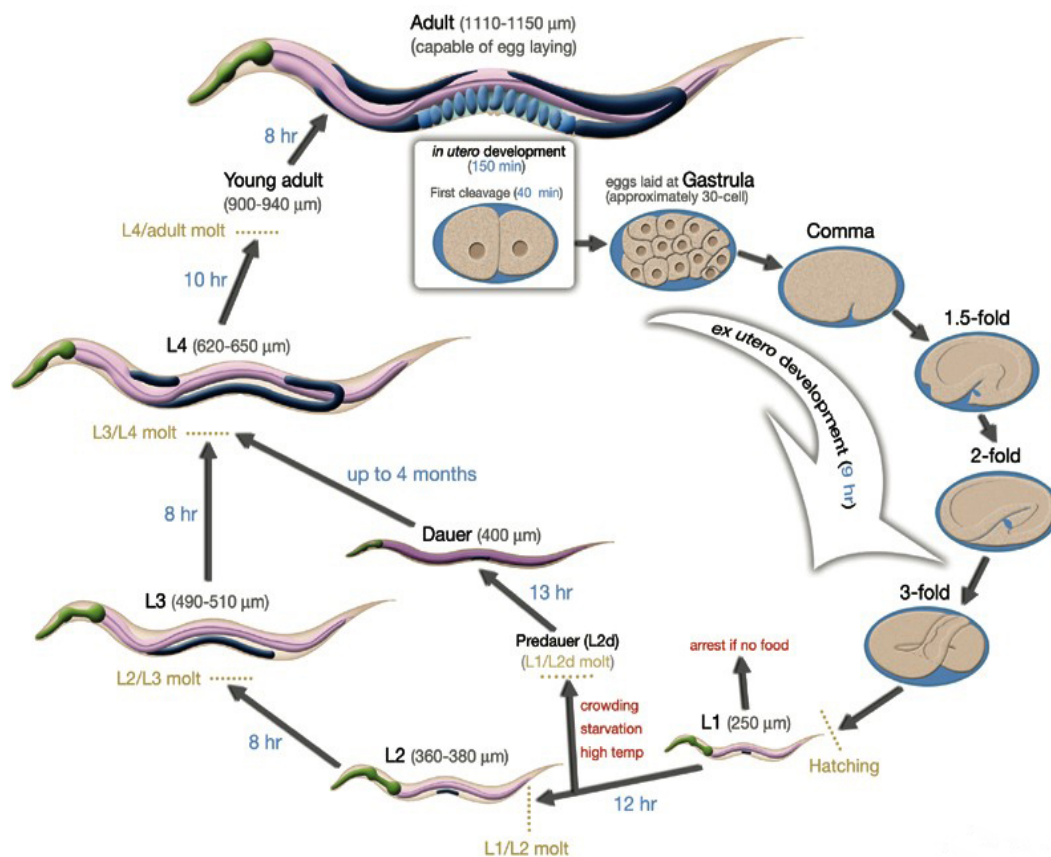


Figure 1.1 Development of the *C. elegans* nematode.

Developmental timing starts at fertilization ($t = 0$ min). The development time at each stage is marked in blue. This image is modified from WormAtlas (<http://www.wormatlas.org>).

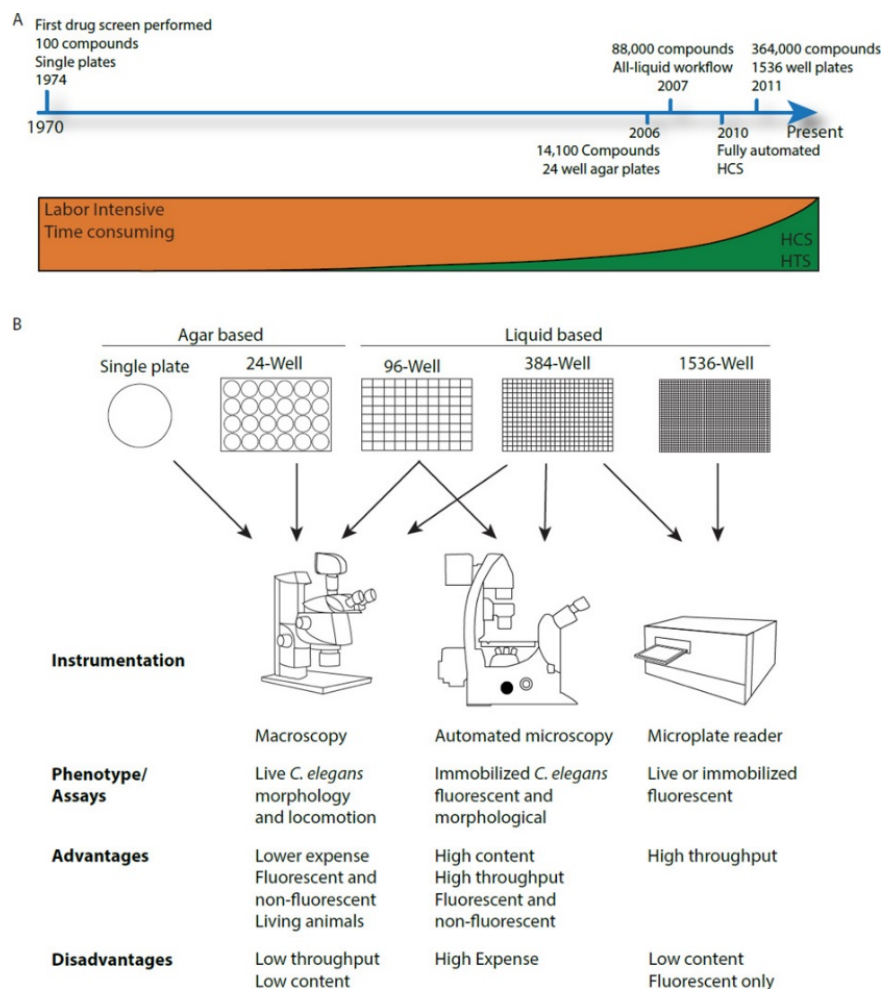


Figure 1.2 Historical timeline of *C. elegans* for drug discovery

(A) Timeline shows major milestones of *C. elegans*-based drug discovery. **(B)** Common instruments currently used for phenotypic assessment of *C. elegans*. (reproduced from [21]).

1.2 The rise of microfluidic technologies

The concept of microfluidics, or the so-called lab-on-a-chip (LOC) field, introduced by Manz *et al.* in the early 1990s [27], has emerged as a distinct new technology. Microfluidic devices can be used to flexibly manipulate the flow of microvolume fluids in microchannels and allow the implementation of complete (bio-)chemical processes, including sample collection, preparation, processing and analysis, in an easy and flexible way. The length scale of microfluidic components are between tens to hundreds of micrometers, *i.e.* the same scale as many biological models or materials such as cells and small organs. These device features allow reducing the compound consumption, in particular of expensive reagents or biochemical compounds, and fluidic manipulation with greater precision, resulting in fast analysis, better process control, massive parallelization, and eventually lower cost and safer platform operation.

Due to the trend of miniaturization and integration of modern scientific and technological development, microfluidic technology has been widely concerned and valued by the international scientific and industrial communities during the last two decades. The LOC field

has been developing rapidly and branched into many different areas, such as biological and chemical analysis, point-of-care testing, clinical and forensic analysis, molecular and medical diagnostics, and certain types of LOC devices have already been commercialized. As a general tool for biology, microfluidics offers numerous benefits to the biology community. Microfluidic devices allow control of chemical and physical properties of *in vivo*-like cellular microenvironments of individual cells, which facilitate the accurate study of cellular behavior *in vitro*. Driven by the rising demand for the point-of-care (POC) market, as well as by the promise of wearable devices, microfluidics technology is progressing steadily, and in turn is promoting the growth of this market, and is more and more thought to revolutionize today's medicine.

1.3 Microfluidic systems for *C. elegans* studies

Microfluidic chip-based assays recently emerged as a new and versatile technology for studies on *C. elegans* [28-53]. Microfluidic approaches allow accurate worm manipulation and advanced handling protocols, for instance for assaying worm populations in specific microchambers, or immobilization of single worms for high-resolution microscopic imaging without using anesthetics. As an example, Chokshi *et al.* developed a device where a worm was pushed and fixed for imaging at the side a microfluidic channel by deformation of a flexible polydimethylsiloxane (PDMS) membrane [28]. Behavioral studies and recording of neuronal activity under stimuli, like exposure to chemical compounds, light and temperature [35, 40, 48], as well as laser ablation [41] and nerve regeneration studies [42, 47] have been performed on-chip. Additionally, high-throughput imaging, phenotyping and screening have been successfully performed by using microfluidics technology [42-46]. More specific microfluidic approaches and on-chips assays reported in literature will be discussed in the corresponding chapters of this thesis.

1.4 Thesis objectives and outline

The goal of this thesis is to develop innovative microfluidic systems for manipulation and biological studies of *C. elegans* to overcome drawbacks of the major conventional methods and eventual existing microfluidic devices.

The thesis encompasses five major topics (see also Fig. 1.3), which are discussed in Chapter 2 to 6: (i) worm sorting, (ii) worm biocommunication, (iii) worm immobilization, (iv) drug studies on early embryos and (v) Single embryo dispensing. In addition to the presentation of own work and results, each chapter comprises an introduction, a state-of-the-art section, and a conclusion of the specific topic. An overall conclusion and an outlook of the research area will be provided in the final chapter (Chapter 7).

In particular the following work will be discussed in this thesis:

Worm sorting (Chapter 2)

I introduce a new and simple microfluidic sorting device based on adjustable filter structures that can be easily tuned by external pressure for a specific size-dependent *C. elegans* worm sorting experiment. A single device can be used for selecting and sorting of all worm stages and single-sex populations on a microfluidic chip, in particular for sorting male and age-matched hermaphrodite *C. elegans* worms.

Worm biocommunication studies (Chapter 3)

I propose a microfluidic system for studying signaling between specific *C. elegans* populations based on secreted diffusive compounds over prolonged durations. In particular, we designed a microfluidic assay to evaluate the problem of male-induced decrepitude, including lifespan shortening and accelerated age-related phenotype alterations in *C. elegans* hermaphrodites in the presence of a physically separated *C. elegans* male population on-chip.

Worm immobilization (Chapter 4)

I introduce two different approaches for reversible immobilization of *C. elegans* nematodes:

(i) A new, simple and versatile method for immobilization of *C. elegans* nematodes, based on a biocompatible and temperature-responsive hydrogel-microbead matrix. This immobilization technique allows the recovery of worms after immobilization, for repeated imaging of the same worm for several days, a feature that presents a significant advantage with respect to conventional immobilization methods.

(ii) Microfluidic approaches, taking advantage of the elastic properties of PDMS, and optimized for different applications. Thanks to size-tunable PDMS structures, both chips can be used for immobilization of worms or larvae at all development stages. Our microfluidic devices provide appropriate on-chip physiological conditions for long-term studies and enable on-chip high-resolution imaging of *in vivo* biological processes. Moreover, we present two applications that are performed on-chip for the first time, *i.e.* *in vivo* live imaging of early embryogenesis and of bacterial colonization of a worm's intestine, respectively.

Drug studies during embryogenesis (Chapter 5)

I report the first fully integrated microfluidic approach for *C. elegans* early embryogenesis studies with unprecedented accuracy and throughput. The device enables on-chip embryo extraction from the uterus of gravid nematodes followed by fast and reliable on-chip immobilization of fragile permeable embryos in a microtrap array. Up to 100 embryos can be immobilized in parallel for on-chip high-resolution live imaging of very early events in embryogenesis, starting from the 1-cell embryo. We also demonstrated well-controlled compound application for versatile microfluidic pharmacological assays on early embryos.

Single embryo dispensing (Chapter 6)

We propose an “*Single Embryo Pipette*” (SEP) that is specifically designed for dispensing single *C. elegans* embryos into standard well plates. Our microfluidic device takes advantage of flexible embryo traps which can easily capture or release single embryos on-demand by mean of tuning the loading pressure. In particular, we evaluate the physiological impact of SEP fluidic manipulations by monitoring the development of the embryos after dispensing with SEP.

Conclusions of this thesis (chapter 7)

The last chapter provides the reader with an overview of the presented results and an outlook on future opportunities in the field.

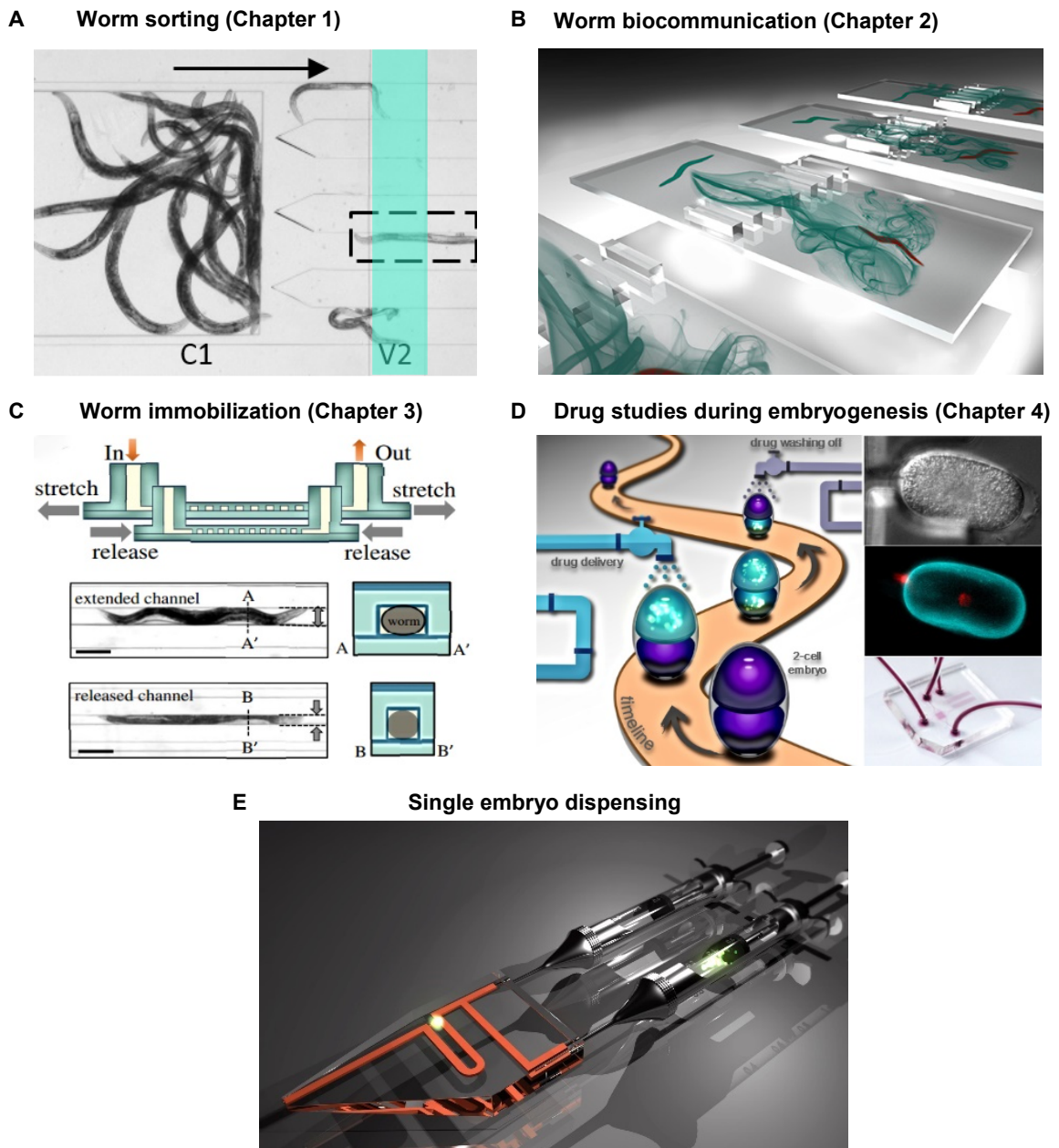


Figure 1.3 Microfluidic *C. elegans* platforms.

Artistic illustrations of the different microfluidic *C. elegans* platforms developed in the frame of this thesis.

Chapter 2 Sorting of *C. elegans* nematodes and embryos on a microfluidic chip

The *C. elegans* life cycle consists of an embryo stage, four larval stages that can be clearly distinguished in size and by different morphological features, and adulthood. Many worm-based bio-assays require stage- or age-synchronized worm populations, for example for studying life cycle and aging of worms under different pharmacological conditions, or to avoid misinterpretation of results due to overlap of stage-specific response in general. Here, we present a new microfluidic approach for size-dependent sorting of *C. elegans* nematodes on-chip. We take advantage of the external pressure-deformable profile of polydimethylsiloxane (PDMS) transfer channels that connect two on-chip worm chambers. The pressure-controlled effective cross-section of these channels creates adjustable filter structures that can be easily tuned for a specific worm sorting experiment, without changing the design parameters of the device itself. By optimizing the control pressure settings, we can extract larvae of a specific development stage from a mixed worm culture with an efficiency close to 100% and with a throughput of up to 3.5 worms per second. Our approach also allows generating mixed populations of larvae of adjacent stages, or to adjust the ratio of these directly in the microfluidic chamber. Moreover, using the same device, we demonstrated extraction of embryos from adult worm populations for subsequent culture of accurately age-synchronized nematode populations or embryo-based assays. Further study and protocol optimization showed that our device is also able to generate single-sex populations, in particular by sorting male and age-matched hermaphrodite *C. elegans* worms. Considering that our sorting device is merely based on geometrical parameters and operated by simple fluidic and pressure control, we believe that it has strong potential for use in advanced, automated, microfluidic *C. elegans*-based assay platforms.

This chapter is an adapted version of the following publications:

L. Dong, M. Cornaglia, T. Lehnert, M. Gijs, “Versatile size-dependent sorting of *C. elegans* nematodes and embryos using a tunable microfluidic filter structure,” *Lab on a Chip* 2016 (3), 574-585.

L. Dong, M. Cornaglia, T. Lehnert, M. Gijs, “Size-dependent Sorting of *C. elegans* Nematodes through An Adjustable Microfluidic Filter Structure,” *The 20th International Conference on Miniaturized Systems for Chemistry and Life Sciences (MicroTAS 2016)*, 2016, Dublin, Ireland.

Contributions: L. D. designed, built, and tested the microfluidic control instrument and conceived the application to the sorting experiments with input from M. C., M. G. and T. L. supervised the research, and provided reagents and funding. All authors reviewed and edited the manuscript.

2.1 Challenges and opportunities for *C. elegans* sorting

C. elegans has been at the forefront of aging research since the first long-living mutant was discovered over 25 years ago [54, 55]. Studies of aging in *C. elegans* focus on the identification of factors that influence lifespan and the analysis of the underlying mechanisms responsible for longevity. Such longitudinal studies are performed best by using stage- and/or age-synchronized cohorts of animals. Likewise, in many other worm assays, synchronized worm populations are also advantageous in view of better targeting specific experiments and reducing the variability of results. For the time being, synchronization still frequently relies on the manual selection of a large number of *C. elegans* larvae [56]. Two classical methods, which are both based on the time synchronization of embryos, are mainly used: (i) exploiting a timed embryo lay or (ii) bleaching of gravid worms to isolate embryos. For synchronization via timed embryo lay, adult worms are allowed to lay embryos for a defined period of time, typically 2–6 h. Subsequently, after a sufficient number of embryos has been produced, all adult worms are removed from the plate [13]. Bleaching dissolves the worm body and liberates the embryos from the adult worm in the medium. However, these methods are time-consuming, labor-intensive and may affect the worm's physiology. On the other hand, automated sorting systems, such as the fluorescence-activated *COPAS Biosort* platform (Fig. 2.1), provide high-throughput and, for instance, enable the isolation of mutants with altered fluorescent protein expression [57]. However, such equipments are expensive and may not be accessible to many labs.

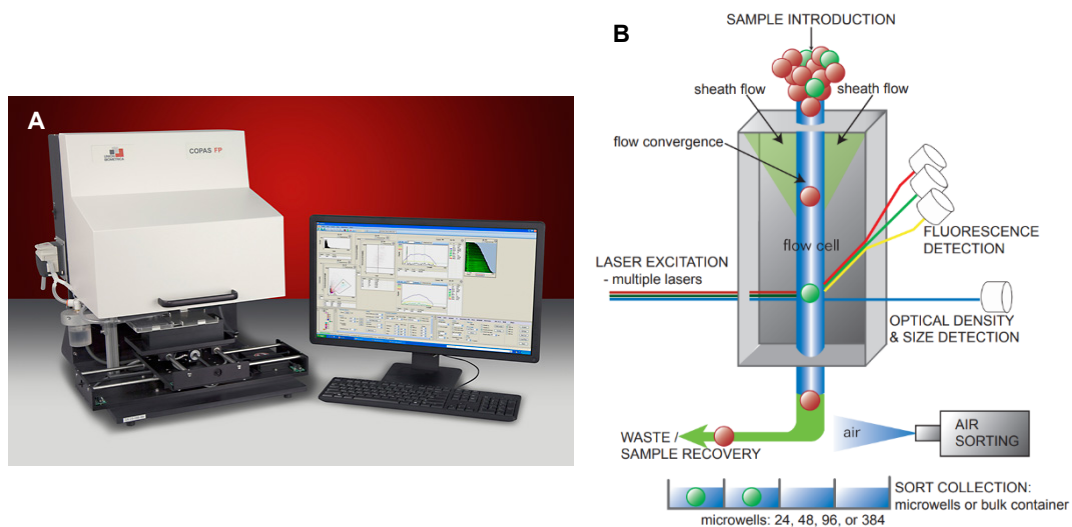


Figure 2.1 *COPAS Biosort* platform overview.

(A) *COPAS Biosort* platform. **(B)** The principle of the *Biosort* system. This image is modified from BIOMETRICA (<http://www.unionbio.com/copas/>).

Several chip-based devices have been developed recently that allow sorting, *i.e.* the extraction of a desired sub-group from a mixed larvae/adult worm population, based on size and/or behavioral differences. For example, one used electrotaxis as driving force, *i.e.* the tendency of nematodes to migrate towards the negative pole of an electric field, often combined with worm behavior in maze arrays, to direct the motion of the animals [58–63]. By collecting animals at a predetermined location, one can achieve motility-based separation as a

function of their arrival time. Solvas *et al.* used a smart microfluidic maze array to passively isolate adult worms from larvae on the basis of size and age [58]. Rezai *et al.* spatially separated different stages of *C. elegans* in two microchambers connected by a constricted electric trap region (Fig. 2.2A) [59]. Han *et al.* proposed micro-bumps arrayed channels which allow size separation due to the restriction of the undulating motion of the worms passing through [60]. While electro-taxis is now a well-known technique of guiding the worm through fluidic microstructures [59, 61], its electro-sensory navigation is still not well understood and it is also known that long time exposure to electric fields may adversely impact the animals' motility, which limits the accuracy of sorting [59, 61]. For the time being, it is not clear to which extent the electric field experienced by the worms has an impact on subsequent bio-assays. Besides, this method suffers from a relatively low throughput and is limited to strains that exhibit electro-taxis [60]. In contrast, Ai *et al.* developed a simple sorting device based on differences in animal size and morphology (Fig. 2.2B) [64]. The device consisted of an array of geometrically optimized pillars that acted as a filter, allowing worms of specific sizes to move through more rapidly. This technique is simple, accurate and allows high-throughput sorting of worms of different sizes. The drawback of all these devices is that they feature filtering structures with fixed geometrical dimensions. As a consequence, for successful sorting or size separation of different worm populations, such as larvae stages, male/hermaphrodite worms or different mutants, the device design and several parameters have to be adapted for each specific experiment. This obviously limits the versatility of the device. Clogging by the debris or *E. coli* clusters may also occur easily, especially when using small filters sizes for young larvae. This issue impedes the continuous and long-term operation of the device.

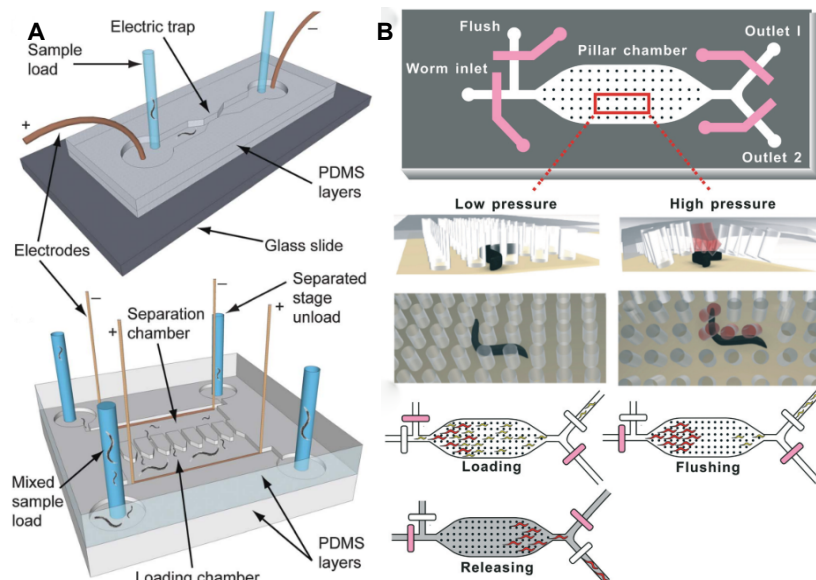


Figure 2.2 Microfluidic technologies for *C. elegans* sorting studies.

(A) Microfluidic devices for worm electro-tactic sorting. The electric field in a channel containing electric traps can cause worms of a specific age to pass through the trap while preventing others (*reproduced from* [59]). **(B)** Another type of device consists of an array of geometrically optimized pillars that act as a sieve to allow worms of specific sizes to rapidly move through (*reproduced from* [64]).

2.2 Microfluidic device design and operation

2.2.1 Overview of the microfluidic device

The layout of our worm sorting device is shown in Fig. 2.3A. The device is built from a two-layer PDMS structure allowing fluidic control (red in Fig. 2.3A) and valve pressure control (green in Fig. 2.3A). Fluidic and control layer are separated by a deformable PDMS membrane. Two worm chambers C1 and C2 (length 5.8 mm, width 1.4 mm, height 150 μm) are connected by four parallel channels (length 2.4 mm, width 200 μm , height 50 μm). The chambers are large enough to accommodate hundreds of *C. elegans* worms. Worm populations are initially loaded into C1 through the fluidic inlet (In), whereas sorted populations may be extracted from the device through a fluidic outlet (Out). Size-selective sorting takes place during the transfer of the worm population from C1 to C2. For this purpose, the effective cross-section and shape of the four transfer channels is adjusted by means of a pneumatic control chamber (width 400 μm , height 60 μm) that is positioned perpendicular and on top of the fluidic transfer channels. It functions as an adjustable valve (V2 in Fig. 2.3A) that compresses all four fluidic channels simultaneously in a well-controlled way. A second valve (V4) has been introduced as a backup of V2. Similar valves are positioned at the inlet and outlet of the chip (V1 and V3, respectively). In contrast to V2 (or V4), V1 and V3 are mainly operated in an open/(nearly)closed state in order to confine worm populations in the chambers for imaging and counting. Schematic cross-sectional views of the parallel arrangement of the four microfluidic channels with valve V2 (along the line A-A') and of chamber C2 (along the line B-B') are also shown in Fig. 2.3A.

A photograph of the whole PDMS chip (76 mm \times 52 mm) with 8 independent sorting units is shown in the upper part of Fig. 2.3B. The middle part of this figure is a zoom showing a single sorting unit, in which the fluidic layer is emphasized by using a red dye solution and the valve pressure control chambers are filled with a green dye solution, respectively. Tuning of the cross-section of a single transfer channel by modifying the valve control pressure is demonstrated in three photographs in the lower part of Fig. 2.3B. The situations (i) to (iii) illustrate how the fluidic path (as revealed by the red color) is progressively obstructed by increasing the valve control pressure values from 0 bar, 0.7 bar to 1.9 bar, respectively. At 0 bar, the transfer channel is fully open. For higher control pressures, the PDMS membrane blocks the central section of the transfer channel, leaving open narrow fluidic paths on each sidewall. Size-filtering of worm populations is achieved by accurately adjusting the cross-section of these residual paths.

Deflection of the PDMS membrane as a function of valve control chamber pressure was quantified by optical image analysis of pictures like the ones shown in the lower part of Fig. 2.3B (i,ii,iii). A series of top-view pictures of a red dye-filled transfer channel situated at valve V2, obtained using increasing pressure values from 0 bar to 1.9 bar to the valve control chamber, was first converted to 8-bit grey pictures. The membrane deformation profiles shown in Fig. 2.3C, *i.e.* the opening sections of the fluidic channel, were obtained by analyzing the grey level values along the cross-section line C-C' in the lower part of Fig. 2.3B. As observed in Fig. 2.3C, the width of the two fluidic paths on each side of the transfer channel can be reliably adjusted as a function of control pressure. This feature is used in our device to realize adjustable filters for size-dependent worm sorting.

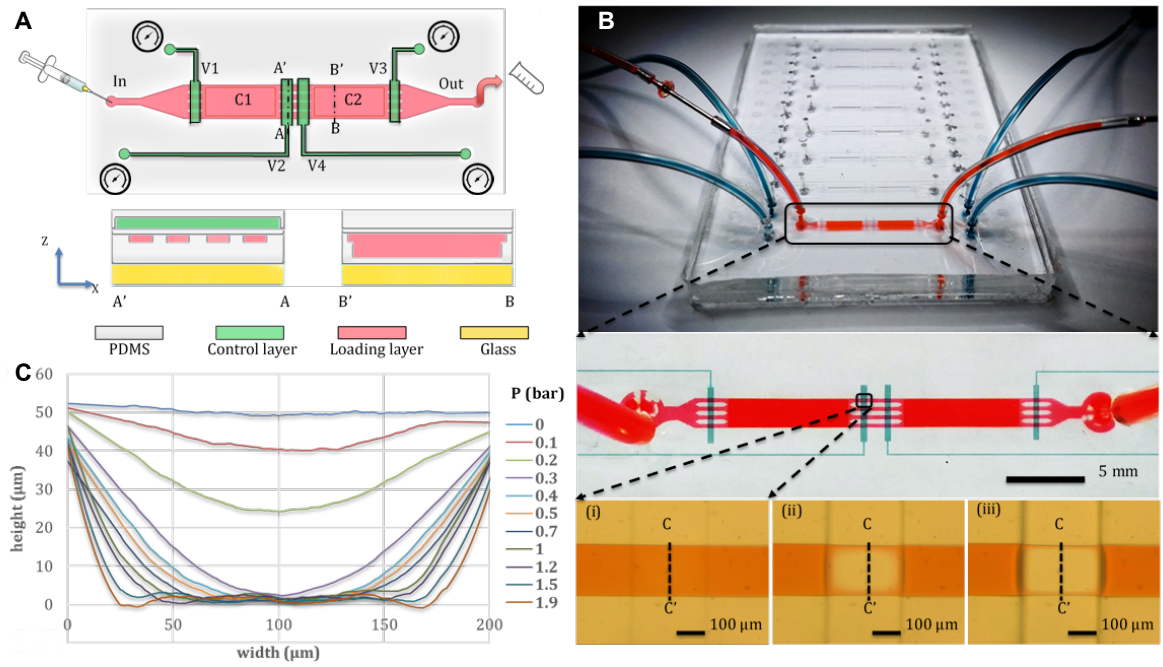


Figure 2.3 *C. elegans* sorting device.

(A) Schematic view of the worm sorting device (not to scale). The device is built from two PDMS layers, one for fluidic control (red) and one for valve pressure control (green), respectively. It comprises a single fluidic inlet (In), two worm chambers (C1, C2), one fluidic outlet (Out) and four valves used either as open/close valves (V1, V3) or as adjustable valves (V2, V4) for size-selective worm filtering. Mixed populations of worms are first loaded into C1. Subsequently, the desired portion of this population is transferred to C2 by adjusting the opening section of the transfer channels of V2 (V4 is not used here). Cross-sectional views of the four transfer channels of the valve V2 (along the line A-A') and of the chamber C2 (along the line B-B') are also shown. **(B)** Device photograph of the full chip with 8 individual worm selection units (one with tubes connected). The middle part shows the arrangement of fluidic and pressure control channels (filled with red and green dye solutions, respectively). The bottom pictures (i,ii,iii) illustrate the different states of a single transfer channel when using a valve control chamber pressure of 0, 0.7, and 1.9 bar, respectively. These images show how the fluidic path (red) is squeezed when pressure in the control channel is increased. **(C)** Deflection of the PDMS membrane (cross-section along the line C-C' in the picture of the lower part of Fig. 2.3B), defining the effective opening of the fluidic channel, as a function of control pressure measured by optical image analysis.

2.2.2 Principle of size-selective sorting

The principle of size-dependent filtering in our device relies on the effective opening of the fluidic transfer channels which is adjusted by pressure control. Fig. 2.4A depicts schematically the cross-sectional view of one partially closed transfer channel due to the deflected PDMS membrane of valve V2. Assuming a circular cross-section of the nematode (diameter D_{worm}), we can set a threshold for passing or blocking worms of a certain size or age, respectively. The geometrical limit for passing the filter corresponds to the maximum diameter of a circle that can be inscribed in the residual fluidic opening path. In Fig. 2.4B, the red curve schematically represents the deflected membrane and the blue circle with radius $O'C$ (center O') is the largest circle that fits in the opening. Here, $C(x,z)$ is the point on the curve that has the minimum distance OC from the point of origin O . The diameter D_{pass} of the biggest worm which can still pass the filter can be determined as

$$D_{\text{pass}} = 2O'C = 2 \frac{OC}{1 + \sqrt{2}}$$

Equation 2.1 Diameter of the biggest worm that can pass the filter.

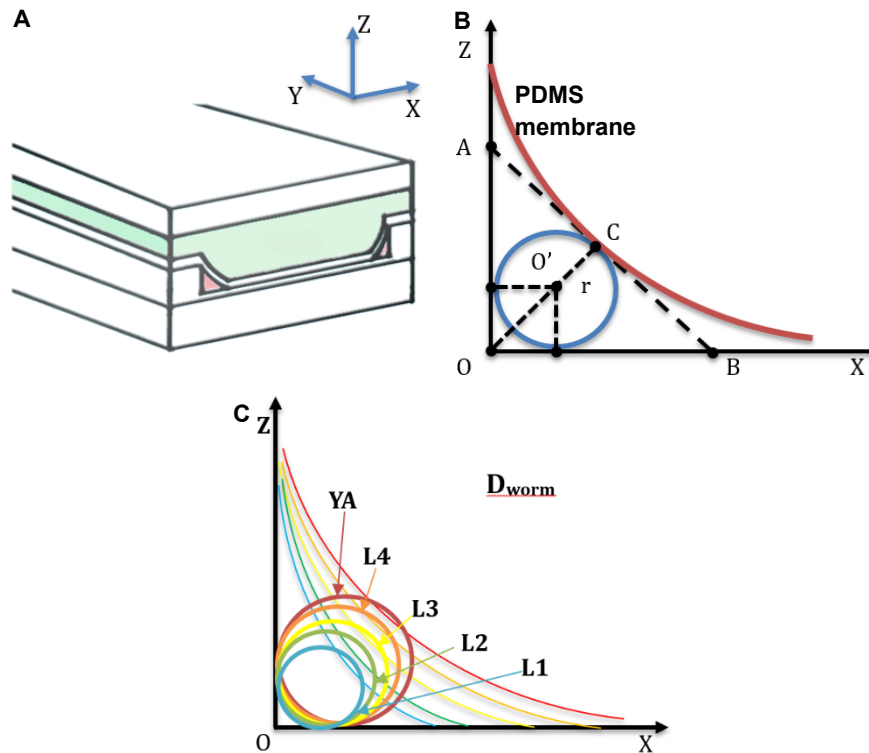


Figure 2.4 Operation of the sorting device.

(A) Schematic view of a single partially closed transfer channel due to the deflected PDMS membrane of valve V2. The pressure applied to the control channel (green) determines the opening section in the fluidic path (red). The compression is symmetric, leaving fluidic path openings on either edge of the channel. (B) Geometrical consideration of the fluidic filter defined by the deflected PDMS membrane (red line). The diameter of the biggest worm which can pass through the filter is given by $D_{pass}=2O'C$, corresponding to the maximum diameter of a circle (center O') that can be inscribed in the open fluidic path. (C) Graph explaining the mechanism of selective size filtering. Circles (diameter D_{worm}) indicate the worm stage (larvae L1 to L4, or YA) that is just blocked by the filter position. The corresponding deflection of the PDMS valve membrane for different applied pressure values is schematically shown (P_0 to P_4 , as reported in Table 2.1).

For size-dependent filtering, smaller worms ($D_{worm} \leq D_{pass}$) are transferred from chamber C1 to chamber C2, while bigger animals ($D_{worm} > D_{pass}$) are blocked by the membrane and retained in C1. This principle is explained in Fig. 2.4C. Different membrane deflections that would just block worms of a specific stage (or larger), the worm diameter represented by corresponding circles, are schematically drawn. Based on this model, we estimated practical values for D_{pass} for the experimentally derived membrane deflection curves that were already shown in Fig. 2.3C. For this purpose, the experimental curves are expressed in (x,z) coordinates and the point $C(x,z)$ can readily be found by minimizing the distance $(x^2+z^2)^{0.5}$ from the origin. Using eqn (2.1), we determine D_{pass} for different membrane deflections, *i.e.* as a function of the applied pressure and compare these values to the diameter D_{worm} of different larvae stages (L1 to L4) and young adult (YA) worms. The relationship between D_{pass} and pressure P applied to the membrane was simulated by the Finite Element Method (FEM, Comsol) for different PDMS membrane thicknesses and PDMS mixing ratios. Results are shown in section 2.2.3 and Fig. 2.5. Values for D_{worm} , D_{pass} and the pressure values (P_0 - P_4) to generate the corresponding membrane deflection are listed in Table 2.1. As an example,

applying a pressure P_3 of about 0.7 bar to the control channel, generates a membrane deflection that allows passing of all larvae stages up to L3 into chamber C2, but retains L4 larvae and adult worms in chamber C1. Average values for *C. elegans* body diameters have been determined by experimental measurements (on average about 30 worms for each population) using a digital microscope (*KEYENCE VHX-700F*). The microscope software tool is used to measure the distance between two points of the worm body width in the observation window. The measurement results are displayed in the observation window and measure result window, and can be saved in CSV format. We found these measurement results correspond well to values reported in literature [65].

Table 2.1 Relevant parameters of the sorting device.

Worm diameters (D_{worm}) for different larvae stages (upper part of the table) and young adult (YA) male/hermaphrodite worms (lower part), and the corresponding pressure values applied to the filter required for larvae or worms of a specific size or larger to be retained. At P_0 (1.9 bar, not listed), *the valve is nearly closed, all larvae are blocked in chamber C1, and only liquid can pass through*. D_{pass} is the maximum diameter of a circle that can be inscribed in the fluidic path opening (see Fig. 2.4). The “nearly-closed” valve configuration is also indicated.

D_{worm} (μm)	L1	L2	L3	L4
	11.7 \pm 0.2	17.0 \pm 0.2	22.1 \pm 0.3	29.5 \pm 0.6
Pressure (bar)	P_1	P_2	P_3	P_4
	1.5	1.1	0.7	0.3
D_{pass} (μm)	13.0 \pm 0.4	18.9 \pm 0.3	24.1 \pm 0.3	33.3 \pm 0.2
D_{worm} (μm)	Male YA 38.5\pm0.6	Herm YA 47.9\pm0.8	<i>Valve nearly-closed</i> <i>(only liquid can pass)</i>	
Pressure (bar)	0.2	0	P_0 1.9	
D_{pass} (μm)	43.3 \pm 0.2	50 \pm 0.1	10.4 \pm 0.3	

2.2.3 Evaluation of D_{pass} for different PDMS membrane thicknesses and mixing ratios

FEM simulations of the membrane deflection have been carried out for different PDMS membrane thicknesses and mixing ratios in order to evaluate D_{pass} , as depicted in Fig. 2.5. To describe hyperelastic properties of PDMS, we used the Mooney-Rivlin model (see Fig. 2.5A-D). In this model, the stress state is determined as the derivatives of the strain energy density W with respect to the strain components. The strain energy density function W is given as:

$$W = C_{10}(\bar{I}_1 - 1) + C_{01}(\bar{I}_2 - 1) + C_{11}(\bar{I}_1 - 1)(\bar{I}_2 - 1) + \frac{1}{d}(J - 1)^2$$

Equation 2.2 The strain energy density in the Mooney-Rivlin model.

where C_{01} , C_{00} , C_{10} are empirically determined material constants, and I_1 , I_2 are strain invariants. I_1 , $I_2 = J^2$, and J is the elastic volume ratio. d is the material constant that control bulk compressibility and set to zero for fully incompressible rubber. The Mooney-Rivlin coefficients determined in our case are shown in Table 2.2 [66]. Computational results for the 25 μm membrane correspond well to our experimental results represented by green dots in Fig. 2.5 (see also Table 2.1). Fig. 2.5E also shows the variation of D_{pass} as a function of applied

pressure for thinner or thicker membranes, respectively. Furthermore, D_{pass} is also a function of the PDMS mixing ratio (base to curing agent), as is shown in Fig. 2.5F for three different ratios. Increasing the amount of base with respect to curing agent (from 5:1 to 15:1) lowers the elastic modulus, resulting in stronger membrane deflection for the same pressure value.

Table 2.2 Material constants of the Mooney-Rivlin model.

Material constants of the Mooney-Rivlin model for different PDMS mixing ratios, as reported in [66].

PDMS (Ratio base:curing agent)			
Mooney-Rivlin model material constant	Ratio 5:1	Ratio 10:1	Ratio 15:1
$C10$	0	0.0308307	0.0013643
$C01$	0.1342	0	0.0878638
$C11$	0.0889167	0.0269727	0.0109259

Unit: Mpa

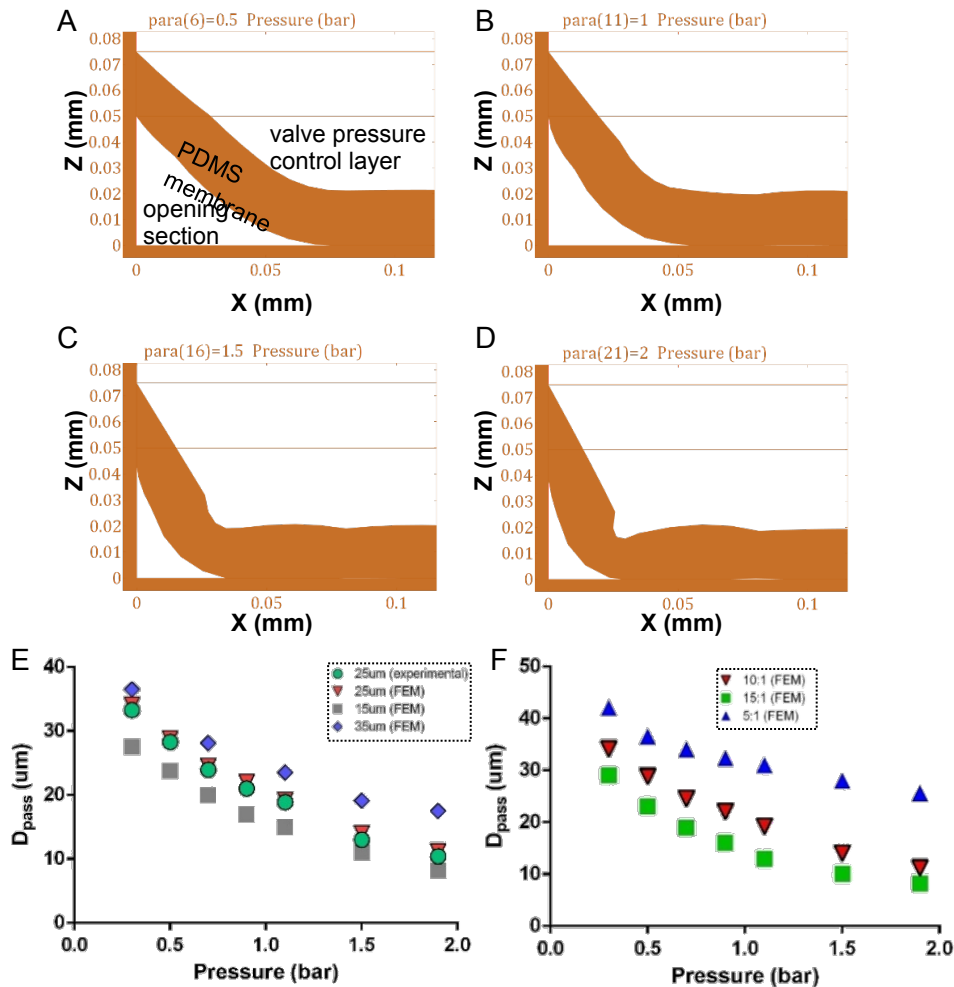


Figure 2.5 Finite Element Method (FEM) simulations of the deflected PDMS filter valve membrane.

(A-D) FEM modeling and simulation under various pressure loads. The graphs show cross-sectional views of the deflected PDMS filter valve membrane with pressure loads from the valve control layer of 0.5 bar (A), 1 bar (B), 1.5 bar (C), and 2 bar, respectively. **(E)** The graph shows the influence of the PDMS membrane thickness on D_{pass} (base:curing agent ratio 10:1). For the 25 μm membrane used in our device, the simulated values agree well to the experimentally observed ones reported in Table 2.1. **(F)** Influence of the PDMS base:curing agent mixing ratio on D_{pass} (membrane thickness 25 μm).

2.2.4 Device operation and sorting procedure

Prior to worm loading, the device was pre-filled with S-medium. Subsequently, a heterogeneous worm population was loaded into C1. For loading, a constant flow rate of 100 nl/s was applied. The corresponding valve configuration is shown in Fig. 2.6A. V1 and V3 are fully open during loading (no pressure applied to their control chambers). V2 is nearly closed by applying P_0 to its control chamber, meaning that all larvae are blocked in chamber C1, but liquid can still pass. The population is then confined in C1 for imaging and counting by applying P_0 to the control chambers of V1 and V2. For worm sorting, pressure on the control chamber V2 was changed to the required value for selecting worms of a certain size as listed in Table 2.1. The selected portion of the initial worm population was pushed through the transfer channels into C2 at a constant flow rate of 100 nl/s. V3 was set to retain the population inside C2 (Fig. 2.6B). After sorting and worm counting in C1 and C2, V3 was opened to collect the filtered worm population at the outlet (Fig. 2.6C). On the other hand, if desired, V3 can also be used as a second serial filter for a subsequent additional sorting step.

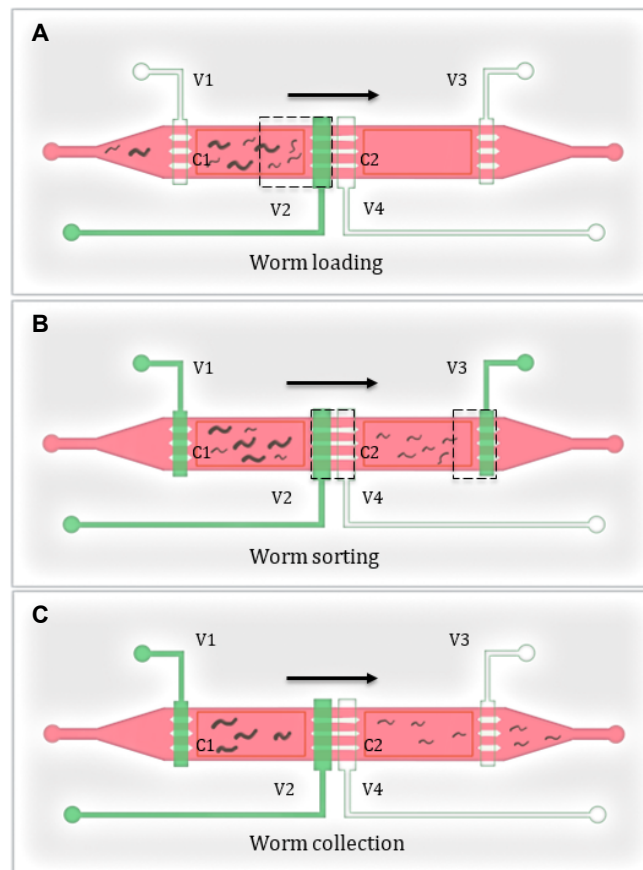


Figure 2.6 Worm sorting protocol.

(A) Worm loading: injection of a heterogeneous population of worms into chamber C1 (P_0 is applied to the control chamber of V2, *i.e.* the transfer channels beneath are nearly closed and only liquid can pass to C2, V1 and V3 are fully open, V4 is not used/ its control chamber never pressurized in this experiment). Subsequently, there is confinement in C1 (P_0 applied to the control chambers of V1 and V2) and counting of larvae and adults is done. **(B)** Worm sorting: application of the required pressures P_1 - P_4 to the control chamber of V2 (see Table 2.1) and transfer of the desired larvae population into C2. V3 is nearly closed by applying a pressure P_0 to its control chamber, keeping all larvae inside C2 (eventually it can be left partially open by applying a pressure P_1 - P_3 , if used as a second serial filter). **(C)** Worm collection: the selected worm population is transferred from C2 to the outlet (V3 open).

2.3 Worm sorting experiments

2.3.1 Larvae and adult worm sorting

The initial heterogeneous population that is loaded into C1 may comprise embryos, larvae at all stages, and adult worms. Specific sorting protocols are performed by adjusting the pressure settings of the different valves of the device, in particular V2 and V3. Our device allows versatile size- and age-dependent sorting resulting in populations comprising a unique larvae stage or only adults, or larvae of two or more different stages. With our approach, simple protocols may be applied to generate mixtures of larvae populations on-chip and different ratios of these. The versatility of the present device is demonstrated by a series of different sorting experiments. An outline of experiments that have been performed is shown in Table 2.3. The corresponding control pressure settings, applied to V2 and V3, respectively, and worm stages present in C1, C2 and at the outlet are summarized. The first and second part of the table explains extraction and isolation of larvae with unique size or of mixed populations in C2, respectively. In this case, an initial population containing larvae at all stages (L1 to L4) and adult worms has been loaded into C1. The third part of the table describes a protocol for adjusting ratios of larvae populations by 3 subsequent steps. For this experiment, a worm population that contains an equal amount of L2 and L1 larvae (ratio 1:1) was loaded into C1. With this protocol, first a population of L1 larvae is transferred from C1 to C2 (P_1 on V2, P_0 on V3). Then the outlet valve is partially opened (P_1 on V3) to release a portion of this population. The amount of L1 larvae transferred to the outlet is controlled by applying flow through the device for a defined time span. In the particular case shown in Table 2.3, 50% of the L1 population in C2 have been removed. After closing the outlet, the whole L2 population may be transferred from C1 to C2 (P_2 on V2, P_0 on V3). The resulting population in C2 is a mixture of L2/L1 larvae at a ratio of 2:1.

Fig. 2.7 shows subsequent steps of a typical sorting experiment. As an example, we have chosen the extraction of L2 larvae from a mixed population of L2, L3 larvae and adult worms (no L1 and L4 are present in this case). Fig. 2.7A-C show photographs of the microfluidic device at important steps of the sorting experiment. Fig. 2.7A shows a picture of the initial heterogeneous worm population in C1 (photograph corresponding to the area defined by the dashed square in Fig. 2.6A). For more accurate counting, worms may be concentrated in a smaller region of C1, corresponding to the field of view of the microscope, by pushing them gently towards valve V2 (Fig. 2.7A, P_0 on V2). The number of L2, L3 and adult worms were counted one by one after closing the inlet valve V1. In order to selectively extract the L2 larvae population from C1, the valve filter V2 was then set to pressure P_2 . Using this pressure value, the effective width of the filter is 18.9 μm thus only L2 larvae having a diameter of typically 17 μm can pass through V2 (see Table 2.1). Fig. 2.7B is a snapshot showing a L2 larva passing through V2 (the photograph corresponds to the area defined by the dashed square in the middle of Fig. 2.6B). Larger animals, *i.e.* L3 larvae and adults in this case, are retained in C1. During this operation, the outlet valve V3 was set to pressure P_1 which corresponds to the threshold for retaining L2 larvae in C2. If present, L1 larvae, embryos but also small debris and bacteria clusters are removed from C1, pass through C2 and are transferred to the outlet. Immediately after the selective transfer, L2 larvae were confined in C2 by closing V3 for counting. It is noted that sometimes a larva gets partially blocked in a valve. However, such larvae do not pass the filter structure and retract back to chamber C1 after a short time, without significant impact on the sorting efficiency. To prevent clogging of the filter structure by young

adults or adult worms, we take advantage of geometrical hindrance. As shown in Fig. 2.3A, worm chambers are three times higher than valve filters (height 150 μm vs 50 μm , respectively). Upon sorting of larvae groups from adults (diameter $\geq 50 \mu\text{m}$) and by using flow rates in the lower range up to 100 nl/s, this height difference acts as a threshold that retains adult worms in chamber C1 at a certain distance from the valve channel (see Fig. 2.7A). In this way, clogging can be safely avoided. After sorting of the larvae population, adults may be pushed towards and through the filter channels by increasing the flow rate (typically to 250 nl/s). Nevertheless, for reliable and reproducible worm sorting protocols, it is convenient to restrict the initial number of worms in chamber C1. This can be achieved by means of V1 and V2, as explained above. According to our observations, the number of adult worms loaded in chamber C1 should not exceed about 30 per experiment (*i.e.* 25 worms/ μL for a chamber volume 1.2 μL) to avoid a ‘steric hindrance’-like effect in sorting. Also the maximum total number for a mixed population loaded in chamber C1 should be around 80 worms (≈ 67 worms/ μL). After each sorting experiment, the surplus worms are washed out, followed by next mixed population loading.

Table 2.3 Possible worm sorting experiments.

List of possible sorting experiments: pressures applied to the control chambers of V2 and V3 to obtain various populations in C2 and to have specific worm populations transferred to the outlet are indicated; sorting of either single-stage larvae or mixed populations is possible. V1 is always in the nearly-closed state after loading (*P0*). The initial worm population loaded before sorting in chamber C1 is a heterogeneous mixture that may contain L1, L2, L3, L4 larvae and adults (A) worms. The third part of the table describes a 3-step protocol for adjusting ratios of larvae populations in C2 or at the outlet.

Sorting protocol	Valve state pressure		Population after sorting		
	V2	V3	C1	C2	Outlet
Single larva population in C2: Initial population in C1: L1, L2, L3, L4, A					
L1 sorting	<i>P1</i>	<i>P0</i>	L2, L3, L4, A	L1	-
L2 sorting	<i>P2</i>	<i>P1</i>	L3, L4, A	L2	L1
L3 sorting	<i>P3</i>	<i>P2</i>	L4, A	L3	L1, L2
L4 sorting	<i>P4</i>	<i>P3</i>	A	L4	L1, L2, L3
Mixed larvae population in C2: Initial population in C1: L1, L2, L3, L4, A					
L1&L2 sorting	<i>P2</i>	<i>P0</i>	L3, L4, A	L1, L2	-
L2&L3 sorting	<i>P3</i>	<i>P1</i>	L4, A	L2, L3	L1
L3&L4 sorting	<i>P4</i>	<i>P2</i>	A	L3, L4	L1, L2
L1, L2 & L3 sorting	<i>P3</i>	<i>P0</i>	L4, A	L1, L2, L3	-
L2, L3 & L4 sorting	<i>P4</i>	<i>P1</i>	A	L2, L3, L4	L1
Adjusting ratios: Initial ratio L2:L1 = (1:1) in C1					
1) Sorting of L1	<i>P1</i>	<i>P0</i>	L2	L1	-
2) Partial release of L1 from C2	<i>P0</i>	<i>P1</i>	L2	L1(50%)	L1(50%)
3) Mixing of L2 & L1 in C2	<i>P2</i>	<i>P0</i>	-	L2:L1 (2:1)	L1

A photograph of the L2 population in C2 is shown in Fig. 2.7C (corresponding to the area defined by the right dashed square in Fig. 2.6B). In order to determine safely the larval stage, the diameter of all larvae present in C2 was measured and compared with typical values listed in Table 2.1. Finally, the selected population may be collected at the outlet of the device. A significant advantage of our device is that by using adjustable filter valves, subsequent sorting steps of the same initial worm population may be readily performed. For instance, in the

present case, the L3 larvae population can be extracted from C1 by applying a pressure value P_3 to valve V2, and P_2 to valve V3, respectively. With this configuration, adult worms will be blocked in C1, L3 and L2 are transferred into C2 where only L3 are retained, whereas L2 pass to the outlet. In this way, serial separation of L2, L3 and adults, in this particular case, can be performed in a single step by applying a constant flow rate (typically 100 nL/s). Throughput of the sorting progress mainly depends on the progress of the sorting experiment, *i.e.* on the actual larva/worm density in chamber C1, and to a minor extent on the larva/worm size. A typical sorting experiment lasts about 1 min. During this period throughput decreases from about 3.5 larvae/sec (≈ 210 worms/min) or 3.0 adults/sec (≈ 180 worms/min) at the beginning of a sorting experiment to about 1.0 ± 0.5 worms/sec towards the end when the population of interest in chamber C1 declines. A detailed study on the evolution of the throughput during a sorting experiment is reported in section 2.3.4 and Fig. 2.11).

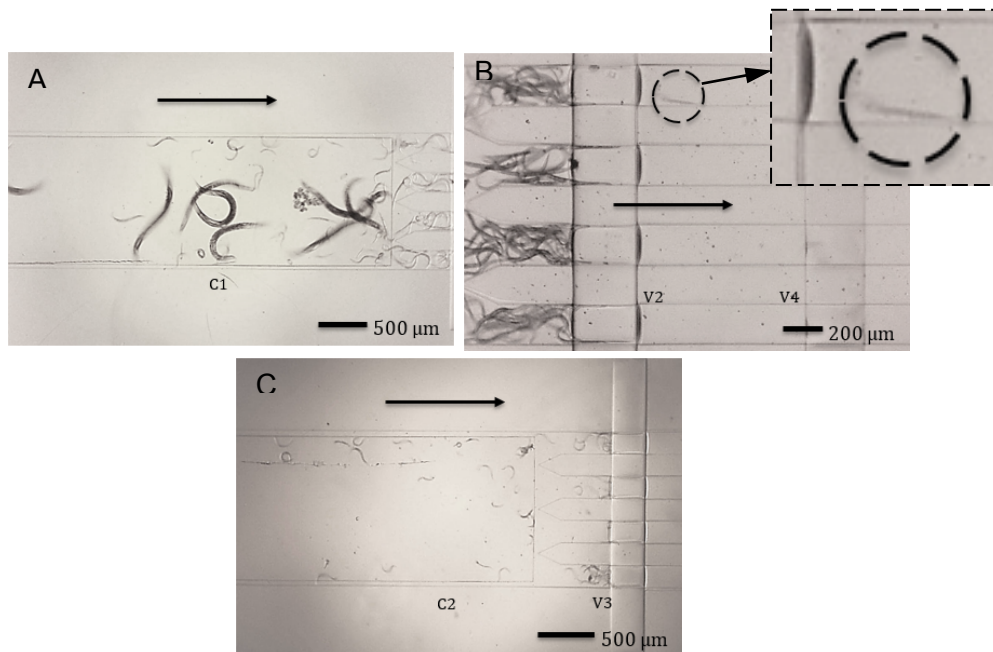


Figure 2.7 Images of size-selective on-chip sorting of L2 larvae from a mixed population of worms.

(A) A heterogeneous population comprising L2, L3 larvae and adult worms has been loaded into chamber C1 (V2 closed). For more convenient counting, the worms have been pushed in the vicinity of valve V2 (corresponding to the area defined by the dashed square in Fig. 2.6A). **(B)** Snapshot of a L2 larva passing through valve V2 where a pressure P_2 has been applied (picture corresponding to the area defined by the left dashed square in Fig. 2.6B). Larger worms are blocked by V2. **(C)** Successful L2 sorting showing only L2 larvae in chamber C2 (picture corresponding to the area defined by the right dashed square in Fig. 2.6B).

Four groups of experiments were used to evaluate the sorting accuracy of the device, as depicted in Fig. 2.8. The images are snapshot photographs of representative events occurring during the separation of L1 from L2 (Fig. 2.8A,B), L2 from L3 (Fig. 2.8C,D), L3 from L4 (Fig. 2.8E,F), and L4 from adults (Fig. 2.8G,H), respectively. The used protocol for these sorting experiments is similar for all stages, but pressure values, in particular the pressure applied to the valve V2, were adjusted to enable sorting of a certain worm stage/size (see Table 2.1). As a representative example, L2 sorting from L3 and adult worms has been explained already in the above (see also Fig. 2.6).

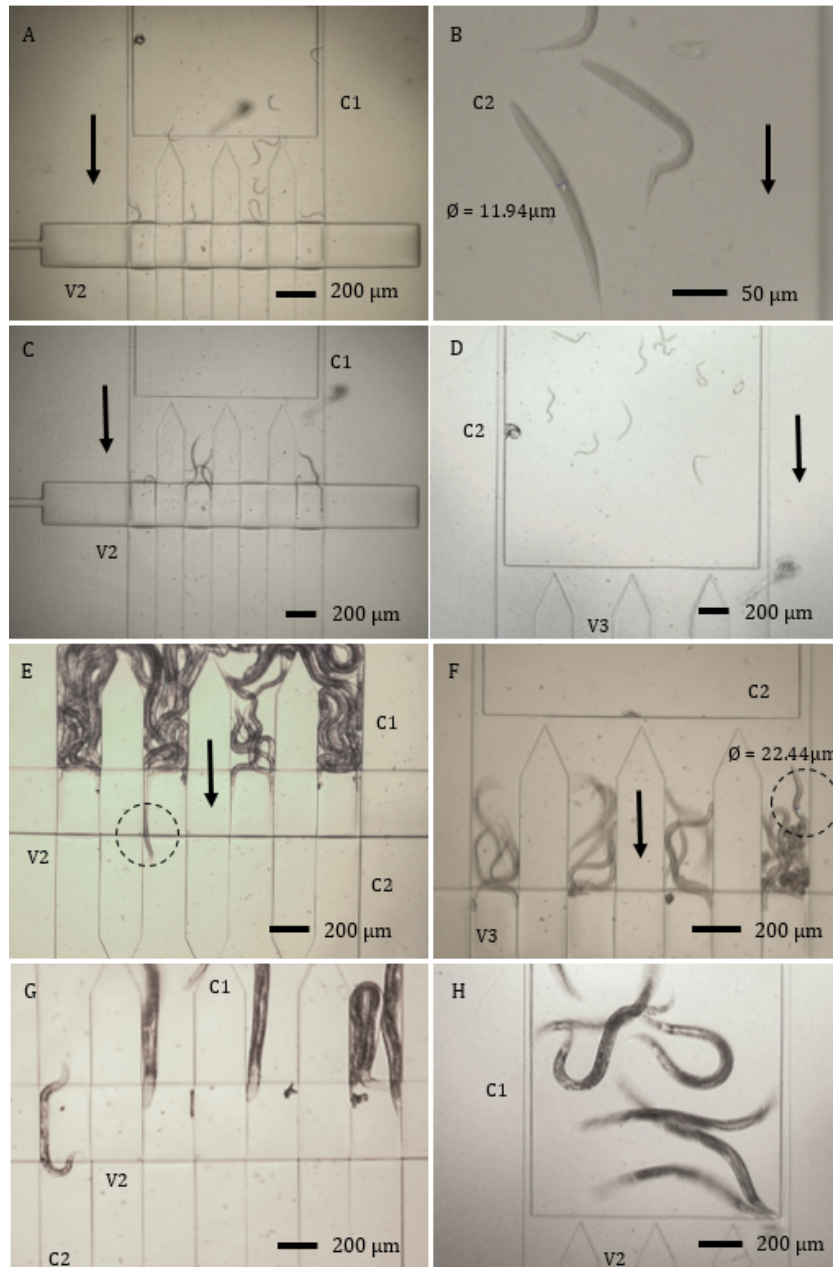


Figure 2.8 Images of sorting of worms having adjacent development stages.

Size-selective on-chip sorting of L1 from L2 (A,B), L2 from L3 (C,D), L3 from L4 (E,F), and L4 from adults (G,H) is demonstrated. **(A)** Before sorting, heterogeneous populations comprising L1 and L2 larvae were loaded into chamber C1 (V2 closed). **(B)** Photograph of L1 larvae in chamber C2 after successful L1 sorting; only L1 larvae are in C2. In order to determine safely the larval stage, the diameter of all larvae present in C2 was measured and compared with typical values listed in Table 2.1. Here, we measured a mean maximum diameter of $11.9 \pm 0.2 \mu\text{m}$ corresponding to the L1 larval stage. **(C)** Snapshot of L2 larvae passing through valve V2, to which a pressure P_2 has been applied. L3 larvae are blocked by V2. **(D)** Photograph of chamber C2 containing only L2 larvae after sorting from a L2&L3 population in chamber C1. **(E)** Snapshot of a L3 larva passing through the valve V2 (indicated by the dashed circle), to which a pressure P_3 has been applied. L4 larvae are seen to be retained in C1 by valve V2. **(F)** After transfer of L3 larvae from C1 to C2, L3 larvae were blocked in chamber C2 by valve V3 for counting and imaging. The measured average diameter of the L3 larvae was $22.4 \pm 0.2 \mu\text{m}$. **(G)** Snapshot of a L4 larva passing through valve V2, to which a pressure P_4 has been applied. **(H)** Successful adult sorting from a mixed L4&adult population, as evidenced by the presence of only adults in C1 after selective transfer of L4 to C2.

2.3.2 Male and hermaphrodites worm sorting

Male worms occur extremely rarely in cultures propagated by hermaphrodite self-fertilization (0.1-0.2%). Here, we further extended our study and protocol optimization for creating single-sex populations on a microfluidic chip, in particular for sorting male and age-matched hermaphrodite *C. elegans* worms. Subsequent steps of a male/hermaphrodite sorting experiment are shown in Fig. 2.9 which are similar to the stage sorting as described above, comprising loading of a mixed population (Fig. 2.9A), selective transfer of male worms through the adjusted filter structure (Fig. 2.9B) and male collection (Fig. 2.9C).

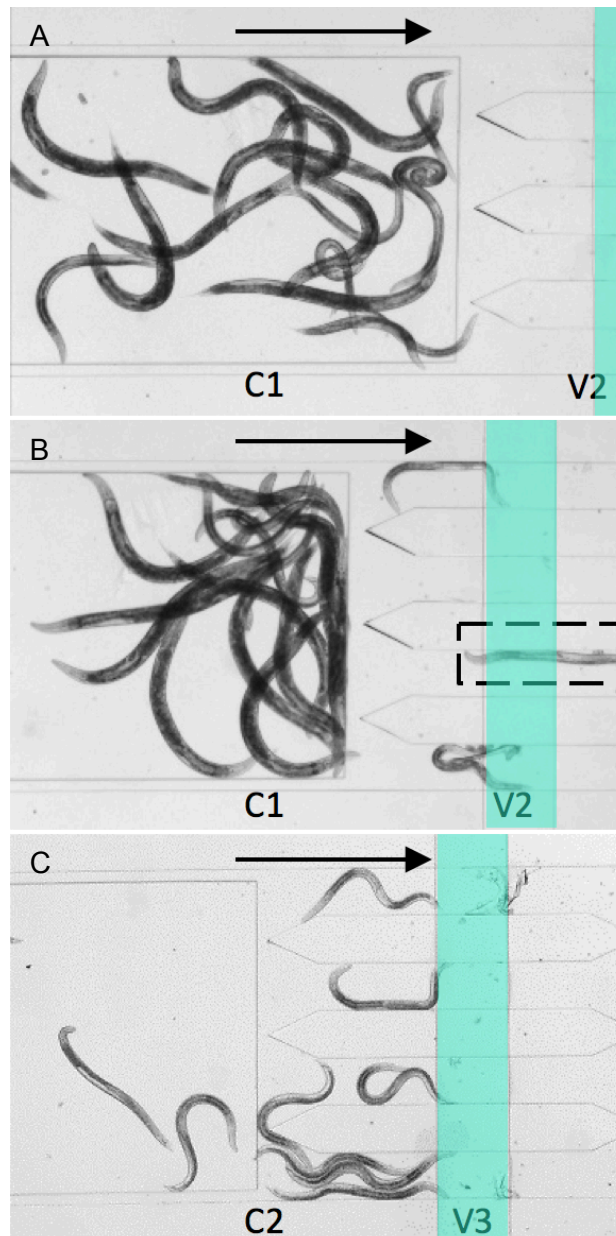


Figure 2.9 Sorting of adult males from same-aged hermaphrodites.

(A) A mixed population has been loaded into chamber C1 (V2 nearly-closed, flow direction as indicated). (B) Snapshot of a male worm passing through V2, to which a pressure has been applied, while hermaphrodites are blocked inside chamber C1. (C) Successful sorting showing only males in chamber C2 (V3 nearly-closed).

2.3.3 Worm sorting purity and efficiency

In order to evaluate the performance of our device, the number of larvae or adult worms was counted in chamber C1 and C2 before and after sorting. The results for N2 hermaphrodite sorting, separating L1 from L2, L2 from L3, L3 from L4, L4 from adult, and for sorting male from hermaphrodite young adults are shown in Fig. 2.10. Overall sorting results were obtained based on the counting of individual worms of a certain population (total population sizes of about 250-350 worms; counting was done from 6-7 independent sorting experiments). According to a definition proposed by Ai *et al.* [64], we define the ‘purity’ of a worm population as the number of target worms in C1 or C2 divided by the total number of worms in that chamber. The ‘efficiency’ of the sorting process is defined as the number of target worms in C1 or C2 divided by the total number of target worms initially loaded in C1, before sorting. The sorting accuracy of the device for separating L1 from L2, L2 from L3, L3 from L4, L4 from adult, and males from hermaphrodite adults, respectively, is also reported in Table 2.4. Representative images of these sorting experiments are shown in (Fig. 2.7-2.9). The device achieved an overall sorting purity and efficiency of close to 95-100 % for all larvae/worm groups.

Table 2.4 Separation purity and efficiency.

Larvae and adult worm separation purity and efficiency. Each value was determined from 6 or 7 independent experiments (shown in Fig. 2.10). Each experiment was performed with a total number of about 50 worms that were recovered from an agar plate and placed in C1. For every sorting experiment, two different populations (*P1* and *P2*) were loaded into C1.

Populations loaded into C1 (<i>P1</i> & <i>P2</i>)	Average purity (%) of populations in C1 before sorting		Average purity (%) of populations in C1 and C2 after sorting		Sorting efficiency (%)	
	<i>P1</i>	<i>P2</i>	C2 (<i>P1</i>)	C1 (<i>P2</i>)	C2 (<i>P1</i>)	C1 (<i>P2</i>)
L1 & L2	31.5	68.5	93 ± 3	98 ± 2	96 ± 1	96 ± 1
L2 & L3	43.3	56.7	98 ± 2	97 ± 3	98 ± 3	98 ± 2
L3 & L4	45.1	54.9	98 ± 2	97 ± 4	98 ± 2	98 ± 3
L4 & adult	48.9	51.1	98 ± 2	98 ± 2	98 ± 2	98 ± 2
male & herm (YA)	45.1	55.5	97 ± 2	98 ± 2	98 ± 2	98 ± 2

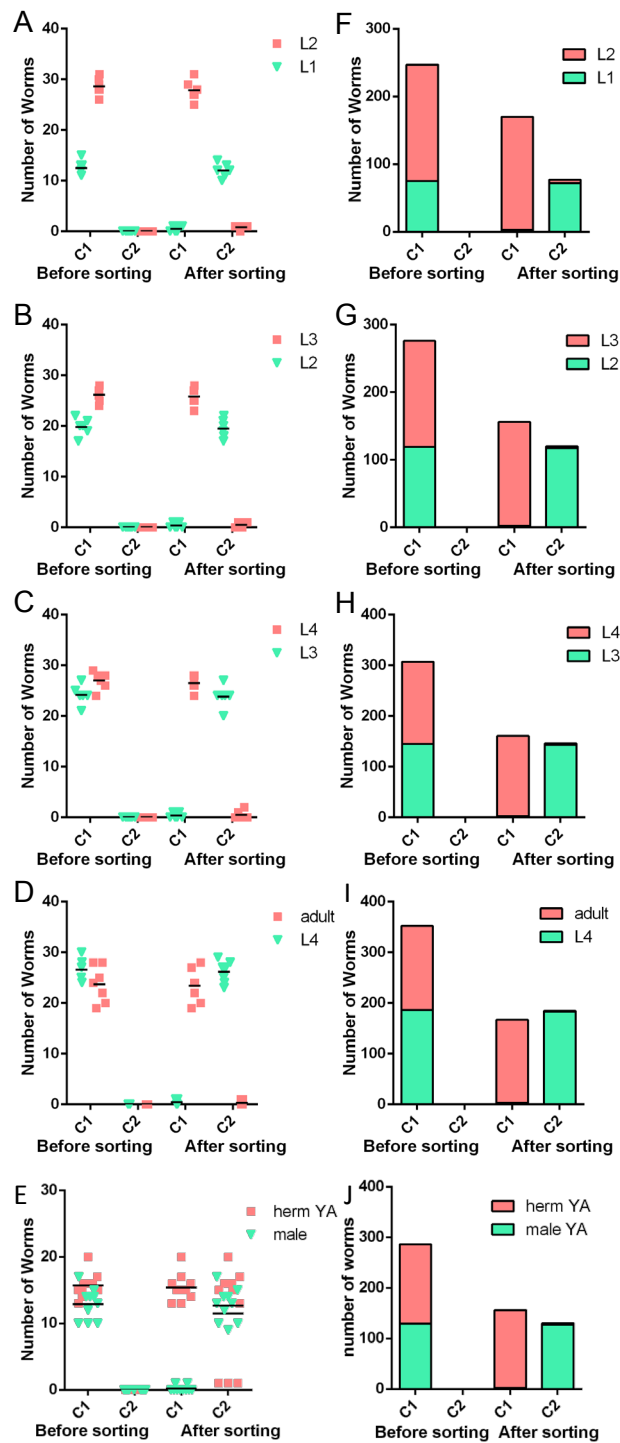


Figure 2.10 Worm counting before and after sorting.

In each experiment, a mixture of 2 populations of larvae and/or worms was introduced in chamber C1. Size-selection was obtained by applying the appropriate pressure to V2, after which the populations were counted in C1 and C2. In (A-E), the number of all individuals in a population counted in a single experiment is represented by a point and a triangle, while the average of similar experiments is represented by the dash. Summation of the counts done in all experiments is represented in (F-J). The two populations and the V2 pressure condition for the various sorting experiments are: (A, F) L1 and L2, 1.5 bar; (B, G) L2 and L3, 1.1 bar; (C, H) L3 and L4, 0.7 bar; (D, I) L4 and adults, 0.3 bar; (E, J) Male and hermaphrodite young adults (YA), 0.2 bar.

2.3.4 Analysis of throughput of the sorting experiments

Sorting throughput in our device appeared to be a function of target worm density in chamber C1. We evaluated this relationship by counting the number of target worms passing through the filter structure during subsequent time windows (of 10 s duration) in the course of a sorting experiment. Density of target worms was defined as the actual average target worm number in C1 for each time window divided by the chamber volume of 1.2 μL . According to our experiments, throughput for “larva & larva” separation is comparable for all protocols, *i.e.* separation of L1 from L2, L2 from L3, and L3 from L4, whereas the separation speed of L4 from adults showed a slightly different behavior. Thus, two groups of the experiments, larva & larva populations and a L4 & adult population, were used to evaluate the throughput. For all experiments, we observe a decreasing sorting speed (throughput) as the sorting process progresses and the target worm density in C1 is decreases. Data comparing L2 & L3 and L4 & adult sorting experiments are shown in Fig. 2.11. In particular, in the beginning of the sorting experiment, we determined a throughput of approximately 3.5 worms/sec (210 worms/min) for the larva & larva populations and around 3.0 worms/s (180 worms/min) for the L4 & adult population for a target worm density in the range of 30 to 40 worms/ μL . The slightly lower value in the latter case may be due to the fact that larger size L4 larvae require a longer transfer time through the filter structure compared to smaller larvae. Towards the end of an experiment, when the number of target worms in C1 strongly decreases, throughput approaches a value of about 0.3-0.5 worms/sec (20-30 worms/min) for larva & larva sorting, whereas for L4 & adult sorting throughput remains slightly higher, *i.e.* about 1.0-1.5 worms/sec (60-90 worms/min). A possible reason for this observation is that adult worm-related hindrance at the height step at the chamber/valve interface (see Fig. 2.3A) has stronger impact at lower worm densities. During larva & larva separation, even at low densities, some of the larger larvae can still temporally block the valve channel, thus reducing slightly the throughput, whereas in L4 & adult separation, adults cannot approach the valve structure (see Fig. 2.7a).

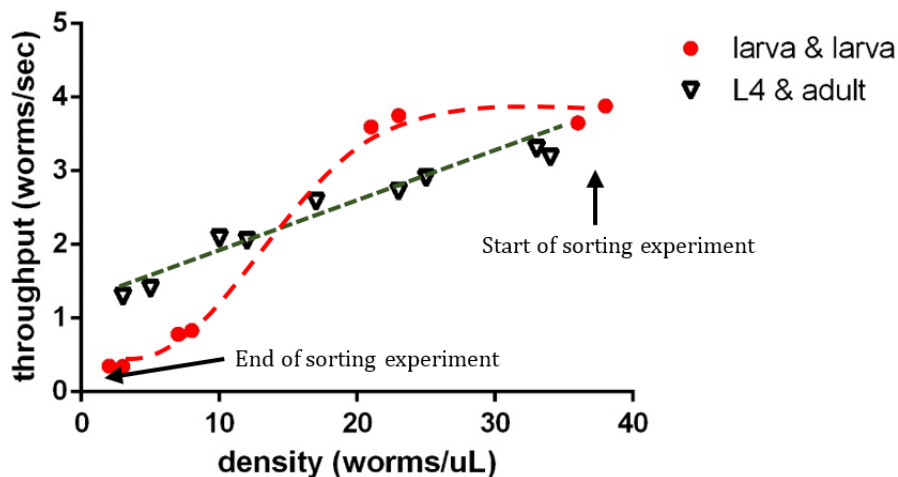


Figure 2.11 Time-dependent throughput during the lapse of a sorting experiment, in particular for L2 & L3 and L4 & adult sorting (2 experiments for each case).

The initial worm density is about 40 worms/ μL , which decreases to 0 worms/ μL at the end of the sorting process. Data was analyzed at different stages of the sorting progress, *i.e.* for decreasing target worm densities in chamber C1. The dashed lines are only intended to be a guide to the eye.

2.3.5 Embryo sorting

As explained in the introduction of this chapter, synchronized populations of worms are required for many worm-based assays in order to eliminate variations of biological parameters due to age difference. Two methods that are commonly used to obtain age-synchronized worm populations are both based on the sorting of embryos: (i) dissolving the adult worms by bleaching and simultaneous release of the embryos in the worm's body, (ii) collecting laid embryos directly from an agar plate. Here we show that we can perform with our device a very simple and efficient protocol to separate embryos from mixed adult worm populations directly in the liquid phase, thus rendering embryos immediately available for incubation. Moreover, if integrated in a microfluidic platform, embryos can be directly transferred to different modules for further processing or studies [67].

For preparing a mixed embryo and adult worm suspension, L1 worms were cultured in S-medium in a 96-well plate. *E. coli* OP50 was added as food source. After 4-5 days of culture at 20 °C in an incubator, the suspension mainly consisted of embryo-laying adult worms. Both embryos and adult worms, were harvested and injected into C1 of the device. Selective transfer of embryos to C2 was achieved by adjusting the filter valve to a suitable opening cross-section (V4 was used here instead of V2). The typical embryo size is around 50 μm \times 30 μm , whereas adult worms have a diameter of larger than 50 μm . Size-separation can be easily achieved as embryos move with longitudinal orientation through the filter. Applying a pressure of 0.6 bar to valve V4 results in an effective D_{pass} of 28.1 μm , which is slightly smaller than the nominal value for a typical embryo diameter.

However, as worm embryos may be slightly deformed, this is a suitable value for efficient sorting of embryos from adult worms, while still ensuring that no mechanical stress could damage the embryos during the separation process. Embryos may subsequently be recovered at the outlet of the chip and used for further culturing and bio-assays. Fig. 2.12A shows a snapshot of an embryo transfer from chamber C1 to C2. An adult worm is blocked by V4, whereas an embryo passes through (V2 fully open in this case). The result of embryo sorting from adults is shown in Fig. 2.12B, C. Before sorting, the ratio of embryos *vs* adults in C1 was about 3:2 for each measurement, corresponding to 10-30 adult worms and 20-50 embryos. After sorting, the purity of adults was 83 \pm 1% in C1 and 100% for embryos in C2, respectively, *i.e.* only embryos were found in C2. This observation demonstrates that a completely pure embryo suspension may be obtained with this method. The efficiency for embryo sorting was 85 \pm 1%. Eight independent experiments were used to evaluate the accuracy of embryo sorting. This result for embryo removal from C1 can be considered as very good, as strong adhesion of the sticky embryos to the chamber walls is commonly observed and represents an important issue in microfluidic manipulation. Sticky embryos also inevitably result in the formation of clusters inside the chamber. These groups are usually an issue for reliable chip operation and handling and separation of single embryos is very difficult. As can be observed in Fig. 2.12A, clusters of embryos are too big to pass through the filter of our device if adjusted by using the indicated pressure value for embryo sorting ($P=0.6$ bar). However, it is possible that fine-tuning of the opening size, *i.e.* fine-tuning of the flow speed and the related shear forces, plays an important role in disrupting clusters of embryos, and consequently improves the efficiency of embryo transfer. Sorting of eggs from L4 larva is still a challenge, since both have a diameter of approximately 30 μm . It is therefore difficult to extract a pure egg suspension from a natural worm population. Again, fine tuning of the flow rate might be a possible solution. On the one hand, one may take advantage of the high mobility of the L4 larvae to improve the filter

selectivity with respect to eggs. On the other hand, eggs form clusters and easily stick to the surface of the PDMS chamber. Thus filtering at low flow rates, where only low shear forces are generated, may retain part of the egg suspension in chamber C1 whereas L4 pass through the filter into chamber C2.

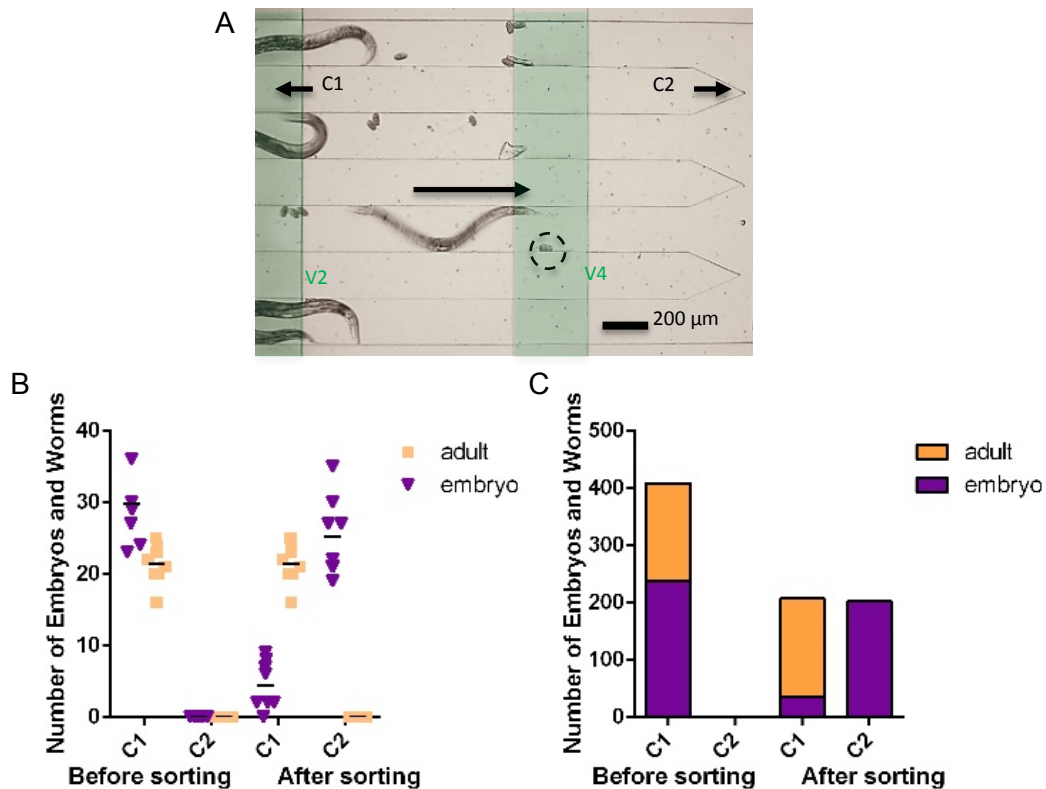


Figure 2.12 Embryo and adult count before and after sorting.

(A) Photograph of an embryo that is present in V4 and transferring from chamber C1 to C2, whereas adult worms and embryo clusters are retained in C1. A pressure of 0.6 bar was applied to valve V4 during sorting (V2 open). The areas enhanced by the color are for indicating the position of V2 and V4, respectively. **(B)** The number of embryos and adults in a population counted in a single experiment is represented by a point and a triangle, while the average of similar experiments is represented by the dash. In each experiment, a mixture of a population of embryos and adult worms was introduced in chamber C1. Summation of all counts done over the independent experiments is represented in **(C)**.

2.4 Materials and methods

2.4.1 Materials

4-inch 550 μm thick Si and float glass wafers were obtained from the EPFL Center of Micro- and Nanotechnology (EPFL-CMI). GM 1075 SU-8 negative photoresist was purchased from Gersteltec (Pully, Switzerland). PDMS *Sylgard 184* was acquired from Dow Corning (Wiesbaden, Germany). 1 mL borosilicate H-TLL-PE syringes were purchased from Innovative Labor Systeme (Stutzerbach, Germany). Microline ethylvinylacetate tubes with 0.51 mm inner and 1.52 mm outer diameters was bought from Fisher Scientific (Wohlen, Switzerland). L-Broth bacterial culture medium was obtained by adding 10 g Bacto-tryptone, 5 g Bacto-yeast, 5 g NaCl, in 1 L of H₂O. S-Basal was obtained by adding 5.85 g NaCl, 1 g K₂ HPO₄, 6 g KH₂PO₄,

1 ml cholesterol (5 mg/ml in ethanol), in 1 L of H₂O. S-medium was obtained by adding 10 ml 1 M potassium citrate pH 6, 10 ml trace metals solution, 3 ml 1 M CaCl₂, 3 ml 1 M MgSO₄ in 1L of S-Basal. S-Basal, L-Broth and S-medium were sterilized by autoclaving. Bleach solution was obtained by adding commercial bleach and NaOH (4 N) at a ratio of 3:2. All the chemicals used in S-Basal, L-Broth, S-medium and bleach solutions were purchased from Sigma-Aldrich (Buchs, Switzerland).

2.4.2 Worm strains culture

A single colony of *E. coli* OP50 was used from the streaked plate and inoculated into L-Broth. The inoculated cultures were shaken and grew overnight at 37°C. *E. coli* OP50 suspension was then ready for use as food source for *C. elegans*. *C. elegans* N2 wild type strains used for all experiments were obtained from EPFL's 'Nestlé Chair in Energy Metabolism' laboratory. The *C. elegans* N2 strain was cultured at 20 °C on nematode growth medium (NGM) plates seeded with *E. coli* OP50. For synchronization, 10–15 reproductively active adults were transferred to a fresh plate seeded with bacteria every four days. The adults were allowed to lay embryos for 2–6 h. After a sufficient number of embryos was produced, all adult worms were removed from the plate. The embryos were then allowed to develop up to the desired larva stage or to adulthood before being used for a specific sorting experiment. Prior to the experiment, the synchronized populations were removed from the NGM plates by washing the plates with filtered S-medium; hereafter they were mixed according the desired sorting experiment requirements. Subsequently, the worms were gently washed twice by centrifugation and resuspension in fresh filtered S-medium. The density of worms was first counted by dropping 5 µL of suspension onto a glass slide. The density was then adjusted to 2 - 5 worm/µL by adding S-medium. A 1 ml syringe was filled with the worm suspension, and connected to the chip inlet. Worm loading was carried out by using a syringe pump (*neMESYS*, Low Pressure Syringe Pump, Cetoni GmbH, Germany). Before each loading experiment, the syringe was shaken or refilled to avoid worm sedimentation in the syringe. For sorting experiments, synchronized populations of L1, L2, L3 or L4 larvae, and adults were used.

2.4.3 Device fabrication

Two dedicated molds were used to fabricate each of the PDMS layers. The mold for the fluidic control layer was made by a two-step process. First, 50 µm deep structures were dry etched into a Si wafer (Alcatel AMS 200 SE) defining the fluidic transfer channels. Subsequently, a 100 µm thick SU8-100 layer was spin-coated on top to define chambers C1 and C2 resulting in a total chamber height of 150 µm. Likewise, the master for the valve pressure control layer was made by etching 50 µm deep structures into a Si wafer. Furthermore, a 25 µm thick PDMS membrane (base-to-curing agent ratio 10:1) was fabricated by spin-coating on a Si blank wafer and cured at 70 °C for 2 h. The two molds and the blank wafer were treated with trimethylchlorosilane (TMCS) in a vacuum desiccator to prevent adhesion of PDMS during the molding process. After air plasma surface activation, the PDMS valve layer was bonded to the PDMS membrane on the blank wafer. The assembly was peeled off and, following another air plasma activation step, fixed to the fluidic layer. Access holes for tube insertion were punched beforehand into the PMDS layers. Finally, the individual PDMS devices were bonded onto a cover glass slide for mechanical support. The four valve control channels were filled with deionized DI water to avoid pressure loss by air diffusion through the PDMS layers (a problem arising when air-filled chambers would be used). Valve pressure was

controlled by syringe pumps and measured by pressure sensors (Pressure Measurement Module Qmix P, Cetoni GmbH) in the connecting tubes.

2.5 Conclusions

C. elegans nematodes develop from hatching to reproductive adulthood through four larval stages (L1 to L4) that exhibit distinctive stage-specific features. For this reason, many biological studies on worms require populations of stage-synchronized animals for reliable interpretation of the results. In this chapter, we presented a new approach for size- and thus stage-specific sorting of heterogeneous worm populations. The sorting principle is based on the selective transfer of larvae through an adjustable microfluidic PDMS filter structure. Filter parameters, *i.e.* the effective cross-section of the fluidic path connecting two worm chambers, may be accurately adjusted through the externally applied control pressure. Compared with other manual, microfluidic or automated synchronization methods, this new approach appears to be very simple and highly efficient, yet is very flexible. Furthermore, since the device operation is merely based on geometrical parameters, *i.e.* filter opening section and animal diameter, instead of behavioral differences of worms, the sorting mechanism is by nature very reliable and reproducible. Also, the throughput, 3.5 worms per second, is higher than shown with electrotaxis-based sorting methods. Further upscaling of the throughput may be readily achieved by increasing the number of parallel filter channels on the chip. Another significant advantage is the versatility of the device. The same chip can be used for performing different sorting experiments with worms at all developmental stages, without changing the external dimensions of the microfluidic channels. The feasibility of worm sorting was demonstrated, among others, by separating groups of adjacent larvae stages (*e.g.* L1/L2) with close to 100% purity and efficiency in a single step. These results indicate that by performing several subsequent filtering steps with appropriate filter settings, a natural mixture of worms could easily be separated into populations of the five developmental stages (L1 to L4 larvae and adults). It is possible to easily implement on-chip such a serial filter structure by using the same fabrication process and design rules. On the other hand, we also demonstrated the possibility to generate on-chip controlled mixed larvae populations (*e.g.* L1&L2 or L1&L2&L3). Furthermore, for the time being, in some biological studies, *e.g.* social interaction pheromone-driven communication [68], different ratios of two worm population are used to study the influence between each other. For the time being, there is no microfluidic device capable of adjusting the ratio of a given mixture of two worm populations. This option is available with our device by means of a simple microfluidic protocol.

For longitudinal developmental studies, an accurately age-matched cohort of animals is required, which can be obtained by isolating a batch of embryos that will hatch into a synchronized population. The adjustable filter structures of our device can be used as a powerful tool to isolate laid embryos from an adult worm population. In this way high purity embryo suspensions could be readily produced. Eventually, the throughput for generating large synchronized populations might be significantly increased with respect to presently used methods, opening the way for more advanced and efficient drug screening assays, for instance. Beside larvae/adult and embryo/adult sorting, fine-tuning of the filter structures may provide a simple solution for any other possible size-dependent sorting protocol, such as mutant/mutant (*e.g.* *lon-3* [69] and *dpy-4* mutants [70, 71]), male/hermaphrodite and *C. elegans*/other nematodes (*e.g.* *P. pacificus*). A potential problem of size filtration is clogging

due to particulates in the filtrate, in particular very sticky bacteria clusters, which hinders repeated or continuous operation of the device. This issue is greatly reduced by the use of filters with adjustable opening. We think that this new and simple sorting device has therefore strong potential for future integrated microfluidic worm assays. For instance, the device can be easily integrated into a platform where stage- and/or age-synchronized populations, that are sequentially transferred to the outlet of the sorting chip, can be directly injected into bio-assay chip modules situated further downstream. This approach opens perspectives for advanced automated worm assays based on well-controlled and highly purified worm populations.

Chapter 3 Microfluidic biocommunication assay for studying male-induced demise in *C. elegans* hermaphrodites

Like other animals, *C. elegans* nematodes have the ability to socially interact and to communicate through exchange and sensing of small soluble signaling compounds that help them coping with complex environmental conditions. For the time being, worm biocommunication assays have been performed mainly on agar plates, however, microfluidic assays may provide significant advantages compared to traditional methods, such as control of signaling molecule concentrations and gradients or confinement of distinct worm populations in different microcompartments. Here, we propose a microfluidic device for studying signaling via diffusive secreted compounds between two specific *C. elegans* populations over prolonged durations. In particular, we designed a microfluidic assay to investigate the biological process of male-induced demise, *i.e.* lifespan shortening and accelerated age-related phenotype alterations, in *C. elegans* hermaphrodites in the presence of a physically separated male population. For this purpose, male and hermaphrodite worm populations were confined in adjacent microchambers on the chip, whereas molecules secreted by males could be exchanged between both populations by periodically activating controlled fluidic transfer of μl -volume aliquots of male-conditioned medium. For male-conditioned hermaphrodites, we observe a reduction in mean lifespan of 4 days compared to non-conditioned on-chip culture. We also observe an enhanced muscle decline, as expressed by a faster decrease of the thrashing frequency and the appearance of vacuolar-like structures indicative for accelerated aging. The chip was placed in an incubator at 20°C for accurate control of the lifespan assay conditions. An on-demand bacteria feeding protocol was applied, and worms were observed during long-term on-chip culture over the whole worm lifespan.

This chapter is an adapted version of the following publications:

L. Dong, M. Cornaglia, T. Lehnert, M. Gijs, “On-chip microfluidic biocommunication assay for studying male-induced demise in *C. elegans* hermaphrodites,” *Lab on a Chip*, 2016 (16), 4534-4545.

L. Dong, M. Cornaglia, T. Lehnert, M. Gijs, “On-Chip Biocommunication through Exchange of Diffusive Compounds Secreted by Male *C. elegans* Nematodes,” *The 20th International Conference on Miniaturized Systems for Chemistry and Life Sciences (MicroTAS 2016)*, 2016, Dublin, Ireland.

Contributions: L. D. designed, built, and tested the microfluidic control instrument and conceived the application to the male secreted phenome studies with input from M. C.. M. G. and T. L. supervised the research, and provided reagents and funding. All authors reviewed and edited the manuscript.

3.1 Introduction

In the *Animalia Kingdom*, patterns and mechanisms of interaction are extremely diverse and creative. More highly developed animals obviously communicate using vocalizations, facial expressions, postures, and gestures. Insects, like honey bees, may develop behavioral movement sequences as part of the communication process. On the other hand, probably for most living organisms, comprehensive communicative interaction based on the exchange of small signaling molecules plays a major role in behavioral, phenotypic and genetic responses to external cues generated by mates from the same or akin species [72]. For instance, quorum sensing bacteria release molecules called autoinducers to monitor one another's presence and to modulate gene expression in response to changes in population density [73]. Such signaling processes are involved in biofilm formation, antibiotic resistance development and virulence factor expression. In the fruit fly *Drosophila melanogaster*, exposure to sex-specific chemical cues strongly affect physiology, stress resistance, and lifespan [74]. Signaling in mammals is based on a wide range of pheromones, from small volatile molecules to large families of proteins, which control innate social behaviors and regulate hormone levels [75].

3.1.1 Molecular signaling in *C. elegans* populations

C. elegans has a highly developed chemosensory system and is able to modulate a variety of behaviors in response to olfactory and gustatory environmental cues carried with food or by other animals [76-79]. Social communication in *C. elegans* populations via small-molecule signaling, including population density sensing and mating behavior, has been increasingly studied over the last years. In particular, the relevance of ascarosides (ascr), a class of glycolipid-based pheromones containing the sugar ascarylose, has been recognized [80-83].

More recent research by Maures *et al.* shows that male-secreted pheromones may act as signals that can shorten the lifespan of recipient hermaphrodite worms and generate male-induced demise (MID), comprising slow movement, paralysis, general decrepitude, increased incidence of vacuole-like structures and structural decline within the cuticle, muscle, pharynx and intestine [68]. For this study, the researchers designed a male-conditioned assay based on conventional agar plate culture. A male-conditioned plate was prepared by placing 30 young adult males on an *E. coli*-seeded plate for 2 days at 20 °C. Subsequently, after removing all males, an equal number of hermaphrodite L1 larvae was added to the male-conditioned plate. The hermaphrodites were transferred to a new male-conditioned plate every 2 days, for the whole duration of lifespan assay. For negative control, 30 L1 hermaphrodites were cultured on non-conditioned plates. The observed hermaphrodite lifespan shortening could possibly be related to mating [84, 85], but it was shown in this study that only exposure to male-conditioned medium is sufficient, confirming that male-secreted molecules are at the origin of MID in hermaphrodites [68].

Communication via small-molecule signaling controls various aspects of *C. elegans* social behavior, including population density sensing and mating behavior. For instance, it was well-known that a small-molecule signaling mechanism, driven by the so-called dauer pheromone, controls *C. elegans*' dauer arrest, an alternative larval developmental process, triggered by starving or crowding. The mechanism allows survival in adverse conditions for prolonged periods [86, 87]. Butcher *et al.* showed that the dauer pheromone actually consists of several structurally related ascarosides [88, 89]. Furthermore, many aspects of sex-specific and social communication in *C. elegans* are controlled by ascarosides or derived compounds. For example, Simon and Sternberg reported evidence of a diffusive mate-finding cue in *C. elegans*

hermaphrodites [90]. Srinivasan *et al.* found that, at high concentrations, the indole-ascarosides icas#3 and icas#9 attract both hermaphrodites and males, whereas, at lower physiological concentrations, only hermaphrodites are attracted. In addition, icas#3 at concentrations as low as 10 fM increases hermaphrodite aggregation on food [91]. Izrayelit *et al.* demonstrated that the hermaphrodite-produced ascaroside ascr#3 repels hermaphrodites and attracts males, whereas male-produced ascr#10 strongly attracts hermaphrodites. Hermaphrodites respond to extremely low quantities of ascr#10 and it appears that the amount of ascr#10 secreted by a single male may be sufficient to affect hermaphrodite behavior [92]. Maures *et al.* showed that male-secreted diffusible pheromones act as signals that shorten the lifespan of recipient hermaphrodites and generate MID [68]. Interestingly, they could demonstrate that hermaphrodite mutants that were deficient for processing sensory signals, including those from pheromones, were not susceptible to MID. Also, male mutants deficient in ascaroside pheromone biogenesis triggered MID less effectively. It thus appears that males excrete a blend of ascaroside which is involved in generating the reported male-induced phenotypes. However, for the time being, it was not possible to identify more specifically the impact of particular molecules.

3.1.2 Challenges and opportunities for *C. elegans* controlled chemical stimuli sensing

Microfluidic technology has been used for a large variety of *C. elegans* assays, as outlined by several review articles [93-96]. Microfluidic chip-based devices allow for accurate fluidic and environmental control on a scale comparable to the worm size. Microfluidic platforms are therefore well-suited tools to study the behavioral and cellular response of *C. elegans* to controlled chemical stimuli [30, 38, 40, 48, 97, 98]. For instance, Chronis *et al.* designed an olfactory chip (Fig. 3.1A) for delivery of chemical stimuli to the worm nose region [30, 97]. Albrecht *et al.* studied locomotory behavior of *C. elegans* in structured arenas as response to different stimulus patterns (Fig. 3.1B) [40]. Gray *et al.* observed, by creating linear spatial oxygen gradients on-chip (Fig. 3.1C), that social feeding occurs only when oxygen exceeds a *C. elegans*' preferred level [38]. Different approaches for on-chip worm manipulation exist, *e.g.* worm immobilization for worm imaging and phenotyping [34, 45, 99] or stage-dependent worm sorting based on different techniques, such as electrotaxis [63], or flow-sorting [58, 100]. Microfluidic chips, including droplet-based systems, have been used for *C. elegans* development studies [51, 101, 102]. Moreover, automated microfluidic platforms have been developed for quantitative analysis of *C. elegans* longevity [103], for longitudinal monitoring of *in vivo* protein aggregation in neurodegenerative disease *C. elegans* models [104], and for *C. elegans* embryo arraying, phenotyping, and long-term live imaging [67]. However, until now, no microfluidic device has been presented being capable of analyzing alterations in behavioral and morphological phenotypes related to small-molecule signaling on *C. elegans* over the entire lifespan. Compared to conventional *C. elegans* social communication assays on agar plates, microfluidic devices open new opportunities to study small-molecule signaling for the following reasons: (i) the concentration of signaling molecules can be enhanced by confinement of the signaling source in a microfluidic chamber; (ii) the exchange of secreted molecules through microchannels may be well-controlled, either by stable diffusion profiles or by active fluidic transport, and (iii) microfluidic devices allow for culture of distinct worm populations without physical contact, a major advantage if mating effects and signaling should be discriminated.

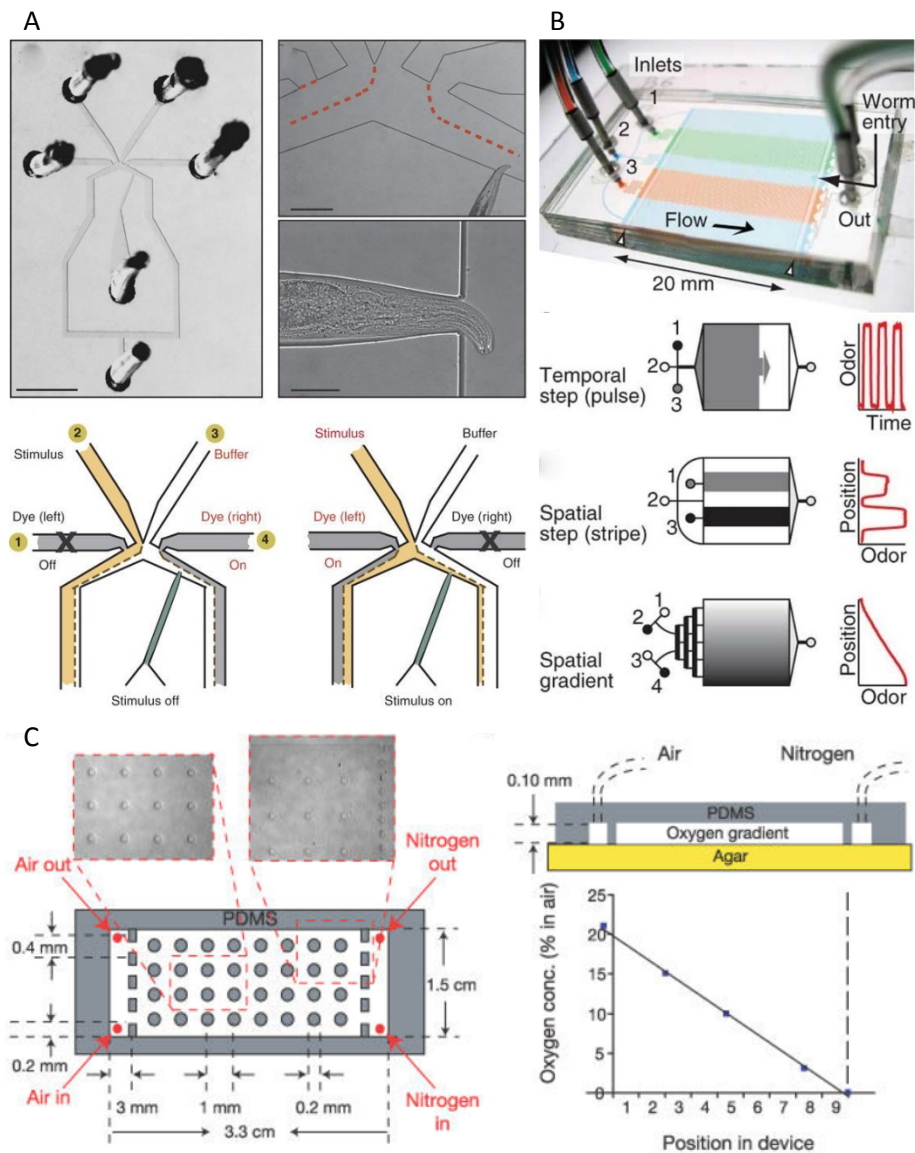


Figure 3.1 Microfluidic technologies for *C. elegans* controlled chemical stimuli sensing.

(A) Olfactory chip. The top view shows a photograph of the chip with a worm loaded and its nose exposure to the chemical delivery channel. The bottom panel shows the control of stimuli loading. Scale bars: left image, 2 mm; right images, 150 μm (reproduced from [30]). **(B)** Stimuli delivery chip. Stimuli can be delivered from the left to the right of the chip with different profiles as shown on the right (reproduced from [40]). **(C)** Oxygen gradient chip (reproduced from [38]).

We propose here a simple and robust microfluidic system that allows studying biocommunication between *C. elegans* populations based on diffusive secreted compounds over the entire lifespan, *i.e.* from L1 larva stage to worm death. Two distinct *C. elegans* populations, consisting of hermaphrodites and male worms, respectively, are cultured in two adjacent chambers of a microfluidic chip. In particular, we designed an on-chip microfluidic assay to evaluate male-induced lifespan reduction and demise in *C. elegans* hermaphrodites in the presence of a physically separated *C. elegans* male population. Controlled exchange of signaling molecules between the two worm populations is performed by periodically activating fluidic transfer of μL -volume aliquots from one chamber to the other. Fine-adjustment of mechanical screw valves allows retaining worms in the chambers during transfer of male-

conditioned medium. An on-demand bacteria supply protocol was applied for worm feeding to meet the specific criteria of this assay, and long-term on-chip culture issues in general. We first confirmed good viability, health and development conditions by on-chip culture of non-conditioned hermaphrodites. Subsequently, lifespan and phenotype alterations of male-conditioned hermaphrodites were analyzed and compared with the non-conditioned control group.

3.2 Microfluidic device design and operation

3.2.1 Overview of the microfluidic device

The *C. elegans* worm chip (Fig. 3.2A) consists of two PDMS worm culture chambers C1 and C2 (5.8 mm long \times 1.4 mm wide \times 150 μ m high) that are connected by a parallel array of 4 fluidic microchannels (2.4 mm long \times 200 μ m wide \times 150 μ m high). Furthermore, each chamber is connected to an outlet (Out1, Out2) via a similar structure. A 10 μ L Eppendorf tip which is plugged into the top PDMS layer of chamber C1 forms a fluidic reservoir that is used as single inlet (In) of the chip (cross-section A-A' in Fig. 3.2A). Worm and bacteria suspensions are first loaded into C1, from where they may be transferred into chamber C2. The microfluidic chambers are large enough to accommodate more than 20 *C. elegans* adult worms. Two different worm populations may be cultured separately in C1 and C2, respectively, in order to study lifespan, phenotype alterations and social behavior under the same environmental conditions but without any physical contact between the two groups. However, diffusive compounds, such as specific signaling molecules released by the worms, and bacteria may be transferred from one chamber to the other through the connecting channel array.

The PDMS chip is clamped mechanically in a PMMA holder (12 cm long \times 10 cm wide). Mechanical screw valves have been developed to confine worm populations in C1 and C2, respectively. For this purpose, 3 small screws (M2 \times 8 mm) have been positioned in the PMMA holder directly above each of the 3 fluidic PDMS channel array in order to control fluidic transfer between the two chambers (valve V2) and towards the outlets (valves V1 and V3, cross-section A-A' in Fig. 3.2A). Rotation of a screw results in downward motion and well-controlled compression of the underlying PDMS layer; thus, the effective cross-section and shape of the 4 channels can be adjusted simultaneously in an accurate and reproducible way (cross-section B-B' in Fig. 3.2A). The valves are operated in an open or nearly-closed state. In the nearly-closed state the effective channel cross-section is so small that only liquid, bacteria suspensions or debris can pass through the valve, whereas larvae and adult worms are retained and remain confined in the chamber for culture and observation. Other screw valves have been reported previously; however, these valves have been incorporated directly into the PDMS chip [105], which makes their fabrication and operation more difficult with respect to our configuration, where a simple rigid PMMA frame is used. A photograph of the whole PDMS chip with 8 independent culture units is shown in Fig. 3.2B. Fig. 3.2C reports a magnified view of a single culture unit with 3 screw valves.

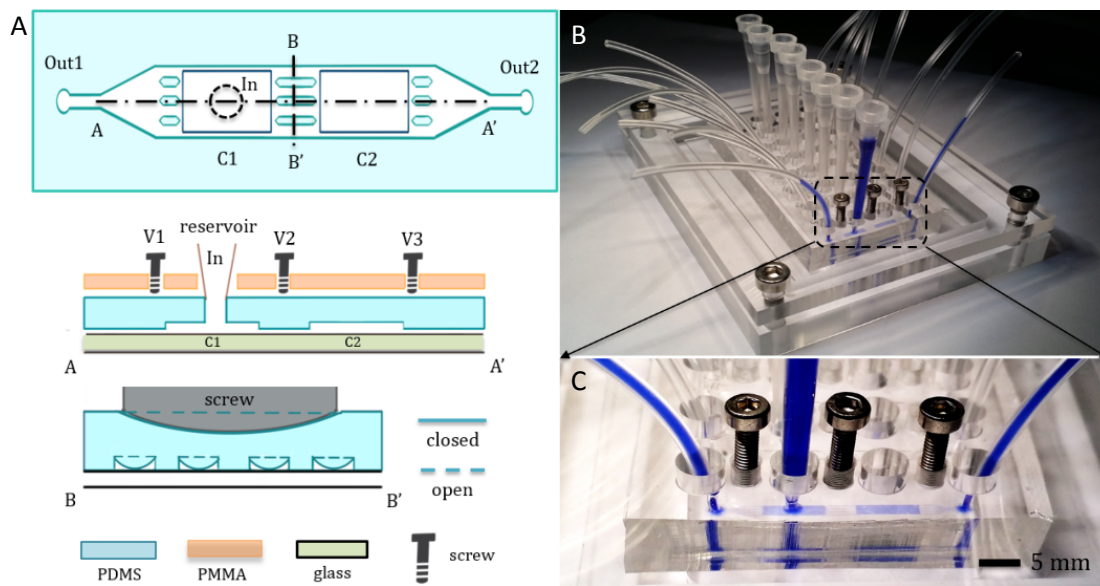


Figure 3.2 Microfluidic worm biocommunication device.

(A) Schematic top and cross-sectional views of the chip layout (not to scale). The PDMS chip (blue) comprises two worm culture chambers (C1, C2) with a reservoir and a single inlet on C1 (In), and two fluidic outlets (Out1, Out2). An array of 4 parallel channels allows for fluidic transfer between C1 and C2, as well as towards the outlets. Three screw valves (V1, V2 and V3) are used for fluidic control and chamber isolation. Cross-section B-B' depicts the working principle of a valve, *i.e.* simultaneous deformation of all 4 channels by controlled pressure applied from the top (solid lines, valve shown in the nearly-closed state, *i.e.* only liquid can pass and worms are blocked). (B) Photograph of the full device with PDMS chip and PMMA holder comprising 8 individual worm culture units. Eppendorf tips used as reservoirs are inserted in the inlet of each chip module. (C) Zoom on a single worm culture unit (filled with blue dye), with tubes connected to the 2 outlets and 3 screws corresponding to valve V1, V2 and V3, respectively.

3.2.2 Device operation

3.2.2.1 Worm loading

After prefilling the device with S-medium, two different worm populations (A and B, male and hermaphrodite worms, for instance) may be introduced in chamber C1 and C2, respectively, by using the same inlet reservoir (In). The loading sequence is depicted in Fig. 3.3A(i)-(iii). 5 μ L of worm A suspension containing typically about 10 worms is first pipetted into the reservoir. Driven by gravity, all worms sink to the bottom of the reservoir and thus into C1 (Fig. 3.3A(i)) after 3 to 5 min. The whole worm A population may then be transferred to C2 by gentle suction through Out2 by means of a glass syringe (Fig. 3.3A(ii)). During transfer, valve V2 is open and valve V3 is in nearly-closed state, meaning that all worms of population A are retained in C2, whereas liquid can be sucked to the outlet. The worm A population is then confined inside C2 for counting by closing V2. Subsequently, worm B population is loaded into the reservoir and settles in C1 (Fig. 3.3A(iii)). An inverted microscope is used for real-time worm observation throughout the whole worm lifespan.

3.2.2.2 *E. coli* supply protocol

For on-chip worm culture, *E. coli* suspensions have to be introduced in the device as food source. A major problem generally encountered in on-chip worm cultures is clogging of fluidic channels and constrictions due to bacterial aggregation and adhesion. Some research groups apply continuous flow protocols for bacteria supply to tackle this problem [101]. However, it

has also been shown that shear forces in flow-through devices, including microfluidic devices, may promote the growth of bacterial biofilms and filamentous structures called streamers, that eventually may clog up a microfluidic structure [106]. More importantly, as our experiments rely on the controlled transfer of diffusive compounds released by the worms, continuous flushing of the two worm culture chambers by bacteria solution could present a significant problem. To circumvent these issues, we apply a sequential an on-demand bacteria supply protocol, thus minimizing the disturbance of the biochemical environment in the worm culture chambers by the liquid flow. The protocol consists in periodically refilling the culture chambers with fresh bacterial suspension (initial concentration in the chamber $\approx 10^9$ cfu/ml), only when food is actually required. For worm feeding, *E. coli* OP50 suspension was pipetted into the reservoir and deposited in C1 after sedimenting for 1 to 2 hours (Fig. 3.3B(i)). Subsequently, part of the *E. coli* suspension is transferred to C2 by suction from Out2. Screw valves V2 and V3 were set to the nearly-closed state to block the worms inside C1 and C2, respectively (Fig. 3.3B(ii)). On-demand filling was repeated at time intervals of 2 to 5 days as a function of food consumption, which varies with age and development stage. Fig. 3.3D shows representative images of bacterial worm feeding. In this case, as in a typical lifespan experiment, L1 larvae were first loaded in C2 (Fig. 3.3D(i), without bacteria), which was then uniformly filled with a bacterial suspension, introduced by transfer from C1 (Fig. 3.3D(ii)). After 3 hours, the bacteria distribution became heterogeneous, showing depleted zones around the larvae (brighter spots in Fig. 3.3D(iii)) and areas with higher concentration (darker zones in Fig. 3.3D(iii)). If bacteria or debris aggregation inside the chambers became too important, fine adjustment of the screw valves allowed rinsing the device with fresh bacterial suspension without removing the worm populations.

3.2.2.3 Progeny removal

During an on-chip lifespan experiment, adult worms produce larvae which make scoring and analyzing of the aging population in the culture chamber more difficult. We therefore removed their progeny from the chambers every 2 days during the worms' reproductive period. In order to separate adults and progeny in a worm culture on agar plate, all adults must be transferred manually onto fresh plates. The situation may be even worse in well-plate liquid cultures, since there is no convenient way to extract progeny from adults, and it is often best to grow just a single generation of worms in order to avoid adverse effects of crowding, such as dauer arrest. With our microfluidic design, selective progeny removal is straightforward. As indicated in Fig. 3.2A (cross section A-A'), worm chambers are three times higher than the connecting channels, including the narrow chamber rims ($150\ \mu\text{m}$ vs $50\ \mu\text{m}$, respectively). At sufficiently low flow rates, this structural hurdle retains adult worms (diameter $\geq 50\ \mu\text{m}$) in C1 or C2, respectively. Screw valves V1 and V3 may be fully opened in order to remove small L1 larvae by applying mild suction either from Out1 or Out2, respectively (Fig. 3.3C).

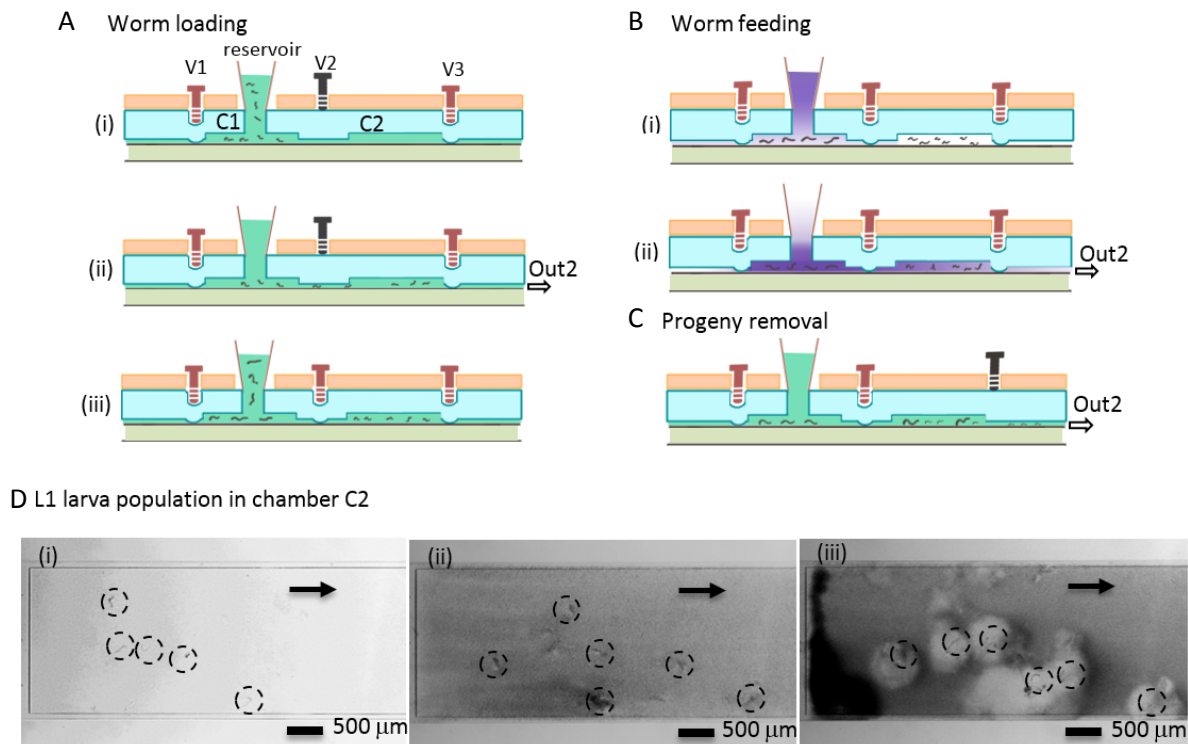


Figure 3.3 On-chip worm handling.

(A) Sequence for loading two different worm populations into chamber C1 and C2, respectively: (i) a suspension of worm A loaded into the reservoir sediments rapidly inside chamber C1; (ii) worms A are transferred to C2 by gentle suction from outlet Out2 (V2 open, V3 nearly-closed state, *i.e.* only liquid can pass); (iii) worms A are confined in C2 (V2 and V3 nearly-closed), and C1 is refilled with a population of worm B. **(B)** Worm feeding: (i) *E. coli* OP50 settle at the bottom of C1 after loading; (ii) partial transfer of *E. coli* into C2 by suction from Out2 (V2 and V3 nearly-closed, *i.e.* only bacteria may pass, worms remain confined in C1 and C2, respectively). **(C)** Progeny removal (in this case from C2): Adult worms are retained in C2 due to the reduced height of the chamber rims and channels, whereas V3 is fully open for L1 larvae transfer to Out2. **(D)** Photographs of *C. elegans* L1 larvae in C2 (highlighted by dashed circles): **(i)** after loading by transfer from C1 (channels on the left border of C2 not visible in the image); **(ii)** uniformly distributed *E. coli* shortly after supply; **(iii)** image taken 3 hours after *E. coli* supply. *E. coli* around the larvae was almost completely eaten (brighter areas), whereas in other regions, bacterial growth increased the *E. coli* density (darker areas).

3.3 Male-conditioned vs non-conditioned on-chip assays

3.3.1 On-chip assays for studying male-induced phenotype alterations

The goal of this work was to demonstrate that biocommunication through diffusive compounds can take place in a microfluidic device via active transfer of μL -aliquots of conditioned medium and controlled exposure of the receiving worm population to this biochemical cue. We demonstrate the feasibility of this approach by monitoring possible effects of the presence of male *C. elegans* nematodes on the opposite sex (hermaphrodites), including the assessment of male-conditioned lifespan shortening and MID. In particular, the chip was designed to test the influence of male-secreted compounds on hermaphrodites that are physically separated from males, so that any observed effect cannot result from mating. We compare two on-chip assays: (i) non-conditioned assays (negative control, Fig. 3.4A),

where only hermaphrodites, which we denote as WT her(-males), were cultured on-chip and (ii) male- conditioned assays (Fig. 3.4B), where we placed males and hermaphrodites separately in chamber C1 and C2 to monitor the lifespan, phenotype and other features of male-conditioned hermaphrodites, which we denote as WT her(+males). The device was placed in an incubator at 20 °C during the entire assay duration, except for short exposure to room temperature during bacteria loading, fluidic operations and observation under the microscope.

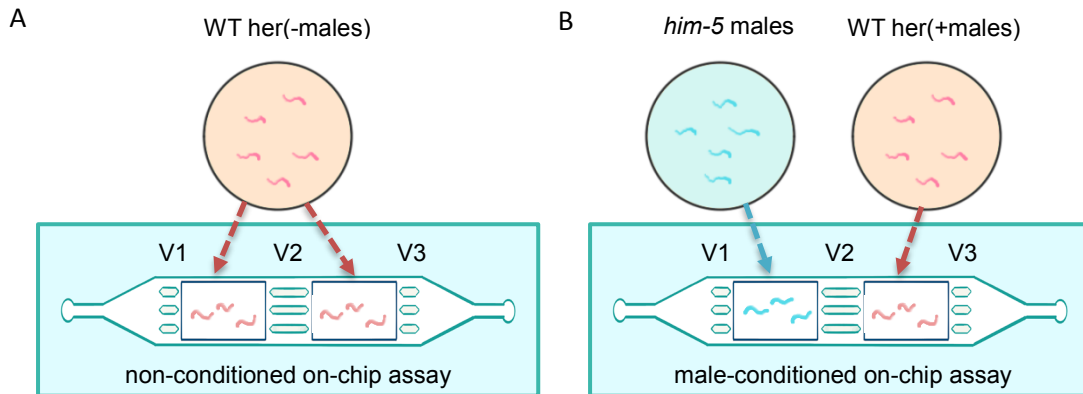


Figure 3.4 On-chip assays for studying male-induced phenotype alterations in *C. elegans* hermaphrodites.

(A) Non-conditioned assay: WT hermaphrodites [WT her(-males)] are simultaneously cultured in both chambers of the chip under equal conditions. **(B)** Male-conditioned assay: *him-5* males and WT hermaphrodites [WT her(+males)] were loaded into chambers C1 and C2, respectively, and cultured simultaneously. Controlled biochemical communication was allowed by activating liquid transfer through the connecting channels between the chambers, whereas worms remained confined in the chambers.

3.3.2 Non-conditioned on-chip assays

3.3.2.1 Early development of hermaphrodites

On-chip culture conditions are very different from conventional agar plate assays and key parameters, in particular efficient bacterial food supply, may have strong impact on the worm development. Lack of healthy conditions can result in premature and unnatural death [107]. We therefore examined how growth of WT hermaphrodite worms without the presence of males in our microfluidic chip compares with culture on agar plates. 10 μ L of L1 larvae (day 1) suspended in S-medium was first loaded in each reservoir of the 8 individual chip modules. All worms were distributed evenly in chamber C1 and C2, and the number of worms was adjusted to 10 ± 2 worms per chamber by fluidic control to avoid effects due to crowding. Subsequently, *E. coli* OP50 was supplied to all chambers. Early development up to young adult (YA) stage of non-conditioned WT her(-males) hermaphrodites was evaluated by measuring the body diameter (Fig. 3.5A, red data triangles) and length (Fig. 3.5B, red data triangles) at four different stages, *i.e.* the larva stages L1 (day 1), L3(day 2), L4 (day 2), and YA stage (day 3). L2 data was not considered here, since the barely visible morphological differences not allow clear distinguishing L1 from L2 worms (L1 data was taken immediately after hatching). The resulting mean values for diameter/length (L1: 12.1 μ m/274 μ m, L3: 20.8 μ m/485 μ m, L4:

44.6 μm /661 μm , YA: 64.0 μm /1036 μm ; N=10) agree well with well-known values obtained with conventional substrates [108], indicating that our chip assay protocol provides adequate conditions for *C. elegans* culture. In order to visually demonstrate normal worm development, viability and embryo production, Fig. 3.6 shows a series of images of WT her(-males), cultured on-chip at different stages of their life from day 2 (L4 stage) to day 19 (adults close to dead).

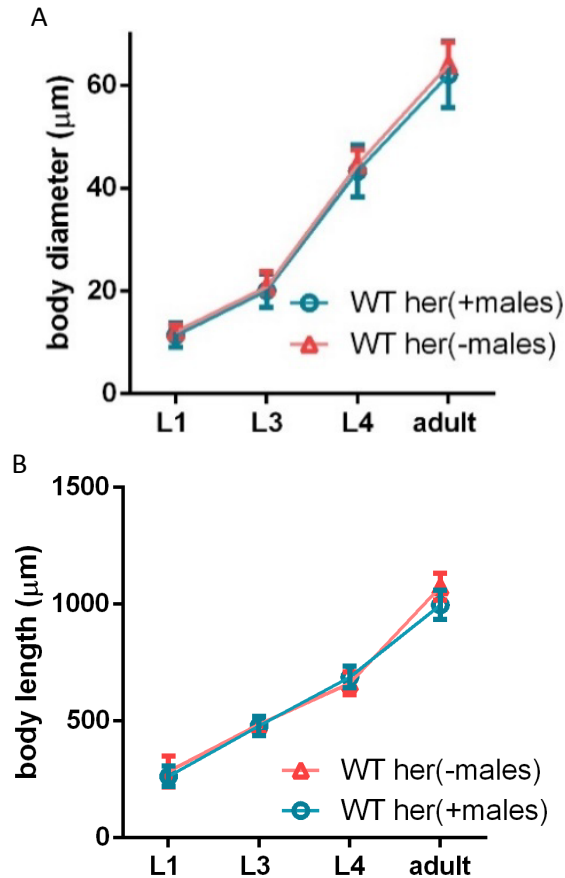


Figure 3.5 Early development of WT *C. elegans* hermaphrodites.

Early development of WT *C. elegans* hermaphrodites in a non-conditioned (WT her(-males), red data triangles) and in a male-conditioned on-chip culture assay (WT her(+males), blue data circles). Body diameter (A) and worm length (B) were measured at larva stage L1, L3, L4 and for adults (data are mean values \pm SD, t -test $P > 0.1$, N=15). The continuous presence of young males since the beginning of the hermaphrodites' life (day 1) did not have an adverse effect on hermaphrodite growth.

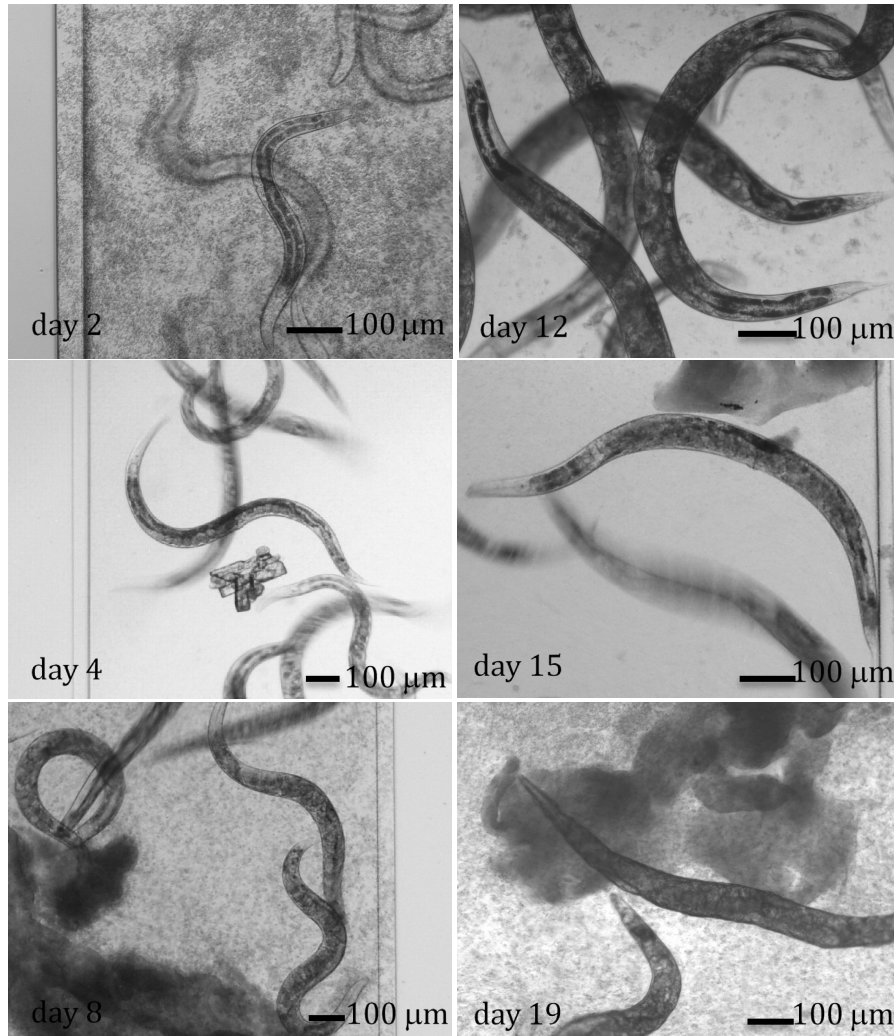


Figure 3.6 Validation of *C. elegans* hermaphrodite on-chip culture over the whole lifespan.

Consecutive images confirm normal development of WT her(-males) worms (no males are present on the chip). After hatching (day 1), L1 larvae were immediately loaded into the chip. The image taken at day 2 corresponds to the L4 larva stage, subsequent images show adult worms, *i.e.* in gravid state (day 4 to 12) or close to dead (day 19). A concentrated *E. coli* suspension has been loaded into the microfluidic chamber anytime when necessary, *i.e.* after nutrient depletion. Images at day 2, 8 or 19 show chambers with high numbers of bacteria, whereas at day 4, 12 and 15 nearly all bacteria have been consumed.

3.3.2.2 Evaluation of lifespan

Most *C. elegans* lifespan studies reported to date have been performed using agar plates or 96-well plates at 20 °C [109]. To evaluate the non-conditioned WT her(-males) on-chip lifespan, hermaphrodites in chamber C2 were scored. Dead or alive state was defined by the presence or absence of swimming motion or ‘thrashing’. At the beginning of an experiment (L1 larva stage, day 1), and every other day, the total number of alive worms was counted and observation was stopped when the last worm died. Worms usually do not thrash all the time, especially under conditions of sufficient feeding. Thus, for reliable observation and counting of thrashes, worms were stimulated by gently oscillating flows or by blue fluorescent light. For worms close to the end of their lifespan, even relatively strong stimuli did not necessarily

induce thrashing anymore. In this case, subtle movements of the pharyngeal terminal bulb due to bacteria ingestion were observed to determine whether the worm was still alive [110]. Moreover, worms exhibiting phenotypes that will lead to early and unnatural death, such as “bagging,” *i.e.* hatching of live progeny inside the hermaphrodite, or vulval rupture, *i.e.* the eruption of the intestine from the worm vulva, were scored as censored, in accordance with what is typically done for agar-based lifespan tests [111]. Fig. 3.7A shows the survival curve of WT her(-males) worms cultured on-chip (red curve, N=68). The mean, median and maximal values for on-chip lifespan were 15, 14 and 19 days, respectively. These values compare well with those reported for agar plate cultures (16, 15 and 24 days) and for liquid culture systems (13, 12 and 22 days) [112].

Until now, to the best of our knowledge, there is no data available showing the entire on-chip *C. elegans* lifespan from L1 to death. Complicate chip operation, parameter control over extended periods and bacteria clogging are issues that may adversely affect long-term culture assays on microfluidic chips. Furthermore, several environmental parameters, in particular temperature, are known to significantly affect *C. elegans* lifespan, so that data provided by different authors often cannot be directly compared. For instance, Hulme *et al.* reported on-chip culture and aging studies from L4 to death that showed an average lifespan of 10 ± 2 days at 24 °C [101]. Other researchers performed on-chip worm culture over shorter periods. For example, Krajniak *et al.* showed a microfluidic chip assay for early stage development from L1 to L3 Larva, at 21 °C [102]. Wen *et al.* presented a multifunctional droplet microdevice enabling culture and study of the developmental process of *C. elegans* from L1 to the adult stage, *i.e.* over 4 days, at 20°C [51]. Cornaglia *et al.* showed L1-to-adult on-chip worm development at 24°C [104]. Xian *et al.* developed a worm culture microfluidic chip for analysis of longevity and lifespan from the second day of adulthood to death, *i.e.* over 12 days at 25°C [103].

3.3.2.3 Thrashing frequency

C. elegans shows certain characteristic phenotypes that can be correlated with aging, such as deterioration in muscle function, and an increase in age-associated autofluorescence in the intestine [110]. Measuring these age- and longevity-associated phenotypes can therefore be a useful way of assessing the rate of aging for a given worm genotype or for specific conditions and can also suggest a mechanism for an observed change in lifespan. Here, we have chosen to assess the thrashing behavior of the worms in the microfluidic chip, in particular the thrashing frequency, to measure the age-related regression. This method is also used with agar plate worm cultures [110]. The thrashing frequency of WT her(-males) was measured from day 3 (YA) until death (Fig. 3.7B, red curve). Fig. 3.7B reveals that there is a slight decline in the thrashing rate during the reproductive period, *i.e.* for about five days after YA stage (*i.e.* from day 3, 55 ± 5 thrashes/30 s to day 8, 50 ± 5 thrashes/30 s). For worms at a more advanced age (>10 days) faster deterioration appears, *i.e.* they cannot sustain high thrashing frequency anymore. Furthermore, the rhythmic pattern of thrashing in aged worms became increasingly irregular compared to smooth thrashing of young adult worms (data not shown). In contrast, in a previously reported assay on agar plate, decline of the thrashing rate started earlier (at day 3 to 4) and decreased in a more continuous manner over the lifespan [113].

3.3.3 Male-conditioned on-chip assays

3.3.3.1 Worm population control

Lifespan, behavior and phenotypes of hermaphrodites were investigated in the presence of males on the chip. For male-conditioned experiments, 8-12 WT hermaphrodites in the L1 larva stage (*i.e.* at day 1 after hatching) were first introduced in chamber C2 of each of the 8 individual worm culture units, according to the worm loading protocol described above. Subsequently, young male worms were selected from *him-5(e1490)* plates and loaded into chamber C1. The male to hermaphrodite ratio was adjusted to one for all chip units. Every 2 or 3 days old *him-5(e1490)* males were removed from C1 by gentle suction through outlet Out1 (V1 open, V2/V3 nearly closed) and were replaced by an equal number of young males, in order to keep a fresh population of males on-chip. Furthermore, the WT hermaphrodite population in C2 was regularly checked for the presence of WT male worms, possibly generated by hermaphrodite self-fertilization. As the larval male is almost indistinguishable from the hermaphrodite, control was carried out after 3 days when worms were adult. In case that males were found, the assay would have been rejected. However, since the natural male production rate is extremely low [114], we never found WT males in our experiments. During the reproductive period, bacteria were added to C2 at the time of progeny removal.

3.3.3.2 Exchange of male-conditioned medium

In our device, male and hermaphrodites are always confined in separate chambers and biochemical communication is possible only by exchange of diffusive secreted compounds through the channel array connecting chambers C1 and C2. An assay merely based on diffusion of the compounds through the microchannels could in principle be implemented. In this case, we may calculate the diffusion coefficient D_{AB} of a solute A (*e.g.* a pheromone) in a solvent B (buffer solution) by using the semi-empirical Wilke–Chang equation:[115]

$$D_{AB} = \frac{7.4 \times 10^{-8} T \sqrt{\varphi_B M_B}}{\eta_B V_A^{0.6}}$$

Equation 3.1 Semi-empirical Wilke–Chang equation.

where T is the absolute temperature, M_B the molecular weight of the diffusing molecule, η_B the viscosity (1.002 mPa for water at 20°C), φ_B is the association coefficient (2.6 for water) and V_A is the molar volume at the normal boiling point. We estimated V_A for a typical ascaroside according to Schoeder's method[116] (ascr#2, $V_A \approx 329$ cm³/mol) and found a diffusion coefficient $D_{AB} \approx 4.7 \times 10^{-6}$ cm²/s. Considering a channel length of $L = 1.4$ mm in our device and a diffusion time $t = L^2 D_{AB}^{-1}$, diffusion of small molecules through the connecting channels would therefore take about 1 hour. Given the long diffusion time scale and related strong concentrations gradients between C1 and C2, an approach merely based on diffusive compound exchange does not seem appropriate for well-controlled assay conditions. Instead, we implemented active liquid transfer of male-conditioned medium from C1 to C2, which is quasi-instantaneous and efficiently increases the exposure of hermaphrodites to male-secreted compounds. For this purpose, about 1 μ L of male-conditioned solution in chamber C1, *i.e.* an aliquot that corresponds approximately to the volume of the microchamber (total volume 1.24 μ L), was transferred into C2 by gentle suction from outlet Out2. Valves V2 and V3 are in the nearly-closed state, *i.e.* only liquid but no worms can pass. A single aliquot was

transferred per day. Transfer was carried out intentionally once per day or coincided with bacterial supply or progeny removal. At this transfer frequency we expect that a reasonably high concentration of freshly secreted compounds can build up in C1 prior to transfer into C2. With this method, diffusive gradients are minimized and the hermaphrodite population in C2 is instantaneously exposed to a uniform compound concentration. Chamber C1 was simultaneously refilled through the reservoir with S-medium and/or OP50 solution.

3.3.3.3 Male-induced reduced lifespan and accelerated aging

The early development of male-conditioned WT hermaphrodites (WT her(+males), blue data circles in Fig. 3.5) was evaluated by measuring the diameter (Fig. 3.5A) and length (Fig. 3.5B) of hermaphrodites at four different stages, *i.e.* larva stages L1 (day 1), L3, L4 (day 2), and YA stage (day 3) with a digital microscope (*Keyences VHX-700F*). Data for non-conditioned hermaphrodites is also reported (WT her(-males), red data triangles in Fig. 3.5). The mean body diameters of WT her(+males) (L1: 11.4 μm , L3: 20.1 μm , L4: 43.3 μm , YA: 62.1 μm , N=10) are very similar to WT her(-males).

Likewise, the mean body lengths of WT her(+males) (L1: 268 μm , L3: 475 μm , L4: 678 μm , YA: 1006 μm , N=10) are comparable to WT her(-males). No male-induced growth rate decline or related demise is observed in this early development phase. This is possibly due to the fact that WT larvae sensing of males is only weakly developed before sexual maturity is reached at the adult stage. Our observation is consistent with a previously published comparable study on agar plates, where no significant difference between two survival curves showing shortened lifespan for WT her(+males), one starting from L1 stage (day 1) and another one starting from adult stage (day 4), was observed [68]. Adequate food supply and accurate temperature control are probably the two most important factors in early development.

Most interestingly, the presence of male worms in an adjacent chamber reduced the lifespan of hermaphrodites on the chip. Fig. 3.7A compares the survival rate of WT hermaphrodites cultured in a male-conditioned chamber and the previously determined curve for a non-conditioned WT hermaphrodite population. In particular, the mean, median and maximal values of lifespan were significantly shorter in the WT her(+males) group (11, 10 and 14 days, respectively; N=61) than in the WT her(-males) group (15, 14 and 19 days, respectively; N=68), corresponding to a more than 26 % decrease in lifespan (Fig. 3.7A). This difference in lifespan is even more pronounced than the about 20% decrease in previously reported experiments performed on male-conditioned agar plates [68]. This finding possibly indicates that exposure to diffusive secreted compounds can be enhanced in our microfluidic chip with respect to agar plates. As the number of worms in the microfluidic chambers was relatively small, and comparable for non-conditioned and male-conditioned on-chip experiments, we conclude that lifespan reduction is not generated by a possible adverse effect due to worm crowding in a confined space. Such lifespan assays were repeated four times using a new microfluidic chip for each experiment (see Table 3.1). Median lifespan values (\pm SD) of the four independent experiments are 9.8 ± 0.3 days for male-conditioned WT her(+males) and 13.5 ± 0.3 days for non-conditioned WT her(-males) assays. Small SD-values indicated a very good reproducibility of successive on-chip assays, despite possible variations in environmental conditions, such as food availability, ambient temperature or number of confined worms.

On-chip cohabitation of males and hermaphrodites also induced behavioral phenotype modifications related to accelerated ageing of the hermaphrodite population. As for non-conditioned experiments, the thrashing behavior was observed in order to evaluate the muscular tissue decline in hermaphrodites. Fig. 3.7B compares the reduction in thrashing

frequency for male-conditioned hermaphrodites to non-conditioned hermaphrodites on-chip and shows that the thrashing curve for WT her(+males) declines faster with increasing age than for WT her(-males). This is in-line with the more pronounced structural decline observable in WT her(+males) hermaphrodites body muscles. Interestingly, in both cases, thrashing starts slowing down already from early adulthood, *i.e.* from about day 3 after hatching, whereas as the lifespan curve starts dropping only at day 7-8 which reveals that all worms suffer from a period of body muscle decline before death.

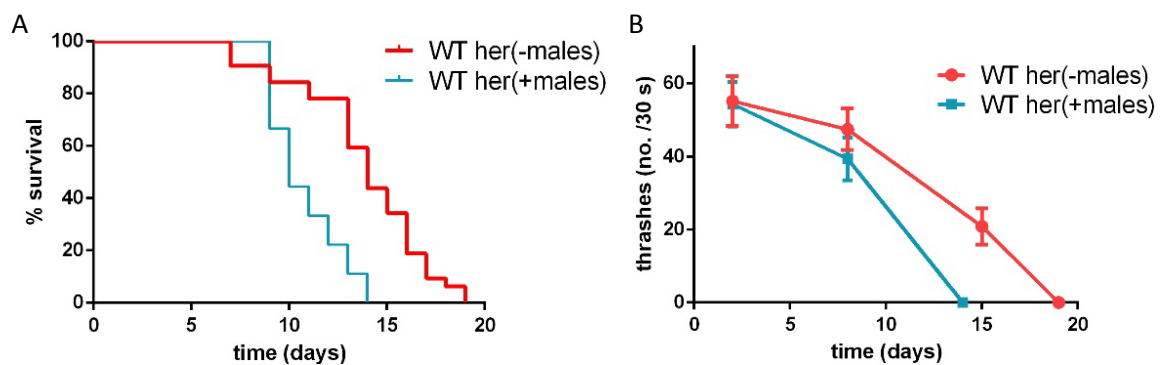


Figure 3.7 Survival rate and behavioral study for WT *C. elegans* hermaphrodites cultured on-chip.

(A) Lifespan of non-conditioned [WT her(-males), red curve] and male-conditioned WT hermaphrodites [WT her(+males), blue curve]. A mean lifespan of 11 days was determined for WT her(+males) whereas the WT her(-males) control group reached a mean value of 15 days (log rank $P < 0.001$). Hermaphrodites' mean lifespan shortened for about 4 days when continuously kept in the presence of young males in an adjacent chamber of the chip from the beginning of their life (day 1). **(B)** Age-related reduction of swimming frequency (thrashing) for WT *C. elegans*, showing faster decline for male-conditioned [WT her(+males), blue data points] with respect to non-conditioned [WT her(-males), red data points] (data are mean values \pm SD, one-way ANOVA post hoc test; $P < 0.0001$).

Table 3.1 Male-conditioned and non-conditioned on-chip assays.

Hermaphrodites' lifespan analysis for male-conditioned and non-conditioned on-chip assays, corresponding to data shown in Fig. 3.7A and repeated experiments. Statistical analysis was performed on Kaplan-Meier survival curves in Prism 6 by log rank tests.

Assay	Lifespan mean/median/max (days)	#Worms	Censored	log rank P value		
1	WT her(-males)	15/14/19	81	13		Fig. 3.7A
	WT her(+males)	11/10/14	69	8	vs WT her(-males), $P < 0.0001$	Fig. 3.7A
2	WT her(-males)	14/13/21	75	16		not shown
	WT her(+males)	11/10/16	86	10	vs WT her(-males), $P < 0.0001$	not shown
3	WT her(-males)	14/13/18	81	17		not shown
	WT her(+males)	10/9/14	71	15	vs WT her(-males), $P < 0.0001$	not shown
4	WT her(-males)	14/14/18	73	20		not shown
	WT her(+males)	11/10/14	64	12	vs WT her(-males), $P < 0.0001$	not shown

3.3.3.4 Male-induced vacuole-like structures

Morphological phenotypes, indicating a general decrepitude due to advanced aging, such as structural decline within the cuticle, muscles, pharynx, and intestine, were also observed on-chip for hermaphrodites exposed to male-secreted compounds. In particular, vacuole-like structures appeared frequently in WT her(+males) bodies, whereas such structures have nearly not been observed in the non-conditioned hermaphrodites. An increased incidence of such structures has been observed earlier on male-conditioned agar plate assays [68]. Images shown in Fig. 3.8 compare the morphology of WT her(+males) at day 4 and day 10, and WT her(-males) at day 10. Images of head, mid-body region and tail are shown. WT her(+males) hermaphrodites at day 4 (Fig. 3.8A-D) do not exhibit any particular morphological abnormality. However, WT her(+males) at day 10 (Fig. 3.8E-H and Fig. 3.8M) revealed vacuolar-like structures appearing in body wall muscles, the intestine and the head. A negative WT her(-males) control group of hermaphrodites cultured in the absence of males (Fig. 3.8I-L) did not show any particular advanced MID at day 10. A direct comparison of WT her(-males) (Fig. 3.8N) and WT her(+males) (Fig. 3.8O) obviously demonstrates a general structural decline at day 12 of a male-conditioned hermaphrodite's life.

For a more detailed evaluation, we calculated the percentage of hermaphrodite worms displaying vacuolar-like structures as a function of age (Fig. 3.9, blue data points). The plot indicates that the first worms display visible vacuolar structures on day 7, *i.e.* roughly at the end of the reproductive period, then the percentage increases to nearly 70% (N=42) at day 12, and remains constant until the end of the lifespan curve for WT her(+males) worms at day 15. For the WT her(-males) negative control (Fig. 3.9a, red data points), only 1.5% of the hermaphrodites (N=1 experiment) showed vacuolar-like structures at day 15 and significantly lower incidence of general structural decline. As notified by Fig. 3.9B, male-induced vacuolar-like structures were mainly found in areas of worm bodies where the main organs, such as pharynx and intestine, are located, *i.e.* in the mid-region (close to 100%) and in the head (about 90%), whereas in the tail these structures appeared to a lower extent (around 45%).

However, the origin of these structures and their impact on the worm physiology is still unclear. Maures *et al.* identified several genes, whose expression was increased in hermaphrodites in response to males. RNA interference (RNAi) used to decrease expression of three specific genes (*ins-11*, *F11A5.3*, and *utx-1*) partially rescued MID [68]. Van Gilst *et al.* showed that deletion of the *C. elegans* NHR gene *nhr-49* yielded worms with elevated fat content and shortened lifespan. In these worms vacuoles appeared in the intestine and gonad [117]. Besides, Herndon *et al.* also found vacuole-like structures in aged hermaphrodite and remarked that these structures are visually similar to neurons that die in response to ion channel injury [118]. As an additional indication in order to evaluate the impact of vacuolar-like structures, we measured the average survival time of the male-conditioned worms after such structures had been first detected in the worm. Fig. 3.9C shows that WT her(+males) worms stayed alive for a mean period of only about 3 days after detecting first vacuolar-like structures. This might suggest that decreased lifespan of hermaphrodites may possibly be related to enhanced wearing out of the body due to such structures.

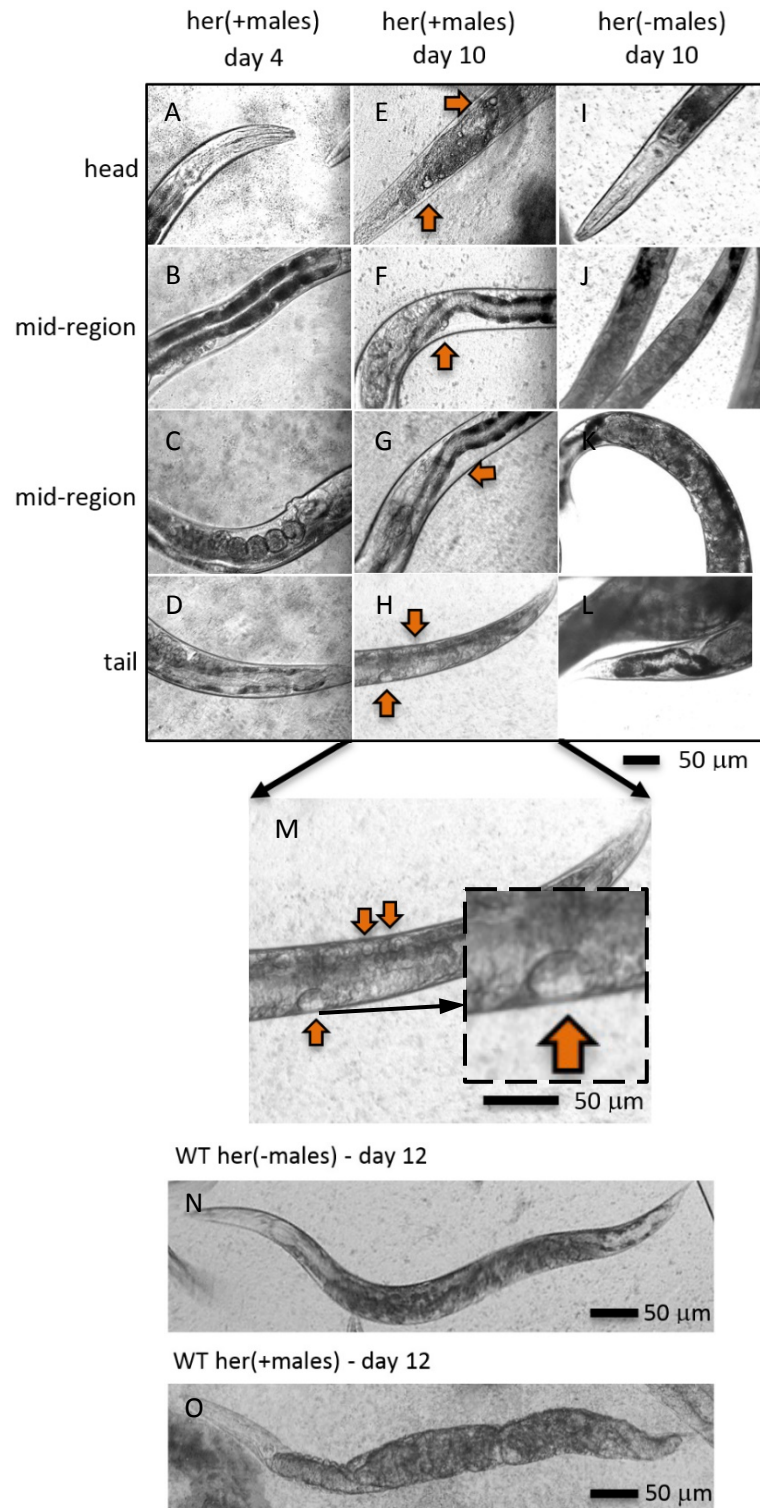


Figure 3.8 WT hermaphrodites with male-induced demise.

Representative images (10x) of different body locations of on-chip cultured male-conditioned WT her(+males) and non-conditioned WT her(-males) hermaphrodites are shown. **(A-D)** Details of WT her(+males) bodies at day 4, showing normal development. **(E-H)** Images taken at day 10, where WT her(+males) worms display vacuolar-like structures (indicated by yellow arrows) that correspond to morphological changes normally observed at a more advanced age. **(I-L)** WT her(-males) at day 10 do not show similar demise. **(M)** Zoom on vacuolar-like structures shown in **(H)**. **(N and O)** A general structural decline in WT her(+males) is clearly visible by comparison with WT her(-males) on day 12.

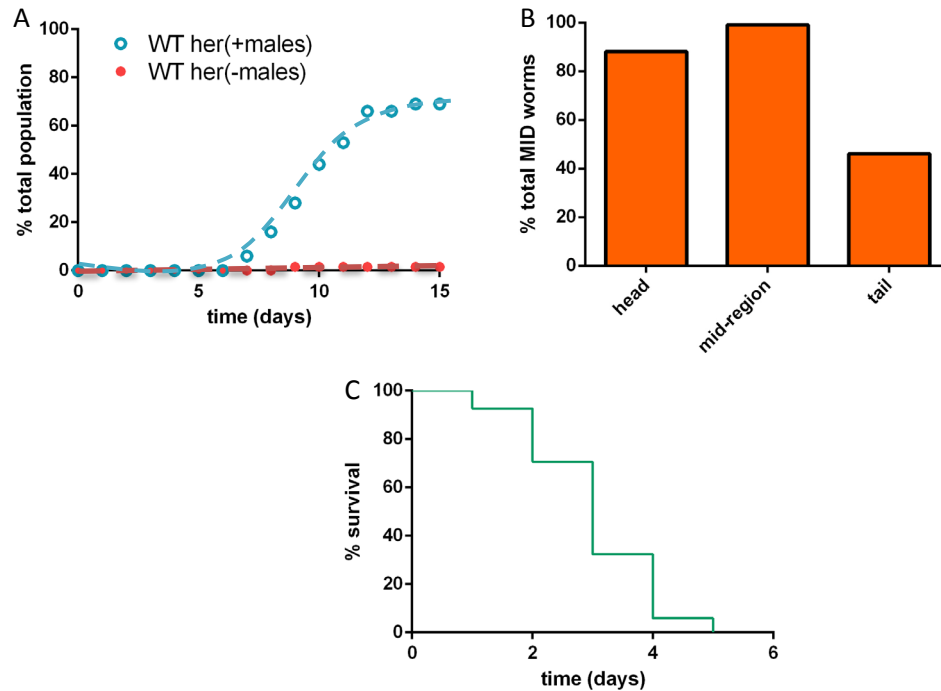


Figure 3.9 Hallmarks for male-induced demise.

(A) Percentage of hermaphrodite worms displaying vacuolar-like structures. In the male-conditioned group [WT her(+males), blue data points] the first worms developed visible vacuolar-like structures on day 7, and on day 15 nearly 70% displayed this type of structure. For the negative control [WT her(-males), red data points], only 1.5% of the hermaphrodites developed vacuolar-like structures at day 9. **(B)** Distribution of vacuolar structures in WT her(+males) worm bodies with MID. In nearly all affected worms, vacuoles mainly appeared in the mid-region of the body and in the head. **(C)** Worm survival time after vacuolar structures had been first detected. WT her(+males) worms stayed alive for a mean period of about 3 days ($N=42$ deaths, log rank $P < 0.0001$) after detecting vacuolar-like structures.

3.4 Materials and methods

3.4.1 Materials

The poly(methyl methacrylate) (PMMA) holder was fabricated by an EPFL workshop (EPFL-ATPR). Microliter glass syringes (ITO corporation, Japan) were purchased from Carl Roth GmbH (Arlesheim, Switzerland) and 1 ml borosilicate H-TLL-PE syringes from Innovative Labor Systeme GmbH (Stutzerbach, Germany). All the other materials are the same as what is shown in section 2.4.1.

3.4.2 Worm strains culture and preparation

Worm culture and synchronization methods are the same as what are introduced in the section 2.4.2. *him-5(e1490)* strain was provided by the Caenorhabditis Genetics Center (University of Minnesota). For transfer into the on-chip reservoir, L1 larvae were collected from the NGM plates by rinsing with filtered S-medium. Subsequently, the worms were gently washed twice by centrifugation and resuspension in fresh S-medium. The worm density was determined by counting the number of L1 worms in a 5 μ L droplet of suspension on a glass slide. The density was then adjusted to 2 - 5 worm/ μ L by adding S-medium. Such populations

consist mainly of WT hermaphrodites, with typically only 0.2 % of male worms [114]. A common way to obtain WT male worms on agar plates is to apply a heat shock treatment on hermaphrodites which increases the male production rate. Subsequently, mating plates with an enhanced number of male worms may be prepared [119]. However, heat shock exposure usually takes about 4 to 6 hours and maintenance of WT males is labor-intensive. To avoid this procedure, we have chosen to use the *him-5(e1490)* mutant strain that generates about 30 % male worms [114]. These mutants do not differ in behavior and anatomy from WT males. To obtain a synchronized population on-chip, young males (day 2) were visually identified, picked out from *him-5(e1490)* plates, and directly loaded into the chip. As food source for the on-chip assay, a single colony of *E. coli* OP50 was taken from a streak plate, inoculated into L-Broth and cultured overnight at 37°C. The bacteria concentration was adjusted to approximately 10¹² cfu/ml prior to loading into the on-chip reservoir. Bacterial suspension was stored at 4 °C when not used for an experiment.

3.4.3 Device fabrication

We used PDMS soft lithography to fabricate the microfluidic chip (blue in Fig. 3.2A, 76 mm long × 52 mm wide). The master mold for the fluidic culture layer was made by a two-step process. First, 50 μm high structures were created by dry etching of a Si wafer (*Alcatel AMS 200SE*) defining the shallower features of the chip, *i.e.* the fluidic transfer channels and the chamber rims. Subsequently, a 100 μm thick SU8-100 layer was spin-coated on the wafer and patterned to increase the total height of C1 and C2 to 150 μm. The surface of the patterned wafer was treated with Trimethylchlorosilane (TMCS) in a vacuum desiccator to prevent adhesion of PDMS upon demolding. PDMS (base-to-curing agent ratio 10:1) was poured onto the mold to obtain a 5 mm thick layer for sufficient mechanical stability of the final chip. After curing at 70 °C for 2 h, the PDMS layer was peeled off and devices were cut into shape. For fluidic connections, access holes for tube insertion and for the reservoir inlet in C1 were punched into the PMDS layer. Individual chips were then bonded to a cover glass slide for channel sealing and mechanical support. Conclusions

3.5 Conclusions

We presented an innovative microfluidic approach for long-term studies of biocommunication based on the exchange of secreted diffusive signaling compounds between distinct *C. elegans* populations. In particular, we designed a microfluidic assay to evaluate male-induced demise and lifespan shortening of *C. elegans* WT hermaphrodites in the presence of a physically separated *C. elegans him-5(e1490)* male population. Compared with traditional studies to assess male-induced effects using agar plates or 96-well plates, our method benefits from well-defined assay conditions, with physical confinement of hermaphrodite and male populations in adjacent microfluidic culture chambers, and actively controlled male- secreted compound exchange through fluidic microchannels. We use an optimized on-demand bacteria feeding protocol to meet the specific requirements of this assay. Implementing mechanical screw valves allowed tuning of fluidic exchange and reliably solved issues related to progeny removal or bacterial clogging, which may dramatically affect the performance of long-term on-chip culture assays.

With this new platform, we performed culture and real-time imaging of hermaphrodites with or without the presence of males over the whole lifespan, *i.e.* over a period of up to 19 days. Most strikingly, the presence of male worms on the chip reduced the lifespan of

hermaphrodites by more than 26%. On-chip cohabitation of males and hermaphrodites also induced behavioral phenotype modifications, such as reduced thrashing frequency of hermaphrodites. Significant male-induced structural decline within the cuticle, muscles, pharynx and intestine was observed at a more advanced stage of the lifespan (> day 10). Such morphological phenotypes indicate a general decrepitude due to accelerated aging in hermaphrodites exposed to male-secreted compounds. Likewise, vacuolar structures appeared in body wall muscles, the intestine and the head of male-conditioned hermaphrodite worms, but did not in non-conditioned ones. On the other hand, hermaphrodite worm growth (body length and diameter) was not affected by the presence of males during the initial development phase (*i.e.* from L1 larva stage to young adult, day 1 to day 3). This result might indicate that WT larvae sensing of males is only weakly developed before reaching sexual maturity.

In conclusion, we could demonstrate that biocommunication can take place in a microfluidic device via active transfer of μL -aliquots of a biochemically conditioned medium and controlled exposure of the receiving worm population to this cue. This was clearly demonstrated by the observation of accelerated male-induced phenotype alterations and lifespan reduction of *C. elegans* hermaphrodites. We anticipate that our microfluidic chip is a powerful tool to analyze other specific molecular communication processes among *C. elegans* populations. Spatial confinement of interacting worm populations with controlled fluidic exchange is advantageous with respect to conventional biological agar plate-based assays and opens the way to more advanced and accurate signaling assays. Such assays may include control of the concentration of secreted molecular compounds, control of worm exposure timing, frequency and duration, and real-time imaging and tracking of small worm populations or single worms over the whole lifespan.

Chapter 4 Reversible immobilization of *C. elegans* worms for high-resolution imaging

Biomedical research and genetic studies using *C. elegans* are often based on high-resolution imaging of dynamic biological processes in the worm body tissues, requiring well-immobilized and physiologically active animals in order to avoid movement-related artifacts and to obtain meaningful biological information. However, existing immobilization methods, based either on anesthetics or severe physical constraints by using glue, may strongly affect physiological processes of the animals. In this chapter, we propose two versatile and reversible *C. elegans* immobilization approaches to cover several aspects of *C. elegans* studies as alternatives that may release the constraints of conventional methods.

In the first part of this chapter (section 4.2), we discuss a simple immobilization protocol that can be readily used in any lab. *C. elegans* nematodes were immobilized by taking advantage of a biocompatible and temperature-responsive hydrogel-microbead matrix. Our gel-based immobilization technique does not require a specific chip design and enables fast and reversible immobilization, thereby allowing successive imaging of the same single worm or of small worm populations at all development stages for several days. We successfully demonstrated the applicability of this method in challenging worm imaging contexts, in particular by applying it for high-resolution confocal imaging of the mitochondrial morphology in worm body wall muscle cells and for the long-term quantification of number and size of specific protein aggregates in different *C. elegans* neurodegenerative disease models. We anticipate that this versatile technique will significantly simplify biological assay-based longitudinal studies and long-term observation of small model organisms.

To meet better the requirements of specific *C. elegans* studies, we developed two new on-chip approaches for *C. elegans* immobilization, taking advantage of the elastic properties of PDMS (section 4.3). We present two different microdevices, using a micropillar array or a stretchable serpentine microchannel, respectively. Both chips consist of size-tunable PDMS structures allowing them to be used for immobilizing worms at all development stages. Our microfluidic approach provides appropriate physiological conditions for long-term studies (*e.g.* worm feeding) and enables worm recovery after the experiment. The device performance was demonstrated by *in vivo* live imaging of *C. elegans* embryo fertilization and early embryogenesis, as well as the observation of bacterial colonization of a worm's intestine.

This chapter is an adapted version of the following publications:

L. Dong, M. Cornaglia, G. Krishnamani, J. Zhang, L. Mouchiroud, T. Lehnert, J. Auwerx, and M. Gijs, "Reversible and Long-Term Immobilization in a Hydrogel-Microbead Matrix for High-Resolution Imaging of *Caenorhabditis elegans* and Other Small Organisms," *PLoS ONE* 2018, (13), e0193989.

L. Dong, J. Zhang, M. Cornaglia, T. Lehnert, M. Gijs, “*C. elegans* Immobilization Using Deformable Microfluidics for *In-Vivo* Studies of Early Embryogenesis and Intestinal Microbiota,” *The 30th IEEE International Conference on Micro Electro Mechanical Systems (MEMS 2017)*, 2017, Las Vegas, USA.

Contributions: L. D. designed and performed the immobilization experiments (4.2.1, 4.2.3-4.2.6, 4.2.8, 4.3). M. C. and G. K. did the Pluronic characterization (4.2.2) and confocal fluorescence imaging (4.2.7). M. G. and T. L. supervised the research, and provided reagents and funding. All authors reviewed and edited the manuscript.

4.1 Challenges and opportunities for *C. elegans* immobilization

Many *C. elegans* research studies rely on high-resolution imaging, *e.g.* based on fluorescence confocal microscopy imaging, and on longitudinal observations of dynamic alterations of mitochondrial networks or cluster morphologies. High-resolution imaging over time spans of minutes up to several hours inevitably requires secure immobilization of the worms. Any residual agitation may blur details of tissue fine structures or of dynamic molecular events, and thus reduce the information content and quality of the assay. Moreover, long-term observation and immobilization should be carried out under physiological conditions with minimal impact on the worms' health. Conventional immobilization methods rely on anesthetic drugs [120], such as sodium azide, phenoxypropanol, and tetramisole, to paralyze the worms, or on mechanical immobilization with glue [121]. However, anesthetics chemically disrupt normal physiological functions of the worms (*e.g.* sodium azide perturbs cellular activity [122]). Both anesthetics and glue immobilization methods inhibit the natural worm development, and worms can usually not be recovered after imaging.

As an alternative to overcome these limitations, microfluidic approaches for on-chip worm manipulation have been developed in recent years [93, 96, 123]. Different on-chip worm immobilization techniques, in particular methods based on mechanical forces, have been proposed, such as arrays of tapered channels, *e.g.* for performing lifelong observation [124], neuronal ablation [125] or electrophysiology experiments [126], and pressure-controlled deflectable membranes, *e.g.* for *in vivo* imaging of dynamic cellular processes [127] or neuronal transport [128], laser axotomy [129] and chemosensing assays [130].

For instance, Hulme *et al.* designed a worm chip with tapered channels to accommodate worms of varying sizes [131]. The worm suspension flowing through the device guides the animals towards these channels, where they can be individually isolated and clamped for imaging (Fig. 4.1A). Chokshi *et al.* developed a microfluidic chip which utilizes a deformable PDMS membrane to mechanically restrict the worm's movement by compression. This 2-layer device operates similarly to on-chip valves. The animals are loaded in the fluidic bottom layer of the device. The control layer on top comprises a wider channel that, when pressurized, deforms the membrane in between the two layers and squeezes the worm (Fig. 4.1B).

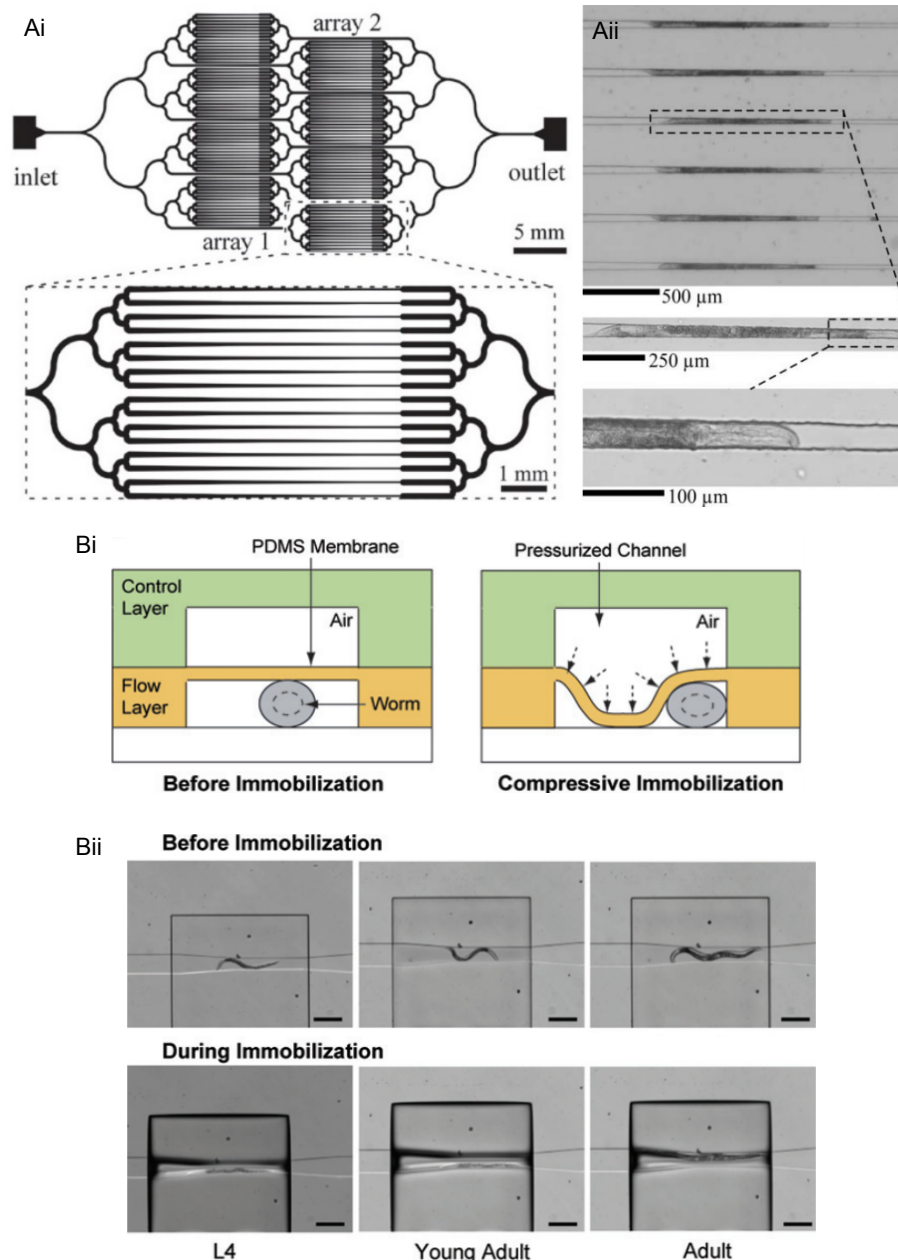


Figure 4.1 Microfluidic devices as tools for *C. elegans* immobilization and imaging.

(A) Worm clamp device (reproduced from [131]). **(Ai)** Branching channel network for worm imaging in a 128-clamp device. **(Aii)** Image of worms immobilized within the tapered microchannels of the worm clamp device. **(B)** Worm immobilization with a flexible PDMS membrane (reproduced from [28]). **(Bi)** Immobilization process. **(Bii)** Images of worms of different ages (and thus of different sizes) before and during compressive immobilization. Scale bar is 500 μm.

Another class of devices takes advantage of Pluronic F127 (PF127), a biocompatible triblock copolymer that, in aqueous solution, undergoes thermogelling at a specific gelation temperature, *i.e.* a reversible sol-to-gel transition upon heating by forming a three-dimensional packing of micelles due to amphiphilic molecule interactions [132, 133]. Gelation temperature and viscosity of the polymer solution depend on the PF127 concentration. PF127 has been implemented in different microfluidic devices, to trigger or improve worm

immobilization through a temperature-induced sol-gel transition, *e.g.* in worm culture chambers [134] or trapping channels [135], in droplet-based devices [136] or in a temperature-controlled microfluidic platform for monitoring *in vivo* protein aggregation in *C. elegans* models [137].

Chuang *et al.* developed an optoelectric device (Fig. 4.2A) based on the simultaneous application of laser irradiation and an electric field to enable selective worm immobilization [138]. The technique was used to track muscular degeneration during aging in a specific transgenic strain. Huang *et al.* proposed a photothermal immobilization method (Fig. 4.2B) based on optical control of the sol-gel transition of the thermosensitive polymer via a photo-absorbing layer on the substrate [99]. This simple method, however, required specific bright field illumination conditions to trigger a sol-gel transition locally, and white light exposure had to be maintained during fluorescent imaging. For these reasons, the technique seems not easily adaptable to high-resolution confocal imaging sessions. Moreover, repeated and relatively long exposure to light stimuli is known to evoke negative phototaxis behavior in *C. elegans* [139].

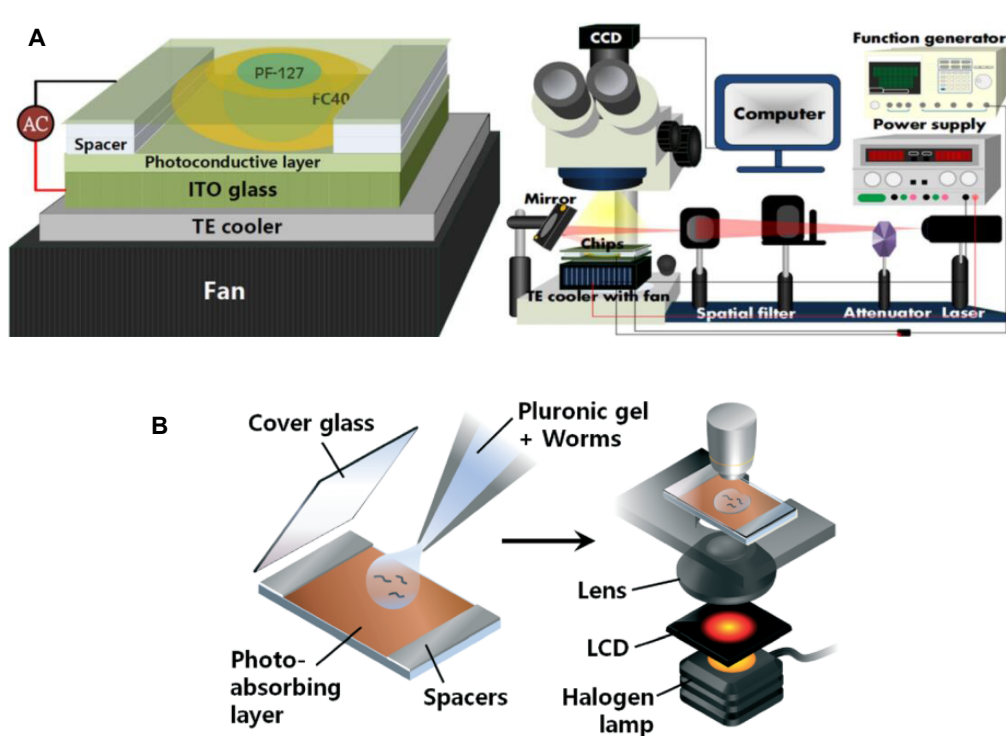


Figure 4.2 Pluronic (PF127) as a tool for *C. elegans* immobilization and imaging.

(A) Close-up view of the optoelectric device and schematic of the overall experimental system. (reproduced from [138]). **(B)** Schematic diagram of a protocol for selective worm immobilization based on photothermal sol-gel transition of Pluronic F127 via conventional microscopic illumination (reproduced from [99]).

All methods or devices discussed so far have specific drawbacks, *e.g.* an unknown or adverse effect on the organism's health, the complexity of the fabrication process, a certain lack of versatility, or the requirement of technical resources that may not be available in standard biomedical research labs. Additionally, major drawbacks of PF127-based microfluidic devices are related to problems with injecting and on-chip manipulation of the viscous solution/gel

and the integration of a chip temperature control system for reversible PF127 thermogelling. Hence, there is a lack of a simple approach that combines the possibility of long-term or periodic high-resolution imaging of a small model organism throughout its lifespan.

To address the above-mentioned requirements and drawbacks, we propose here two new versatile methods for *C. elegans* immobilization and imaging. In section 4.2, we focus first on a protocol based on a hydrogel-microbead matrix for fast and reliable, yet reversible immobilization, in particular of *C. elegans* at all development stages, as well as other small organism (*D. melanogaster* larvae and *T. brucei*). It is easy to use and does not rely on a specific chip design and requires only minimal manual operation. The immobilization principle is based on the combined action of hydrogel in its highly viscous state and moderate compression of the worms, which is well-controlled through the microbead spacers. As a proof-of-concept, we employed this simple technique for *in vivo* confocal fluorescent high-resolution imaging of mitochondrial networks in the body wall muscle cells of *C. elegans*. We demonstrated that our approach is suitable for the accurate observation of the long-term dynamics of mitochondrial fusion and fission processes in worms subjected to different RNA interference (RNAi) treatments. Moreover, we analyzed protein aggregate progression in *C. elegans* neurodegenerative models in a quantitative manner.

Furthermore, as explained in section 4.3, we aim to apply lab-on-chip techniques to meet special demands of *C. elegans* immobilization experiments. We propose two different microdevices, a micropillar array and a serpentine microchannel, respectively, both taking advantage of the elastic properties of a custom-designed PDMS structure and allow reliable and simple immobilization of worms at all development stages in medium containing bacterial food. The microfluidic approach provides appropriate physiological conditions for long-term studies and enables worm recovery after the experiment. The performance of our devices is demonstrated by two different imaging experiments. The micropillar array chip is used for *in vivo* live imaging of *C. elegans* embryo fertilization, early embryogenesis and embryo laying. The straight stretchable channel device was specifically designed for 3D rapid high-resolution scanning. In particular, bacterial colonization of a worm's intestine was observed.

4.2 *C. elegans* immobilization using a hydrogel-microbead matrix

4.2.1 Gel-based immobilization protocol

For immobilization experiments, PF127 in water (30% w/v) was used, either mixed with polystyrene microbeads (for *C. elegans* adult worms) or as pure hydrogel (for *C. elegans* larvae, *D. melanogaster* larvae and *T. brucei*). To obtain a low viscosity Pluronic solution (liquid state), a 1 ml syringe filled with PF127 was stored at 4 °C before and after each experiment. The worm immobilization protocol comprises the steps depicted in Fig. 4.3. First, a 10 μ L droplet of S-medium was pipetted on a glass slide to provide a suitable liquid environment for the worms. About 10 worms were then transferred from a NGM agar plate into the droplet by using a worm pick (Fig. 4.3A). In the next step, the precooled low-viscous PF127 solution or PF127-microbead suspension was applied around the S-medium droplet on the glass slide (Fig. 4.3B) and on a coverslip, which was placed upside down over the worms (Fig. 4.3C). Thereby S-medium was expelled from the center area, leaving the worms in the gel matrix. Gelation prior to imaging was obtained by thermalization of the PF127 solution in between the glass slides at room temperature. For this reason, manipulation at room temperature had to be done reasonably fast (≤ 2 min).

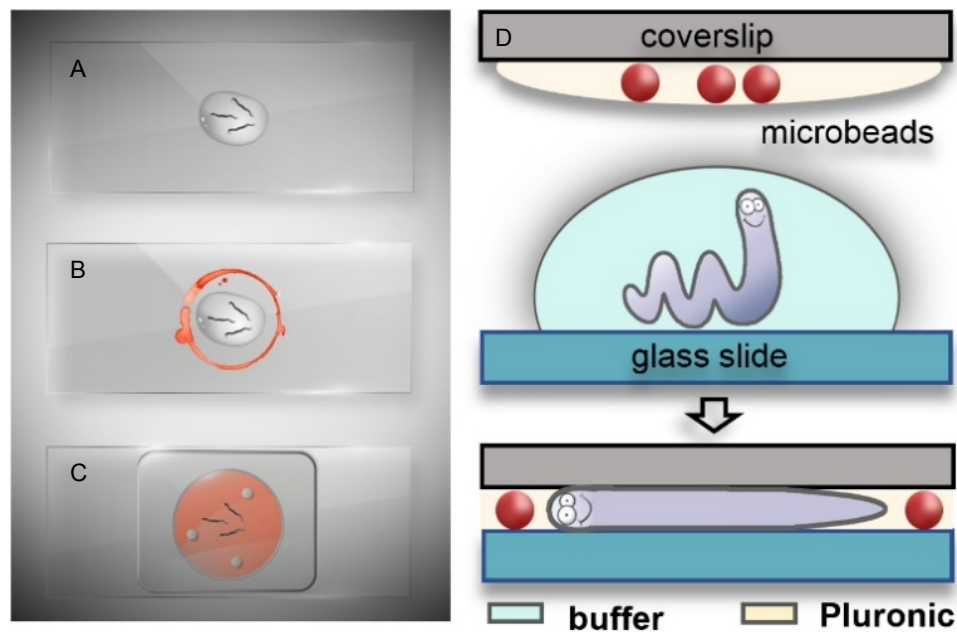


Figure 4.3 *C. elegans* immobilization protocol using a hydrogel-microbead matrix.

(A) Worms are transferred from an agar plate into a droplet of liquid S-medium on a glass slide. (B) Precooled (~ 4 °C) liquid Pluronic-microbead suspension is applied on the glass slide around the S-medium (red trace) and on a coverslip (not shown here). (C) The coverslip is positioned upside down and worms are immobilized in the gel-microbead matrix (red) in between the two glass substrates after thermalization ($T \approx 25$ °C). (D) Schematics of the worm immobilization technique with microbead spacers.

The principle of adult worm confinement and immobilization is schematically shown in Fig. 4.3D. Applying a uniform pressure onto the coverslip results in an evenly distributed monolayer of beads and worms trapped within the gel matrix. The presence of microbeads with suitable diameter ($30 \mu\text{m}$ or $40 \mu\text{m}$ in our experiments) between the two glass surfaces prevents damage to the worms, thereby allowing gentle and well-controlled compression of the worms' body.

For worm recovery after immobilization, worms were released by carefully lifting the coverslip. The hydrogel then formed a dendritic structure on the surface of the glass slide, where worms could be easily found. Worms were set free by rapid dissolution of the surrounding gel in a small drop of S-medium. Then they could be easily placed back onto an agar plate by pipetting the liquid.

4.2.2 Thermogelling of aqueous Pluronic solutions

The accessible parameter range for worm immobilization was first assessed via viscosity measurements of PF127 solutions of different concentrations and over the temperature range of interest (Fig. 4.4A). The sol-gel transition temperature showed a linear drop with increasing PF127 concentration and the viscosity reached at room temperature (25°C) depends quadratically on the polymer concentration (Fig. 4.4B). 30% w/v of PF127 in water is the highest concentration that can conveniently be prepared at room temperature. For our experiments, we used this concentration, as it has the highest viscosity in the gel phase and a convenient sol-gel transition temperature of 12.0 ± 0.5 °C.

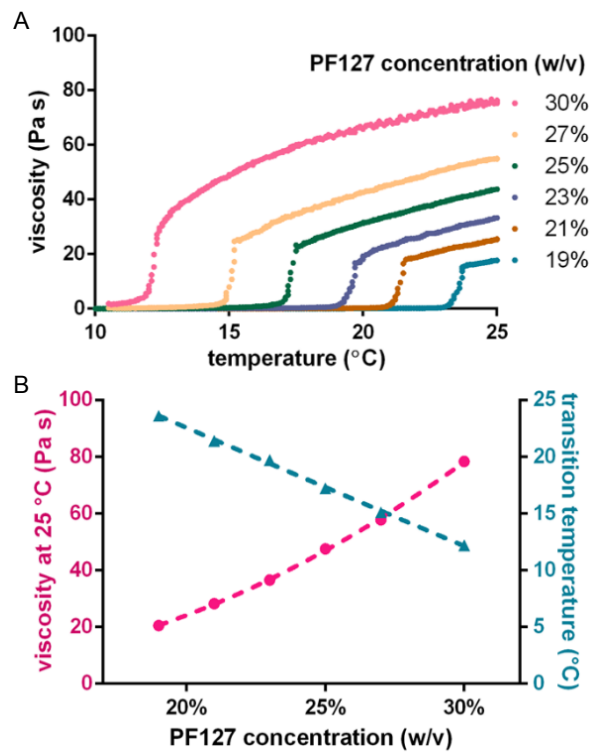


Figure 4.4 Characterization of different Pluronic (PF127) solutions.

(A) PF127 viscosity as a function of temperature for a range of concentrations, measured with a cone-plate viscometer. The viscosity curves show a sharp rise at a specific temperature, corresponding to the sol-gel transition. (B) The viscosity at 25 °C follows a quadratic progression as a function of PF127 concentration. The sol-gel transition temperature decreases linearly with increasing Pluronic concentration.

4.2.3 Immobilization of *C. elegans* larvae

Larvae were incorporated in a pure droplet of PF127 solution (no microbeads) which was sandwiched in between the two glass slides. In this case, the coverslip was only gently pressed from the top to flatten the Pluronic droplet in order to loosely align the larvae in the focal plane for imaging. The spacing is comparable or slightly larger than the body diameter, thus no mechanical compression of the larvae themselves occurred, nor was required for full immobilization. Using PF127 (30% w/v), viscoelastic forces at room temperature (25°C) within the gel matrix were sufficient for full immobilization of *C. elegans* larvae at all stages from L1 to L4 (body length in the range from ~250 μm to ~650 μm [140], diameter from ~10 μm to ~25 μm [141], respectively).

4.2.4 Adult worm immobilization using a gel-microbead matrix

Worms have strong somatic muscles for locomotion based on lateral undulatory motion patterns. Thus, accurate immobilization with negligible residual motion for long-term imaging merely based on viscoelastic forces, as for larvae, is not feasible. To immobilize adult *C. elegans*, we added microbeads to the PF127 gel matrix that function as spacers between the two glass slides, providing a well-defined vertical confinement of the worms. Fig. 4.5A depicts this principle in detail. In the uncompressed state, viscous forces on the worm body dominate, and significantly slow down the worms' motion. But even with the highly viscous Pluronic 30%

w/v gel at 25 °C, such forces are not sufficient to fully inhibit motion of adult worms. Slight compression of a worm in between the two glass interfaces, however, increases friction forces between the worm body and the adjacent glass substrates. If the combined effect of friction and viscoelastic gel forces exceeds the worms' body forces, worms' motion may be inhibited.

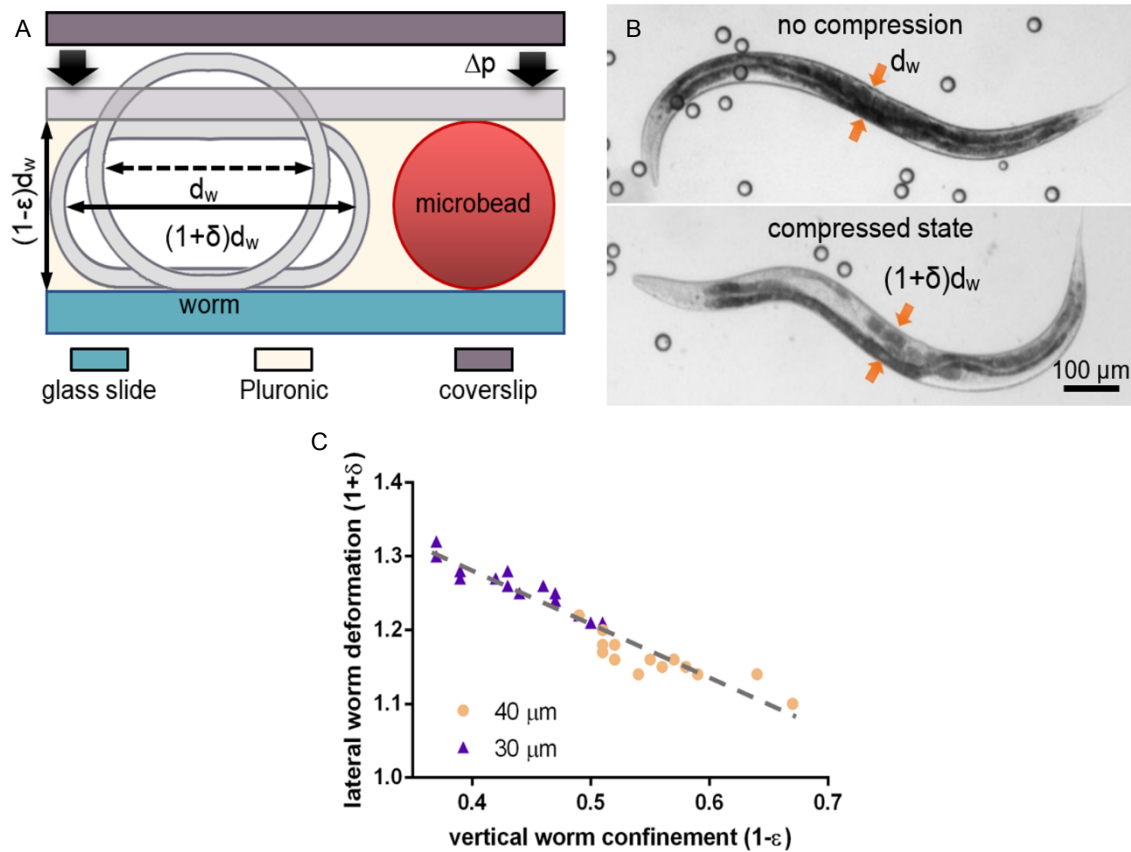


Figure 4.5 The mechanism of *C. elegans* worm immobilization in the hydrogel-microbead matrix.

(A) Application of compression in the normal direction increases friction between the worm body and the glass surfaces. $(1-\epsilon)$ and $(1+\delta)$ denote the vertical and lateral deformation of a worm with a body diameter d_w . (B) Bright field images of an adult hermaphrodite worm in a hydrogel-microbead matrix on a glass slide: freely moving (without coverslip), and in a compressed state with coverslip. The vertical confinement is defined by the bead diameter. Arrows indicate the location where the lateral dorsoventral deformation of the worm body was measured. (C) Worm body extension $(1+\delta)$ as a function of the degree of compression/confinement $(1-\epsilon)$ for two different microbead spacers (40 μm and 30 μm). The range of values is determined by body diameter variations of the unsynchronized worm population used here ($N=15$ for each group).

To observe physiological processes, and possibly to recover the worms after imaging, the worm body has to be compressed to a level that is not harmful. In order to choose the adequate size for the microbeads, we first evaluated the degree of compression of the worm body for different bead diameters. For this, we assume that a worm with a circular cross-section d_w is subjected to a vertical confinement $(1-\epsilon)\cdot d_w$ in between the two glass slides, which causes a lateral extension with a dorsoventral width $(1+\delta)\cdot d_w$ at mid-body location (Fig. 4.5A). Typical values for d_w are the range of 60 to 80 μm , increasing slightly from the young adult to the old adult stage. Representative bright field images of an adult worm are shown in Fig. 4.5B, in the

uncompressed and in the compressed state, respectively. To evaluate the maximum pressure that adult worms can bear, we tested 40 μm , 30 μm and 15 μm microbeads as spacers, corresponding to increasing amounts of vertical and lateral deformation of the worms. According to our study, worms can safely withstand deformations limited by 40 μm ($\varepsilon \approx 0.33-0.52$ and $\delta \approx 0.10-0.22$) and 30 μm microbeads ($\varepsilon \approx 0.50-0.63$ and $\delta \approx 0.21-0.30$), respectively. However, with 15 μm beads compression was too strong ($\varepsilon \approx 0.75$), causing irreversible physical damage to the worms (body burst). For this evaluation, worm populations have not been age-synchronized, thus the range of ε and δ values is determined by the variation of worm body diameters in the adulthood stage. In Fig. 4.5C we plotted experimental values for the lateral worm body deformation ($1+\delta$) as a function of the vertical confinement ($1-\varepsilon$).

Our method differs from another bead-based technique proposed by Kim *et al.* [142]. These authors evaluated the immobilization of worms placed on agarose pads mixed with nanoparticles (diameters 0.05 μm , 0.1 μm , 0.2 μm or 0.5 μm) and hypothesized that the large surface area of small diameter beads may play a role in increasing both contact area and the interfacial shear strength with the agarose matrix, thereby increasing friction. In this case, the spacing of the glass slides is larger than the worms' diameter, nevertheless the worm body dorsoventral width increased up to 40% (for 10% agarose in NGM buffer) by compression due to the stiffness of the agarose. A inconvenience of this approach is that agarose pads do not provide the versatility of repeated PF127 thermogelling. Furthermore, adult worms can swallow beads up to a diameter of a few micrometer [143], thus using nanobeads that can be ingested might have an adverse effect on the worm's physiological condition.

4.2.5 Quantification of worm motility in different media

In order to evaluate more accurately the importance of the hydrogel-microbead matrix for worm immobilization, we applied different degrees of compression (no compression, *i.e.* without beads and a loosely positioned coverslip for aligning worms in the focal plane, and compression limited by 40 μm or 30 μm spacer microbeads). We compared the impact on worm motility in buffer solution or in PF127 (30% w/v) gel, respectively. Fig. 4.6A-C shows two superimposed bright field images of a worm's position in buffer solution for the three configurations. This image series, exhibiting the typical wave-like motion of worms swimming in aqueous solution, reveals stronger restriction of motion with increasing confinement of the worms, and a transition from C-shape (free motion) to more S-shape patterns (worm confinement at the body center). Likewise, Fig. 4.6D-F shows snapshots of worms in PF127 for the different compressive states. In the gel matrix, the worm motion patterns are dramatically different. Due to high viscoelastic forces, the worms can hardly perform lateral undulations but exhibit mainly forward-backward locomotion, similar to their characteristic crawling behavior on agar plates. Displacement amplitudes are considerably smaller than in buffer solution, and we used false colors to highlight two extreme worm positions. As emphasized visually in Fig. 4.6F, using 30 μm spacer beads in the gel matrix, an adult worm can be immobilized nearly completely over the full body length (except a small section of the head). Dashed rectangles in Fig. 4.6C and 3.6F indicate the regions of interest for the bio-assays and imaging experiments performed in the frame of this work. Comparing both pictures clearly reveals significantly improved and apparently complete immobilization of this portion of the worm body in the PF127-microbead matrix.

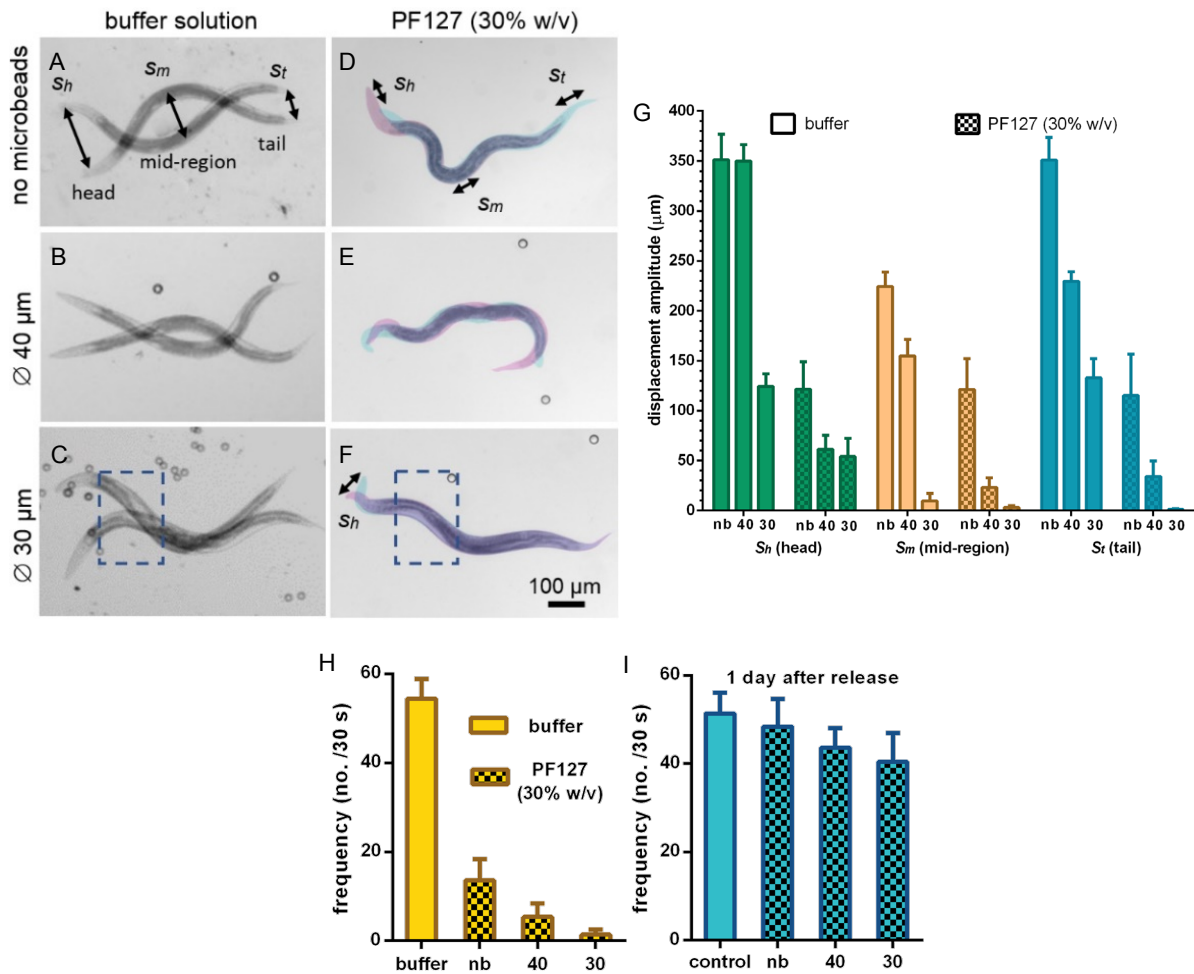


Figure 4.6 Evaluation of *C. elegans* immobilization and recovery for different conditions.

(A-F) Pairs of successive bright field images give an indication of adult worm motility under different conditions: (A-C) in buffer solution (one stroke intervals) and (D-F) in a PF127 (30% w/v) hydrogel matrix (using false colors to visualize two successive snapshots (30 s intervals)). 3 different degrees of worm compression have been applied in either case: (A, D) no compression (no microbeads), and vertical confinement defined by 40 μm (B, E) or 30 μm (C, F) spacer microbeads, respectively. Rectangles indicate regions of interest for high-resolution imaging. Displacement amplitudes of 3 distinct worm body regions (head, mid-region and tail), as indicated in (A) or (D), were measured. (G) Mean amplitude of displacement of the 3 worm body regions, in buffer solution or in PF127 under different conditions: no beads/no compression (nb), and with 40 μm or 30 μm spacer beads (N=15 for each group). (H) Frequency of repeating motion patterns for freely moving adult worms (thrashes in buffer) and during immobilization under different conditions in PF127 (mainly forward-backward motion). (I) Evaluation of worm recovery from long-term (1 hour) immobilization in PF127 (30% w/v). The thrashing frequency was measured in buffer solution 1 day after release of the immobilized worms. The control population was maintained in buffer solution all the time. Data is presented as mean \pm SD (each group N=15).

To assess the worms' motility quantitatively, we measured the displacement amplitudes of three distinct body regions, *i.e.* s_h of the head, s_m the mid-body region and s_t the tail, corresponding to oscillation amplitudes in buffer solution or to the amplitudes of longitudinal displacement in the gel matrix, respectively (as indicated in Fig. 4.6A and 4.6D). The results are summarized in Fig. 4.6G. In buffer solution, the thrashing amplitude s_m without compression in the mid-body region is 225 ± 15 μm , whereas s_h and s_t reach values up to 350 ± 30

μm . Upon compression using 30 μm beads, s_m decreases to 10 ± 5 μm . Head and tail regions, having smaller diameters than the mid-body region, still show strong undulation in this case, with amplitudes in the range of 120-130 μm . In PF127 (30% w/v) gel at room temperature, overall displacement amplitudes in all three worm body regions were significantly reduced. A mid-body amplitude s_m of 120 ± 30 μm was measured without compression. Using 40 μm beads in PF127 gel, s_m decreased to 25 ± 5 μm , a value that still might be too large for most high-resolution imaging protocols. Upon further compression with 30 μm spacer beads, however, the stroke amplitude s_m of the mid-body and s_t of the tail region fell to values in the range of the accuracy of measurement (20x objective, $s_m = 2.2\pm 2.1$ μm and $s_t = 1.3\pm 0.5$ μm , respectively). This configuration was suitable to perform the high-resolution wide field and confocal imaging experiments described below. A small part of the head region (*i.e.* an about 50 μm long portion of the mouth) is only weakly compressed due to its conical shape and still wiggles continuously ($s_m = 55\pm 15$ μm). However, as emphasized by the corresponding false-color image shown in Fig. 4.6F, this agitation is not transmitted to the worm body, in particular to regions where imaging of organs or cells would take place. It is worth to mention, that even in the hypothetical case of perfect immobilization of the worm's cuticle, the residual motion of inner organs or body wall muscles, exhibiting pulsating displacements in the range of a few μm , imposes a natural limit to high-resolution imaging of living physiologically active worms.

The imaging resolution is also affected to a certain extent by the speed or characteristic time scale of the displacement, which should be compared to the exposure time required for the experiment. For very short exposure times in the ms-range, ideally full-worm scale images could be even obtained from worms moving freely in aqueous solution if high-speed sensitive cameras are used. However, tracking a worm in a population or localizing specific features inside a worm would not be possible in this case. Much longer exposure times (hundreds of ms) are necessary for low-intensity signals and/or high magnification imaging, thus requiring adequate worm immobilization. In this regard, we determined the thrashing frequency for freely moving worms in buffer solution and during the different immobilization conditions. Fig. 4.6H summarizes these values, showing that also this parameter decreases drastically with increasing compression.

4.2.6 Worm recovery after immobilization

Worm recovery and possible adverse effects of the gel-based technique on worm physiology were assessed by measuring the worms' motility one day after immobilization. In these experiments, worms were recovered from the chip either after short-term (10 min) or long-term immobilization (60 min) and the thrashing frequency was measured. Typically, for standard imaging techniques, immobilization durations no longer than a few minutes are required. For instance, with the fluorescence wide field imaging used in this work, immobilization of 2-3 minutes is sufficient for localizing a worm of interest and taking a picture. For confocal imaging, the time range required to run through a z-stack is in the range of ~1 min up to 5-6 minutes (depending on the depth of the scan and the averaging number). For this operation range (*i.e.* for ≤ 10 min, 30 or 40 μm beads), we did not observe a statistically significant decrease of the thrashing frequency after worm recovery (data not shown). We conclude that immobilization conditions with our methods are suitable for common imaging protocols. In Fig. 4.6I, values of the thrashing frequency after recovery from long-term immobilization are plotted and compared to a control population that was maintained in buffer solution (no immobilization). For the extreme case of maximum compression (60 min,

30 μm beads), a reduction of only about 20% in the thrashing frequency of the released worms was observed, indicating still a reasonably good physiological state of the worms.

4.2.7 Study of *C. elegans* models of neurodegenerative disease with a hydrogel-microbeads technique

4.2.7.1 *C. elegans* as model organism for neurodegenerative diseases

Additionally, a large number of orthologues of human disease genes and disease pathways has been found, which is a major reason why *C. elegans* has become an attractive model organism for the study of human diseases, aging and for drug discovery [144-148]. For instance, in *C. elegans* models for neurodegenerative diseases, such as Alzheimer's, Parkinson's or Huntington's disease, disease progression can be assessed by monitoring cluster formation of specific proteins in the worm's body tissue [149]. Protein aggregation is a common hallmark of most neurodegenerative diseases. Furthermore, in *C. elegans*, as in humans, a decline in mitochondrial function plays a key role in the aging process, while altered mitochondrial dynamics is known to be implicated in many diseases, including neurodegenerative disorders [150-153]. Inhibition of mitochondrial division, for instance, attenuates disease-associated phenotypes in multiple models of neurodegenerative disease [153, 154]. Mitochondrial fission and fusion therefore represent a potential therapeutic target for neurodegeneration and needs to be further explored in relevant animal models, in particular *C. elegans*. As a proof of concept, the hydrogel-microbead technique is applied for high-resolution confocal imaging of mitochondrial morphology in worm body wall muscles cells and for the quantification of protein aggregation in different *C. elegans* neurodegenerative disease models.

4.2.7.2 High-resolution confocal fluorescent imaging of mitochondrial networks in *C. elegans* using two different immobilization techniques

Prior to the imaging of protein aggregation in neurodegenerative worm strains by wide field fluorescence microscopy, we evaluated our gel-based immobilization technique through the challenging application of confocal imaging of mitochondrial morphology, which has also been associated to several neurodegenerative disorders [148]. Using a transgenic strain expressing the GFP in mitochondria under the control of the muscle-specific *myo-3* promoter (*Pmyo-3::mito::GFP* reporter), we compared the quality of the acquired images obtained with the gel-based technique and with the traditional anesthetics-based immobilization using tetramisole. Fig. 4.7A schematically compares the two techniques. Here, as in the following experiments, PF127 with 30 μm spacer microbeads was used for immobilization. For this evaluation, worms have been immobilized continuously during 3 hours. Thanks to very stable worm immobilization provided by both techniques, the features of interest could be imaged without re-adjusting the objective position over the entire observation time. Fig. 4.7B shows high-resolution time-lapse confocal fluorescent pictures of mitochondrial networks of immobilized worms. For both methods, mitochondrial networks maintained an organized interconnected morphology over 1.5 hours and started displaying signs of fragmented pre-apoptotic mitochondria after ~3 hours of immobilization. Both techniques show a similar degeneration of the mitochondrial network over time, indicating that this evolution is actually not merely a side effect of anesthesia. The observed alteration of the network is probably due to different stress factors experienced by the worm, *e.g.* a lack of food or oxygen deprivation with both methods during this long immobilization interval. Anoxic and hypoxic conditions are known to induce mitochondrial fission [155]. Such harsh conditions are not an issue for imaging

experiments discussed in this work, which, as mentioned earlier, require maximum continuous immobilization intervals lasting not more than ~10 min. As outlined above, the major advantage of the PF127 immobilization protocol is its reversibility, thus opening the possibility of longitudinal studies over several days (see below). Furthermore, the anesthetics-based technique requires extra preparatory steps, *e.g.* for the creation of an agar pad. Also, agar is not a good optical medium due to its yellowish translucent coloring, whereas PF127 gel is perfectly transparent, thus improving the imaging quality. Due to the slight compression of worms with our technique, a slightly larger portion of the worm muscle cells are located within the imaging focal plane, allowing for a more extensive visualization of the mitochondrial network.

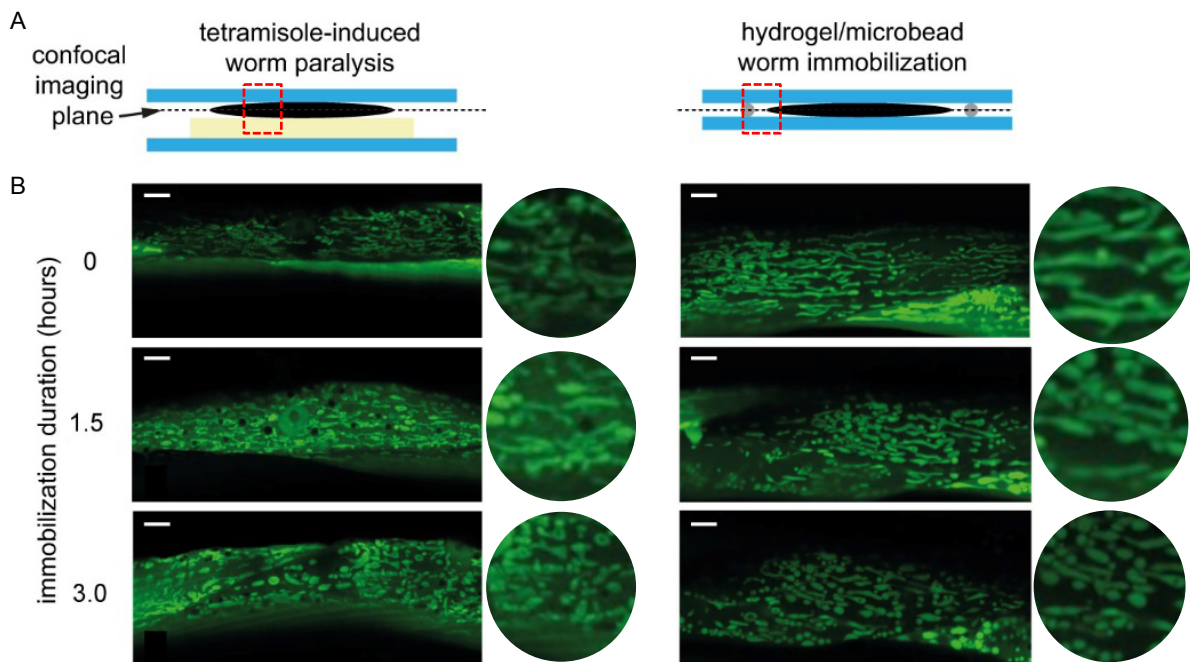


Figure 4.7 High-resolution confocal imaging of mitochondrial morphology in *C. elegans* (A) Schematics of an immobilized adult worm (side view) using two different techniques, *i.e.* tetramisole-induced worm paralysis (current gold standard) and our gel-based method (dashed rectangles indicate the location of the imaging areas). (B) Representative time-lapse confocal fluorescent images of dynamic alterations of mitochondrial networks in *C. elegans* body wall muscle cells during continuous immobilization up to 3 hours, visualized using the *Pmyo-3::mito::GFP* reporter. Images are taken through a 63× NA 1.4 oil immersion objective using the standard immobilization method (left panels) and our technique (right panels). Scale bars = 5 μm. Figures are provided by M. Cornaglia and G. Krishnamani.

4.2.7.3 Mitochondrial morphology progression during worm aging and for different RNAi conditions

As a proof-of-concept for performing longitudinal studies based on high-resolution confocal imaging of *C. elegans*, we investigated mitochondrial morphology in the body wall muscle cells of worms under different RNAi conditions and at different timing during their early adult life. In mammals, mitochondrial fission is mediated by a single protein called DRP1, whereas fusion requires two families of proteins, MFN1/MFN2 and OPA1 [156]. Mitofusins MFN1/MFN2, or *C. elegans* homologue *fzo-1*, are required for the mitochondrial outer

membrane fusion [157] and OPA1, or *C. elegans* homologue *eat-3*, is required for the inner membrane fusion [158]. *fzo-1* depleted worms are known to display a fragmented and disorganized mitochondrial network morphology [159]. On the other hand, *drp-1* deficient worms display disorganized aggregated and globular mitochondria that can be visualized as large blebs [160]. The mitochondrial network in wild-type animals is well-organized and highly interconnected [159].

These observations were confirmed using the gel-based imaging technique, with 63x confocal imaging of the mitochondrial structures in the body wall muscle cells of *C. elegans* (Fig. 4.8). For this study, worms were immobilized in the PF127-microbead matrix for imaging at day 1 and day 3 of adulthood, and allowed to grow on agar plates in the interval. In control worms, treated with an empty RNAi vector, the mitochondrial network was well interconnected on day 1 (young adult stage), but began to fragment with age on day 3 (Fig. 4.8, Inset A). During cell death, it is known that mitochondria dramatically fragment as a consequence of an increased recruitment of *drp-1* to mitochondria [161]. *fzo-1* knockdown inhibited mitochondrial fusion and produced many fragmented mitochondria (Fig. 4.8, Inset B), whereas *drp-1* knockdown inhibited division and produced larger aggregated mitochondria (Fig. 4.8, Inset C). There was a certain degree of heterogeneity between different muscle cells of the same worm, probably pointing to the limited efficiency of the RNAi treatment (images not shown). The digital zooms shown as insets in Fig. 4.8 reveal submicrometer-size features, emphasizing the stability of worm immobilization with our technique.

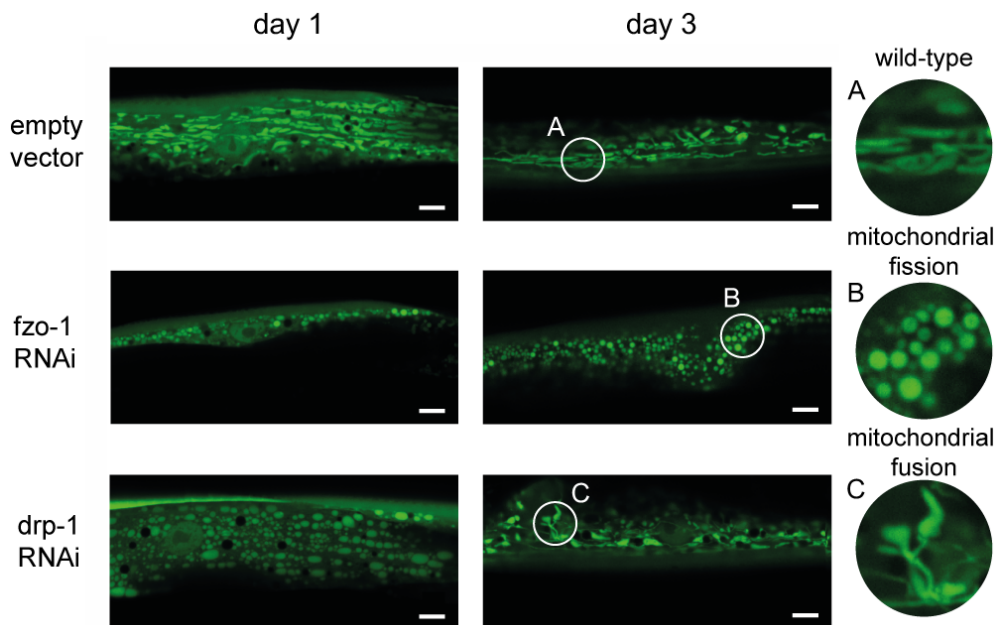


Figure 4.8 Longitudinal analysis of mitochondrial morphology in the body wall muscle cells of *C. elegans* worms under different RNAi conditions.

In wild-type control worms (empty vector), the mitochondrial network is well interconnected on day 1, but begins to fragment with age on day 3 (inset A). *fzo-1* knockdown inhibits mitochondrial fusion and produces many fragmented mitochondria patterns (fission, inset B), whereas *drp-1* knockdown inhibits division and produces larger aggregated networks (fusion, inset C). Images are representative of N=4-6 worms analyzed per condition, visualized via confocal microscopy (63x NA 1.4 oil immersion objective) using the *Pmyo-3::mito::GFP* reporter. Scale bars = 5 μ m. Insets A, B and C are digital zooms (x3.6) of the indicated circular areas. Figures are provided by M. Cornaglia and G. Krishnamani.

4.2.7.4 High-resolution imaging of progressing protein aggregation in different *C. elegans* neurodegenerative disease models

Protein aggregation in *C. elegans* models of Huntington's disease (HD), Parkinson's disease (PD), and Amyotrophic Lateral Sclerosis (ALS) was characterized by wide field high-resolution fluorescence imaging of distinct proteins within the worm muscular tissues. In particular, for HD the AM140 transgenic strain was used, showing Q35::YFP expression in the body wall muscles [162]. For ALS, we employed the AM725 strain, encoding a mutated form of human SOD1::YFP expressed in body wall muscle cells [163]. PD was modeled using the NL5901 strain, featuring α -syn::YFP expression in body wall muscles [164]. Aggregate morphology and accumulation were observed using the described gel-based technique. Each disease model was found to display different aggregate morphologies and evolution with aging. For HD, the AM140 strain was chosen for imaging due to easier visualization of aggregates in the large body wall muscle cells. In this model, polyglutamine (polyQ) repeats progressively underwent a transition from a soluble non-aggregated form to the insoluble aggregate formation with age (Fig. 4.9A) [165]. In contrast, ALS worms with mutant SOD1 aggregation displayed aggregate formation right from the embryo stage (figures not shown), pointing to the permanent instability of the protein. Disease progression, in this case, is more due to the increased expression and accumulation of mutated SOD1 in the worm's body wall cells (Fig. 4.9B). In the case of PD, α -syn aggregates were difficult to visualize at full-worm scale (*i.e.* through a 10x microscope objective), due to their much smaller size with respect to the largely elongated foci formed by polyQ repeats and SOD1 aggregates. Nevertheless, the high stability performance offered by our worm immobilization method allowed obtaining clear images of small α -syn aggregates as well, by using higher magnification objectives (20x and 50x in Fig. 4.9C). In this case, aggregate counting and statistical size quantification per worm would be hence possible by stitching multiple pictures to cover the entire worm body.

For the HD and ALS worm models, quantitative information related to the average size, number and total area of aggregates could be extracted over multiple days through basic image processing. The total aggregate area is not an independent parameter but the product of the number and the average size of aggregates. Interestingly, in the HD model, the number of aggregates increased significantly with aging, but with the aggregate size remaining nearly constant (Fig. 4.9D). For the ALS model, however, this effect was reversed and the aggregate size was the main indicator of disease progression (Fig. 4.9E).

4.2.8 Immobilization of other small model organisms

Finally, to test the versatility of our immobilization protocol, we applied it to other small biological model organisms, such as *D. melanogaster* larvae and *T. brucei* unicellular parasites. Both these organisms could actually be immobilized in PF127 (30% w/v) hydrogel only (no microbeads were required). In the case of *D. melanogaster*, this is somewhat surprising, as *D. melanogaster* larvae are much larger (length ~2 mm in the first instar stage, <4 mm in the prepupal stage), and possibly develop stronger locomotion forces than *C. elegans* adult worms (length ~1 mm) (Fig. 4.10A). However, due to the larger body size, they are also subjected to higher viscous forces. Importantly, there is also a major difference in the natural body motion pattern, which is composed of lateral undulations in the case of *C. elegans* worms, whereas *D. melanogaster* larvae locomotion is induced by circular muscles squeezing and extending the larval body along its axis. In order to evaluate the effect of the PF127 concentration, in this case, we measured the frequency of the small lateral head thrashes and

found that for Pluronic concentrations $\geq 27\%$ w/v *D. melanogaster* larvae can be well immobilized (Fig. 4.10C). On the other hand, *T. brucei* is a very small undulating organism (length 20 to 30 μm) that cannot generate forces strong enough, similar to small *C. elegans* larvae, to move in highly viscous Pluronic gels (Fig. 4.10B). In this case, we evaluated, as for *C. elegans*, the frequency of locomotory body thrashes and found that for a PF127 concentration of 20% w/v *T. brucei* becomes immobile (Fig. 4.10C).

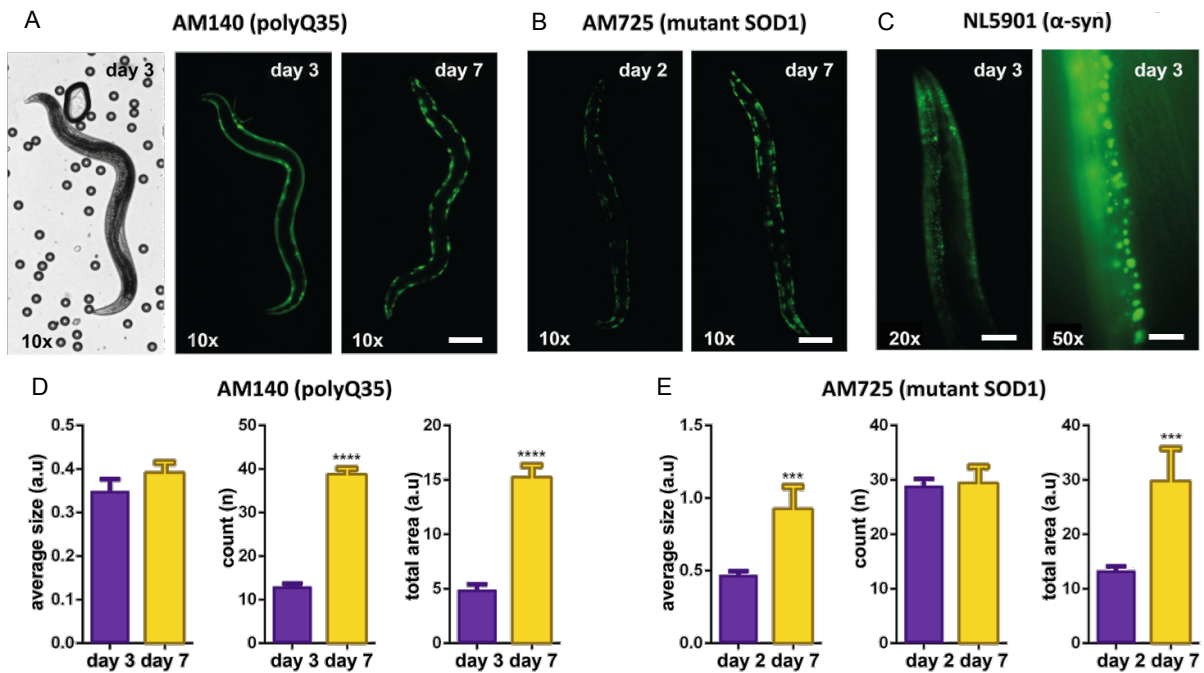


Figure 4.9 Protein aggregate morphology and progression in different *C. elegans* neurodegenerative disease models.

(A) Time-lapse bright field and fluorescent wide-field images of an AM140 worm (Huntington's disease model) immobilized in the gel-microbead matrix. PolyQ35 proteins exhibit a transition from a soluble state to an aggregated form as the worm ages from day 3 to day 7 of adulthood (10x objective, scale bar = 100 μm). **(B)** Time-lapse fluorescent pictures of an AM725 worm (Amyotrophic Lateral Sclerosis model) displaying aggregated SOD1 proteins throughout its adulthood (day 2 to day 7), with aggregate size growing over time (10x objective, scale bar = 100 μm). **(C)** Fluorescent images of α -syn aggregates in a NL5901 worm (Parkinson's disease model), allowing accurate visualization of smaller aggregates (20x and 50x objectives, scale bars = 50 μm and 20 μm , respectively). **(D-E)** Temporal evolution (from day 2 or 3 to day 7) of the average aggregate size, number of aggregates and total aggregate area per worm, in **(D)** AM140 and **(E)** AM725 worms. Data is presented as mean+SEM, *** $p \leq 0.001$ ($N=15-20$ for each group). Figures are provided by M. Cornaglia and G. Krishnamani.

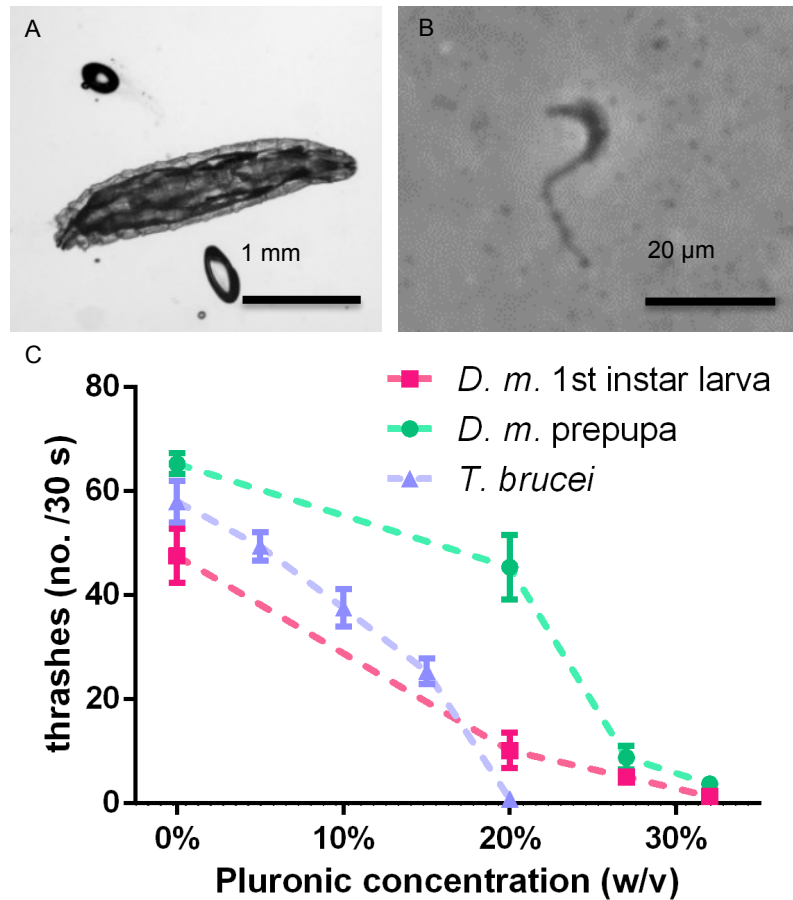


Figure 4.10 Gel-based immobilization of other small organisms.

(A) Image of an immobilized *D. melanogaster* 1st instar larva (length ~2 mm). (B) Image of an immobilized *T. brucei* unicellular parasite (length ~20 μm). (C) Pluronic hydrogel concentration-related reduction of head thrashes for *D. melanogaster* 1st instar larvae, *D. melanogaster* larvae in the prepupal stage (N=15 for each group), and reduction of body thrashes (swimming frequency) for *T. brucei* (N=20). Data is mean \pm SD.

4.2.9 Materials and methods

4.2.9.1 Materials

Polystyrene microbeads with diameters of 15 μm , 30 μm and 40 μm (std. dev. <0.5 μm , coeff. var. <2%) were purchased from Sigma-Aldrich (Buchs, Switzerland). Standard glass slides (76 mm \times 25 mm \times 1 mm) and coverslips (22 mm \times 22 mm \times 0.17 mm) were obtained from Carl Roth GmbH (Arlenheim, Switzerland). Pluronic (PF127) and tetramisole hydrochloride were acquired from Sigma-Aldrich. Lysogeny broth (LB) bacterial culture medium was prepared by adding 10 g BactoTM tryptone, 5 g BactoTM yeast and 5 g NaCl in 1 L of DI H₂O. Tetracycline and ampicillin were purchased from Sigma-Aldrich and Eurobio (Les Ulis, France), respectively. S-medium was prepared by adding 10 ml of 1 M potassium citrate pH 6, 10 ml of trace metals solution, 3 ml 1 M CaCl₂ and 3 ml 1 M MgSO₄ in 1 L of S Basal. S Basal, LB and S-medium were sterilized by autoclaving. All chemicals used in S Basal, LB and S-medium solutions were purchased from Sigma-Aldrich.

4.2.9.2 Bacterial food source

Bacterial culture of *E. coli* OP50 was obtained by inoculating a small amount of OP50 glycerol stock in LB medium without antibiotic. The bacteria were grown at 37 $^{\circ}\text{C}$ overnight in

an orbital shaker and kept at 4°C. Bacterial culture of the HT115 bacteria strain was done in two steps. For the first culture, bacteria were grown at 37 °C overnight in an orbital shaker in LB medium with tetracycline (0.0125 mg/ml final concentration) and ampicillin (0.1 mg/ml final concentration). The following day, for the second culture, they were allowed to grow for 8 hours in LB medium with only ampicillin at the same concentration as before. These bacterial solutions were used to seed NGM agar plates on the same day. The plates were left to dry overnight before worm transfer.

4.2.9.3 Worm culture

C. elegans strains used were wild-type Bristol N2, SJ4103 (zcIs14 [*myo-3::GFP(mit)*]), AM140 (rmIs132[*unc-54p::Q35::YFP*]), NL5901 (pkIs2386[*unc-54p::alphasynuclein::YFP + unc-119(+)*]) and AM725 (rmIs290[*unc-54p::Hsa-sod-1(127X)::YFP*]). All strains were provided by the Caenorhabditis Genetics Center (University of Minnesota). *C. elegans* strains were cultured at 20 °C on NGM plates seeded with *E. coli* OP50 as a food source. Bacteria cultures were grown overnight at 37 °C. Silencing of *fzo-1* and *drp-1* genes were obtained using the RNAi technique by feeding worms with bacteria expressing dedicated double-stranded RNA [166]. *fzo-1* (ZK1248.14), *drp-1* (T12E12.4) and *E. coli* HT115 (empty vector) clones were obtained from the Ahringer *C. elegans* RNAi feeding library.

4.2.9.4 Confocal imaging of mitochondrial morphology

For confocal imaging, a *C. elegans* strain expressing mitochondrial-targeted Green Fluorescent Protein (GFP) driven by the muscle-specific *myo-3* promoter (SJ4103) was used. Worms were immobilized using the gel-based technique detailed in this paper or with 6 mM solution of tetramisole hydrochloride (control group) in S-medium and mounted on 6% agarose pads on glass slides. Images of worms were acquired using a Zeiss LSM 700 upright confocal microscope (Carl Zeiss AG, Oberkochen, Germany, 63x NA 1.4) under non-saturating exposure conditions. All pictures of mitochondrial morphology were taken in body wall muscles from the upper or lower part of the worm, excluding the regions of oesophagus and vulva.

4.3 *C. elegans* immobilization using deformable microfluidics

4.3.1 Micropillar array device for embryo fertilization and embryogenesis studies

4.3.1.1 Design overview

The device is based on a 16 × 16 mm² PDMS micropillar array chip, mounted in a height-adjustable polymethylmethacrylate (PMMA) holder for applying compressive stress (Fig. 4.11A,B). The pillars feature a specific dual-stage design with a 40 μm high foldable, crescent-shaped part on top of a 20 μm high, more stable, cylinder-shaped base part (Fig. 4.11C,D). In the released non-compressed state, the total height and the lateral spacing of the pillars is 60 μm, thus arrays may accommodate freely moving adult worms ($\varnothing \approx 60 \mu\text{m}$). Prior to worm loading, a 10 μL droplet of M9 buffer solution was introduced at the center of the micropillar array chip to provide a suitable liquid environment for the worms. Then, 10 to 20 individual worms were transferred from an agar plate and carefully placed into the droplet area. Subsequently, the pillar array was covered with a glass coverslip and placed in the PMMA holder for observation under the microscope. Finally, the distance of PMMA holder plates was adjusted via the incorporated screws, resulting in uniform compression of the PDMS pillar array. As not only the height but also the effective spacing between the compressed pillars decreases progressively with increasing pressure, the worms' movement may be restricted in

a well-controlled manner and without excessively squeezing the worm bodies. This procedure may be applied to worms of all development stages. Examples for an adult worm, a L3 larva and a L1 larva are shown in Fig. 4.11E, F, and G, respectively. The pillar interstitial spaces leave enough room for allowing embryo laying and on-chip feeding during long-term immobilization.

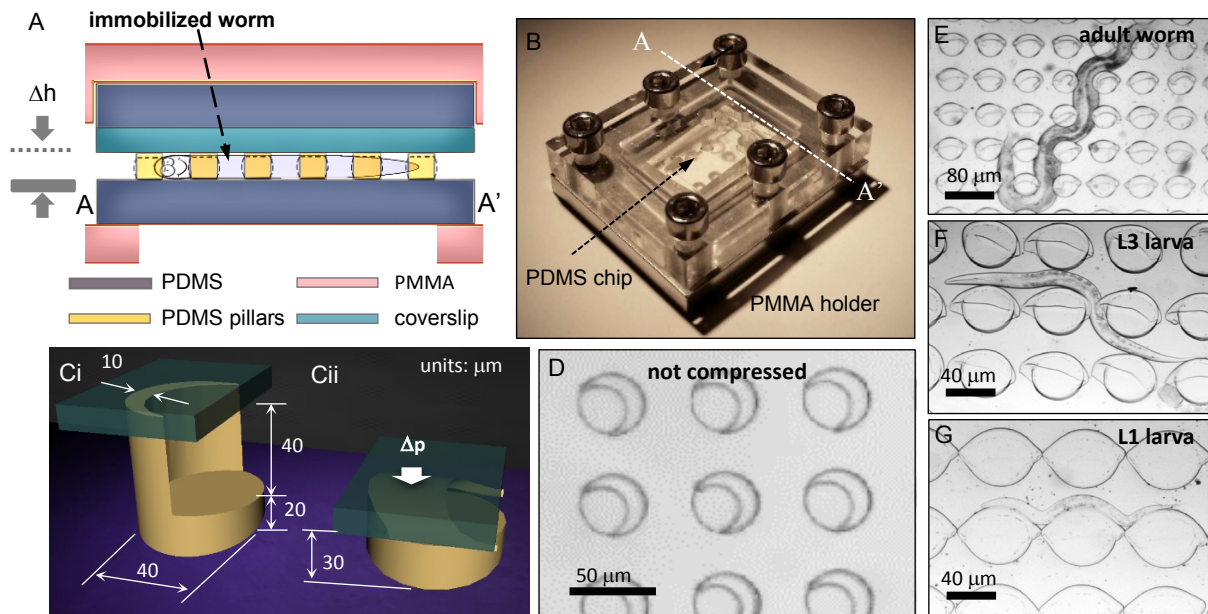


Figure 4.11 Micropillar array device for *C. elegans* immobilization.

(A) PDMS pillar array chip for worm clamping using a height-adjustable PMMA frame (cross-section). (B) Photograph of the device. (C) Schematic 3D view of a single pillar: (i) in the released state (height 60 μm) where the chip may accommodate adult worms or larvae; (ii) immobilization of adult worms is achieved by compressing the upper crescent-shaped part that collapses on the pillar base. (D) Top view of a portion of the full array showing nine crescent-shaped pillars in the uncompressed state. (E) Image of an immobilized adult worm ($\varnothing \approx 60 \mu\text{m}$). Increasing the applied pressure also deforms the PDMS pillar base allowing immobilization of larvae at all stages, e.g. (F) L3 ($\varnothing \approx 25 \mu\text{m}$) or (G) L1 ($\varnothing \approx 12 \mu\text{m}$).

4.3.1.2 Studies of *C. elegans* embryo fertilization and embryogenesis

For each experiment, up to 20 worms were transferred onto the pillar array and securely immobilized. Worms were slightly squeezed by adjusting the height of the PMMA holder until residual movements of the body ceased. Nevertheless, this approach still allows agitation of the worm's head, an important requirement for maintaining adequate feeding conditions with *E. coli* that has been introduced on the chip prior to worm loading. As mentioned above, this immobilization protocol may be applied to worms at all development stages (Fig. 4.11E, F, and G). An on-chip egg-laying event was captured after immobilizing a gravid adult worm for about 1 hour on the pillar array (Fig. 4.12), demonstrating that this technique provides physiological conditions for normal worm behavior. Moreover, we have performed two specific *in vivo* high-resolution imaging experiments. First, an oocyte-to-embryo transition in a worm's uterus was recorded. Fig. 4.13 shows the process of fertilization occurring in the spermatheca located at the end of a gonad of an adult *C. elegans* hermaphrodite. Contractions of the oviduct force an oocyte to move towards (Fig. 4.13A), and finally into the spermatheca (Fig. 4.13B) where fertilization takes place. Subsequently, early embryogenesis may be directly studied *in vivo* in

the uterus of the worm, starting from the first mitotic cellular division (~19 min after fertilization). Fig. 4.13C and Fig. 4.13D emphasize an embryo in the 1-cell and in the 2-cell stage, respectively.

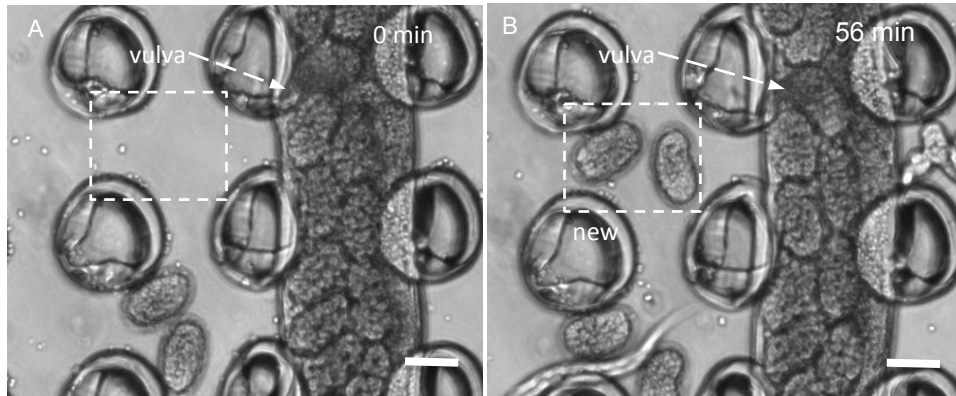


Figure 4.12 Live imaging (bright field) of a *C. elegans* wild-type worm immobilized on the pillar array chip over long periods.

(A) Detail of a gravid worm showing embryos *in utero*. (B) Two freshly laid embryos appeared on an image taken after 56 min. This observation demonstrates that egg laying occurs on-chip during immobilization, which is an indicator of good worm's health. The location of the worm's vulva is indicated. Scale bars = 30 μm .

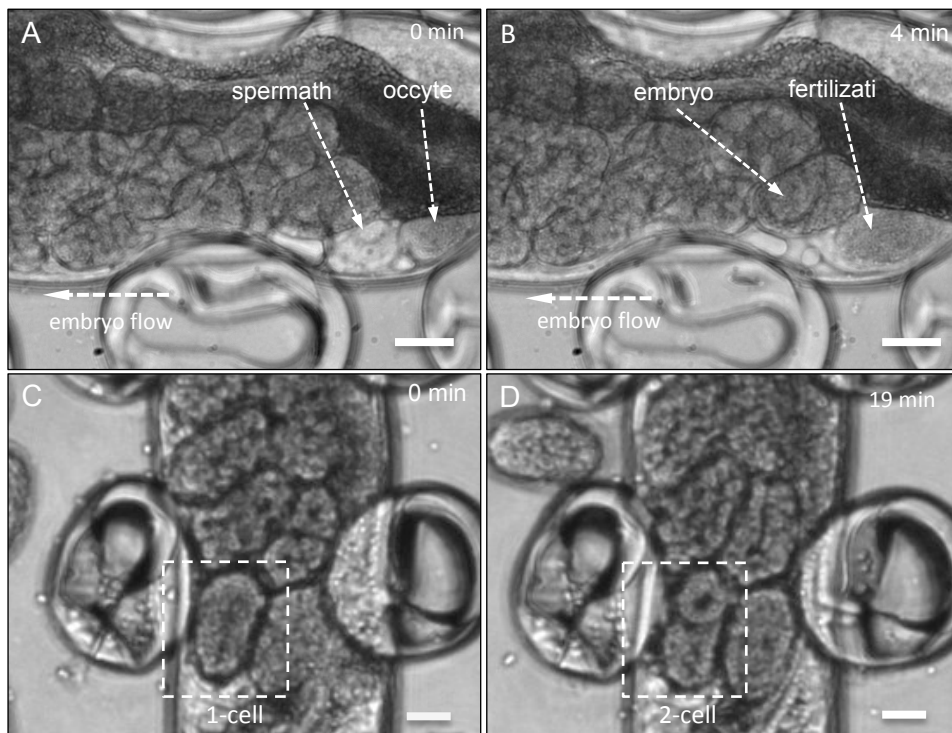


Figure 4.13 *In vivo* observation of early embryo development on the pillar array chip.

The images show a portion of the uterus of an immobilized gravid *C. elegans* hermaphrodite. All embryos slowly move to the left upon egg laying. (A) An unfertilized oocyte in the gonad is approaching the spermatheca. (B) After 4 minutes, the oocyte moved into the spermatheca. (C) A fertilized embryo in the one-cell stage appeared in the worm's uterus after passing the spermatheca (dashed frame). (D) The same embryo after 19 minutes, *i.e.* after the first cellular division. Scale bars = 20 μm .

4.3.2 Stretchable channel device for linear alignment of *C. elegans* worms

4.3.2.1 Design overview

The second device is a full PDMS chip that comprises a 15 μm wide and 40 μm high serpentine microfluidic channel. Worm suspensions are introduced through a single fluidic inlet, and eventually recovered at the outlet, respectively. The serpentine channel has 30 parallel channel sections with a length of about 10 mm each. This PDMS chip, which is stretchable by its nature, is mounted on a commercial tensile stage (Fig. 4.14A). Tensile stress is applied perpendicular to the parallel channel sections, by which the effective cross-section of these may be increased prior to worm loading (Fig. 4.14B). Subsequently, upon release of tensile stress, worms are securely immobilized and aligned (Fig. 4.14C). Applied tensile stress values and/or geometrical dimensions of the channel can be adjusted for immobilizing worms at all development stages. For long-term immobilization (>30 min), *E. coli* is introduced during worm loading for food supply. A photograph of the whole stretchable channel set-up is shown in Fig. 4.14D.

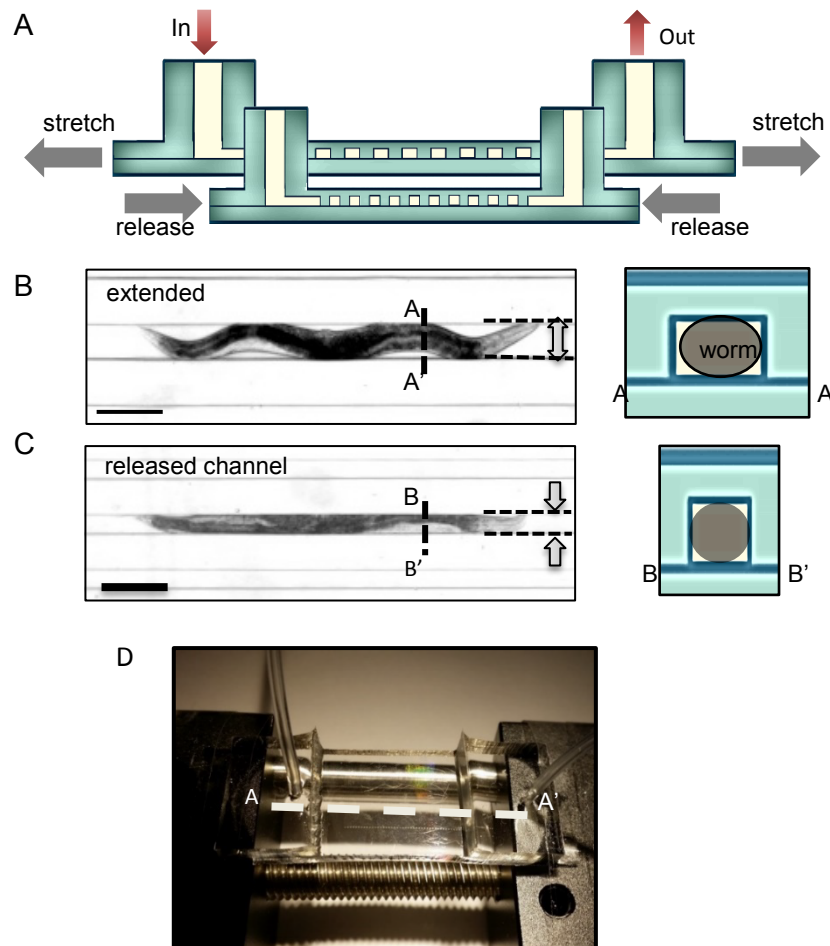


Figure 4.14 PDMS device with stretchable channel sections for immobilization and linear alignment of *C. elegans* worms.

(A) The PDMS chip, which is attached to a tensile stage (not shown), comprises a single serpentine microchannel that receives the worm suspension. The cross-section in the figure reveals the parallel sections of the serpentine channel. (B) Image of an undulating adult worm during loading in the extended PDMS channel (width $\approx 80 \mu\text{m}$, worm diameter $\varnothing \approx 60 \mu\text{m}$). (C) Immobilized, slightly compressed and aligned worm in the released channel structure (width $\approx 40 \mu\text{m}$). Scale bar = 100 μm . (D) Photograph of the set-up.

4.3.2.2 3D imaging of *C. elegans* with visible optical coherence microscopy

3D imaging of biological processes *in vivo* is of major interest for *C. elegans* studies. Confocal fluorescence microscopy as the conventional method for 3D imaging of living *C. elegans* requires biological samples that are treated with fluorescent dyes or labeled with fluorescent proteins (*e.g.* GFP) to make selected objects visible. Recently, visible optical coherence microscopy (visOCM) has been used for label-free *in vivo* imaging of whole *C. elegans* worms down to the sub-cellular level [167]. However, image acquisition and processing is very time-consuming and depends on the worm's shape and position. In a typical visOCM set-up, the illumination beam is raster-scanned over a $100 \times 100 \mu\text{m}^2$ sample area. Several 3D stacks need to be acquired to cover the whole worm body ($80 \mu\text{m}$ wide \times 1 mm long for adult worms). As the beam can only scan along x and y directions, the required scanning area is much larger than the actual worm shape. Fig. 4.15A shows an image acquisition sequence for an anesthetized worm. In this case, the sequence comprises 21 3D stacks to cover the whole worm body. The resulting images are finally assembled into a mosaic using an algorithm for stitching of tiled 3D microscopic images (available in ImageJ) [168]. In the case shown in Fig. 4.15A, it took ≈ 30 minutes for scanning each individual area, and up to 13 hours of processing time for the image stitching.

Our stretchable channel device provides a simple solution to decrease scanning and processing durations of visOCM for *C. elegans* 3D imaging. As worms may be immobilized in a straight position (Fig. 4.15B), a set of approximately only 9 3D stacks is sufficient to cover the entire adult worm with sub-micrometer resolution. Besides, each stack has no more than two edges that need to be stitched, which strongly reduces the post-acquisition processing time. Taking advantage of our on-chip technique, the data acquisition and processing time could be shortened to 18 minutes and 2 hours, respectively, for the example shown in Fig. 4.15B. Furthermore, a representative high-resolution section scan image is shown in Fig. 4.15C, showing two early embryos under cell division.

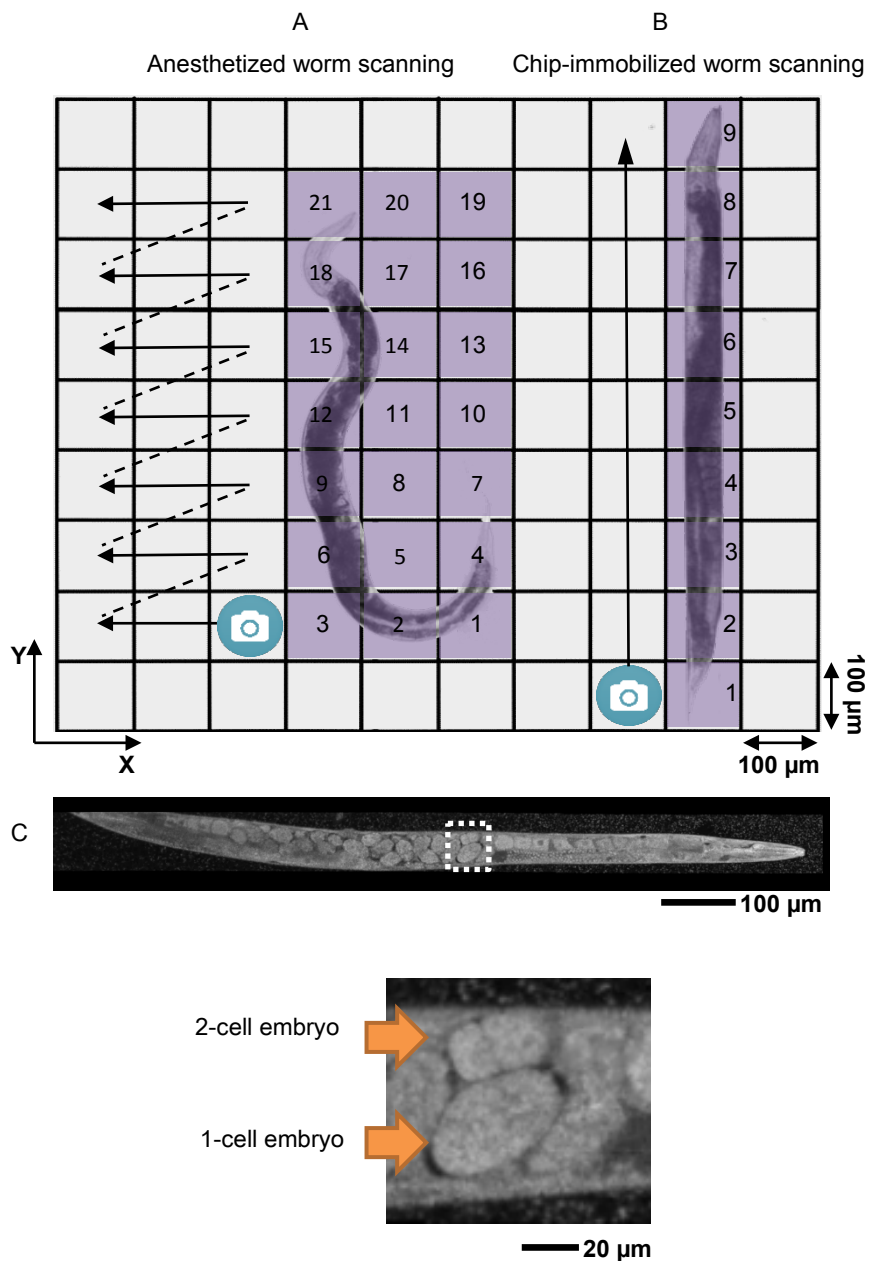


Figure 4.15 visOCM 3D imaging of an adult *C. elegans* worm.

(A) Scanning of an anesthetized worm. The curved worm body shape requires a set of 21 stacks, *i.e.* a large scanning area to cover the whole body. Depending on the location, each stack has 3 or 4 edges to be stitched after image acquisition. **(B)** Scanning of a worm immobilized in the stretchable microchannel device. The straight worm body is aligned with the scanning direction. A set of 9 stacks is needed for scanning the whole worm body. Each stack has only 1 or 2 edges to be stitched. **(C)** Sectional scan of an adult worm (provided by EPFL Laboratoire d'Optique Biomedicale). The picture shows two developing embryos *in vivo*.

4.3.2.3 Study of bacterial colonization in the *C. elegans* intestine

Linear alignment of the worm body, thus of its inner organs, as enabled by the stretchable channel chip, also presents advantages for fast image acquisition in high-resolution wide field and fluorescence microscopy of the worm's intestine. For instance, studies of host-microbiota interactions in diverse animals demonstrate the importance of the gut microbiota for the host

health [169]. *C. elegans* has become a new model to characterize microbial populations and proliferation *in vivo*, as well as the possible impact on the host physiological state, including the emergence of specific diseases [170].

In order to demonstrate the utility of the stretchable channel chip for such studies, bacterial colonization of an aligned worm's intestine was visualized by high-resolution fluorescence imaging. For that purpose, a group of adult worms was fed on agar plate with the pGFPuv-expressing *E. coli* HT115 bacterial strain. For on-chip imaging, worms were picked up manually from the agar plates, suspended in the bacteria solution and introduced in the serpentine channel for immobilization. Immobilization and on-chip imaging of the worm's intestine was performed at day 2 and at day 5 of adulthood. Worms were recovered after each experiment and placed again on an agar plate. At day 2 no significant fluorescent signal was observed (Fig. 4.16a). However, at day 5 a clear GFP signal appeared all over the worm's intestine, generated by invasion of the worm's intestine with pGFPuv-expressing *E. coli* HT115 bacteria (Fig. 4.16b). Bacterial invasion of the worm's intestine could be due to an age-related abrasion of the worm's pharyngeal grinder, resulting in poor mechanical reduction of the bacterial food and incomplete digestion [171].

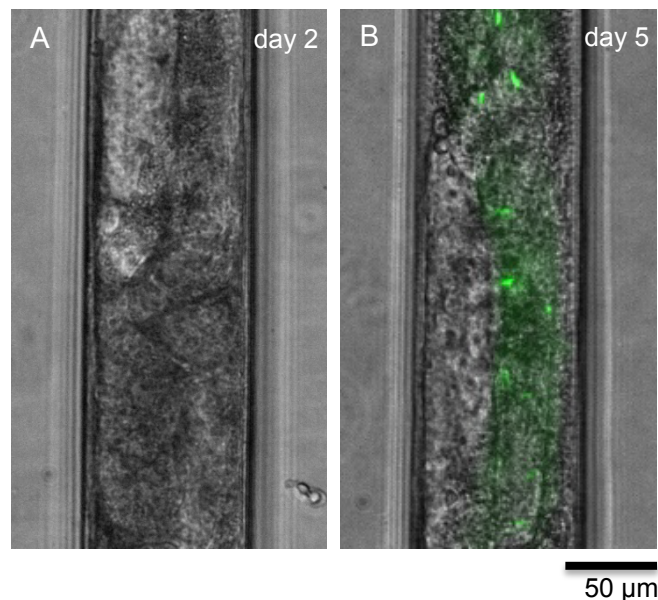


Figure 4.16 High-resolution *in vivo* imaging of bacterial colonization of the intestine of an aligned adult *C. elegans* worm.

Worms were fed off-chip with a GFP-expressing *E. coli* bacterial strain and securely immobilized on a stretchable PDMS channel chip for imaging. **(A)** At day 2 of adulthood no fluorescent signal was observed. **(B)** At day 5, a GFP signal appeared in the worm's intestine, indicating that worms at an advanced age were not able to grind and digest all of the consumed bacterial food.

4.3.3 Materials and methods

4.3.3.1 Materials

L-Broth bacterial culture medium was obtained by adding 10 g Bacto-tryptone, 5 g Bacto-yeast, 5 g NaCl, in 1 L of H₂O. S-Basal was obtained by adding 5.85 g NaCl, 1 g K₂ HPO₄, 6 g KH₂PO₄, 1 ml cholesterol (5 mg/ml in ethanol), in 1 L of H₂O. S-medium was obtained by adding 10 ml 1 M potassium citrate pH 6, 10 ml trace metals solution, 3 ml 1 M CaCl₂, 3 ml 1 M MgSO₄ in 1L of S-Basal. S-Basal, L-Broth and S-medium were sterilized by autoclaving. All

the chemicals used in S-Basal, L-Broth and S-medium solutions were purchased from Sigma-Aldrich (Buchs, Switzerland).

4.3.3.2 Worm strains culture and bacterial strains

The *C. elegans* N2 wild-type strain used in this work was cultured at 20 °C on NGM plates seeded with *E. coli* OP50. The same bacteria were also used as food source for *C. elegans* in the microfluidic chips. A single colony of *E. coli* OP50 was taken from a streaked plate and inoculated into lysogeny broth (LB). The inoculated cultures were shaken and grown overnight at 37 °C. These suspensions were directly injected into the chip for worm feeding. For monitoring bacterial colonization of *C. elegans* by fluorescence microscopy, pGFPuv-expressing *E. coli* HT115 were used. The pGFPuv plasmid (Clontech Laboratories, Inc., USA), carrying a gene for a green fluorescent protein (GFP) variant optimized for maximal fluorescent response, was introduced into *E. coli* HT115 by electroporation. The pGFPuv-expressing *E. coli* HT115 strain was maintained in LB medium containing ampicillin (100 µg/ml) for selective growth.

4.3.3.3 Device fabrication

The micropillar array device was fabricated using standard soft lithography. The master mold was made by a two-step SU-8 on silicon process. First, the master structure for the foldable parts of the pillar array were created on a Si wafer by plasma etching (structure height 40 µm). Subsequently, a 20 µm thick SU-8 layer was spin-coated on the wafer and patterned to form the non-compressible pillar base structures. PDMS was poured onto the mold to obtain a 1 mm thick layer. The PDMS layer was cured at 80 °C for 1 hour (base to curing agent ratio 10:1). Beforehand, mold surfaces were treated with TMCS for 60 min to facilitate PDMS demolding.

For the stretchable device, a 40 µm high SU-8 serpentine structure was patterned on a silicon wafer and replicated in a 1 mm thick PDMS layer. The chip was plasma-bonded onto a second 1 mm flat PDMS layer to close the fluidic structures. All PDMS layers were cured at 80 °C for 1 hour (base to curing agent ratio 10:1). Mold surfaces were treated with trimethylchlorosilane.

4.4 Conclusions

Until now, no single worm immobilization method exists that can satisfy the full range of requirements for *C. elegans* studies and imaging. In this chapter, we reported several new, versatile and reversible *C. elegans* immobilization techniques: (i) a “chip-less” hydrogel-microbead method and (ii) two chip-based devices taking advantage of deformable microfluidic PDMS structures.

(i) Immobilization of small organisms in a biocompatible and temperature-responsive Pluronic-microbead matrix was achieved by thermalization of the glass/PF127 substrate at room temperature, thus no specific equipment or technical skills are required, making the technique readily operational in any biological laboratory. The technique allows recovery of the worms, *e.g.* for repeated imaging of the same worm over a time span of several days, a feature that presents a significant advantage with respect to conventional anesthetics- or glue-based methods. Furthermore, in Pluronic only, *i.e.* without microbeads, immobilized animals often rotate around their longitudinal axis, hence preventing stable observation and imaging of specific features in their body. This happens in particular during fluorescence imaging, since such movement can be triggered by the worm’s propensity to avoid blue light. As with our

method, taking advantage of microbead spacers, the worm is slightly compressed in a well-controlled manner, rotation around its axis cannot take place.

To test the performance of the gel-based technique, we focused on biological applications requiring challenging longitudinal high-resolution imaging and data quantification related to the morphology, size and/or counting of specific shapes within the worms' tissues. In particular, we demonstrated high-quality *in vivo* imaging of mitochondrial morphology in the body wall muscle cells of *C. elegans* by confocal fluorescence microscopy on immobilized worms. This allowed successfully observing the long-term dynamics of the mitochondrial fusion and fission processes with unprecedented simplicity and accuracy. Likewise, the progression of protein aggregates, one of the major hallmarks of many neurodegenerative diseases, was assessed quantitatively in different *C. elegans* models of human neurodegenerative diseases, namely ALS, HD, and PD. In this study, our method enabled the longitudinal quantification of size and number of specific protein aggregates in each worm, revealing clear differences in the temporal evolution of the protein aggregation patterns in HD and ALS, while allowing the observation of particularly small aggregates, via high-magnification imaging of PD worm models.

(ii) Microfluidics technology is perfectly adapted for the study of *C. elegans*. We reported here two new and simple on-chip immobilization methods for experiments requiring continuous feeding and high-resolution imaging of *C. elegans* nematodes. Immobilization of worms under physiological conditions is a feature that presents a clear advantage with respect to the hydrogel-microbead method. In contrast to other existing on-chip immobilization methods that are designed for a specific worm size or age [93, 94, 96], our methods enable immobilizing *C. elegans* of all development stages, thanks to tuning of specific geometrical parameters of deformable structures. Both devices enable high-quality and long-term *in vivo* imaging of dynamic biological processes in *C. elegans* with unprecedented accuracy and simplicity. In particular, we demonstrate the feasibility of *in vivo* observation of oocyte fertilization and of early embryogenesis on the micropillar array device under normal bacterial feeding conditions. Furthermore, linear on-chip alignment of a worm provided by the stretchable microchannel device has been particularly useful for advanced automated scanning imaging experiments. The efficiency of data acquisition and processing time of visOCM for 3D imaging of *C. elegans* could be significantly reduced by using our stretchable channel device. Similarly, bacterial colonization of adult worms was monitored by fluorescence imaging of the worm's intestine.

Chapter 5 On-chip drug studies during *C. elegans* early embryogenesis

Small-molecule inhibitors are powerful tools for studying multiple aspects of cell biology and stand at the forefront of drug discovery pipelines. However, in the early *C. elegans* embryo, which is an interesting model system for cell and developmental studies, the use of small-molecule inhibitors has been limited by the impermeability of the embryonic eggshell, the low-throughput manual embryo isolation method and the lack of well-controlled drug delivery protocols. This work reports a fully integrated microfluidic approach for studies of *C. elegans* early embryogenesis, including the possibility of testing small-molecule inhibitors with increased throughput and versatility. The set-up enables robust on-chip extraction of embryos from gravid adult worms in a dedicated pillar array chamber by mechanical compression, followed by rapid fluidic transfer of embryos into an adjacent microtrap array. Parallel analysis of ~100 embryos by high-resolution time-lapse imaging from the 1-cell stage zygote until hatching can be performed with this device. The implementation of versatile microfluidic protocols, in particular time-controlled and reversible drug delivery to on-chip immobilized embryos, demonstrate its potential for biochemical and pharmacological assays.

This chapter is an adapted version of the following publications:

L. Dong, R. Jankele, T. Lehnert, P. Gönczy, M. Gijs, “On-chip drug studies to *C. elegans* early embryogenesis,” *Advanced Science*, 2018 (5), 1700751.

L. Dong, J. Zhang, R. Jankele, T. Lehnert, P. Gönczy, M. Gijs, “*C. elegans* Immobilization Using Deformable Microfluidics for In-Vivo Studies of Early Embryogenesis and Intestinal Microbiota,” *The 30th IEEE International Conference on Micro Electro Mechanical Systems (MEMS 2017)*, 2017, Las Vegas, USA.

Contributions: L. D. designed, built, and tested the microfluidic control instrument and conceived the application to the drug studies with input from R. J., M. G., T. L. and P. G supervised the research, and provided reagents and funding. All authors reviewed and edited the manuscript.

5.1 Early *C. elegans* embryos as model system

Over the last decades, the *C. elegans* embryo has been proven to be an excellent system to study diverse complex events in cellular processes, ranging from the regulation of cell cycle control and mitosis to proliferation and differentiation [164], as well as to study the biology of centrioles and centrosomes. In that system, the stereotypic cleavage of the embryo follows a series of programmed events that exist similarly in most cell types, offering several key advantages for the following reasons: (i) the worm's genome is fully sequenced offering the possibility to perform a comprehensive analysis; (ii) the large cell size and optical transparency of the eggshell allows analyzing the dynamics of the cell components and perturbations of biological processes with high spatial and temporal resolution, by combining advanced time-lapse imaging techniques, such as differential interference contrast (DIC), fluorescence, or confocal laser scanning microscopy; and (iii) RNA-interference (RNAi) based analysis can generate extensive phenotypic datasets. By neutralizing targeted mRNA molecules, RNAi is able to inhibit a given gene in the embryo. This is known to be a precise and efficient technology for gene suppression, allowing researchers to identify evolutionary conserved pathways and proteins, *e.g.* the cell polarity establishment or PAR proteins for the asymmetric division [168].

To date, the majority of studies in *C. elegans* utilized larval or adult worms, thus missing the unique opportunities provided by the early embryo, which is an excellent model system for analyzing fundamental cellular processes, such as cytoskeletal biophysics, cell cycle progression and developmental regulation [172]. Thanks to the optical transparency of the *C. elegans* embryo, perturbations of cellular processes in this system can be observed with high spatial and temporal resolution by light and fluorescence microscopy. Currently, the application of small-molecule inhibitors to early *C. elegans* embryos is limited by the low rate of embryo harvesting and by only partially controllable drug delivery. For the time being, there is no high-throughput method specifically designed for the handling and the treatment of such fragile drug-permeable early embryos of *C. elegans*.

5.2 *C. elegans* embryogenesis

5.2.1 The reproductive system of *C. elegans* hermaphrodites

The reproductive system of *C. elegans* hermaphrodites provides the environment for oocyte fertilization and egg laying. It consists of 3 major parts (Fig. 5.1): the egg-laying apparatus, the somatic gonadal sheath and the germline cells. The germline and somatic gonad together form two U-shaped gonad arms, which are connected to the uterus and egg laying apparatus through the spermathecae. The germline stem cells move out from the distal tip of a gonad arm and then go through a mitotic stage, before entering meiosis and arresting in prophase I. Meiosis resumes after fertilization, which takes place as the oocyte is pushed into the spermatheca by contraction force generated by the oviduct [173]. The side of the sperm entry appoints the future posterior end of the embryo. The posterior end is normally the site, where the oocyte first penetrates into the spermatheca. The oocyte nucleus is located at the opposite end, which becomes the future anterior end of the embryo.

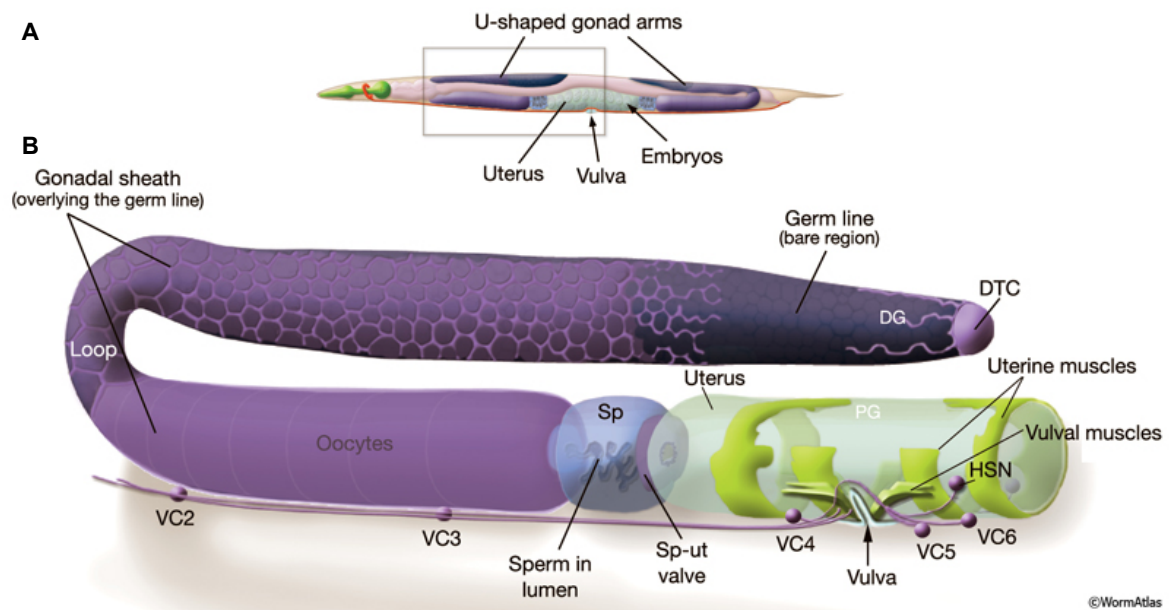


Figure 5.1 The *C. elegans* hermaphrodite reproductive system.

(A) Schematic of the adult hermaphrodite with twofold symmetry, consisting of two U-shaped gonad arms linked to a common uterus. (B) Enlarged view of the left gonad arm, showing, among others, the distal tip cell (DTC), the distal gonad (DG), the proximal gonad (PG), the spermatheca (Sp), and the spermathecal-uterine valve (Sp-ut). The figure is reproduced from [174].

5.2.2 The timeline of embryogenesis

In *C. elegans*, the self-fertilizing XX wild-type hermaphrodite is the most common sex compared with a small percentage (0.1%) of XO males. In general, gravid adult hermaphrodite lay about 200 embryos within 2.5 - 6 days, resulting in genetically identical progeny [140]. Before reaching the L1 larva stage, the *C. elegans* embryos pass through several distinct stages (Fig. 5.2). *C. elegans* embryogenesis may be roughly divided into two phases: *in utero* development (0 - 150 min) and *ex utero* development (150 - 840 min) at 20-22°C. *In utero* development involves cell divisions from the 1-cell stage to the beginning of the gastrula stage (about 30-cell stage), which encompasses the time from zygote formation to the generation of embryonic founder cells. Subsequently, the embryo is laid outside and cell proliferation continues. At the end of the three-fold stage, the worm can twist inside the embryo eggshell, indicating advanced motor system development. L1 larva hatching occurs at around 800 min [175].

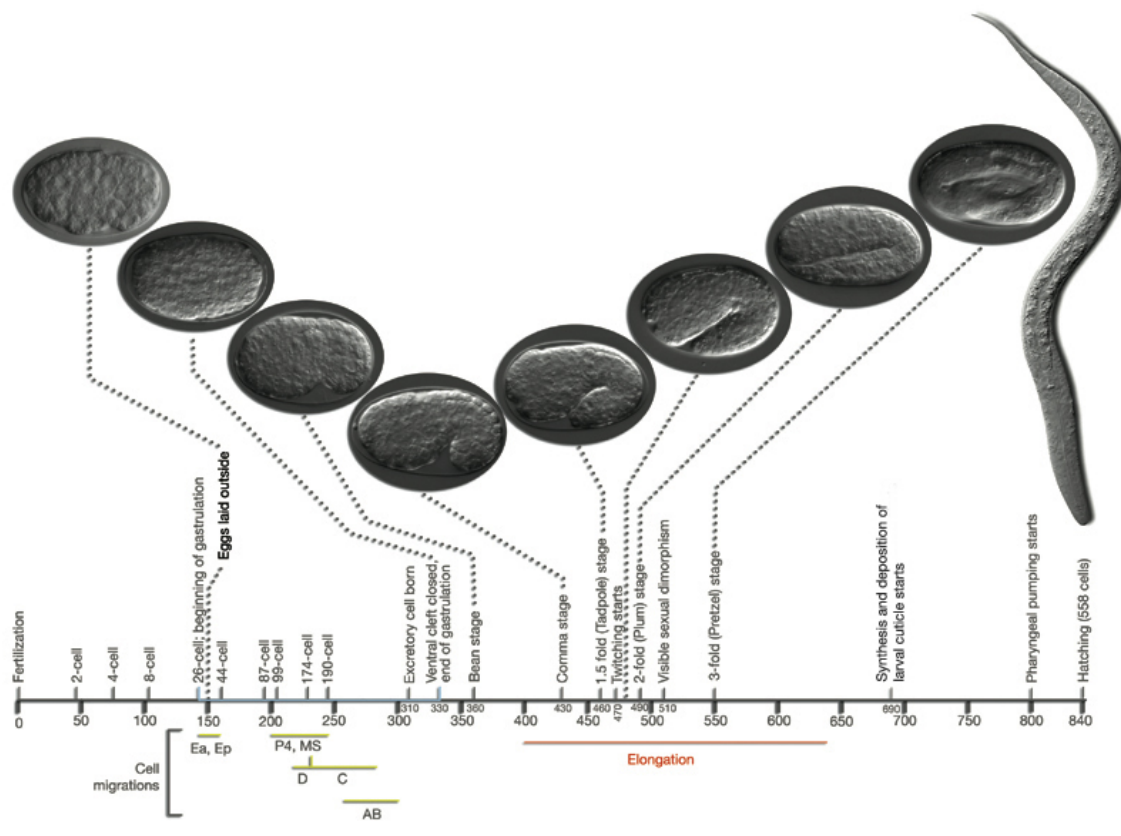


Figure 5.2 Timeline of *C. elegans* embryogenesis.

Timeline with key events of the *C. elegans* embryonic development from the 1-cell stage up to hatching (wild-type worms, for 22°C). Reproduced from [140].

5.2.3 The early stage *C. elegans* embryo

5.2.3.1 1-cell to 4-cell: Generation of the founder cells

The stereotypic cleavage pattern during *C. elegans* embryogenesis is normally invariable in WT hermaphrodite embryos and has been studied in detail [175]. Therefore, the fate of every embryonic cell is known. The oocyte nucleus completes meiosis I and meiosis II within ~20 min and ~30 min after fertilization at 20–22°C, respectively (Fig. 5.3A). The male and female pronuclei (*i.e.* sperm and oocyte-driven pronuclei) then start migrating and fusing with each other. The metaphase of mitosis occurs shortly thereafter. During the first asymmetric division, the anterior-posterior (AP) embryonic axis is established, followed by a series of asymmetric division derived from the anterior AB and posterior P1 blastomere. During the first five divisions, six founder cells are generated: AB, MS, E, C, D, and P4, whose descendants each produce specific cell types (Fig. 5.3B) [175].

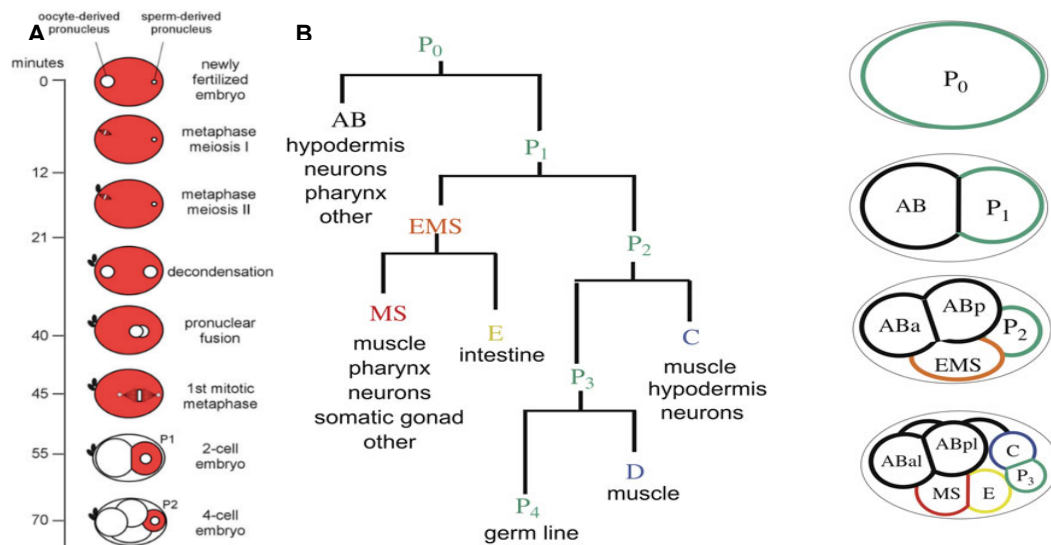


Figure 5.3 Embryogenesis of the early *C. elegans* embryo.

(A) Schematic of events following *C. elegans* embryos fertilization. The timeline of the embryonic cell cycle from the newly fertilized 1-cell stage ($t = 0$ min) to the 4-cell embryo stage ($t = 70$ min) is shown (for 20–22°C). **(B)** Generation of founder cells in the early embryo: Cell lineage of the early embryo (left) and schematic diagram of cell positions at different stages (right). Reproduced from [176].

5.2.3.2 Events in 1-cell stage

Here, we focus on the most important events that occur during the 1-cell embryonic cell division (Fig. 5.4). After pronuclear fusion, prometaphase starts abruptly with the breakdown of the nuclear envelope. Chromosomes can now attach to spindle microtubules via their kinetochores and undergo active movement. Subsequently, at metaphase and anaphase, the chromosomes are aligned at the equator of the spindle, midway between the spindle poles. The sister chromatids synchronously separate to form two daughter chromosomes, and each is pulled slowly towards the spindle pole it faces. During telophase and cytokinesis, the two sets of daughter chromosomes arrive at the poles of the spindle and decondense. The cytoplasm is then divided by a contractile ring of actin and myosin filaments, which pinches the cell to create two daughters, each with one nucleus (2-cell stage).

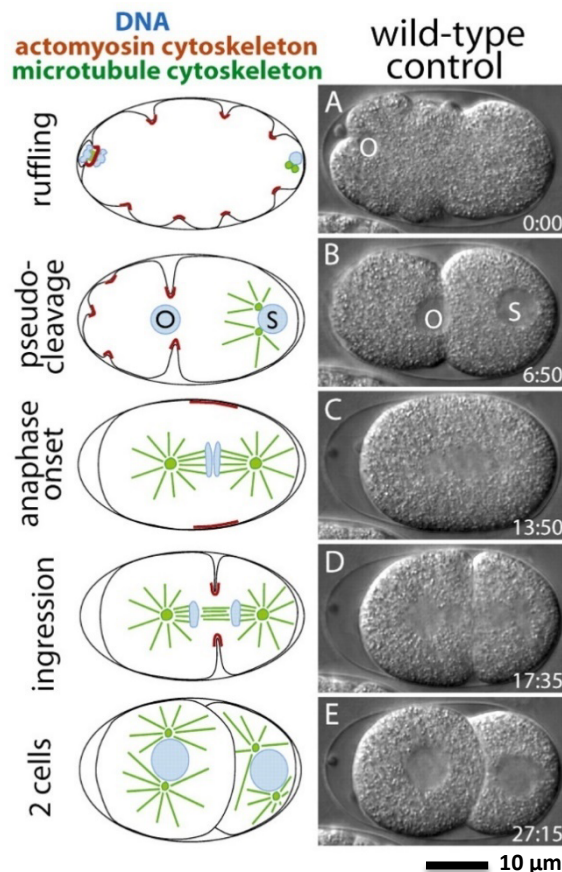


Figure 5.4 *C. elegans* 1-cell embryo stage.

Schematics illustrating major events in the 1-cell stage of a *C. elegans* embryo from meiosis to cytokinesis and corresponding embryo images selected from time-lapse DIC sequences (A-E). The embryo anterior is on the left-hand side, the posterior (defined by the site of sperm entry) is on the right-hand side. Scale bar = 10 μm . Reproduced from [177].

5.2.4 The role of actin and myosin II in cytokinesis

5.2.4.1 The contractile ring

A cell cycle typically ends with cytokinesis, *i.e.* the division of the cytoplasm. Typically, cytokinesis follows every mitosis, despite some cell types exist, *e.g.* in early *Drosophila* embryos, that don't show cytokinesis and thereby acquire multiple nuclei during mitosis. In *C. elegans* embryo cells, as in most animal cells, cytokinesis starts in anaphase and ends after the completion of mitosis in the telophase. The most obvious change during cytokinesis in the animal cell cycle is the fast formation of a cleavage furrow on the cell surface. The cleavage furrow rapidly shrinks and contracts inward until the parent cell is divided into two daughter cells. In animal cells, this composite structure is also called contractile ring, which is dynamically assembled by actin filaments, myosin II filaments, and many structural and regulatory proteins. Fig. 5.5A shows some drawings of the assembly of the contractile ring beneath the plasma membrane during anaphase. SEM images of the contractile ring and the enlarged furrow are shown in Fig. 5.5B and 5.5C.

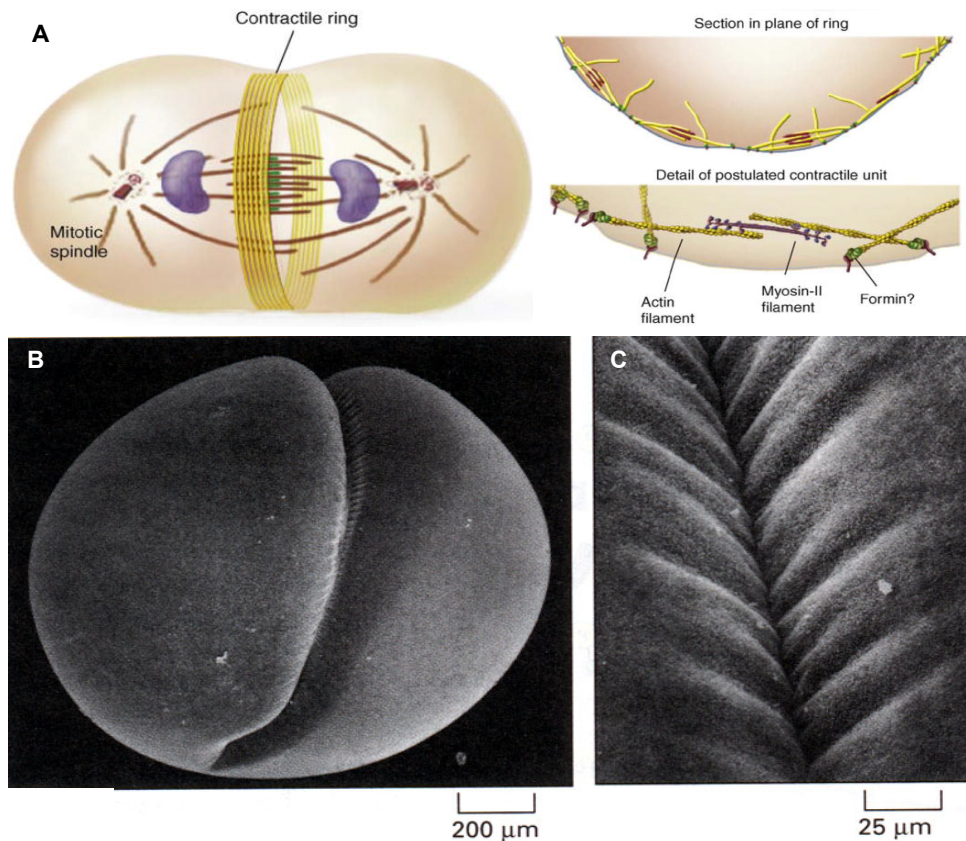


Figure 5.5 Generation of the contractile ring during cytokinesis.

(A) Schematic drawings of a contractile ring. Actin-myosin bundles of the contractile ring are shown, which pull the cell plasma membrane inwards. Reproduced from [178, 179]. **(B)** SEM picture of a cleaving frog egg. The insertion of the cell membrane is caused by the action of the contractile ring beneath the membrane. Due to its large size, the egg cleavage furrow is especially well-defined. **(C)** High magnification SEM micrograph of the furrow. (B, C) Reproduced from [178].

5.2.4.2 Actin-binding small-molecule drugs

Specific small molecules are one of the most widely used inhibitor groups for researchers studying multiple aspects of cell biology, ranging from control of cell cycle to gene expression and signaling pathway [180]. For the actin filament dynamics studies, small molecules such as Phalloidins, Latrunculin A, Cytochalasin B, Cytochalasin D, Jasplakinolide and Dihydrocytochalasin B are widely used, due to their ability to alter actin dynamics. However, these unmodified drugs have proven to be unsuitable for pharmacological treatments, as they feature a poor capability to permeate the cell membrane or even have adverse effects on the cell (Fig. 5.6A). Phalloidin functions by binding and stabilizing filamentous actin (F-actin) and effectively prevents the depolymerization of actin fibers. The properties of its derivatives have been widely used in microscopy to stain actin filaments in biomedical research by labeling phalloidin with fluorescent tags. Jasplakinolide is known as a toxin which binds to F-actin competitively with phalloidin. It stabilizes actin monomers (G-actin), thereby accelerating filament assembly [181]. Cytochalasin D, a well-known actin polymerization inhibitor, binds F-actin at the barbed end to prevent actin filament assembly and disassembly at that end. Its effect results in disruption of the actin filaments of the cytoskeleton, which has proven to be a useful tool allowing visualization of the corresponding changes made to cellular processes (Fig.

5.6 B, C). The property of Latrunculin A is similar to that of cytochalasin D which binds to actin monomers (G-actin) to inhibit their polymerization and disassembly.

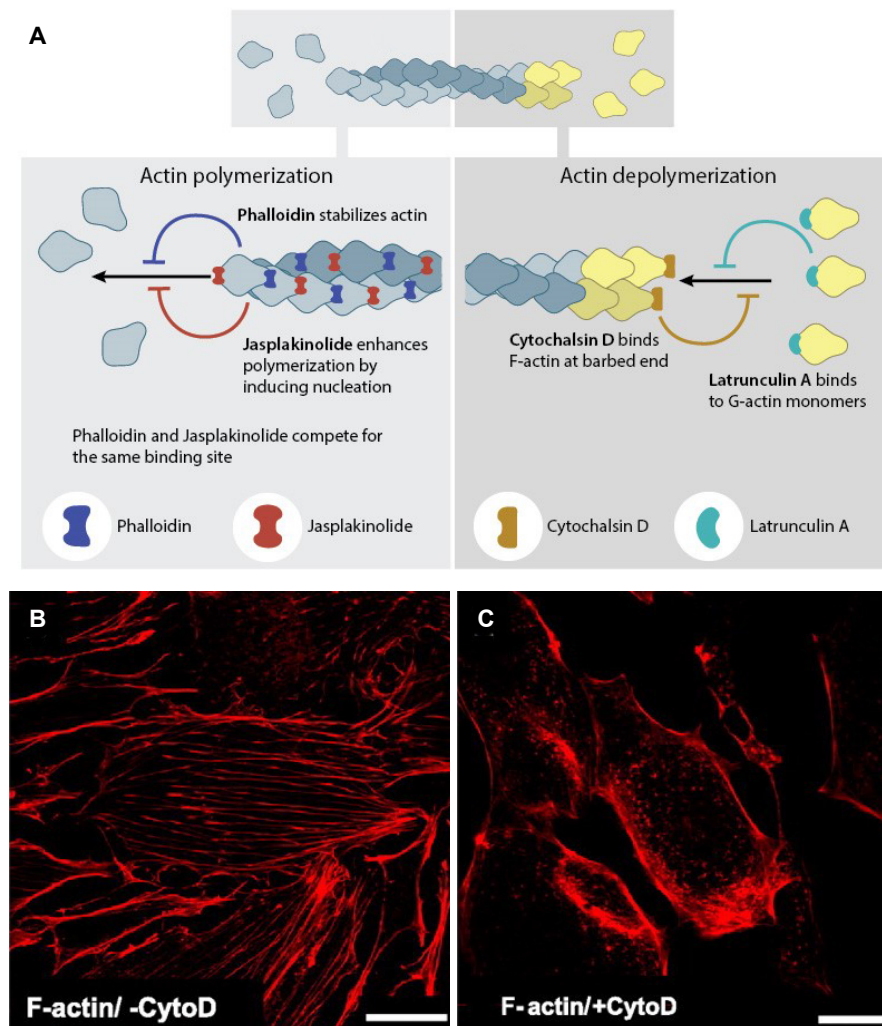


Figure 5.6. Actin-binding small-molecule drugs.

(A) A number of small-molecule drugs can bind to actin either during polymerization or depolymerization, with varying effects on the actin filament dynamics. Reproduced from [182]. (B) In untreated cells, GFP-CD151 shows a co-localization with actin filaments. (C) After inhibition of actin polymerization, GFP-CD151 actin rich spots were evident. Scale bar = 25 μ m. Reproduced from [183].

5.3 The challenges and opportunities for drug studies during *C. elegans* early embryogenesis

Typically, early embryos are obtained by manual dissection of adult hermaphrodite worms and are subsequently transferred onto agarose pads prepared on a microscope slide for imaging [172] by the following steps: (i) agarose pads are prepared by adding a drop of 2% w/v agarose to the clean, pre-warmed glass slide; (ii) pick around 5 adult hermaphrodite worms from NGM or RNAi plates and release them in a well with M9 buffer solution on a depression slide; (iii) use a scalpel to cut the worms into half near the either of spermatheca in order to release early embryos into the buffer solution (Fig. 5.7A); (iv) transfer the released embryos

with a mouth pipette to a second well containing M9 buffer, to get rid of worm debris from the embryos; (v) suck the embryos onto the prepared agarose pads; (vi) collect the embryos close to each other with an eyelash to make them fill into the same x and y plane; and (vii) cover the agarose pads with coverslips and seal the edges with liquid (petroleum jelly, lanolin and paraffin; melted and combined 1:1:1) to prevent dehydration of the embryos (Fig. 5.7B). Despite the fact that a trained person can isolate embryos relatively quickly, dissection sometimes must be repeated several times to capture the desired early embryo stage, in particular in mutant or RNA interference (RNAi)-mediated conditions.

Another main limitation is the drug-impermeability of the embryo shell which prevents the drug accessing inside the embryo. Hyman *et al.* reported a laser beam punching technique allowing the permeabilization of the embryo shell and access to substances from the surrounding solution [184]. For this method, a nitrogen-pulsed dye laser was installed on a fluorescence microscope and was set up to focus on the middle plane of embryo close to the anterior end of the embryo. The challenge faced by the laser punching technique is that it is difficult to judge the permeabilization success of the embryo after punching. Besides, the drug entry is confined to a narrow punching hole which leads to non-uniform inhibitor diffusion into the embryo cells. Hill *et al.* proposed an embryo crush method for permeabilization by applying pressure on the coverslip [185]. However, this compression method is difficult to control. Edgar *et al.* demonstrated that the embryo shell can be permeabilized by bleaching. This method requires accurate bleaching time control, which is difficult to execute consistently.

Carvalho *et al.* reported a RNAi-based method for the permeabilization of *C. elegans* embryo shell, which allows small-molecule soaking into the embryo. RNAi knockdown of the *perm-1* gene has been used to render the embryonic eggshell permeable to small molecules, with minimal deleterious effects on normal cell processes during the early embryonic development [186]. However, permeabilized embryos are very fragile, making manual manipulation and drug application even more cumbersome. Carvalho *et al.* proposed to address this issue arising during *perm-1* (RNAi) protocols by manually pushing embryos into a dedicated microwell array right after dissection (Fig. 5.8) [186]. The device consists of a PDMS worm reservoir and an embedded dissection board coverslip located on one side, whereas the 16 microwells are positioned on the other side, as shown in Fig. 5.8B. The gravid worms were first placed in the reservoir for manual dissection, and the released embryos were then immobilized by moving them into the microwells with an eyelash for further imaging under a microscope (Fig. 5.8C). During the experiment, the buffer/drug solution can be exchanged. This device provides some convenience for the fragile embryo handling; however, for the time being, there is no automated and high-throughput method specifically designed for handling and drug treatment of fragile drug-permeable *C. elegans* early embryos.

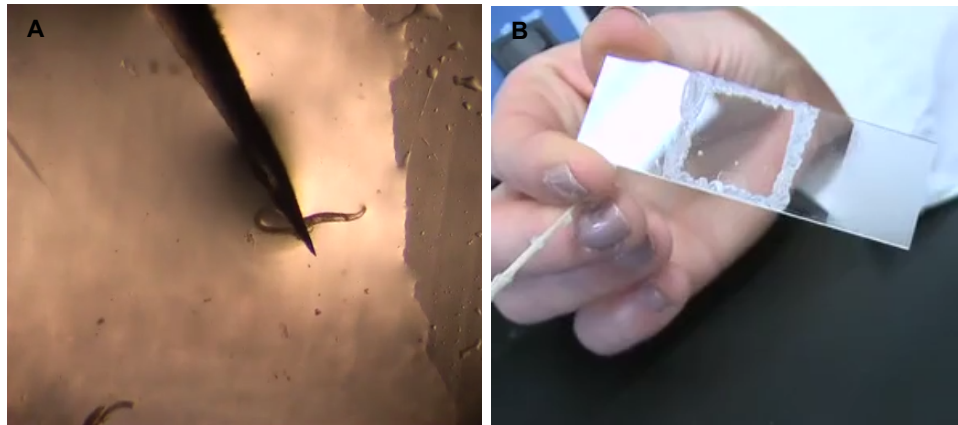


Figure 5.7 Conventional *C. elegans* embryo slide preparation.

(A) A sterilized scalpel is used to cut the worms on either side of the spermatheca (or alternatively near the vulva) to release embryos into the solution. (B) Embryo slide with a coverslip, and sealed with pre-heated liquid VALAP (petroleum jelly, lanolin and paraffin; 1:1:1) to prevent dehydration of the embryos during imaging. Reproduced from [187].

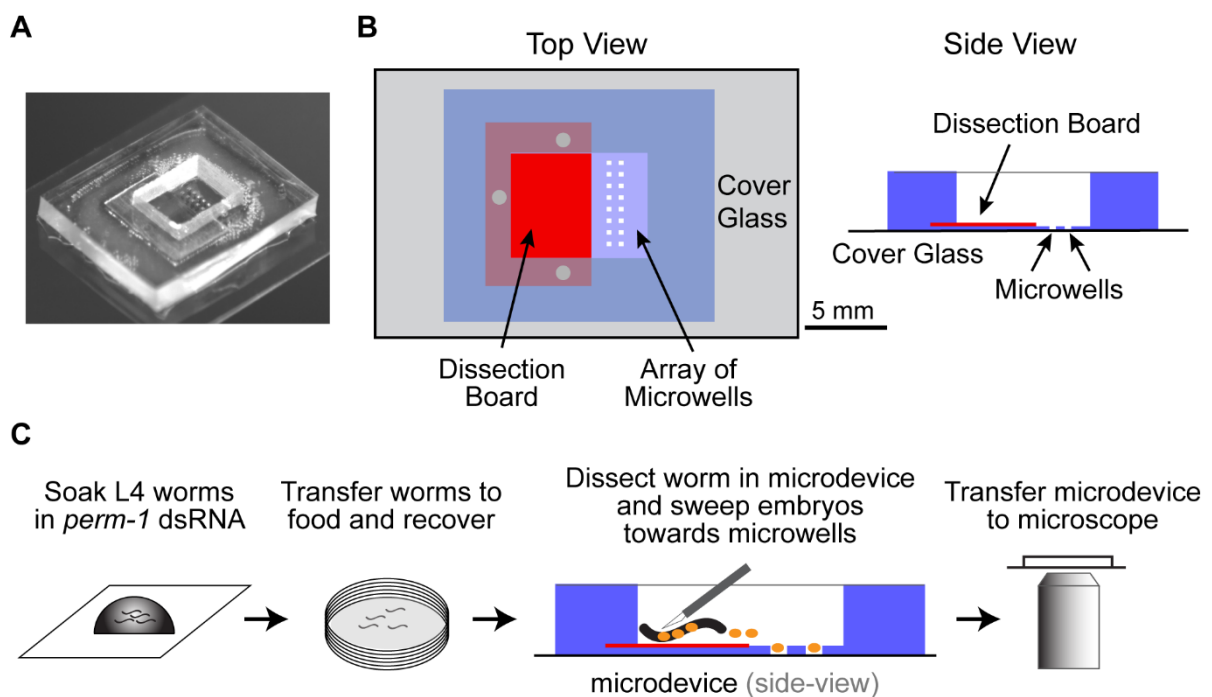


Figure 5.8 A microdevice for immobilization of permeable embryos, imaging and small-molecule drug application.

(A) Photograph of the microdevice. (B) Schematic drawings of the top and side views of the microdevice. (C) Schematic depicting the procedure for preparing permeabilized embryos for drug treatment and imaging. *C. elegans* hermaphrodites at the L4 larval stage are soaked in a drop of *perm-1* dsRNA for 4 hours at 20°C. The worms are transferred to a plate with bacteria and allowed to recover for 16 hours at 16°C. 1–3 worms are placed on the dissection board of the microdevice after filling it with ~100 µL of media. Worms are dissected with a scalpel and the released early embryos are swept into the microwells with an eyelash tool. The microdevice is transferred to the microscope and the embryos are imaged. When the desired stage is reached, the medium in the microdevice is replaced with fresh medium containing the drug of interest. Reproduced from [186].

5.4 Microfluidic platform for early embryo trapping and drug delivery

Previously, our group introduced a microfluidic device for trapping non-permeabilized embryos naturally laid by gravid *C. elegans* adults [188]. This device allowed studying the different phases of embryogenesis after egg laying, which occurs typically after gastrulation has been initiated at the ~30 cell stage. In this section, we describe the development of a novel integrated microfluidic approach enabling: (i) rapid and highly efficient extraction of embryos at earlier stages of development directly from gravid adults without perturbing embryo physiology, (ii) fluidic transfer and immobilization of single embryos in a microtrap array for high-resolution imaging and analysis of development starting from the 1-cell stage, and (iii) precise handling and transport of small liquid quantities for controlled drug applications. We demonstrate the potential of the new device using time-controlled delivery of the actin-polymerization inhibitor Cytochalasin D to prevent cytokinesis in early embryos [189].

5.4.1 Chip design for embryo extraction and trapping

Our device comprises two main functional PDMS components (Fig. 5.9A): an embryo extraction chamber including an array of partly compressible PDMS pillars featuring an innovative design for embryo extraction without damage (Fig. 5.9B), and the linear trapping array for aligning immobilized individual embryos (Fig. 5.9C). The extraction chamber (length 2 mm, width 2 mm, height 60 μm) is large enough to accommodate up to 20 *C. elegans* adult worms. It is bordered by specific on-chip filter structures (leading to a spacing of 60 μm) for the confinement of adult worms, selective transfer of embryos and debris removal. The principle underlying embryo extraction relies on their mechanical expulsion from the uterus of the worms via the application of manual pressure pulses to the roof of the extraction chamber. This step is monitored under a stereo microscope. To prevent embryos from being smashed between the roof of the chamber and the coverslip during extraction, we developed an array of custom-designed PDMS pillars, which securely maintains a minimal height of 30 μm when a pulse is applied on the roof of the chamber. These pillars feature two parts: a 40 μm high compressible and foldable crescent-shaped structure and a 20 μm high, essentially incompressible, cylinder-shaped pad on top of it. The pillar array can be either in a released or a compressed state (Fig. 5.9D). In the released state, the pillar height is 60 μm , corresponding to the typical body centroid diameter of adult worms. By compressing the chamber, the foldable part of the pillars collapses onto the cylinder-shaped pillar pad, eventually resulting in virtually incompressible structures. Considering the elastomeric properties of PDMS, we adjusted the geometrical parameters of the pillars to obtain a total height of ~30 μm for the compressed structure. This arrangement is insensitive to variations in the pulses of applied manual pressure, such that embryos, whose centroid diameter is ~30 μm , are shielded during the extraction procedure. Photographs of the pillar array in either state and of the full PDMS chip sealed to a glass coverslip are shown in Fig. 5.9E, F and G, respectively.

We used standard PDMS soft lithography techniques to fabricate the microfluidic chips. The master mold was made by a two-step process. First, patterns for all fluidic structures, in particular the trapping array and the foldable parts of the pillar array, were created on a silicon wafer by plasma etching (structure height 40 μm). Subsequently, a 20 μm thick SU-8 layer was spin-coated on the wafer and patterned to form the non-compressible pillar top pads, as

well as to increase the total height of the main chamber and of the In1-Out1 fluidic path to 60 μm (Fig. 5.9A and 5.9D).

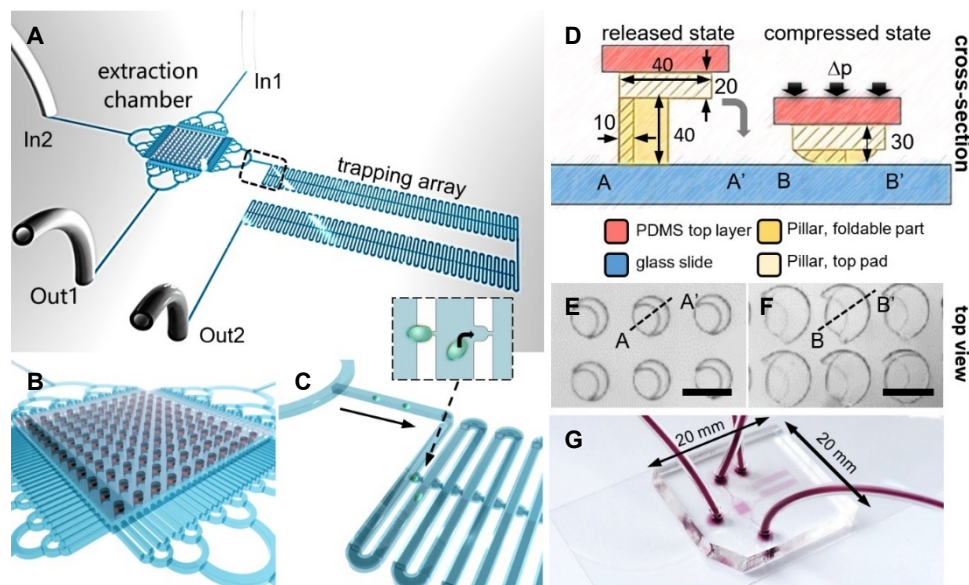


Figure 5.9 Microfluidic embryo harvesting and drug delivery chip.

(A) The integrated chip comprises a chamber with a reversibly compressible PDMS pillar array for extraction of embryos from gravid *C. elegans* worms, and an adjacent embryo trapping array. The device has two fluidic inlets (In1, In2) and two outlets (Out1, Out2). **(B)** Schematic view of the extraction chamber, and **(C)** of the embryo transfer into the trapping array. The inset shows a magnified view of the single-embryo trapping process. **(D)** Cross-sectional views of a PDMS pillar (units are μm), built from a foldable crescent-shaped structure and a solid top pad, in its released (60 μm high) and in its compressed state (~ 30 μm high), respectively. The foldable part faces the glass substrate. Pressure is applied on the chamber roof (a 5 mm thick PDMS top layer, not to scale in the figure). **(E, F)** Top view images of a detail of the pillar array in the released **(E)** and compressed state **(F)**, respectively. Scale bar = 50 μm . **(G)** Photograph of the PDMS-on-glass chip (20 mm \times 20 mm) with fluidic connections. Microfluidic features are dyed in red.

5.4.2 Chip operation

The device is equipped with external flow control through two inlets (In) and two outlets (Out), via computer-controlled syringe pumps that enable rapid and time-controlled fluidic operations. First, a suspension of 10-15 gravid worms is introduced in the extraction chamber through the In1-Out1 fluidic path (Fig. 5.10A). Worms are blocked inside the extraction chamber by the bordering PDMS filter structures (Fig. 5.10B). After mechanical expulsion of the embryos from the worms' uterus through the application of pressure, the embryos are dispersed in the chamber (Fig. 5.10C). In general, almost all the embryos are released from the gravid worms after pressing 3 times on the chamber roof. Thereafter, activation of flow along the In1-Out2 path transfers the embryos into the trapping array that is 40 μm in height, where they are immobilized by passive hydrodynamic action (Fig. 5.10D). Each microtrap accommodates a single embryo (Fig. 5.10E). A transfer and trapping rate analysis is shown in Table 5.1. The yield of successful transfer of the released embryos was 91 ± 3 %, with the remaining embryos sticking to the walls of the extraction chamber. The trapping rate of transferred embryos was 96 ± 1 %. The total timespan from embryo extraction to imaging is 2-

3 min. Thanks to the accurate geometric alignment of the microtraps, the locations of selected embryos can be readily recorded for subsequent imaging. An XYZ microscopy stage is used to scan the array to find and mark positions of those traps containing embryos at the desired stage. The embryo array can receive up to 100 individual embryos at development stages that reflect the natural *in utero* distribution since most embryos are expelled from the adult worms during extraction. Depending on the initial number of worms, the array filling rate is typically 60-90 %. In this way, about 10 1-cell stage embryos can be captured per experiment and selected for further analysis. Importantly, drug compounds can be simultaneously applied to all embryos trapped in the device via the In2-Out2 fluidic path (Fig. 5.10F), and dynamic cellular processes can then be analyzed at high resolution. Laminar flow conditions and computer-control allow for fast and reproducible fluidic exchange on-chip (~70 s at 100 nl/s), enabling accurate drug delivery protocols. The chip can be reused after rinsing with deionized water. A typical bright field image of a 1-cell wild-type embryo in a microtrap is shown in Fig. 5.10G.

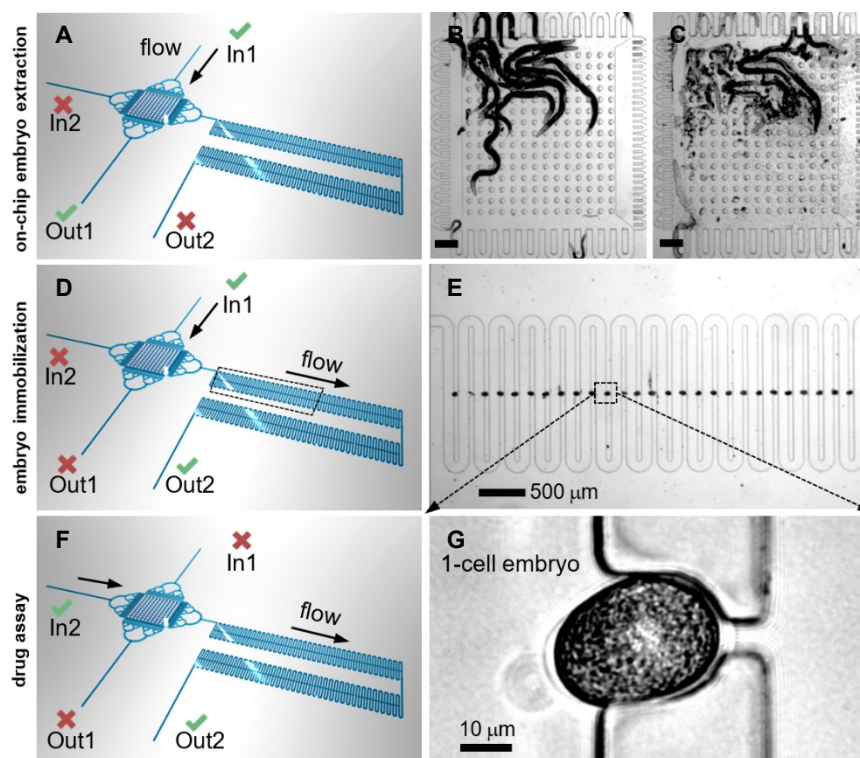


Figure 5.10 Fluidic operations and embryo handling.

(A, B) Protocol for on-chip embryo extraction: **(A)** Fluidic configuration for loading a suspension of adult worms into the extraction chamber (In1-Out1 open, In2-Out2 closed). **(B)** Image of 14 adult worms confined in the chamber. The PDMS micropillar array is in the released state. **(C)** Chamber after squeezing the worms by application of a pressure pulse on the chamber roof. A large number of extracted embryos populates the chamber. Scale bar = 200 μm. **(D, E)** Microtrap array for embryo immobilization: **(D)** Fluidic configuration for embryo transfer from the extraction chamber to the array (In2-Out1 closed, In1-Out2 open). **(E)** Serpentine microchannel with microtraps for hydrodynamic immobilization of the embryos. The image shows a nearly completely filled portion of the array. **(F, G)** Drug assay: **(F)** Fluidic configuration for the perfusion of drug compounds on early embryos (In2-Out2 open, In1-Out1 closed). Drug compounds may be applied through the serpentine channel in a well-controlled manner. **(G)** A zoom on a 1-cell embryo securely positioned in a microfluidic trap adjacent to the serpentine channel (bright field, 50×/0.55 objective).

Table 5.1 Embryo transfer and trapping rate.

‘Transfer rate’ is defined as the number of embryos ($t1$) entering the trapping array divided by the total number of released embryos (re) in the extraction chamber. ‘Trapping rate’ is defined as the number of immobilized embryos ($t2$) divided by the number of embryos ($t1$) entering the trapping array. The present on-chip embryo transfer and trapping rate analysis is based on three subsequent experiments.

assay	# worms		# embryos			transfer rate	trapping rate
	loaded	compressed	released (re)	transferred ($t1$)	trapped ($t2$)		
1	11	8	82	75	72	0.91	0.96
2	10	9	105	92	87	0.88	0.95
3	11	9	84	79	76	0.94	0.96

5.5 *C. elegans* early embryos on-chip drug assays

5.5.1 Study of complete *C. elegans* embryogenesis on-chip

To test whether wild-type *C. elegans* embryos develop normally in the microfluidic device, we monitored embryogenesis from the 1-cell stage all the way to hatching. For clarification, a graphical side view of a gravid adult *C. elegans* hermaphrodite is shown in Fig. 5.11. We found that our device enables the extraction and *ex utero* monitoring of early stages of development on-chip without any apparent damage to embryo physiology (using flow rates ≤ 100 nl/s). Fig. 5.11A-I is a sequence of representative bright field images of a wild-type embryo captured in a microtrap after mechanical on-chip extraction as described above. Several key events of embryogenesis are shown in Fig. 5.11A-I. Fig. 5.11A-C depicts the 1- to 4-cell stage, for instance. At the end of the 3-fold stage (Fig. 5.11H), the embryo starts moving inside the egg, indicating advanced motor system development. Hatching occurs ~ 800 min after fertilization at 20°C (Fig. 5.11I), in line with established values on agar substrates [175]. The on-chip hatching rate of the trapped early embryos was $97 \pm 3\%$. A more detailed hatching rate analysis is provided in Table 5.2. Embryo development and successive hatching events can be observed. These observations indicate that our device and protocol provide adequate assay conditions. In particular, our chip allows secure *ex utero* manipulation of 1-cell embryos, which is most challenging because the eggshell is not fully established at this stage [190].

Table 5.2 Hatching rate for on-chip embryogenesis assays.

On-chip hatching was analyzed for wild-type *C. elegans* early embryos comprising the 1- to 8-cell stage, as well as for embryos at later development stages (>8 cells). Here, the ‘early embryo hatching rate’ is defined by the ratio of hatched embryos with respect to trapped early embryos ($h1/t1$). The ‘total embryo hatching rate’ is defined by $(h1+h2)/(t1+t2)$. Unfertilized embryos do not fully develop (not included in the $t1$ or $t2$ count). This hatching rate analysis is based on 3 subsequent experiments (see also Fig. 5.11).

assay	1-cell to 8-cell (early embryos)		>8 -cell		unfertilized		hatching rate	
	trapped ($t1$)	hatched ($h1$)	trapped ($t2$)	hatched ($h2$)	trapped	hatched	early embryos	total embryos
1	31	31	38	35	3	0	1.00	0.96
2	37	35	45	42	5	0	0.95	0.94
3	33	32	37	34	6	0	0.97	0.94

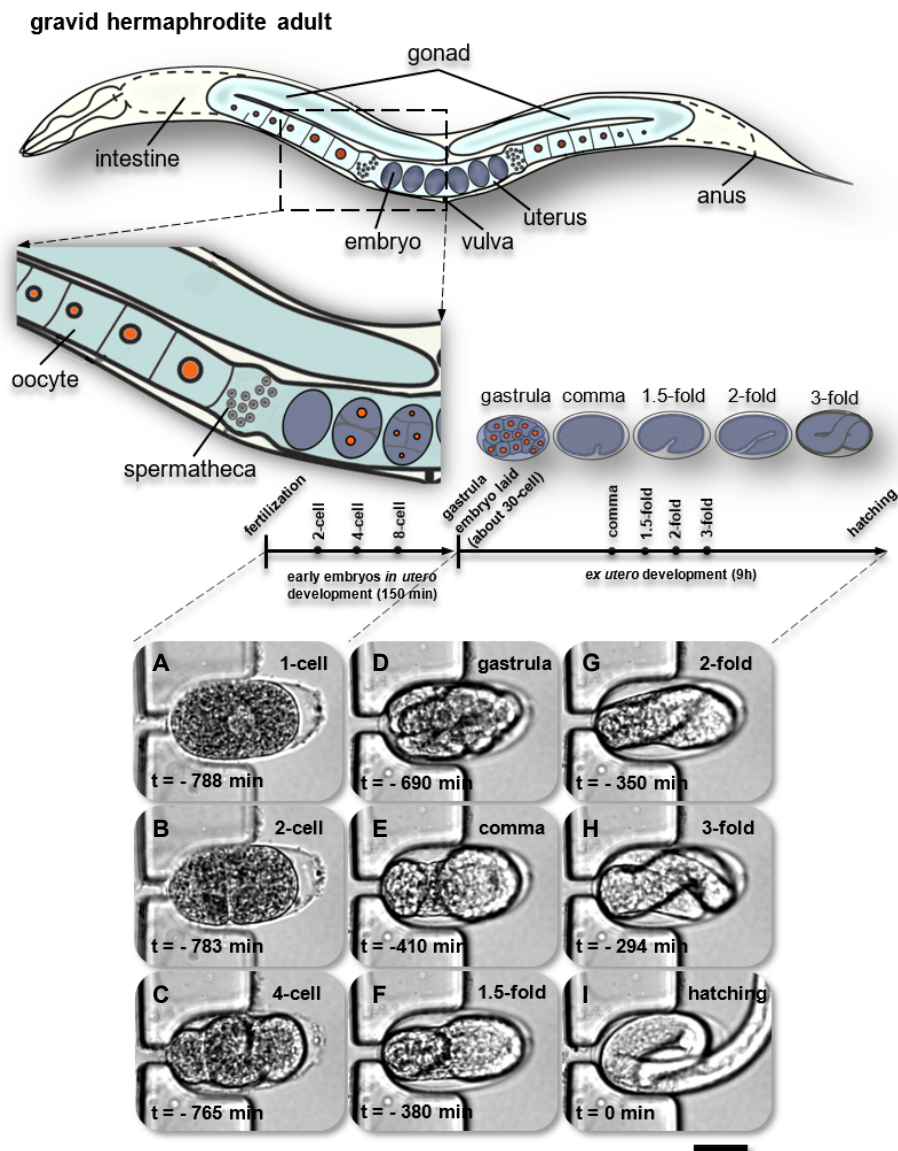


Figure 5.11 Study of complete *C. elegans* embryogenesis on-chip.

Schematic of anatomical structures of a gravid *C. elegans* hermaphrodite with two bilaterally symmetric gonad arms that are connected to a central uterus through the spermatheca. Embryos are shaded in blue-gray. The embryonic development timeline shows several key events with clearly distinguishable morphological changes during *in utero* (1-cell to gastrula, ~30 cells) and *ex utero* development (gastrula to hatching). **(A-I)** Live imaging of normal on-chip embryogenesis from the 1-cell division to larva hatching ($T = 23^{\circ}\text{C}$). Bright field images ($50\times/0.55$ objective) of a microfluidic trap located in between two parallel sections of the serpentine channel in the trapping array (see Fig. 5.10). An immobilized *C. elegans* embryo is shown in the 1-cell stage (A), and in subsequent main embryonic development phases **(B-I)**. The moment of hatching defines the time $t=0$ min. This sequence was taken over a timespan of about 13 hours (at time points indicated in the figure), demonstrating reliable embryo positioning over prolonged periods. Scale bar = $20\ \mu\text{m}$.

5.5.2 Study of drug treatment in *C. elegans* embryogenesis

The relatively big size and transparency of *C. elegans* embryos represent obvious advantages for analysis of mutant and RNAi conditions, and offers a potentially favorable setting for studying drug-induced effects on cellular physiology and development. In particular, early embryogenesis has great potential for drug testing thanks to the relative

simplicity and stereotypic spatiotemporal pattern of cell divisions allowing for automated and quantitative analysis. During the first few cleavage divisions, 6 embryonic founder cells are generated (*P4*, *D*, *C*, *E*, *MS*, *AB*), whose descendants generate specific cell types and tissues; for instance, the *E* cell is the sole precursor of the whole intestine (Fig. 5.12A) [175]. In order to test the potential of our newly developed device for performing drug assays, we set out to treat early *C. elegans* embryos transiently with Cytochalasin D (CD), a well-established actin polymerization inhibitor [189]. Among other functions, the actin cytoskeleton is critical for cytokinesis, the final step of cell division, during which two daughter cells are produced from the mother cell by a contracting actin-myosin ring which forms perpendicular to and in the middle of the mitotic spindle [191]. Accordingly, CD can effectively block cytokinesis in mammalian cells and in *C. elegans* embryos [185, 189].

For our study, we used drug-permeable embryos extracted on-chip from *perm-1(RNAi)*-treated gravid adult worms. The embryos were immobilized in the microfluidic trapping array and 1-cell embryos were selected for imaging prior to drug application. Whereas wild-type adults produce healthy early embryos in the trapping compartment (see Table 5.2), we found that this was not always the case for *perm-1(RNAi)*. Biomolecular mechanisms inherent to this mutant or, owing to the unusual fragility of the permeabilized embryo membrane, mechanical stress, in particular during immobilization, may be at the origin of the reduced normal development rate. Abnormal development could be observed at any stages, with one or several embryonic cells not developing properly. Nevertheless, in a typical experiment, 2 to 5 healthy *perm-1(RNAi)* embryos can be found in the micro-array, for which normal early development was observed (*i.e.* at least up to the 16-cell stage). Embryos expressing GFP-PH (pleckstrin homology (PH) domain from rat Phospholipase-C [192]) for visualizing cell membranes and mCherry-H2B (histone-H2B) for marking the chromatin were observed by wide field fluorescence time-lapse microscopy. Fig. 5.12B demonstrates on-chip drug treatment of an immobilized early embryo, and compares its early development to that of a control *perm-1(RNAi)* embryo exposed to 0.1% dimethyl sulfoxide (DMSO), which exhibited a normal division pattern (Fig. 5.12B- control row). In particular, it can be seen that the anterior *AB* cell divides ~2 min before the smaller posterior *P₁* cell (Fig. 5.12B- control row, 22:00 min and 24:00 min, respectively) [193]. For the drug assay, 10 μ M CD was applied onto *perm-1(RNAi)* embryos through the serpentine microchannel of the trapping array at a flow rate of 20 nl/s from $t = 12$ min to 24 min in Fig. 5.12B. During this time, failure of cytokinesis was observed in both *AB* and *P₁* blastomeres, resulting in the absence of cell division and the presence of two nuclei per cell in each case (Fig. 5.12B, arrowheads in the CD rows at 22:30 min and 24:00 min, respectively). Subsequently, the drug was readily washed out at $t = 24$ min within 3 minutes, and cytokinesis was rescued as a consequence (Fig. 5.12B, arrowhead in the CD row at $t = 27:00$ min). Interestingly, we observed that whereas *P₁* could initiate cytokinesis in a delayed manner at this time point, this was not the case in *AB*, where cytokinesis occurred only after the subsequent S-phase ($t = 40:00$ min), producing two instead of four *AB* descendant cells. We observed similar reversible effects on cytokinesis in four embryos in three experiments that contained suitably permeable *perm-1(RNAi)* embryos.

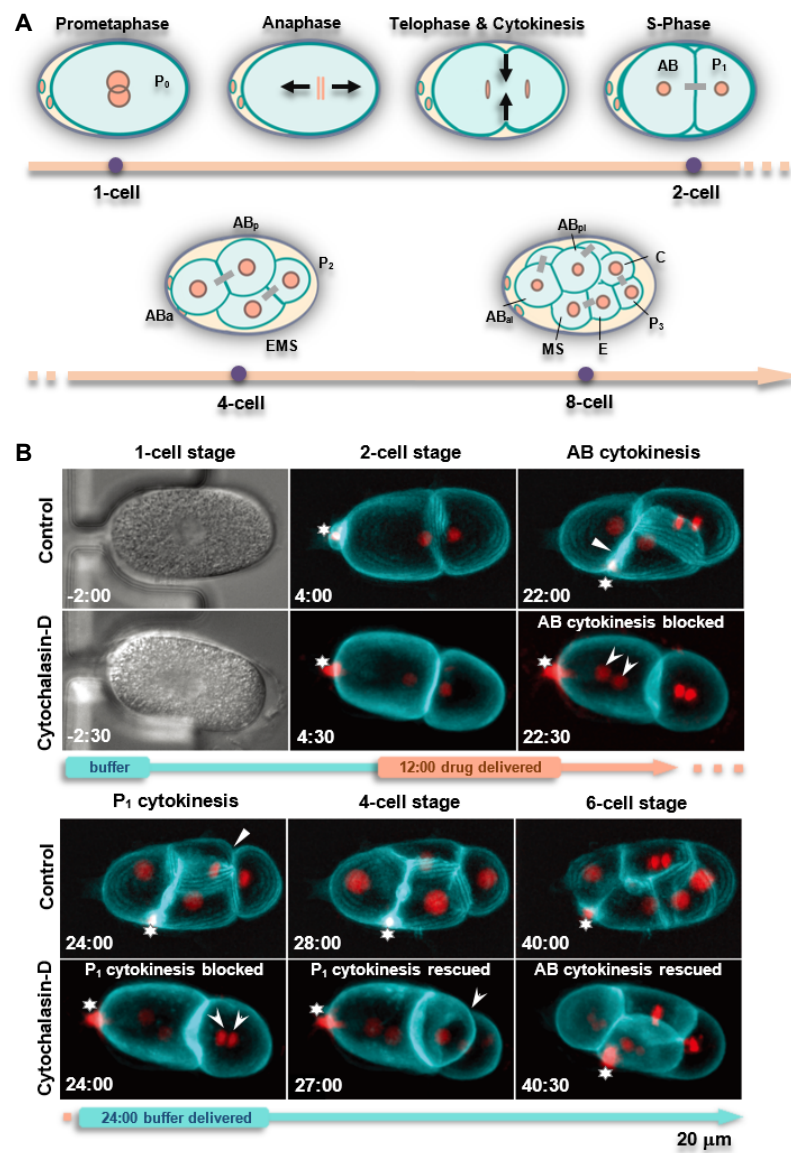


Figure 5.12 Early embryogenesis and on-chip drug treatment.

(A) Schematic diagram of mitosis in the 1-cell stage and cell arrangement in the 4- and 8-cell stage. Daughter cells coming from a common mother cell are connected with a gray bar; black arrows indicate movement of chromosomes in the anaphase and the constriction of the membrane during cytokinesis.

(B) Snapshots of the development from time-lapse recordings of permeable *perm-1(RNAi)* embryos expressing GFP-PH on the membrane (cyan) and mCherry-histone-H2B labeling chromatin (red) (63×/1.2 objective). Time is indicated in minutes. The 1st and 3rd rows of images show normal development of an untreated embryo immobilized in a microtrap (control), from prophase in the 1-cell stage until the 6-cell stage (white arrows indicate completed cytokinesis in AB and P₁ cells, note that AB normally divides two minutes before P₁). The 2nd and 4th row of images show temporary drug delivery to a permeable embryo (indicated on the timeline by the orange section). Subsequent to drug delivery at the 2-cell stage (t = 12:00 min) for a duration of 12 minutes, cytokinesis was blocked in both AB and P₁ cells, resulting in the presence of two nuclei in each cell (marked by arrowheads at t = 22:30 min and 24:00 min). After the drug was washed-off, cytokinesis in P₁ was rescued (t = 27:00 min) demonstrating that Cytochalasin-D was successfully washed-off. AB underwent cytokinesis only after completion of the next S-phase. Time stamps were synchronized with respect to the first metaphase. The star indicates a polar body containing highly compacted DNA extruded during the female meiotic divisions, which is highly mobile.

5.5.3 Materials and methods

5.5.3.1 Materials

L-Broth bacterial culture medium was prepared by adding 10 g Bacto™ tryptone, 5 g Bacto™ yeast and 5 g NaCl in 1 L of DI H₂O. L-Broth was sterilized by autoclaving. All chemicals used in L-Broth were purchased from Sigma-Aldrich (Buchs, Switzerland). Meiosis buffer was prepared by adding 350 µL of heat inactivated (30 min, 56°C) fetal calf serum (FCS, Gibco BRL) to 650 µL of Shelton buffer [194]. Cytochalasin D was obtained from AppliChem (Darmstadt, Germany). It was dissolved in dimethyl sulfoxide (DMSO) at 5 mg/ml (~10 mM) and stored at -20°C. It was then diluted in the meiosis buffer at 10 µM before use. DMSO was purchased from Sigma-Aldrich (Buchs, Switzerland).

5.5.3.2 Worm strains culture

N2 wild-type *C. elegans* worms and worms expressing mCherry::H2B to mark chromatin and GFP::PH to mark cell membranes (strain GZ1326, generated by crossing strains OD57 and OD58 [192] from the Caenorhabditis Genetics Center) were used in this work. Strains were maintained at 25°C on NGM agar plates seeded with the auxotrophic *E. coli* strain OP50 according to standard methods [4]. In order to obtain embryos with a drug-permeable eggshell, the bacterial feeding strain expressing dsRNA against *perm-1* (*To1H3.4*) gene was retrieved from the Ahringer RNAi feeding library [70]. Bacteria were grown overnight at 37 °C in LB medium with 100 µg/ml ampicillin at 250 RPM. The culture was then diluted 1:10 in LB with 100 µg/ml ampicillin and grown at 37 °C until reaching an optical density at 600 nm (OD₆₀₀) between 0.5 - 0.7. Then, the expression of dsRNA was induced with 1 mM isopropyl-β-D-thiogalactopyranosid (IPTG) and the culture was allowed to grow for one hour. The bacterial suspension was then spread on NGM agar plates (6 cm, ~350µL/plate) containing 0.1 mM IPTG. Plates were dried in a sterile hood for ~1 hour and left at room temperature for at least 24 hours before the use. Subsequently, 20 to 30 young adults were transferred onto each plate and incubated at 20 °C for 12 - 15 hours. As reported previously [186], *perm-1*(RNAi) needs to be carefully calibrated, as insufficient inactivation results in embryos that are not permeable enough, whereas excess inactivation increases the lethality of early embryos to a point that renders experiments unfeasible. Inactivation conditions between these two extremes led to suitably permeable and viable embryos as shown in Fig. 5.12.

5.5.3.3 Time-lapse microscopy

Fig. 5.11: Bright field images were obtained with a *Carl Zeiss Axiovert 100* inverted microscope, a *LD EC Epiplan-Neofluar 50×/0.55 BD DIC* objective and a *Hamamatsu Orca-ER High Resolution Digital B/W CCD C4742-95* camera. Images were captured every 60 s.

Fig. 5.12: Time-lapse dual DIC and fluorescence microscopy was performed with a *Carl Zeiss Axio Observer.D1* inverted fluorescence microscope equipped with motorized XY stage and piezo Z insert (both from Ludl Electronics Products, Ltd.), an *C-Apochromat 63×/1.2 W DIC* high-resolution water-immersion objective and an *Andor Zyla 4.2 PLUS sCMOS B/W* camera, and a *SOLA LED light-engine* (Lumencor, Inc.). One z-stack image (spacing 2 µm, 15 images per time point) was captured every 90 s in all three channels (DIC, GFP, RFP) using 50 and 75 ms exposure for GFP and mCherry, respectively (at 5% light output).

5.6 Conclusions

In summary, we report the first fully integrated microfluidic device for drug studies on *C. elegans* early embryos. The new device enables direct on-chip extraction of early embryos

from gravid *C. elegans* hermaphrodites, starting from the 1-cell stage. Released embryos are transferred into an adjacent microtrapping array for on-chip immobilization and high-resolution time-lapse imaging. The overall harvesting rate of released embryos is about 90% on a timescale of a few minutes. In a typical experiment, 60 to 90 embryos are captured, of which, in the case of the *perm-1(RNAi)* worms used in this work, 2-5 are healthy 1-cell embryos that are suitable for on-chip early embryogenesis studies. The microfluidic protocol enables fast compound exchange and its simultaneous delivery to all embryos in the array. This feature allows accurate drug delivery protocols, for instance the application and removal of a compound at specific stages of embryonic development. In particular, we demonstrated arrest and then rescue of cytokinesis in immobilized drug-permeable early embryos following time-controlled delivery of Cytochalasin D. Further improvement of our device may include separate drug delivery channels and/or a second on-chip array for simultaneous control assays. For a fully automated system, the manual pressure application for embryo extraction may be readily replaced by a computer-controlled device. We anticipate that, thanks to the accurate microfluidic control and the on-chip array architecture, our approach will enable the implementation of drug-screening assays based on *C. elegans* early embryos with clearly increased throughput and versatility. We note that our chip could be readily used for mutational screens in early embryos. In these regards, our device provides a novel and promising tool for future embryonic biological research or pharmacological studies based on the important *C. elegans* model organism.

Chapter 6 Single embryo pipette for accurate *C. elegans* bioassays

The nematode *Caenorhabditis elegans* (*C. elegans*) is a powerful model organism for addressing fundamental biological questions related to human disease and aging. Accurate control of the number of worms is a primary step for quantitative biological or biochemical worm analysis and assays. However, conventional single-worm isolation methods often encounter operational complexity, involving manual manipulation steps that result in relatively low throughput and a lack of accuracy, with possible physical damage of the worms. Here, we propose an “*Single Embryo Pipette*” (SEP) that was specifically designed for rapid and highly efficient dispensing of single *C. elegans* embryos, from an embryo suspension directly into standard microtiter plates. Our microfluidic device takes advantage of pressure-tuned flexible embryo microtraps by means of which single embryos can be easily captured and released on-demand. SEP fluidic manipulations do not have an adverse impact on embryo or worm physiology as monitored by normal development of the embryos after dispensing.

This chapter is an adapted version of the following publications:

L. Dong, J. Zhang, T. Lehnert, M. Gijs, “8-Channel Single Embryo Pipette for Accurate *C. elegans* Bioassays,” *The 31th IEEE International Conference on Micro Electro Mechanical Systems (IEEE-MEMS 2018)*, Belfast, UK.

L. Dong, J. Zhang, T. Lehnert, M. Gijs, “Single Embryo Pipette for Accurate *C. elegans* Bioassays,” *The 21st International Conference on Miniaturized Systems for Chemistry and Life Sciences (MicroTAS 2017)*, Savannah, USA.

Contributions: L. D. designed, built, and tested the microfluidic control instrument with input from J. Z., M. G., T. L. and P. G supervised the research, and provided reagents and funding. All authors reviewed and edited the manuscript.

6.1 Challenges and opportunities for *C. elegans* single embryo pipette

The accurate control of the number of worms per test condition is a prerequisite for meaningful and quantitative worm-based bioassays, *e.g.* for social behavior study [84], drug screening or toxicity testing [21]. Furthermore, for longitudinal studies of worm development and aging, it is important to be able to isolate and to track single worms over the whole lifespan. Currently, two main conventional approaches for accurate control of the number of worms exist: (i) Manual worm manipulation, including mouth pipetting and worm picking. Manual picking is a time-consuming and labor-intensive operation, and possibly has adverse effects on the worms' physiology [195]; (ii) Commercial automated sorting devices are available, such as the COPAS Biosorter, that can be used to sort and dispense worms as I introduced previously. This approach, however, is expensive and may not be accessible to many labs [196]. For the time being, only a few microfluidic systems have been developed that are capable of capturing and monitoring single worms on-chip. For instance, Hulme *et al.* introduced a microfluidic device for liquid culture and tracking of 16 single worms throughout their adult lifespan (Fig. 6.1A) [124]. Aubry *et al.* developed a microfluidic device for imaging and sorting of single early larval *C. elegans* in hydrogel droplets (Fig. 6.1B) [136]. However, a simple direct and stand-alone approach for the isolation and transfer of single worms into standard microliter plates or Petri dishes is not available for the time being. Moreover, dispensing directly a precise number of *C. elegans* embryos, combined with standard assays formats, has not been reported so far. Here, we describe a microfluidic pipetting device that enables rapid and sequential dispensing of single embryos into microtiter plates, for subsequent liquid culture and analysis of individual worms confined in separated reservoirs. This approach has a high potential for next-generation worm-based bio-assays with increased throughput and accuracy, *e.g.* the method can be applied to screen genetic variations within a given embryo or worm population with single animal resolution.

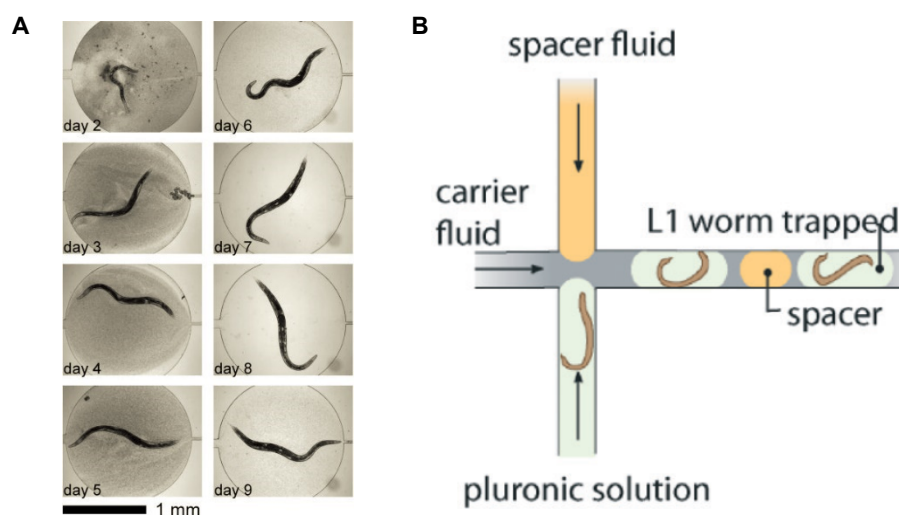


Figure 6.1 Microdevices for capturing and monitoring single worms.

(A) Microfluidic device for the liquid culture of many individual nematode worms in separate chambers. The figure is reproduced from [124]. (B) Design of an integrated system with microfluidics and Pluronic hydrogel to manipulate and image single *C. elegans* larvae. The figure is reproduced from [136].

6.2 Microfluidic device design and operation

6.2.1 Overview of the microfluidic device

Our novel device (Fig. 6.2) has a single PDMS fluidic layer featuring a single embryo trapping unit, for isolating and dispensing a single *C. elegans* embryo per well into a microtiter plate. Two syringes (S1 and S2) are connected to inlets In1 and In2 of the SEP chip for embryo suspension and buffer solution manipulation, respectively. Fig. 6.2A shows the design of a single embryo trapping unit. The core feature of the unit is a flexible PDMS on-chip microtrap structure for capturing a single *C. elegans* embryo and subsequent on-demand release. A photograph of the SEP chip is shown in Fig. 6.2B.

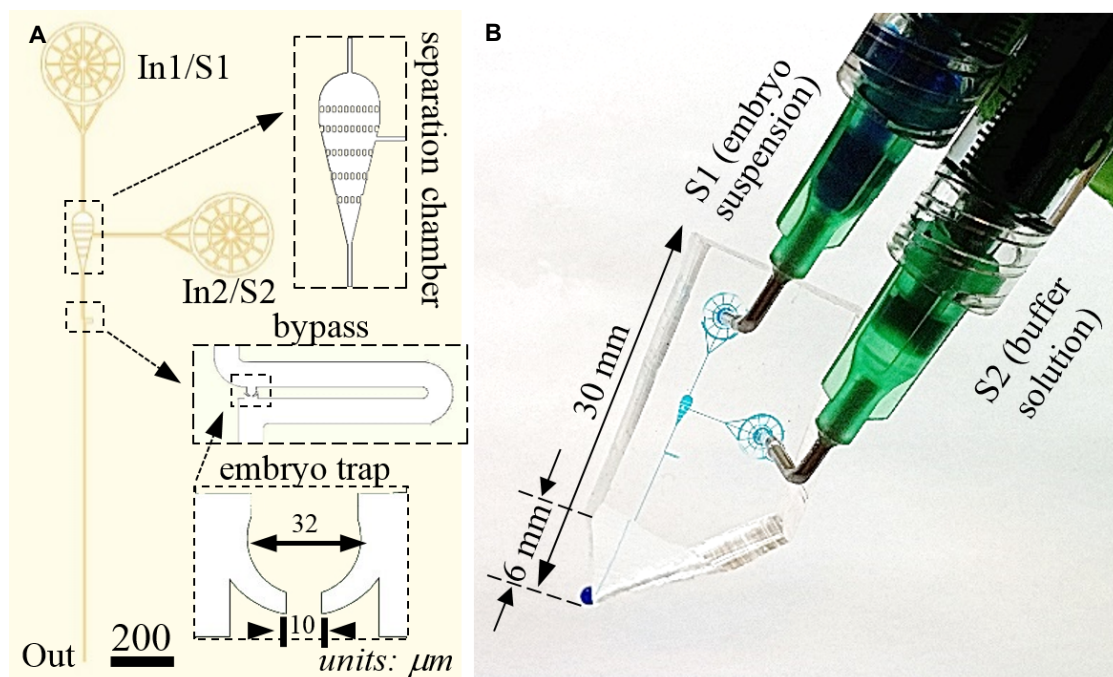


Figure 6.2 Microfluidic “Single Embryo Pipette” (SEP).

(A) Our SEP prototype is built up from a tapered microfluidic PDMS chip connected to two syringes (S1 and S2). The main feature of the SEP chip (inlets In1 and In2, outlet Out, channel height 35 μm) is an embryo trap for single embryo capture, positioned in between the two arms of a fluidic bypass, and a preceding pillar array structure for dispersing clusters of sticky embryos (separation chamber). (B) Photograph of the SEP chip connected to the syringes. The tip of the chip fits into the wells of a 96-well plate for convenient pre-loading of the embryos in the syringe. Microfluidic features are dyed in blue.

6.2.2 Device operation and sorting procedure

Single embryo dispensing is achieved by four steps: chip filling, embryo capture, washing and embryo release. Fig. 6.3 depicts this operation sequence of a single embryo trapping unit. 500 μL of an embryo suspension are loaded into the dedicated syringe (S1) by suction through the tip of the chip (Fig. 6.3A). Next, the flow is inverted and a small volume of embryo suspension ($\sim 10 \mu\text{L}$) is gently pushed through the chip (Fig. 6.3B). Thanks to its specific shape, a single embryo is securely immobilized in the embryo trap (Fig. 6.3E and F). The surplus of embryos is washed out and disposed by a buffer solution flow (syringe S2, Fig. 6.3C).

Subsequent release of the trapped embryo through the expandable PDMS gate structure of the trap is achieved by application of a short pressure pulse Δp (syringe S2, Fig. 6.3D and G). The embryo is then resuspended (Fig. 6.3H). This sequence may be repeated several times without reloading syringe S1.

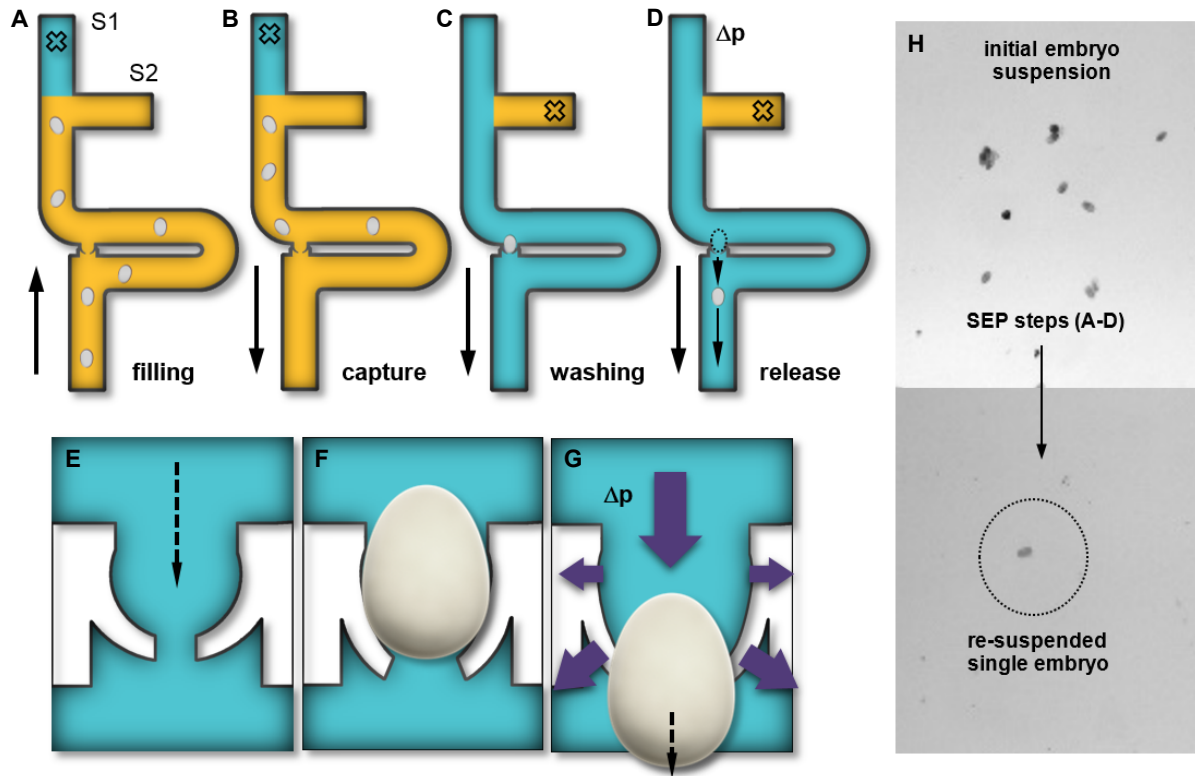


Figure 6.3 Single Embryo Pipette operation.

(A-D) Successive SEP manipulation steps, *i.e.* syringe filling (S1) with a *C. elegans* embryo suspension by suction through the chip, flow inversion for single embryo capture, washing and embryo release (S2). **(E-G)** schematic view of an extensible PDMS embryo trap; no embryo (gate gap 10 μm), immobilized embryo (width $\sim 30 \mu\text{m}$, length $\sim 50 \mu\text{m}$), and release of the embryo by applying a pressure pulse Δp (gate gap extends to 20-30 μm). **(H)** A single embryo isolated from a suspension by SEP operation.

Numerical simulations of the flow pattern around and through the trap structure reveal the passive hydrodynamic trapping mechanism (Fig. 6.4A). We characterized the device as a function of the fluidic resistance ratio of the bypass *vs* the embryo trap path (Fig. 6.4B), and design parameters were optimized for high single embryo capture efficiency ($\sim 75\%$) and moderate values for the required applied release pressure ($p_{in} \approx 1.5 \text{ bar}$).

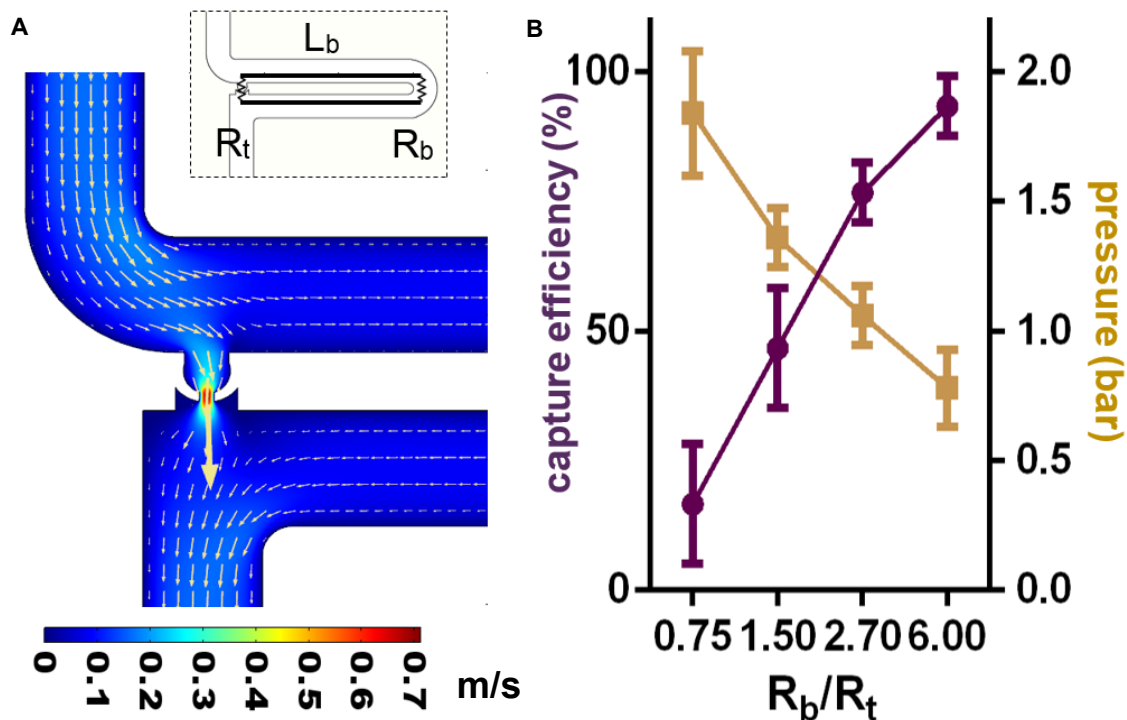


Figure 6.4 Microfluidic “Single Embryo Pipette” (SEP) characterization.

(A) Finite element analysis (FEA) of the flow velocity in the vicinity of the embryo trap (pressure 0.1 bar at In1, as is typically used for capture). The flow velocity vectors suggest how an embryo is deviated into the trap. The inset indicates important design parameters, i.e. the flow resistances R_t of the trap and R_b of the bypass (adjusted through the channel length L_b). **(B)** Single embryo capture efficiency (using a 10 embryos/ μ l suspension), and release pressure applied to In2, as a function of R_b/R_t ($n=5$). A ratio $R_b/R_t = 2.70$ was chosen for optimum operation conditions (Release pressure ≈ 1.5 bar, capture efficiency $\sim 75\%$).

An image sequence of single embryo capture and release is shown in Fig. 6.5. Due to the large fluidic resistance of the long bypass compared to the short capture path, an approaching embryo preferentially moves towards the microtrap where it is captured (Fig. 6.5 A,B). After immobilization of the embryo, the capture path is blocked, resulting in a strongly increased fluidic resistance. Thus, excess embryos are forced to flow along the bypass path and may be easily washed out with buffer solution (S2, Fig. 6.5C). Subsequently, the pressure pulse is applied through In2/S2 for embryo release (Fig. 6.5D). The embryo is recovered in the liquid droplet that forms at the outlet of the chip and may be resuspended. In order to evaluate the physiological impact of SEP fluidic manipulations, wild-type *C. elegans* embryos were dispensed on a glass slide for high-resolution brightfield imaging and monitoring of embryo development. Fig. 6.6A-F shows normal embryogenesis up to hatching, confirming that on-chip operations are carried out under benign conditions.

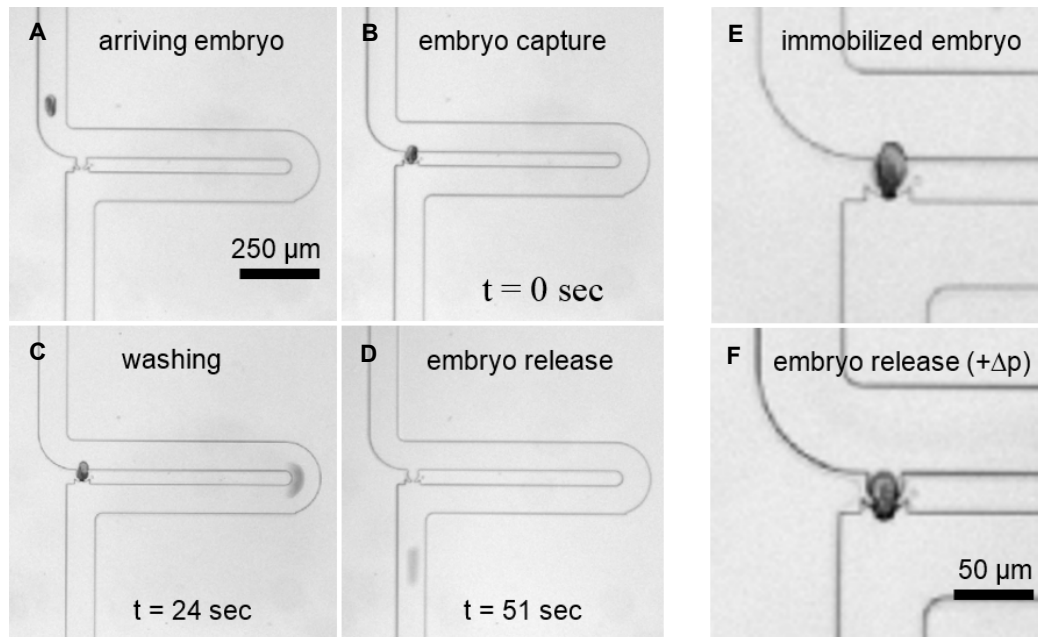


Figure 6.5 Live imaging of single embryo dispensing.

(A-D) Embryo capture and release. (E-F) Enhanced view of an embryo pushed through a trap immediately before release.

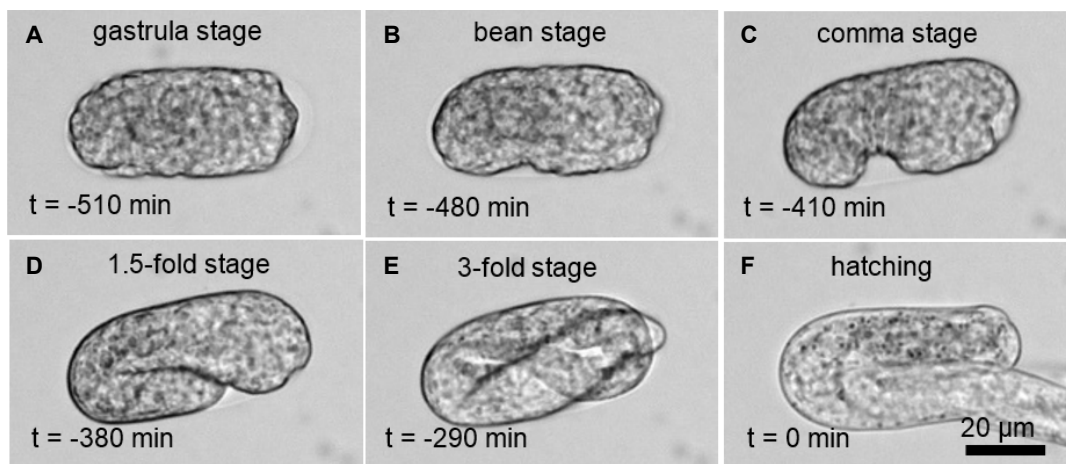


Figure 6.6 Embryogenesis of an embryo after dispensing with the SEP.

Normal development is observed, indicating benign operation conditions (brightfield images, 50 \times /0.55 NA objective, T = 23 $^{\circ}$ C): (A) Gastrula stage (~30 cells), (B-E) Subsequent main embryonic development phases, and (F) larva hatching. The hatching time defines t = 0 min.

6.3 Materials and methods

6.3.1 Materials

All the materials are the same as what is shown in section 2.4.1.

6.3.2 Worm strains culture and embryo preparation

Worm culture and synchronization methods are the same as what are introduced in the section 2.4.2. The embryos were then allowed to develop up adulthood. Prior to the experiment, the synchronized gravid adults were removed from the NGM plates by washing the plates with filtered S-medium. Subsequently, the worms were gently bleached and washed twice by centrifugation. Embryos were resuspended in fresh filtered S-medium. The embryo density was first counted by dropping 5 μ L of suspension onto a glass slide and was then adjusted to 10 embryos/ μ l by adding S-medium.

6.3.3 Device fabrication

We used standard polydimethylsiloxane (PDMS) soft lithography techniques to fabricate the microfluidic chips. The master mold was made by a one-step process. First, a 35 μ m thick SU-8 layer was spin-coated on a Si wafer and patterned to form the fluidic structures. The mold surface was treated with trimethylchlorosilane for 60 min to facilitate PDMS demolding. PDMS was poured over the SU-8/Si mold to form a 5 mm thick layer and cured at 80 °C for 1 hour. PDMS chips were plasma-bonded onto 1 mm thick PDMS membrane.

6.4 Conclusions

In summary, we reported the first chip-based “*Single Embryo Pipette*” for sequential on-demand dispensing of single *C. elegans* embryos onto segmented substrates, in particular microtiter plates, for subsequent culture and study of individual worms. Our single embryo dispensing method has key features of fast speed, high efficiency and low cost. Using pressure-tuned flexible embryo microtraps, single embryos can be easily captured and released on-demand into a well. Furthermore, any defined number of embryos is attainable by repeating the capture - release sequence several times, providing an approach for quantitative worm analysis. We demonstrated that SEP fluidic manipulations do not have an adverse impact on embryo or worm physiology, as monitored by normal development of the embryos after dispensing. We believe this powerful tool opens the way to increased versatility and throughput of assays requiring single-organism resolution with controlled micro-environmental conditions.

Chapter 7 Conclusions

7.1 Main results achieved in this thesis

In recent years, the lab-on-a-chip concept has become one of the most promising tools for studies at the micro- to nanoscale in biological research, including research using *C. elegans*. The use of microfluidics has been successfully demonstrated to provide platforms for easier worm handling, enabling many *C. elegans* biological studies and experiments that are not possible with conventional methods, such as behavior analysis under precise chemical stimulation, for instance. Because of low fabrication costs, better process control and other advantages, we anticipate that microfluidics will further increase its impact as a research tool for studies based on the *C. elegans* model organism.

In the light of the above, the aim of this thesis was to explore the opportunities for developing innovative application-specific microfluidic chip-based approaches and platforms. In particular, this work covered five applications, *i.e.* worm sorting (chapter 2), worm biocommunication (chapter 3), worm immobilization (chapter 4), drug studies during early embryogenesis (chapter 5), and single embryo dispensing (chapter 6).

For accurate and meaningful worm-based bioassays, age-synchronized or single-sex *C. elegans* populations are often required. In **chapter 2**, I introduced a new and simple microfluidic sorting device in order to obtain such populations. Our worm sorting device takes advantage of the pressure-deformable profile of a PDMS membrane. This adjustable filter structure can be tuned for size-dependent sorting of mixed hermaphrodite larvae/adult populations, hermaphrodite/male age-matched populations, and adult/embryo populations. With our device, we could achieve a purity and efficiency of close to 100% for all worms sorting experiments, with a throughput of up to 3.5 worms per second for isolating hermaphrodite larvae from a mixed worm culture. In this way, throughput for generating large and high purity synchronized populations might be significantly increased with respect to presently used methods, opening the way for more advanced and efficient drug screening assays, for instance. One of the limitations of this size-based sorting technique is that the device has not the capability to sort mixed populations with similar body size, *e.g.* L4 hermaphrodite larvae and male adults. Also, embryo sorting has been demonstrated, but more research is required to improve the efficiency. The strong adhesion of the sticky embryos to the chamber walls, as well as the formation of embryo clusters inside the chambers, represented important issues in the microfluidic manipulation. We expect, however, that for all commonly required worm sorting protocols, this simple and versatile sorting approach, providing at the same time high accuracy and throughput, will be a powerful tool for integration in advanced and automated *C. elegans* assay platforms.

Social communication in *C. elegans* populations through exchange and sensing of chemical compounds plays an important role in animal behavior, sociobiology, neurobiology, and animal cognition. In **chapter 3**, I presented a microfluidic system for studying signaling between specific *C. elegans* populations based on secreted diffusive compounds over

prolonged durations. We concluded that biocommunication can take place in a microfluidic device via active transfer of μL -aliquots of a biochemically conditioned medium and controlled exposure of the receiving worm population to this cue. This was clearly demonstrated by the observation of accelerated male-induced phenotype alterations and lifespan reduction of *C. elegans* hermaphrodites. A limitation of this device was that the male-secreted small molecules could not be accumulated in a permanent manner and at high concentration in the microfluidic chambers during the whole worm lifespan. A certain amount of these molecules was washed out with the larva removal process during the embryo laying period. It would be interesting to develop a novel larva removal strategy, to avoid refreshing the buffer medium during the lifespan culture. In conclusion, our chip is a powerful, and to the best of our knowledge also the first, microfluidic tool for analyzing specific cues of social or biochemical communication behavior in *C. elegans* populations. We anticipate that the spatial confinement of interacting worm populations with controlled fluidic exchange of diffusive compounds may significantly improve conventional biological agar plate-based assays.

Worm bioassays are often based on high-resolution imaging of dynamic biological processes in worm body tissues, requiring reliable immobilization of the nematodes. In **chapter 4**, I reported two reversible worm immobilization techniques as an alternative for existing immobilization methods, employing the application of either anesthetics or severe physical constraints, which in some cases may strongly affect physiological processes of the animals. I first proposed a new simple gel-microbeads based method for fast and stable, yet reversible worm immobilization, which we employed for *in vivo* confocal fluorescence imaging of mitochondrial networks within *C. elegans* living cells. With our approach, immobilization of small organisms in the precooled Pluronic gel is achieved by natural thermalization of the glass/PF127 substrate at room temperature, thus no specific equipment or technical skills are required, making the technique readily operational in any biological laboratory. Because of its performance, versatility and ease of use, we believe that our immobilization technique represents a valid alternative to currently used practice, with high potential to improve the quality of biological assays and longitudinal studies based on long-term observation and imaging of single worms or small worm populations. I then presented two new microfluidic methods to meet better the requirements of specific *C. elegans* studies. In contrast to conventional methods or our gel-microbeads matrix, the new micropillar array chip provided adequate bacterial feeding conditions for long-term on-chip immobilization. On the other hand, linear on-chip alignment of a worm by the stretchable microchannel device improved the data acquisition and post-processing time of high-resolution scanning imaging of *C. elegans* worms. A further study could assess the long-term immobilization effect during the whole worm lifespan. We believe that our worm immobilization technique will represent a valid alternative to the current gold standard method and possibly replace it for many applications.

Study of early embryogenesis plays an important role in mechanistic and functional genomic analysis of cellular processes. In **chapter 5**, I reported the first fully integrated microfluidic device for drug studies on *C. elegans* early embryos. Compared with the traditional method, our new device enables direct on-chip extraction of early embryos from gravid *C. elegans* hermaphrodites, and individual tracking of a large number of embryos including fragile mutants with drug-permeable eggshells. The capability to perform high-resolution live imaging of very early events in embryogenesis, starting from the 1-cell stage, was demonstrated with our device. Furthermore, the feasibility of well-controlled compound application in versatile microfluidic pharmacological assays performed on early embryos, was

shown. An issue that was not directly addressed in this the frame of this study, is further automation of the protocol. Computer-controlled application of the pressure pulses for embryo extraction should be implemented in a fully automated system. However, the features of the new device discussed so far, present significant advantages with respect to conventional embryogenesis assays, in particular in terms of throughput, versatility and ease of manipulation. We anticipate that our approach will enable the implementation of early *C. elegans* embryo drug studies with increased throughput and versatility.

The accurate control of the number of worms per test condition is a prerequisite for meaningful and quantitative worm-based bioassays. In **chapter 6**, I introduced a “*Single Embryo Pipette*” (SEP) that is specifically designed for dispensing single *C. elegans* embryos into standard microtiter plates. Compared with other manual, microfluidic or automated single worm methods, this new approach appears to be very simple and highly efficient yet is very flexible. Furthermore, since the device operation is merely based on flow pressure, *i.e.* the low flow pressure is used for the embryo loading and the surplus removal while the higher pressure for the single embryo release, the dispensing mechanism is by nature very reliable and reproducible. Further researches that we need to focus on is still the sticky embryos as we claimed in chapter 2. The embryos sticking to the chamber walls may be released with the trapped embryos, which may affect the dispensing accuracy. We believe our dispensing method provides a novel tool for future worm biological researches, wherein simple and efficient isolation of single or defined numbers of worms is required.

7.2 Future opportunities for microfluidics-based *C. elegans* studies

Fully automated C. elegans culture and imaging systems

Although results presented in this thesis take advantage of integrated microfluidic devices or platforms, fully automated and computer-controlled systems, in particular for *C. elegans* on-chip culture (Chapter 3), are not readily available. Furthermore, a mixed strategy combining microchips and highly performant conventional analytical methods might be useful, instead of aiming integration of all functionalities on a single microfluidic platform. In this view, the following points deserve further research and development: (i) Current microfluidic devices use integrated microfilters to confine worms in on-chip culture chambers, making recovery of worms from the chip difficult. However, in many biological assays subsequent off-chip processing or worm handling worm using Eppendorf tubes or microtiter plates is required, *e.g.* for centrifugation, PCR, or gene sequencing. An option to circumvent this issue is to design an openable device, from which worms can be easily recovered. Such an approach would allow combining the advantages of microfluidic and conventional techniques, thus eventually could extend the range of applications of worm-on-chip devices; (ii) another issue is to develop on-chip culture systems with robust and integrated feeding, larva removal, immobilization and imaging functionalities. To realize this goal, more advanced feedback systems are required, based on readout and imaging of the actual status of each microchamber on the chip, *e.g.* bacteria concentration, larva density, worm stages, survival rates, or worm trapping position. For instance, accurate control of the on-chip bacterial food concentration is a major issue for long-term culture. Such improvements are especially important for some high-throughput assays, such as toxicity test or drug screening, that require tracking of the worm’s state over the whole lifespan.

References

1. White, J.G., et al., *The structure of the ventral nerve cord of Caenorhabditis elegans*. Philos Trans R Soc Lond B Biol Sci, 1976. **275**(938): p. 327-48.
2. Ward, S., et al., *Electron microscopical reconstruction of the anterior sensory anatomy of the nematode Caenorhabditis elegans.* J Comp Neurol, 1975. **160**(3): p. 313-37.
3. Sulston, J.E. and S. Brenner, *The DNA of Caenorhabditis elegans*. Genetics, 1974. **77**(1): p. 95-104.
4. Brenner, S., *The genetics of Caenorhabditis elegans*. Genetics, 1974. **77**(1): p. 71-94.
5. Koelle, M.R. and H.R. Horvitz, *EGL-10 regulates G protein signaling in the C. elegans nervous system and shares a conserved domain with many mammalian proteins*. Cell, 1996. **84**(1): p. 115-25.
6. Hengartner, M.O. and H.R. Horvitz, *C. elegans cell survival gene ced-9 encodes a functional homolog of the mammalian proto-oncogene bcl-2*. Cell, 1994. **76**(4): p. 665-76.
7. Fraser, A.G., et al., *Caenorhabditis elegans inhibitor of apoptosis protein (IAP) homologue BIR-1 plays a conserved role in cytokinesis*. Curr Biol, 1999. **9**(6): p. 292-301.
8. Himmelhoch, S. and B.M. Zuckerman, *Xiphinema index and Caenorhabditis elegans: preparation and molecular labeling of ultrathin frozen sections*. Exp Parasitol, 1982. **54**(2): p. 250-9.
9. Hall, D.H. and R.L. Russell, *The posterior nervous system of the nematode Caenorhabditis elegans: serial reconstruction of identified neurons and complete pattern of synaptic interactions*. J Neurosci, 1991. **11**(1): p. 1-22.
10. Ashrafi, K., et al., *Genome-wide RNAi analysis of Caenorhabditis elegans fat regulatory genes*. Nature, 2003. **421**(6920): p. 268-72.
11. Braungart, E., et al., *Caenorhabditis elegans MPP+ model of Parkinson's disease for high-throughput drug screenings*. Neurodegener Dis, 2004. **1**(4-5): p. 175-83.
12. Voisine, C., et al., *Identification of potential therapeutic drugs for huntington's disease using Caenorhabditis elegans*. PLoS One, 2007. **2**(6): p. e504.
13. Stiernagle, T., *Maintenance of C. elegans*. WormBook, 2006.
14. Hengartner, M.O. and H.R. Horvitz, *The ins and outs of programmed cell death during C. elegans development*. Philosophical Transactions of the Royal Society of London B: Biological Sciences, 1994. **345**(1313): p. 243-246.
15. Kenyon, C., et al., *A C. elegans mutant that lives twice as long as wild type*. Nature, 1993. **366**(6454): p. 461-464.
16. Fire, A., et al., *Potent and specific genetic interference by double-stranded RNA in Caenorhabditis elegans*. nature, 1998. **391**(6669): p. 806-811.
17. Levitan, D., et al., *Assessment of normal and mutant human presenilin function in Caenorhabditis elegans*. Proceedings of the National Academy of Sciences, 1996. **93**(25): p. 14940-14944.

18. Braungart, E., et al., *Caenorhabditis elegans* MPP+ model of Parkinson's disease for high-throughput drug screenings. *Neurodegenerative Diseases*, 2004. **1**(4-5): p. 175-183.
19. Ogg, S., et al., *The Fork head transcription factor DAF-16 transduces insulin-like metabolic and longevity signals in C. elegans*. *Nature*, 1997. **389**(6654): p. 994-999.
20. Perrimon, N., *Signalling pathways initiated by receptor protein tyrosine kinases in Drosophila*. *Current opinion in cell biology*, 1994. **6**(2): p. 260-266.
21. O'Reilly, L.P., et al., *C. elegans in high-throughput drug discovery*. *Advanced drug delivery reviews*, 2014. **69**: p. 247-253.
22. Strange, K., *Drug discovery in fish, flies, and worms*. *ILAR journal*, 2016. **57**(2): p. 133-143.
23. Brindley, P.J., et al., *Helminth genomics: The implications for human health*. *PLoS neglected tropical diseases*, 2009. **3**(10): p. e538.
24. Schulenburg, H., C. Léopold Kurz, and J.J. Ewbank, *Evolution of the innate immune system: the worm perspective*. *Immunological reviews*, 2004. **198**(1): p. 36-58.
25. Chen, X., et al., *Using C. elegans to discover therapeutic compounds for ageing-associated neurodegenerative diseases*. *Chemistry Central Journal*, 2015. **9**(1): p. 65.
26. Lepesant, J.-A., *The promises of neurodegenerative disease modeling*. *Comptes rendus biologies*, 2015. **338**(8): p. 584-592.
27. Manz, A., N. Graber, and H.á. Widmer, *Miniaturized total chemical analysis systems: a novel concept for chemical sensing*. *Sensors and actuators B: Chemical*, 1990. **1**(1-6): p. 244-248.
28. Chokshi, T.V., A. Ben-Yakar, and N. Chronis, *CO2 and compressive immobilization of C. elegans on-chip*. *Lab Chip*, 2009. **9**(1): p. 151-7.
29. Yanik, M.F., C.B. Rohde, and C. Pardo-Martin, *Technologies for micromanipulating, imaging, and phenotyping small invertebrates and vertebrates*. *Annu Rev Biomed Eng*, 2011. **13**: p. 185-217.
30. Chronis, N., M. Zimmer, and C.I. Bargmann, *Microfluidics for in vivo imaging of neuronal and behavioral activity in Caenorhabditis elegans*. *Nat Methods*, 2007. **4**(9): p. 727-31.
31. Chronis, N., *Worm chips: microtools for C. elegans biology*. *Lab Chip*, 2010. **10**(4): p. 432-7.
32. Zimmer, M., et al., *Neurons Detect Increases and Decreases in Oxygen Levels Using Distinct Guanylate Cyclases*. *Neuron*, 2009. **61**(6): p. 865-879.
33. Zhang, Y., H. Lu, and C.I. Bargmann, *Pathogenic bacteria induce aversive olfactory learning in Caenorhabditis elegans*. *Nature*, 2005. **438**(7065): p. 179-184.
34. Rohde, C.B., et al., *Microfluidic system for on-chip high-throughput whole-animal sorting and screening at subcellular resolution*. *Proceedings of the National Academy of Sciences of the United States of America*, 2007. **104**(35): p. 13891-13895.
35. McCormick, K.E., et al., *Microfluidic Devices for Analysis of Spatial Orientation Behaviors in Semi-Restrained Caenorhabditis elegans*. *Plos One*, 2011. **6**(10).
36. Lockery, S., *Channeling the worm: microfluidic devices for nematode neurobiology*. *Nature Methods*, 2007. **4**(9): p. 691-692.
37. Hulme, S.E., S.S. Shevkoplyas, and A. Samuel, *Microfluidics: streamlining discovery in worm biology*. *Nature Methods*, 2008. **5**(7): p. 589-590.
38. Gray, J.M., et al., *Oxygen sensation and social feeding mediated by a C. elegans guanylate cyclase homologue*. *Nature*, 2004. **430**(6997): p. 317-22.
39. Chalasani, S.H., et al., *Dissecting a circuit for olfactory behaviour in Caenorhabditis elegans*. *Nature*, 2007. **450**(7166): p. 63-+.

40. Albrecht, D.R. and C.I. Bargmann, *High-content behavioral analysis of Caenorhabditis elegans in precise spatiotemporal chemical environments*. Nat Methods, 2011. **8**(7): p. 599-605.
41. Ben-Yakar, A. and F. Bourgeois, *Ultrafast laser nanosurgery in microfluidics for genome-wide screenings*. Curr Opin Biotechnol, 2009. **20**(1): p. 100-5.
42. Guo, S.X., et al., *Femtosecond laser nanoaxotomy lab-on-a-chip for in vivo nerve regeneration studies*. Nat Methods, 2008. **5**(6): p. 531-3.
43. Crane, M.M., et al., *Microfluidics-enabled phenotyping, imaging, and screening of multicellular organisms*. Lab Chip, 2010. **10**(12): p. 1509-17.
44. Crane, M.M., K. Chung, and H. Lu, *Computer-enhanced high-throughput genetic screens of C. elegans in a microfluidic system*. Lab Chip, 2009. **9**(1): p. 38-40.
45. Chung, K., M.M. Crane, and H. Lu, *Automated on-chip rapid microscopy, phenotyping and sorting of C. elegans*. Nat Methods, 2008. **5**(7): p. 637-43.
46. Chung, K. and H. Lu, *Automated high-throughput cell microsurgery on-chip*. Lab Chip, 2009. **9**(19): p. 2764-6.
47. Ben-Yakar, A., N. Chronis, and H. Lu, *Microfluidics for the analysis of behavior, nerve regeneration, and neural cell biology in C. elegans*. Curr Opin Neurobiol, 2009. **19**(5): p. 561-7.
48. Qin, J. and A.R. Wheeler, *Maze exploration and learning in C. elegans*. Lab Chip, 2007. **7**(2): p. 186-92.
49. Stirman, J.N., et al., *High-throughput study of synaptic transmission at the neuromuscular junction enabled by optogenetics and microfluidics*. J Neurosci Methods, 2010. **191**(1): p. 90-3.
50. Sivagnanam, V. and M.A. Gijs, *Exploring living multicellular organisms, organs, and tissues using microfluidic systems*. Chem Rev, 2013. **113**(5): p. 3214-47.
51. Wen, H., et al., *A droplet microchip with substance exchange capability for the developmental study of C. elegans*. Lab Chip, 2015. **15**(8): p. 1905-11.
52. Johari, S., et al., *On-chip analysis of C. elegans muscular forces and locomotion patterns in microstructured environments*. Lab Chip, 2013. **13**(9): p. 1699-707.
53. Liu, P., R.J. Martin, and L. Dong, *Micro-electro-fluidic grids for nematodes: a lens-less, image-sensor-less approach for on-chip tracking of nematode locomotion*. Lab Chip, 2013. **13**(4): p. 650-61.
54. Klass, M.R., *A method for the isolation of longevity mutants in the nematode Caenorhabditis elegans and initial results*. Mech Ageing Dev, 1983. **22**(3-4): p. 279-86.
55. Kenyon, C., et al., *A C. elegans mutant that lives twice as long as wild type*. Nature, 1993. **366**(6454): p. 461-4.
56. Jorgensen, E.M. and S.E. Mango, *The art and design of genetic screens: caenorhabditis elegans*. Nat Rev Genet, 2002. **3**(5): p. 356-69.
57. Pulak, R., *Techniques for analysis, sorting, and dispensing of C. elegans on the COPAS flow-sorting system*. Methods Mol Biol, 2006. **351**: p. 275-86.
58. Solvas, X.C.i., et al., *High-throughput age synchronisation of Caenorhabditis elegans*. Chemical Communications, 2011. **47**(35): p. 9801-9803.
59. Rezai, P., et al., *Electrical sorting of Caenorhabditis elegans*. Lab on a Chip, 2012. **12**(10): p. 1831-1840.
60. Han, B., et al., *A sorting strategy for C. elegans based on size-dependent motility and electrotaxis in a micro-structured channel*. Lab on a Chip, 2012. **12**(20): p. 4128-4134.
61. Maniere, X., et al., *Running worms: C. elegans self-sorting by electrotaxis*. PLoS One, 2011. **6**(2): p. e16637.

62. Yuan, J., et al., *High-throughput, motility-based sorter for microswimmers such as C. elegans*. Lab Chip, 2015. **15**(13): p. 2790-8.
63. Wang, X., et al., *Highly efficient microfluidic sorting device for synchronizing developmental stages of C. elegans based on deflecting electrotaxis*. Lab on a Chip, 2015. **15**(11): p. 2513-2521.
64. Ai, X., et al., *A high-throughput device for size based separation of C. elegans developmental stages*. Lab on a Chip, 2014. **14**(10): p. 1746-1752.
65. Maguire, S.M., et al., *The C. elegans touch response facilitates escape from predacious fungi*. Curr Biol, 2011. **21**(15): p. 1326-30.
66. Kim, T.K., J.K. Kim, and O.C. Jeong, *Measurement of nonlinear mechanical properties of PDMS elastomer*. Microelectronic Engineering, 2011. **88**(8): p. 1982-1985.
67. Cornaglia, M., et al., *An automated microfluidic platform for C. elegans embryo arraying, phenotyping, and long-term live imaging*. Sci Rep, 2015. **5**: p. 10192.
68. Maures, T.J., et al., *Males shorten the life span of C. elegans hermaphrodites via secreted compounds*. Science, 2014. **343**(6170): p. 541-4.
69. Nystrom, J., et al., *Increased or decreased levels of Caenorhabditis elegans lon-3, a gene encoding a collagen, cause reciprocal changes in body length*. Genetics, 2002. **161**(1): p. 83-97.
70. Simmer, F., et al., *Genome-wide RNAi of C. elegans using the hypersensitive rrf-3 strain reveals novel gene functions*. PLoS Biol, 2003. **1**(1): p. E12.
71. Kamath, R.S., et al., *Systematic functional analysis of the Caenorhabditis elegans genome using RNAi*. Nature, 2003. **421**(6920): p. 231-7.
72. Wyatt, T.D., *Fifty years of pheromones*. Nature, 2009. **457**(7227): p. 262-3.
73. Waters, C.M. and B.L. Bassler, *Quorum sensing: cell-to-cell communication in bacteria*. Annu Rev Cell Dev Biol, 2005. **21**: p. 319-46.
74. Gendron, C.M., et al., *Drosophila life span and physiology are modulated by sexual perception and reward*. Science, 2014. **343**(6170): p. 544-8.
75. Liberles, S.D., *Mammalian pheromones*. Annu Rev Physiol, 2014. **76**: p. 151-75.
76. de Bono, M., et al., *Social feeding in Caenorhabditis elegans is induced by neurons that detect aversive stimuli*. Nature, 2002. **419**(6910): p. 899-903.
77. Liu, K.S. and P.W. Sternberg, *Sensory regulation of male mating behavior in Caenorhabditis elegans*. Neuron, 1995. **14**(1): p. 79-89.
78. Yamada, K., et al., *Olfactory plasticity is regulated by pheromonal signaling in Caenorhabditis elegans*. Science, 2010. **329**(5999): p. 1647-50.
79. Bargmann, C.I., E. Hartwig, and H.R. Horvitz, *Odorant-selective genes and neurons mediate olfaction in C. elegans*. Cell, 1993. **74**(3): p. 515-27.
80. Butcher, R.A., et al., *Biosynthesis of the Caenorhabditis elegans dauer pheromone*. Proc Natl Acad Sci U S A, 2009. **106**(6): p. 1875-9.
81. Ludewig, A.H. and F.C. Schroeder, *Ascaroside signaling in C. elegans*. WormBook, 2012.
82. Srinivasan, J., et al., *A blend of small molecules regulates both mating and development in Caenorhabditis elegans*. Nature, 2008. **454**(7208): p. 1115-8.
83. Pungaliya, C., et al., *A shortcut to identifying small molecule signals that regulate behavior and development in Caenorhabditis elegans*. Proc Natl Acad Sci U S A, 2009. **106**(19): p. 7708-13.
84. Shi, C. and C.T. Murphy, *Mating induces shrinking and death in Caenorhabditis mothers*. Science, 2014. **343**(6170): p. 536-40.
85. Gems, D. and D.L. Riddle, *Longevity in Caenorhabditis elegans reduced by mating but not gamete production*. Nature, 1996. **379**(6567): p. 723-5.

86. Cassada, R.C. and R.L. Russell, *The dauerlarva, a post-embryonic developmental variant of the nematode Caenorhabditis elegans*. Dev Biol, 1975. **46**(2): p. 326-42.
87. Golden, J.W. and D.L. Riddle, *A pheromone influences larval development in the nematode Caenorhabditis elegans*. Science, 1982. **218**(4572): p. 578-80.
88. Butcher, R.A., et al., *A potent dauer pheromone component in Caenorhabditis elegans that acts synergistically with other components*. Proceedings of the National Academy of Sciences of the United States of America, 2008. **105**(38): p. 14288-14292.
89. Butcher, R.A., et al., *Small-molecule pheromones that control dauer development in Caenorhabditis elegans*. Nat Chem Biol, 2007. **3**(7): p. 420-2.
90. Simon, J.M. and P.W. Sternberg, *Evidence of a mate-finding cue in the hermaphrodite nematode Caenorhabditis elegans*. Proc Natl Acad Sci U S A, 2002. **99**(3): p. 1598-603.
91. Srinivasan, J., et al., *A modular library of small molecule signals regulates social behaviors in Caenorhabditis elegans*. PLoS Biol, 2012. **10**(1): p. e1001237.
92. Izrayelit, Y., et al., *Targeted Metabolomics Reveals a Male Pheromone and Sex-Specific Ascaroside Biosynthesis in Caenorhabditis elegans*. Acs Chemical Biology, 2012. **7**(8): p. 1321-1325.
93. Bakhtina, N.A. and J.G. Korvink, *Microfluidic laboratories for C. elegans enhance fundamental studies in biology*. Rsc Advances, 2014. **4**(9): p. 4691-4709.
94. Sivagnanam, V. and M.A.M. Gijs, *Exploring Living Multicellular Organisms, Organs, and Tissues Using Microfluidic Systems*. Chemical Reviews, 2013. **113**(5): p. 3214-3247.
95. Shi, W., et al., *Microfluidic platform for the study of Caenorhabditis elegans*. Top Curr Chem, 2011. **304**: p. 323-38.
96. Gupta, B.P. and P. Rezai, *Microfluidic Approaches for Manipulating, Imaging, and Screening C. elegans*. Micromachines, 2016. **7**(7): p. 123.
97. Chokshi, T.V., D. Bazopoulou, and N. Chronis, *An automated microfluidic platform for calcium imaging of chemosensory neurons in Caenorhabditis elegans*. Lab Chip, 2010. **10**(20): p. 2758-63.
98. McCormick, K.E., et al., *Microfluidic devices for analysis of spatial orientation behaviors in semi-restrained Caenorhabditis elegans*. PLoS One, 2011. **6**(10): p. e25710.
99. Hwang, H., et al., *On-demand optical immobilization of Caenorhabditis elegans for high-resolution imaging and microinjection*. Lab on a Chip, 2014. **14**(18): p. 3498-3501.
100. Dong, L., et al., *Versatile size-dependent sorting of C. elegans nematodes and embryos using a tunable microfluidic filter structure*. Lab Chip, 2016. **16**(3): p. 574-85.
101. Hulme, S.E., et al., *Lifespan-on-a-chip: microfluidic chambers for performing lifelong observation of C. elegans*. Lab Chip, 2010. **10**(5): p. 589-97.
102. Krajniak, J. and H. Lu, *Long-term high-resolution imaging and culture of C. elegans in chip-gel hybrid microfluidic device for developmental studies*. Lab Chip, 2010. **10**(14): p. 1862-8.
103. Xian, B., et al., *WormFarm: a quantitative control and measurement device toward automated Caenorhabditis elegans aging analysis*. Aging Cell, 2013. **12**(3): p. 398-409.
104. Cornaglia, M., et al., *Automated longitudinal monitoring of in vivo protein aggregation in neurodegenerative disease C. elegans models*. Molecular Neurodegeneration, 2016. **11**.

105. Hulme, S.E., S.S. Shevkoplyas, and G.M. Whitesides, *Incorporation of prefabricated screw, pneumatic, and solenoid valves into microfluidic devices*. Lab Chip, 2009. **9**(1): p. 79-86.
106. Karimi, A., et al., *Interplay of physical mechanisms and biofilm processes: review of microfluidic methods*. Lab Chip, 2015. **15**(1): p. 23-42.
107. Seidel, H.S. and J. Kimble, *The oogenic germline starvation response in C. elegans*. PLoS One, 2011. **6**(12): p. e28074.
108. Altun, Z.F. and D.H. Hall, *INTRODUCTION TO C. elegans ANATOMY*. WormAtlas, 2009: p. <http://www.wormatlas.org/ver1/handbook/anatomyintro/anatomyintro.htm>.
109. Solis, G.M. and M. Petrascheck, *Measuring Caenorhabditis elegans life span in 96 well microtiter plates*. J Vis Exp, 2011(49).
110. Huang, C., C. Xiong, and K. Kornfeld, *Measurements of age-related changes of physiological processes that predict lifespan of Caenorhabditis elegans*. Proc Natl Acad Sci U S A, 2004. **101**(21): p. 8084-9.
111. Amrit, F.R., et al., *The C. elegans lifespan assay toolkit*. Methods, 2014. **68**(3): p. 465-75.
112. Win, M.T., et al., *Validated Liquid Culture Monitoring System for Lifespan Extension of Caenorhabditis elegans through Genetic and Dietary Manipulations*. Aging Dis, 2013. **4**(4): p. 178-185.
113. Mulcahy, B., L. Holden-Dye, and V. O'Connor, *Pharmacological assays reveal age-related changes in synaptic transmission at the Caenorhabditis elegans neuromuscular junction that are modified by reduced insulin signalling*. J Exp Biol, 2013. **216**(Pt 3): p. 492-501.
114. Hodgkin, J. and T. Doniach, *Natural variation and copulatory plug formation in Caenorhabditis elegans*. Genetics, 1997. **146**(1): p. 149-64.
115. Miyabe, K. and R. Isogai, *Estimation of molecular diffusivity in liquid phase systems by the Wilke-Chang equation*. J Chromatogr A, 2011. **1218**(38): p. 6639-45.
116. Baum, E.J., *Chemical Property Estimation: Theory and Application*. 1997: CRC Press 400.
117. Van Gilst, M.R., et al., *Nuclear hormone receptor NHR-49 controls fat consumption and fatty acid composition in C. elegans*. PLoS Biol, 2005. **3**(2): p. e53.
118. Herndon, L.A., et al., *Stochastic and genetic factors influence tissue-specific decline in ageing C. elegans*. Nature, 2002. **419**(6909): p. 808-14.
119. He, F., *Making Males of C. elegans*. Bio-protocol, 2011: p. <http://www.bio-protocol.org/e58>.
120. Lewis, J.A., et al., *The genetics of levamisole resistance in the nematode Caenorhabditis elegans*. Genetics, 1980. **95**(4): p. 905-928.
121. Goodman, M.B., et al., *Active currents regulate sensitivity and dynamic range in C. elegans neurons*. Neuron, 1998. **20**(4): p. 763-772.
122. Massie, M.R., et al., *Exposure to the metabolic inhibitor sodium azide induces stress protein expression and thermotolerance in the nematode Caenorhabditis elegans*. Cell stress & chaperones, 2003. **8**(1): p. 1-7.
123. Sivagnanam, V. and M.A. Gijs, *Exploring living multicellular organisms, organs, and tissues using microfluidic systems*. Chemical reviews, 2013. **113**(5): p. 3214-3247.
124. Hulme, S.E., et al., *Lifespan-on-a-chip: microfluidic chambers for performing lifelong observation of C. elegans*. Lab on a Chip, 2010. **10**(5): p. 589-597.
125. Lee, H., et al., *A multi-channel device for high-density target-selective stimulation and long-term monitoring of cells and subcellular features in C. elegans*. Lab on a Chip, 2014. **14**(23): p. 4513-4522.

126. Gonzales, D.L., et al., *Scalable electrophysiology in intact small animals with nanoscale suspended electrode arrays*. Nature Nanotechnology, 2017.
127. Gilleland, C.L., et al., *Microfluidic immobilization of physiologically active *Caenorhabditis elegans**. Nature protocols, 2010. **5**(12): p. 1888-1902.
128. Mondal, S., et al., *Imaging in vivo neuronal transport in genetic model organisms using microfluidic devices*. Traffic, 2011. **12**(4): p. 372-385.
129. Gokce, S.K., et al., *A fully automated microfluidic femtosecond laser axotomy platform for nerve regeneration studies in *C. elegans**. PLoS one, 2014. **9**(12): p. e113917.
130. Wang, J., et al., *Development of an integrated microfluidic device for evaluating of in vivo chemo-sensing of intact *Caenorhabditis elegans**. Sensors and Actuators B: Chemical, 2013. **178**: p. 343-349.
131. Hulme, S.E., et al., *A microfabricated array of clamps for immobilizing and imaging *C. elegans**. Lab Chip, 2007. **7**(11): p. 1515-23.
132. Basak, R. and R. Bandyopadhyay, *Encapsulation of hydrophobic drugs in Pluronic F127 micelles: effects of drug hydrophobicity, solution temperature, and pH*. Langmuir, 2013. **29**(13): p. 4350-4356.
133. Shachaf, Y., M. Gonen-Wadmany, and D. Seliktar, *The biocompatibility of Pluronic® F127 fibrinogen-based hydrogels*. Biomaterials, 2010. **31**(10): p. 2836-2847.
134. Krajniak, J. and H. Lu, *Long-term high-resolution imaging and culture of *C. elegans* in chip-gel hybrid microfluidic device for developmental studies*. Lab on a Chip, 2010. **10**(14): p. 1862-1868.
135. Krajniak, J., et al., *CLIP—continuous live imaging platform for direct observation of *C. elegans* physiological processes*. Lab on a Chip, 2013. **13**(15): p. 2963-2971.
136. Aubry, G., M. Zhan, and H. Lu, *Hydrogel-droplet microfluidic platform for high-resolution imaging and sorting of early larval *Caenorhabditis elegans**. Lab on a Chip, 2015. **15**(6): p. 1424-1431.
137. Cornaglia, M., et al., *Automated longitudinal monitoring of in vivo protein aggregation in neurodegenerative disease *C. elegans* models*. Molecular neurodegeneration, 2016. **11**(1): p. 17.
138. Chuang, H.-S. and W.-Y. Chuang, *Rapid, Reversible and Addressable Immobilization of *Caenorhabditis elegans* in Pluronic F-127 using an Optoelectric Device*. Sensors and Actuators B: Chemical, 2017.
139. Ward, A., et al., *Light-sensitive neurons and channels mediate phototaxis in *C. elegans**. Nature neuroscience, 2008. **11**(8): p. 916-922.
140. Altun, Z.F. and D.H. Hall, *INTRODUCTION TO *C. elegans* ANATOMY*. WormAtlas, 2017.
141. Dong, L., et al., *Versatile size-dependent sorting of *C. elegans* nematodes and embryos using a tunable microfluidic filter structure*. Lab on a Chip, 2016. **16**(3): p. 574-585.
142. Kim, E., et al., *Long-term imaging of *Caenorhabditis elegans* using nanoparticle-mediated immobilization*. PLoS one, 2013. **8**(1): p. e53419.
143. Avery, L. and B.B. Shtonda, *Food transport in the *C. elegans* pharynx*. Journal of Experimental Biology, 2003. **206**(14): p. 2441-2457.
144. Hulme, S.E. and G.M. Whitesides, *Chemistry and the worm: *Caenorhabditis elegans* as a platform for integrating chemical and biological research*. Angewandte Chemie International Edition, 2011. **50**(21): p. 4774-4807.
145. Curran, S.P. and G. Ruvkun, *Lifespan regulation by evolutionarily conserved genes essential for viability*. PLoS genetics, 2007. **3**(4): p. e56.
146. Kenyon, C.J., *The genetics of ageing*. Nature, 2010. **464**(7288): p. 504-512.

147. Kaletta, T. and M.O. Hengartner, *Finding function in novel targets: C. elegans as a model organism*. Nature reviews Drug discovery, 2006. **5**(5): p. 387-399.
148. Sebastián, D., M. Palacín, and A. Zorzano, *Mitochondrial dynamics: Coupling mitochondrial fitness with healthy aging*. Trends in Molecular Medicine, 2017.
149. Li, J. and W. Le, *Modeling neurodegenerative diseases in Caenorhabditis elegans*. Experimental neurology, 2013. **250**: p. 94-103.
150. Lin, M.T. and M.F. Beal, *Mitochondrial dysfunction and oxidative stress in neurodegenerative diseases*. Nature, 2006. **443**(7113): p. 787-795.
151. Cho, D.-H., T. Nakamura, and S.A. Lipton, *Mitochondrial dynamics in cell death and neurodegeneration*. Cellular and Molecular Life Sciences, 2010. **67**(20): p. 3435-3447.
152. Archer, S.L., *Mitochondrial dynamics—mitochondrial fission and fusion in human diseases*. New England Journal of Medicine, 2013. **369**(23): p. 2236-2251.
153. Lackner, L.L. and J. Nunnari, *Small molecule inhibitors of mitochondrial division: tools that translate basic biological research into medicine*. Chemistry & biology, 2010. **17**(6): p. 578-583.
154. Cui, M., et al., *Perturbations in mitochondrial dynamics induced by human mutant PINK1 can be rescued by the mitochondrial division inhibitor mdivi-1*. Journal of Biological Chemistry, 2010. **285**(15): p. 11740-11752.
155. Kim, H., et al., *Fine-tuning of Drp1/Fis1 availability by AKAP121/Siah2 regulates mitochondrial adaptation to hypoxia*. Molecular cell, 2011. **44**(4): p. 532-544.
156. Nunnari, J. and A. Suomalainen, *Mitochondria: in sickness and in health*. Cell, 2012. **148**(6): p. 1145-1159.
157. Chan, D.C., *Dissecting mitochondrial fusion*. Developmental cell, 2006. **11**(5): p. 592-594.
158. Kanazawa, T., et al., *The C. elegans Opal1 homologue EAT-3 is essential for resistance to free radicals*. PLoS genetics, 2008. **4**(2): p. e1000022.
159. Palikaras, K., E. Lionaki, and N. Tavernarakis, *Coordination of mitophagy and mitochondrial biogenesis during ageing in C. elegans*. Nature, 2015. **521**(7553): p. 525-528.
160. Labrousse, A.M., et al., *C. elegans dynamin-related protein DRP-1 controls severing of the mitochondrial outer membrane*. Molecular cell, 1999. **4**(5): p. 815-826.
161. Frank, S., et al., *The role of dynamin-related protein 1, a mediator of mitochondrial fission, in apoptosis*. Developmental cell, 2001. **1**(4): p. 515-525.
162. David, D.C., et al., *Widespread protein aggregation as an inherent part of aging in C. elegans*. PLoS biology, 2010. **8**(8): p. e1000450.
163. Gidalevitz, T., et al., *Destabilizing protein polymorphisms in the genetic background direct phenotypic expression of mutant SOD1 toxicity*. PLoS genetics, 2009. **5**(3): p. e1000399.
164. Van Ham, T.J., et al., *C. elegans model identifies genetic modifiers of α -synuclein inclusion formation during aging*. PLoS genetics, 2008. **4**(3): p. e1000027.
165. Morley, J.F., et al., *The threshold for polyglutamine-expansion protein aggregation and cellular toxicity is dynamic and influenced by aging in Caenorhabditis elegans*. Proceedings of the National Academy of Sciences, 2002. **99**(16): p. 10417-10422.
166. Kamath, R.S., et al., *Effectiveness of specific RNA-mediated interference through ingested double-stranded RNA in Caenorhabditis elegans*. Genome Biol, 2001. **2**(1): p. RESEARCH0002.
167. Coquoz, S., et al., *Label-free three-dimensional imaging of Caenorhabditis elegans with visible optical coherence microscopy*. PloS one, 2017. **12**(7): p. e0181676.

168. Preibisch, S., S. Saalfeld, and P. Tomancak, *Globally optimal stitching of tiled 3D microscopic image acquisitions*. Bioinformatics, 2009. **25**(11): p. 1463-1465.
169. Compant, S., et al., *Diversity and occurrence of Burkholderia spp. in the natural environment*. FEMS microbiology reviews, 2008. **32**(4): p. 607-626.
170. Berg, M., et al., *Assembly of the Caenorhabditis elegans gut microbiota from diverse soil microbial environments*. The ISME journal, 2016. **10**(8): p. 1998.
171. Sifri, C.D., J. Begun, and F.M. Ausubel, *The worm has turned—microbial virulence modeled in Caenorhabditis elegans*. Trends in microbiology, 2005. **13**(3): p. 119-127.
172. Gönczy, P., et al., *Dissection of cell division processes in the one cell stage Caenorhabditis elegans embryo by mutational analysis*. The Journal of cell biology, 1999. **144**(5): p. 927-946.
173. Ward, S. and J.S. Carrel, *Fertilization and sperm competition in the nematode Caenorhabditis elegans*. Dev Biol, 1979. **73**(2): p. 304-21.
174. Lints, R. and D.H. Hall, *Reproductive system, overview*. WormAtlas, 2009.
175. Sulston, J.E., et al., *The embryonic cell lineage of the nematode Caenorhabditis elegans*. Developmental biology, 1983. **100**(1): p. 64-119.
176. Robertson, S. and R. Lin, *The oocyte-to-embryo transition*, in *Germ Cell Development in C. elegans*. 2013, Springer. p. 351-372.
177. Maddox, A.S., et al., *Distinct roles for two C. elegans anillins in the gonad and early embryo*. Development, 2005. **132**(12): p. 2837-2848.
178. Pollard, T.D., *Mechanics of cytokinesis in eukaryotes*. Current opinion in cell biology, 2010. **22**(1): p. 50-56.
179. Huber, F., et al., *Emergent complexity of the cytoskeleton: from single filaments to tissue*. Advances in physics, 2013. **62**(1): p. 1-112.
180. McEnerney, M.P. and M.P. Styczynski, *Small molecule signaling, regulation, and potential applications in cellular therapeutics*. Wiley Interdisciplinary Reviews: Systems Biology and Medicine, 2017.
181. Visegrády, B., et al., *The effect of phalloidin and jasplakinolide on the flexibility and thermal stability of actin filaments*. FEBS letters, 2004. **565**(1-3): p. 163-166.
182. <https://www.mechanobio.info/figure/actin-binding-small-molecules/>.
183. Blumenthal, A., et al., *Morphology and migration of podocytes are affected by CD151 levels*. American Journal of Physiology-Renal Physiology, 2012. **302**(10): p. F1265-F1277.
184. Hyman, A.A. and J.G. White, *Determination of cell division axes in the early embryogenesis of Caenorhabditis elegans*. The Journal of cell biology, 1987. **105**(5): p. 2123-2135.
185. Hill, D.P. and S. Strome, *Brief cytochalasin-induced disruption of microfilaments during a critical interval in 1-cell C. elegans embryos alters the partitioning of developmental instructions to the 2-cell embryo*. Development, 1990. **108**(1): p. 159-172.
186. Carvalho, A., et al., *Acute drug treatment in the early C. elegans embryo*. PloS one, 2011. **6**(9): p. e24656.
187. Wernike, D., C. van Oostende, and A. Piekny, *Visualizing Neuroblast Cytokinesis During C. elegans Embryogenesis*. Journal of visualized experiments: JoVE, 2014(85).
188. Cornaglia, M., et al., *An automated microfluidic platform for C. elegans embryo arraying, phenotyping, and long-term live imaging*. Scientific reports, 2015. **5**.
189. Casella, J.F., M.D. Flanagan, and S. Lin, *Cytochalasin D inhibits actin polymerization and induces depolymerization of actin filaments formed during platelet shape change*. Nature, 1981. **293**(5830): p. 302-305.

190. Bembenek, J.N., et al., *Cortical granule exocytosis in C. elegans is regulated by cell cycle components including separase*. *Development*, 2007. **134**(21): p. 3837-3848.
191. Robinson, D.N. and J.A. Spudich, *Towards a molecular understanding of cytokinesis*. *Trends in cell biology*, 2000. **10**(6): p. 228-237.
192. McNally, K., et al., *Katanin controls mitotic and meiotic spindle length*. *J Cell Biol*, 2006. **175**(6): p. 881-891.
193. Rose, L. and P. Gönczy, *Polarity establishment, asymmetric division and segregation of fate determinants in early C. elegans embryos*. *WormBook*, 2005.
194. Shelton, C.A. and B. Bowerman, *Time-dependent responses to glp-1-mediated inductions in early C. elegans embryos*. *Development*, 1996. **122**(7): p. 2043-2050.
195. Aitlhadj, L. and S.R. Stürzenbaum, *The use of FUdR can cause prolonged longevity in mutant nematodes*. *Mechanisms of ageing and development*, 2010. **131**(5): p. 364-365.
196. Pulak, R., *Techniques for analysis, sorting, and dispensing of C. elegans on the COPAS™ flow-sorting system*. *C. elegans: methods and applications*, 2006: p. 275-286.

Curriculum Vitae

Li DONG

+41 (0)76 623 4146 | dliepfl@gmail.com | Av. de Montoie 37, Lausanne 1007
<https://www.linkedin.com/in/li-dong/>

EDUCATION	Ph.D., Microsystems and Microelectronics	2013-2018
	Ecole Polytechnique Fédérale de Lausanne (EPFL), Lausanne, CH	
	M.S., Electrical Engineering	2010-2013
	Peking University, Beijing, CN	
	B.S., Electrical Engineering	2006-2010
	Shenzhen University, Shenzhen, CN	

RESEARCH EXPERIENCE

Ecole Polytechnique Fédérale de Lausanne (EPFL) **Lausanne, CH**
Doctoral Assistant Supervisor: Prof. Martin Gijs **2013 – 2018**

Thesis: Lab-On-Chip Technologies for Manipulation and Imaging of *C. elegans* worms and embryos

- Developing bio-MEMS systems for the small organism based bioassays.
 - Design, modeling and simulation of microfluidic devices and bio-MEMS; optimization of cleanroom fabrication processes; development of biological protocols for lab-on-a-chip devices; use of advanced microscopy techniques, image processing and data analysis tools.

Peking University **Beijing, CN**
Graduate Researcher **2010 – 2013**

Thesis: Highly Sensitive Detection of DNA with Silicon Nanowire CMOS Biosensor

- Development of a novel semiconducting silicon nanowire CMOS biosensor array for label-free and real-time detection of nucleic acids.
- Modeling and fabrication of submicron silicon masters and PDMS replicas with high-aspect ratio.
- Publication of 2 papers as the first author on top conferences of MEMS and of 1 patent.

SKILLS AND TECHNIQUES

- Language skills: Chinese (native language), English (fluent), German (basic)
- IT skills:
 - Professional: L-edit, Verilog, C, MATLAB, COMSOL, AutoCAD, SOLIDWORKS, LabVIEW, Conventor
 - Graphics & office: Photoshop, Illustrator, Maya, ImageJ, Prism, MS Office
- Micro/Nanotechnology skills: Extensive experience of IC & MEMS design and fabrication, including finite element analysis and self-assembly based patterning.
- Biotechnological skills: Wide field and fluorescence microscopy, *C. elegans* and bacteria culture, and biometric analysis.

GRANTS AND AWARDS

- China National Award for Outstanding Oversea Students Finalist – China Scholarship Council **2017**
- *Lab on a chip* Poster Prize - Symposium Latsis EPFL **2016**
- Academic Scholarship - Peking University **2010-2013**

JOURNAL PUBLICATIONS

- **L. Dong**, J. Zhang, T. Lehnert, M. Gijs, “Single Embryo Pipette for Accurate *C. elegans* Bioassays,” *Lab on a chip* (In preparation).
- **L. Dong**, M. Cornaglia, G. Krishnamani, J. Zhang, L. Mouchiroud, T. Lehnert, J. Auwerx, and M. Gijs, “Reversible and Long-Term Immobilization in a Hydrogel-Microbead Matrix for High-Resolution Imaging of *Caenorhabditis elegans* and Other Small Organisms,” *PLoS ONE* 2018, (13), e0193989.
- **L. Dong**, R. Jankele, M. Cornaglia, T. Lehnert, P. Gönczy, M. Gijs, “On-Chip Drug Studies to *C. elegans* Early Embryogenesis,” *Advanced Science*, 2018 (5), 1700751.
- **L. Dong**, M. Cornaglia, T. Lehnert, M. Gijs, “On-Chip Microfluidic Biocommunication Assay for Studying Male-Induced Demise in *C. elegans* Hermaphrodites,” *Lab on a Chip*, 2016 (16), 4534-4545.
- **L. Dong**, M. Cornaglia, T. Lehnert, M. Gijs, “Versatile Size-Dependent Sorting of *C. elegans* Nematodes and Embryos Using a Tunable Microfluidic Filter Structure,” *Lab on a Chip* 2016 (3), 574-585.
- E.T. Bowyer, B.J. Villis, J. Li, K.L. Litvinenko, B.N. Murdin, M. Erfani, G. Matmon, G. Aeppli, J. Ortega, R. Prazeres, **L. Dong**, X. Yu, “Picosecond Dynamics of a Silicon Donor Based Terahertz Detector Device,” *App. Phys. Lett.*, 2014 (105) 021107-021107.

CONFERENCE PRESENTATIONS

- **L. Dong**, J. Zhang, T. Lehnert, M. Gijs, “8-Channel Single Embryo Pipette for Accurate *C. elegans* Bioassays,” *The 31th IEEE International Conference on Micro Electro Mechanical Systems (IEEE-MEMS 2018)*, Belfast, UK.
- **L. Dong**, J. Zhang, T. Lehnert, M. Gijs, “Single Embryo Pipette for Accurate *C. elegans* Bioassays,” *The 21st International Conference on Miniaturized Systems for Chemistry and Life Sciences (MicroTAS 2017)*, Savannah, USA.
- **L. Dong**, J. Zhang, M. Cornaglia, T. Lehnert, M. Gijs, “*C. elegans* Immobilization Using Deformable Microfluidics for In-Vivo Studies of Early Embryogenesis and Intestinal Microbiota,” *The 30th IEEE International Conference on Micro Electro Mechanical Systems (IEEE-MEMS 2017)*, Las Vegas, USA.
- **L. Dong**, R. Jankele, J. Zhang, M. Cornaglia, T. Lehnert, P. Gönczy, M. Gijs, “An Integrated Microfluidic Device for *C. elegans* Early Embryogenesis Studies and Drug Assays,” *The 30th IEEE International Conference on Micro Electro Mechanical Systems (IEEE-MEMS 2017)*, Las Vegas, USA.
- **L. Dong**, M. Cornaglia, T. Lehnert, M. Gijs, “On-Chip Biocommunication through Exchange of Diffusive Compounds Secreted by Male *C. elegans* Nematodes,” *The 20th International Conference on Miniaturized Systems for Chemistry and Life Sciences (MicroTAS 2016)*, Dublin, Ireland.
- **L. Dong**, M. Cornaglia, T. Lehnert, M. Gijs, “Size-dependent Sorting of *C. elegans* Nematodes through An Adjustable Microfluidic Filter Structure,” *The 20th International Conference on Miniaturized Systems for Chemistry and Life Sciences (MicroTAS 2016)*, Dublin, Ireland.

- **L. Dong**, X. Yu, “Highly Sensitive Detection of DNA with HNA Defined Silicon Nanowire FET,” *The 17th International Conference on Miniaturized Systems for Chemistry and Life Sciences (MicroTAS 2013)*, Freiburg, Germany.
- **L. Dong**, X. Yu, “Fabrication of Submicron Silicon Masters and PDMS Replicas with High-Aspect Ratio,” *The 6th IEEE International Conference on Nano/Molecular Medicine and Engineering (IEEE-NanoMed 2012)*, Bangkok, Thailand.

